2011

The Application Of Chemometrics To The Detection And Classification Of Ignitable Liquids In Fire Debris Using The Total Ion Spectrum

Jennifer N. Lewis
University of Central Florida

THE APPLICATION OF CHEMOMETRICS TO THE DETECTION AND CLASSIFICATION OF IGNITABLE LIQUIDS IN FIRE DEBRIS USING THE TOTAL ION SPECTRUM

by

JENNIFER N. LEWIS
B.S. University of Florida, 2008

A thesis submitted in partial fulfillment of the requirements
for the degree of Master of Science
in the Department of Chemistry
in the College of Sciences
at the University of Central Florida
Orlando, Florida

Fall Term
2011

Major Professor: Michael E. Sigman

ABSTRACT

Current methods in ignitable liquid identification and classification from fire debris rely on pattern recognition of ignitable liquids in total ion chromatograms, extracted ion profiles, and target compound comparisons, as described in American Standards for Testing and Materials E1618-10. The total ion spectra method takes advantage of the reproducibility among sample spectra from the same American Society for Testing and Materials class. It is a method that is independent of the chromatographic conditions that affect retention times of target compounds, thus aiding in the use of computer-based library searching techniques. The total ion spectrum was obtained by summing the ion intensities across all retention times. The total ion spectrum from multiple fire debris samples were combined for target factor analysis. Principal components analysis allowed the dimensions of the data matrix to be reduced prior to target factor analysis, and the number of principal components retained was based on the determination of rank by median absolute deviation. The latent variables were rotated to find new vectors (resultant vectors) that were the best possible match to spectra in a reference library of over 450 ignitable liquid spectra (test factors). The Pearson correlation between target factors and resultant vectors were used to rank the ignitable liquids in the library. Ignitable liquids with the highest correlation represented possible contributions to the sample. Posterior probabilities for the ASTM ignitable liquid classes were calculated based on the probability distribution function of the correlation values. The ASTM ignitable liquid class present in the sample set was identified based on the class with the highest posterior probability value.

Tests included computer simulations of artificially generated total ion spectra from a combination of ignitable liquid and substrate spectra, as well as large scale burns in 20'x8'x8' containers complete with furnishings and flooring. Computer simulations were performed for each ASTM ignitable liquid class across a range of parameters. Of the total number of total ion spectra in a data set, the percentage of samples containing an ignitable liquid was varied, as well as the percent of ignitable liquid contribution in a given total ion spectrum. Target factor analysis was them performed on the computer-generated sample set. The correlation values from target factor analysis were used to calculate posterior probabilities for each ASTM ignitable liquid class. Large scale burns were designed to test the detection capabilities of the chemometric approach to ignitable liquid detection under conditions similar to those of a structure fire. Burn conditions were controlled by adjusting the type and volume of ignitable liquid used, the fuel load, ventilation, and the elapsed time of the burn. Samples collected from the large scale burns were analyzed using passive headspace adsorption with activated charcoal strips and carbon disulfide desorption of volatiles for analysis using gas chromatography-mass spectrometry.

This work is dedicated to all those who have inspired and supported me.

ACKNOWLEDGMENTS

I would like to thank my parents for always encouraging and supporting me in my educational interests and never letting me get discouraged; my graduate advisor and chair of my thesis committee, Dr. Sigman, for repeatedly explaining principal components analysis even when I thought comprehension was not possible; Dr. Andres Campiglia and Dr. Christian Clausen for serving on my thesis committee; the State of Florida Bureau of Forensic Fire and Explosive Analysis and the Florida State Fire College for providing resources and expertise in structure fires; Mary Williams for her help, guidance, and advice on everything from instrumentation to organization; my undergraduate research assistant, Matt Manney, for normalizing hundreds of spectra and introducing me to addictive websites; and my fellow graduate students at the National Center for Forensic Science for their invaluable insight, patience, and advice. I would like to thank Caitlin Rinke for helping me assemble furniture in all types of weather conditions; Erin Waddell for being an amazing study partner; Katie White for the multiple late-night brainstorming sessions; and Kelly McHugh-Pitan for turning over the reins of this research project. I would like to thank all of my friends who supported me, calmed me down at all hours of the night whenever I felt overwhelmed, feigned interest and excitement when listening to my research ideas and results, and reminded me that anything is possible with the right amount of dedication and moral support.

"Logic will get you from A to Z; imagination will get you everywhere."
- Albert Einstein

TABLE OF CONTENTS

LIST OF FIGURES

LIST OF TABLES

LIST OF ABBREVIATIONS

ACS	Activated charcoal strip
AR	Aromatic product
ASTM	American Standards and Testing Materials
AUC	Area under curve
DRMAD	Determination of Rank by Median Absolute Difference
EI	Electron ionization
EIC	Extracted ion chromatogram
FID	Flame ionization detector
GC	Gas chromatography
HAR	Heavy aromatic product
HPD	Heavy petroleum distillate
IL	Ignitable liquid
ILR	Ignitable liquid residue
ILRC	Ignitable liquid reference collection
IRMS	Isotope ratio mass spectrometry
ISO	Isoparaffinic product
LAR	Light aromatic product
LPD	Light petroleum distillate
MAD	Median absolute deviation
MAR	Medium aromatic product

MISC	Miscellaneous
MPD	Medium petroleum distillate
MS	Mass spectrometry
NAL	Normal alkane product
NCFS	National Center for Forensic Science
NP	Naphthenic-paraffinic product
OXY	Oxygenated product
PC	Principal component
PCA	Principal components analysis
PD	Petroleum distillate
PDF	Probability density function
ROC	Receiver operating characteristic
RSD	Residual standard deviation
SPME	Solid phase microextraction
TFA	Target factor analysis
TIC	Total ion chromatogram
TIS	Total ion spectrum

CHAPTER 1
INTRODUCTION

Fires are responsible for thousands of deaths, injuries and billions of dollars from property loss each year. Although Florida has a death rate by fire that is lower than the national average, fires still represent a large source of property damage. The United States has one of the highest fire-related death rates. In the year 2000 alone, there were over 1 million fires reported that cost an estimated $11 billion in property loss. Of the 1.7 million fires started in 2000, only about 4% were reported as suspicious, but accounted for 12% of the fatality rate and caused $1.3 billion in property damage.[1] In the year 2007, structure fires accounted for 85% of fire-related deaths and 82% of the total dollar loss related to property damage.[2]

Arson is difficult to successfully prosecute because there is little to no physical evidence linking a suspect to the crime. The analysis of fire debris samples for the presence of ignitable liquids is therefore an important component of arson investigations. This thesis examines the detection of ignitable liquids in fire debris samples using the total ion spectrum. This work investigates a method of classification of ignitable liquids in fire debris based on posterior probabilities calculated from correlation values between ignitable liquid spectra in a reference library to a dataset of spectra from fire debris samples.

Fire Debris Analysis

The American Society for Testing and Materials (ASTM) has classified ignitable liquids (ILs) into seven classes: gasoline, petroleum distillates (PD), isoparaffinic products (ISO), aromatic products (AR), naphthenic-paraffinic products (NP), normal alkane products (NAL), and oxygenated solvents (OXY). An eighth category, miscellaneous (MISC), has been created as a classification for those ignitable liquids that do not readily classify into one of the seven main categories. Ignitable liquids can be grouped into the different ASTM categories based on their chemical composition. The common components found in ignitable liquids and the prominent associated ions produced by electron ionization (EI) mass spectrometry (MS) are listed in Table 1.[3] The different categories of ignitable liquids are a product of the different types of refining processes of petroleum, as seen in Figure 1.[4]

Table 1: Major Compounds In Mass Spectra With Associated Common Ions

Compound	*m/z* Ratio
Alkane	43, 57, 71, 85, 99
Cycloalkane & Alkene	55, 59
n-Alkylcyclohexane	82, 83
Aromatic-alkylbenzene	91, 105, 119; 92, 106, 120
Indane	117, 118; 131, 132
Alkylnaphthalenes	128, 142, 156, 170
Alkylstyrenes	104, 117, 118, 132, 146
Alyklanthracenes	178, 192, 206
Alkylbiphenyls/Acenaphthenes	154, 168, 182, 196
Monoterpenes	93, 136
Ketones	43, 58, 72, 86
Alcohols	31, 45

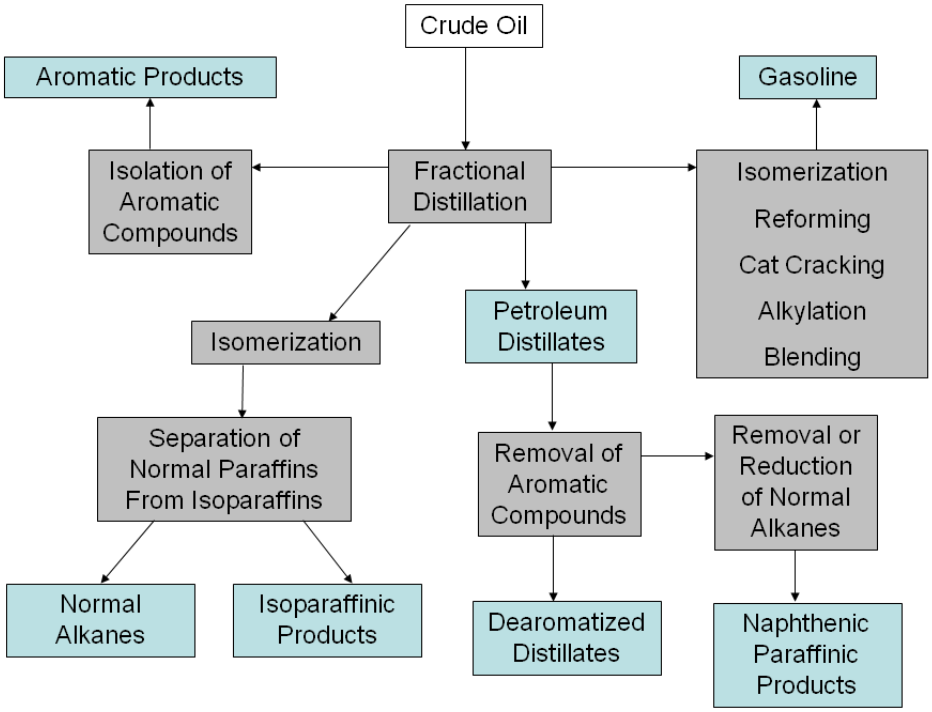

Figure 1: Schematic of Petroleum Refining Processing

Ignitable liquids within a category can be further subclassified based on the boiling point range or volatility of the liquid. The light subclassification includes compounds ranging from C_4 to C_9, the medium subclassification includes compounds ranging from C_8 to C_{13}, and the heavy subclassification includes compounds ranging from C_8 to C_{20} and greater. The medium and heavy subclassifications have significant overlap in the carbon range, which is addressed in ASTM E1618.[4]

Fire debris analysis is a complicated field due to the nature of the ignitable liquids, the complicated matrix of fire debris samples, and the presence of pyrolysis products.[5] Pyrolysis is a chemical process where a compound degrades into smaller volatile components by heat in the absence of oxygen or other oxidants.[4] Pyrolysis products complicate fire debris analysis because

they can contain the same compounds as an ignitable liquid. When volatiles from fire debris samples are extracted for analysis, the presence of these compounds may not be indicative of an ignitable liquid since they can also originate from pyrolysis products. This complicates detection and classification of an ignitable liquid based on target compounds. Therefore, it is essential that analysts be able to identify the target compounds from ignitable liquids in the presence of pyrolysis products and not attribute the presence of certain compounds to an ignitable liquid when they actually originated from pyrolysis products. Some of the compounds from pyrolysis products that could potentially interfere with the detection and classification of an ignitable liquid in fire debris include alkyl benzenes, styrene naphthalenes, methylnaphthalenes, n-alkanes, and branched alkanes.[5] Common substrates submitted for analysis include carpet and carpet padding, wood, fabric, paper, and vinyl flooring or other plastics. Most of these substrates are composed of synthetic materials, which produce organic compounds when burnt. These compounds can be identical to those found in ignitable liquid residues (ILRs) extracted from fire debris samples, thus complicating the ability to correctly identify the IL class present.[4]

Residue Extraction Methods

Ignitable liquids used in fire debris range in volatility, flammability, and other chemical properties making one specific method of ignitable liquid residue extraction from fire debris samples an impractical option. As of 2004, there are six ASTM standards regarded sampling methods of ignitable liquid residues from fire debris: steam distillation (E1385), solvent extraction (E1386), headspace vapor sampling (E1388), passive headspace concentration with activated charcoal (E1412), dynamic headspace concentration (E1413), and passive headspace with solid phase microextraction (SPME) (E2154). Steam distillation techniques have been

replaced by more modern techniques like adsorption or headspace extraction techniques.[4] Ignitable liquid residues can be extracted from fire debris samples by sampling headspace vapors above the fire debris. Volatiles in the headspace can be adsorbed onto activated charcoal or absorbed by a polydimethylsiloxane solid phase microextraction fiber.

Solvent Extraction

Solvent extraction techniques use various solvents to extract ILRs from fire debris samples. The sample is placed in the solvent and the ILRs that are adsorbed on the substrate are then distributed into the solvent, allowing for analysis of the solvent in order to identify the ILRs present. An ideal solvent is one that would not be used as an ignitable liquid and has a high extraction efficiency. Because most ILRs are nonpolar, most extraction solvents used are also nonpolar, such as carbon disulfide (CS_2), pentane, and hexane because they have a greater extraction efficiency. Fire debris samples suspected of containing a polar ignitable liquid, such as alcohols or other oxygenated compounds would be more efficiently extracted by a polar solvent like diethyl ether. Solvent extraction is performed by extracting any ILR from the substrate, filtering the solvent to remove any debris or impurities, and concentrating the sample if necessary by evaporating the solvent without losing any ILR in the solvent.[4] One advantage of this method of ILR extraction is the non-preferential extraction of ILR based on volatility, specifically heavier components displacing lighter components on adsorption materials like activated charcoal strips used in passive headspace sampling.[6]

Headspace Sampling

Headspace sampling (E1388) extracts ILRs from fire debris samples by taking a sampling of the headspace above the substrate. It is a simple, fast, and nondestructive technique requiring only a

heating assembly used to increase the amount of ILRs in the headspace and an airtight syringe to sample the headspace. It is ideal for highly volatile compounds like oxygenated products and does not expose the analyst to toxic solvents necessary for other extraction methods. However, headspace sampling can result in the identification of ILR compounds that are not representative of those adsorbed onto the substrate because ILRs may not be present in the same proportions in the headspace as they are on the fire debris sample. Headspace sampling is described as the least sensitive of the sampling methods and is disadvantageous for extraction of heavier compounds.[4]

Adsorption Methods

Adsorption methods can be divided into two groups based on the type of extraction, passive mode or dynamic mode. Passive adsorption methods include SPME and the use of activated charcoal. Both methods use an adsorbent material that is placed in the headspace of the fire debris sample to allow vapors to adsorb onto the material. In dynamic headspace concentration, the sample is under positive or negative pressure during the adsorption phase of sampling (E1413). Positive pressure systems subject the sample to a flow of nitrogen gas while being heated, whereas negative pressure systems apply a vacuum. The vaporized analytes will adsorb onto an adsorbent material. The adsorbent is then desorbed in a solvent so that the analytes of interest, the ILRs, are in solution. A portion of the solution is injected into the injection port of the gas chromatogram (GC) for analysis by GC or gas chromatography-mass spectrometry (GC-MS). This is a sensitive technique however it is also destructive, meaning that samples tested using this method of ignitable liquid extraction cannot be resampled.[7] Passive headspace concentration uses an adsorbent material, typically activated charcoal that is suspended in the headspace of a fire debris sample container. The sample is heated to facilitate the adsorption of

ILRs onto the activated charcoal. The activated charcoal is then desorbed in an appropriate solvent (E1412). The type of activated charcoal used for the purposes of this research was an activated charcoal strip (ACS), manufactured by Albrayco Technologies (Cromwell, CN). The strip is a mixture of activated charcoal and Teflon used to bind the charcoal together.[4] The ACS is desorbed with carbon disulfide or diethyl ether, and a portion of the solvent is analyzed using GC or GC-MS. Using activated charcoal adsorption is preferable when there is a low concentration of ignitable liquid residue present in the sample.[8] As of 2004, the most commonly used method of extracting ILR from fire debris samples is passive headspace with activated charcoal following the ASTM E1412 guideline.[1] The advantages of the use of ACS include the simplicity of the sampling procedure, sensitivity, and potential for GC-MS automated analysis. Passive headspace sampling with ACS is also advantageous because it is a nondestructive sampling method and allows for easy archiving of a portion of the ACS for future analysis. The primary disadvantage of using ACS is the exposure to toxic chemicals, such as carbon disulfide, which are required for chemical desorption, compared to the thermal desorption process used in SPME.[9]

Solid phase microextraction is a specific passive adsorption extraction technique that is used as a concentration technique to sample ignitable liquid residues from fire debris samples. This method only recovers small amounts of ignitable liquid residues, allowing the samples to be retested due to the nondestructive properties of the method, and can be used with aqueous samples. A fused silica fiber coated with polydimethylsiloxane is exposed to the headspace above the sample. The ignitable liquid residues adsorb onto the fiber and are thermally desorbed in the injection port of the GC.[10] Solid phase microextraction has the disadvantage of required

expensive fibers, which are not as easily retained for archiving as activate charcoal strips. Additionally, autosampling of SPME fibers requires an expensive instrumental setup. The advantages of SPME include the ability to reuse fibers for additional sample extractions, and because ILRs are thermally desorbed from the fiber the need for toxic solvents is eliminated.[1] The use of SPME for ILR extraction in fire debris analysis is not as common as headspace sampling, and is recommended by the ASTM standard E2154 to be used as a screening technique.[9]

Sample Analysis Instrumentation

The previously mentioned sampling techniques serve to extract volatiles from a fire debris sample into a solvent that can be used for instrumental analysis. The most common of these analytical methods is gas chromatography (GC) interfaced with mass spectrometry (MS).

Gas Chromatography

Gas chromatography is an analytical separation technique that uses a mobile gaseous phase to carry the sample onto the column, where the analytes interact with the stationary phase. The main components of a GC instrument include the carrier gas system, sample injection system, column, oven, and detector.[11] The carrier gas is a chemically-inert gas that acts as the eluent, or mobile-phase, for separation during gas chromatography. The sample injection system is important since maximum column efficiency requires the sample be introduced as a "plug" of sample, rather than a slow injection that could lead to band broadening effects being seen in the chromatogram. The liquid sample is injected into the GC system, where it is vaporized by

exposure to heat in the injection port. The vapor plug is then directed into the column, which is contained in an oven programmed to specific temperatures.

In general, separation of the analytes of the sample occurs based on their chemistry, which affects the analytes affinity for the stationary phase. Analytes with a strong affinity for the stationary phase will be retained longer and elute later compared to analytes that have little to no affinity for the stationary phase, so therefore would not be retained and would elute out of the column first. The degree of separation can be controlled by adjusting the flow rate, temperature of the column, and the type of column used.[1]

Mass Spectrometry

Prior to the introduction of mass spectrometers, flame ionization detectors (FIDs) were commonly used as gas chromatography detectors. However, these have largely given way to mass analyzers due to their increased sensitivity and higher information content of the resulting data. Mass spectrometry is an analytical technique that sorts ions based on their *m/z* ratio. The analytes separated by GC pass through the ion source of the MS, where the molecules are ionized. Quadrupole mass analyzers coupled with electron ionization is the most commonly used detector in fire debris analysis.[4] During electron ionization, electrons produced by the heated filament bombard analyte molecules and remove an electron from analyte molecules. The ionization of an analyte molecule is a high energy reaction that causes the molecule to fragment. The charged molecules and fragment ions now have specific *m/z* ratios and are sorted in the mass analyzer according to this ratio. The detector measures the intensity of each *m/z* ratio and the relative intensities of each are presented in a visual representation called a mass spectrum.[12] The fragmentation patterns produced by EI at 70 eV are very reproducible, allowing for easy

comparison of mass spectra to libraries and databases. Mass spectrometry is highly selective since it can detect changes in m/z values down to 1 amu, which allows for greater sensitivity when identifying compounds. The scan range used for the data acquisition was from *m/z* 30-350, which was further limited to *m/z* 30-200. The scan range was narrowed to eliminate the abundance of background ions or noise, since the analytes and pyrolysis products being considered for this type of analysis fell within the *m/z* range of 30-200.

Data Analysis Methods

The methods of data analysis may inevitably vary among laboratories depending on instrumentation available and prior experience or training in certain techniques, but as a general practice, fire debris samples are analyzed by GC-MS and any ILR is identified by a combination of pattern recognition, target compound identification, and extracted ion matching.

Current Methods in Fire Debris Analysis

The American Standards and Testing Materials (ASTM) outlined a test method for the analysis of extracted ignitable liquids from fire debris samples. The methods for gas chromatography-mass spectrometry analysis of fire debris samples listed in the ASTM method ASTM E1618-06 include visual comparisons of total ion chromatograms (TICs), extracted ion profiling for major characteristic ions, see Table 1, and target compound analysis.

Pattern recognition involves comparing the TIC of a fire debris sample to a known reference or standard. One of the most easily identifiable TIC patterns is a general Gaussian shape, indicative of petroleum distillates. This shape is due to the normal distribution of the boiling

points of the compounds within the petroleum-based ignitable liquid that occurs during the distillation process as part of the refinement of crude-oil. Visual pattern recognition compares the specific compounds identified by GC-MS analysis and relies heavily on the experience of the analyst to recognize not only compounds present in a chromatogram, but also whether these compounds are found in the appropriate ratios. For example, the presence of normal alkane compound(s) in a TIC does not automatically mean a petroleum distillate is present, but rather the ratio of the normal alkane compound(s) to other target compounds of the petroleum distillate class are necessary to identify a petroleum distillate as being present in the fire debris sample.

Target compound analysis is also related to pattern recognition, since compounds must be present in certain ratios depending on the ignitable liquid class. ASTM E1618-06 recommends comparing target compounds corresponding to a class of ignitable liquids to fire debris samples as a means of identifying the ignitable liquid class present. The presence of target compounds can be used to support the identification of an ignitable liquid in a fire debris sample.[5]

Challenges Associated with Current Methods

Fire debris samples are a complex matrix and successful determination of the class of ignitable liquid that may be present in debris samples depends on the ability to separate signal from the matrix from that associated with the ignitable liquid. This is especially true for samples containing low concentrations of an ILR.

Current methods of fire debris analysis primarily use TICs and associated extraction ion chromatograms (EICs) as a means of ignitable liquid identification. There are several potential problems associated with using the TIC as the primary means of ignitable liquid identification.

Variations in instrumental parameters and laboratory conditions produce inherent noise that overlay and can even mask the sample signal. In addition, differences between instrumentation can result in inconsistent retention times, even among GC-MS instruments in the same laboratory. Also, there are factors that may distort the pattern of the TIC. One distortion effect called weathering is the preferential loss of the lighter and more volatile components of an ignitable liquid upon heating. The loss of lighter components of an IL can be seen in the series of TICs in Figure 2, which depicts the same medium petroleum distillate (MPD) at several degrees of weathering. When comparing the top TIC of the unweathered MPD to that of the 90% weathered MPD TIC, there is a definite loss of the lighter more volatile analytes from the unweathered MPD.

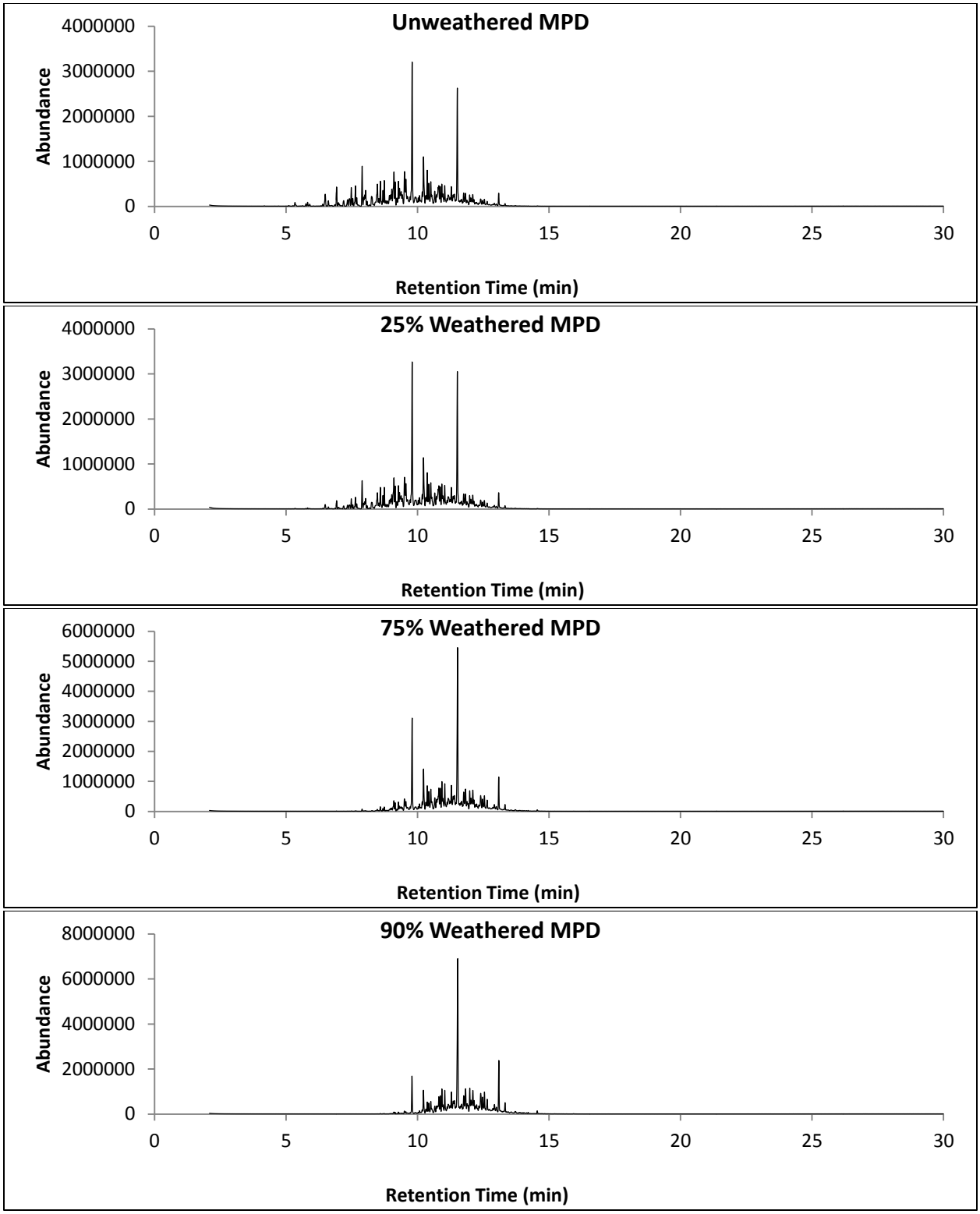

Figure 2: Weathered Series of Medium Petroleum Distillate

Another method of chromatogram distortion occurs during the ILR extraction process with activated charcoal and passive headspace sampling. Activated charcoal strips (ACS) are a common method used in forensic fire debris analysis, but ACS have been shown to preferentially adsorb compounds with a higher molecular weight, ie. heavier and less volatile. This type of chromatographic distortion results in a chromatogram that appears to have a weathered ignitable liquid present, when in fact the actual ignitable liquid present may be unweathered.[6] The analyst then relies on pattern recognition and comparing ratios of target compounds, per the ASTM E1618-06 standard guidelines based on a distorted chromatogram.[5]

The ASTM E1618 standard states that pattern recognition by comparison of a fire debris sample to that of a reference sample and comparisons of target compounds may be used as a means of identifying the presence of an ignitable liquid. As a primary means of ILR identification and classification, visual pattern recognition can be subjective and contingent on the analyst's experience.[13] This method may not provide consistent results among analysts or laboratories and may prove difficult in situations where chromatographic data has been distorted. The challenge with comparing target compounds from a class of ignitable liquids to those present in a fire debris sample is that the matrix can also contribute target compounds. When burned, some materials commonly found in residential and non-residential structures can produce the same target compounds present in ignitable liquids, thus complicating the identification of an ignitable liquid. Sources of target compounds other than the ignitable liquid include background products from substrate materials, pyrolysis products, and combustion products.[5]

New Methods for Data Analysis

Instead of using the TIC to classify ignitable liquids present in a fire debris sample, the goal of this research was to investigate a method using the total ion spectrum (TIS) to determine the presence and classification of ignitable liquid residues. The TIS of a sample is generated by summing all intensities of each m/z value across the length of the chromatographic period, as shown pictorially in Figure 3, which is a representation of a 3-dimensional data set obtained by GC-MS analysis. The TIS is equivalent to the average mass spectrum taken across the chromatographic profile.[14] The intensities are normalized to a total intensity of one, allowing for comparisons between other TISs. The advantage of using the TIS is that the spectrum generated is independent of time, hence shifts in retention time that can be problematic with comparisons and analyses using a TIC are eliminated. However, sampling and analysis methods that exclude or lose the lighter or heavier components will result in incomplete or distorted TIS, which would complicate ILR classification. The total ion spectrum has been shown to contain enough chromatographic information to allow for library or database searching.[14]

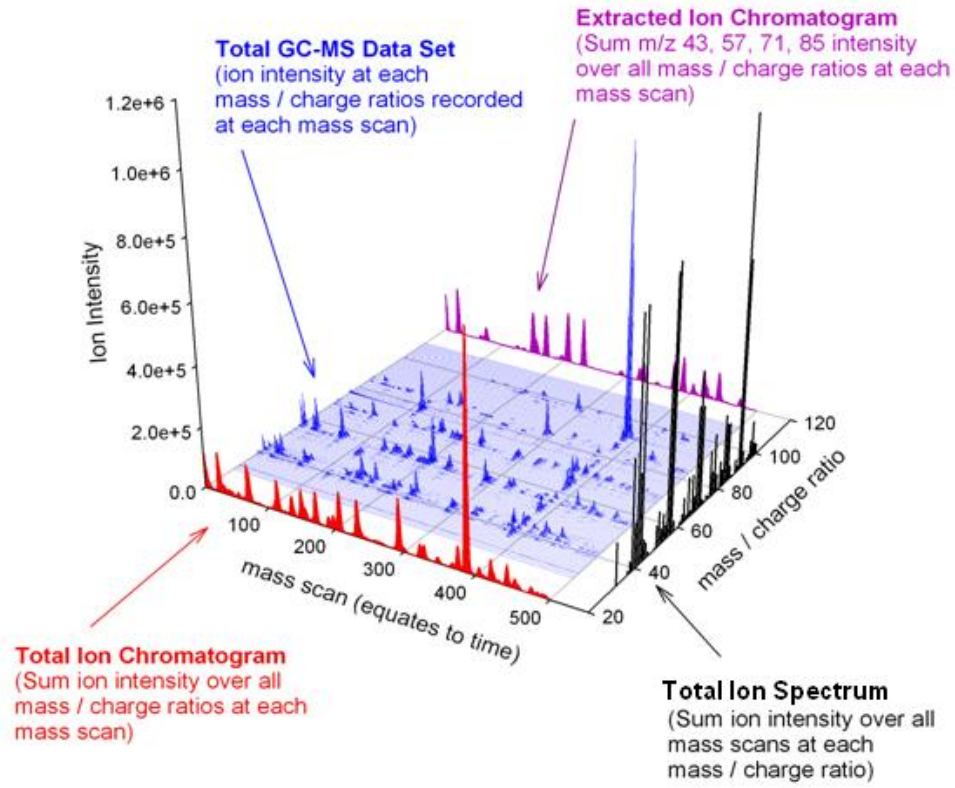

Figure 3: TIS from GC-MS Data*
* Used with permission from the National Center for Forensic Science

Visual pattern recognition, as previously mentioned, is dependent on the experience of the analyst. The inconsistencies in this type of analysis can be largely eliminated by the use of chemometrics or multivariate statistics.[13] Previous uses of multivariate statistics have included principal component analysis (PCA) to eliminate the subjectivity of analysts' interpretations of GC-MS data for the classification of gasoline.[13]

The data set of TIS from multiple fire debris samples is a data set amenable to chemometric analysis, and when used in conjunction with chemometrics can largely eliminate analyst discretion, as previously shown by the use of PCA for gasoline classification. Principal components analysis gave a correct classification rate between 80-93% using Mahalanobis

distances calculated from PCA scores when differentiating between premium and regular gasoline.[13] Principal components analysis also was successful in differentiating unevaporated gasoline and grouping the gasoline samples based on brand.[15] The reduced-dimensionality data set generated by PCA can then be analyzed by target factor analysis (TFA) to aid in library searching. The aim of this research was to investigate an IL classification method by applying chemometrics to the TIS generated from GC-MS analysis of fire debris samples.

Statistical Analysis

Chemometrics is the multivariate statistical analysis of chemical data, including chromatography data. When applied to fire debris analysis, chemometrics can be used to aid in ignitable liquid comparisons and classifications, and is beneficial in pattern comparisons since it largely removes analyst discretion from data interpretation.[4] One of the main multivariate statistics used in the comparison of GC-MS data is PCA.[9] The abstract solutions resulting from PCA are then transformed by TFA. The resulting data can be compared against a reference library and the resulting correlation values between the test and library vectors can be used to determine the ASTM class of IL present in one or more of the original fire debris samples.

Principal Components Analysis

Principal components analysis (PCA) produces a reduced-dimensionality data set using the minimum number of factors possible before the error is also reproduced. The justification for PCA is that spectra, chromatograms, and mass spectra are comprised of redundant data, so it is

possible to reduce the dimensionality of the data set without significant loss of distinguishing information.[16] Before PCA can be applied to a data set, it must conform to the equation:

$$d_{i,k} = \left(\sum_{j=1}^{n} r_{i,j} c_{j,k} \right) + error \qquad [1.1]$$

where the terms *r* and *c* are cofactors, and the number of terms, *n*, in the summation is the number of terms required to reproduce the data. The maximum number of terms that can be used to reproduce the data set is the smaller of the two matrix dimension values, *i* or *k*.

Each data set can be written in terms of matrix notation as:

$$[D] = [R][C] \qquad [1.2]$$

where each column in the scores matrix $[R]$ and each row in the loadings matrix $[C]$ is a factor.[17] The rows in the column matrix $[C]$ correspond to the eigenvalues, λ, which corresponds to the associated variation from the eigenvectors.[9] The eigenvalues correspond to the variance of a specific principal component and the eigenvectors represent the correlations with each variable in the corresponding principal component.[16] The data is arranged in $[D]$ with each sample spectra arranged in rows, so that each column corresponds to a variable, the *m/z* ratio, as shown in Equation [1.3].[9]

$$\overset{s\downarrow}{[D]} = \overset{s\downarrow}{[R]}\ \overset{n\downarrow}{[C]} \qquad \text{(m/z → for [D] and [C], n → for [R])} \qquad [1.3]$$

The loadings matrix typically does not correspond to any physically-relevant solution, but rather to a set of abstract solutions that are ortho-normal. The $[R]$ and $[C]$ matrices are generated by a singular value decomposition of the data matrix $[D]$.

A data matrix $[D]$ with the dimensions $n \times m$ where $n \geq m$ has a singular value decomposition in the form of the Equation [1.4]:

$$[D] = [U][S][V]^T \quad [1.4]$$

where $[U]$ is an ortho-normal $n \times n$ matrix, $[S]$ is a diagonal $n \times m$ matrix with $d_1 ... d_r$ singular values of $[D]$ along the diagonal with r corresponding to the rank of $[D]$ and contains the square roots of the eigenvalues from $[U]$, and $[V]$ is an orthogonal $m \times m$ matrix. In relation to the covariance matrix, the first r columns of $[V]$ correspond to the eigenvectors of $[D] \cdot [D]^T$ where $[D] \cdot [D]^T$ is equivalent to the covariance matrix of $[D]$ when $[V]$ contains a row for each variable, the *m/z* values for the purposes of this research, and $[U]$ contains a row for each sample.[9]

Based on how$[U]$, $[S]$, and $[V]$ are defined, the scores matrix $[R]$ from Equation [1.2] corresponds to the singular value decomposition matrices based on Equation [1.5]:

$$[R] = [U] \times [S] \quad [1.5]$$

The loadings matrix $[C]$ from Equation [1.2] contains the eigenvectors corresponding to the singular decomposition matrix based on Equation [1.6]:

$$[C] = [V]^T \quad [1.6]$$

The row-values in $[C]$ are ranked in decreasing order of importance with respect to the amount of variation accounted for in the data.[17] The first row in $[C]$ is the vector corresponding to the first factor, which accounts for the greatest amount of variation in the data set $[D]$.

The goal of PCA is to determine the number of factors, *n*, that can be retained that would allow the greatest amount of variance in the data set to be reproduced, without reproducing any of the inherent error. By eliminating any factors associated with the error in$[D]$, the data set can be reduced to only those factors that are useful. Then the reduced-dimensionality PCA solutions $[R']$ and $[C']$ of linear combinations of variables can be analyzed by target factor analysis against a library of TIS.

To determine the number of principal components to retain, the total variance was calculated. The variance of a PCA score is a measure of how much of the total variance of the data set is in a specific principal component (PC), with the cumulative variance being equal to the sum of the variances for a set of principal components. The individual eigenvalues, see Equation [1.3], represent the variance of each corresponding principal component. By summing the eigenvalues, the cumulative variance can be determined.[16] A scree plot depicts either the variance or cumulative variance plotted against the number of principal components, see Figure 4, based on

the theory that "after a certain number of principal components, the residual variance should level off" indicating any additional principal components would only contribute to reproducing the inherent error.[17] The points of each principal component are connected to aid in visually determining where the breaking point is between principal components contributing significant variance and those contributing to the error.

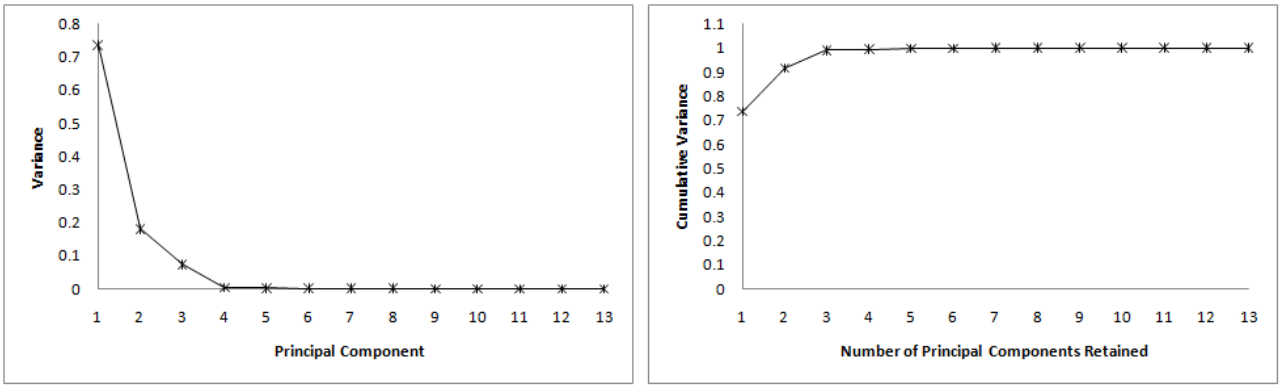

Figure 4: Example of Scree Plots

As seen in Figure 4, there is a breaking point in the scree plot at the number of principal components to retain. The breaking point in the scree plot of the cumulative variance with the corresponding principal component (right) is identical to that of a scree plot of the eigenvalues with the corresponding principal component (left).[9]

Target Factor Analysis

After determining the number of factors *n* to retain, Equation [1.2] can be redefined using the reduced dimensionality $[R']$ and $[C']$ matrices by Equation [1.7]:

$$[D'] = [R'][C'] \qquad [1.7]$$

where $[R']$ and $[C']$ retain only the first *n* columns and rows of $[R]$ and $[C]$, respectively. The abstract solutions obtained from principal components analysis are then transformed into physically meaningful solutions by factor analysis by one of two approaches: target testing or abstract rotation, to transform the matrix $[C]$ into physically meaningful solutions.[17] The transformation of $[R']$ into solutions that are physically meaningful is accomplished by Equation [1.8]:

$$[\bar{R}] = [R'][T] \quad [1.8]$$

where $[\bar{R}]$ is the row matrix of the predicted scores, and $[T]$ is the transformation matrix with dimensions $n \times n$. The transformation of $[C']$ into physically meaningful solutions is accomplished by premultiplying $[C']$ by the inverse of the transformation matrix $[T]^{-1}$ as shown in the Equation [1.9]:

$$[\bar{C}] = [T]^{-1}[C'] \quad [1.9]$$

The relation between $[R']$, $[C']$ and $[D']$ can be seen by manipulation of Equation [1.7] as shown below:

$$[D'] = [R'][T][T]^{-1}[C'] \quad [1.10]$$

where the $[R'][T]$ factor corresponds to $[\bar{R}]$ by Equation [1.8] and the $[T]^{-1}[C']$ factor equals $[\bar{C}]$ as seen in Equation [1.9]. The transformation matrix is obtained by target transformation of $[C']$. The principal components of $[C]$ are rotated since $[C']$ corresponds to the m/z values, that

are known for the data set. The values of $[C']$ which are analogous to intensities of the *m/z* values are projected onto test vectors that are from the library spectra. The goal is to find a rotation of the principal components that produces a predicted vector that is similar to the test vector.

As shown in Equation [1.11], test vectors $\overline{\overline{C_l}}$ can be searched for individually, which means a sample can be compared individually to a library of reference ignitable liquids to determine a set of real factors. The goal of target transformations is to find a transformation vector T'_l calculated by Equation [1.11], which is then applied to the reduced dimensionality matrix $[C']$ obtained from PCA to find a predicted vector $\overline{C_l}$ by Equation [1.12].

$$T'_l = \overline{\overline{C_l}}[C']^T \quad [1.11]$$

The predicted vector is produced by target transformation based on Equation [1.12] by multiplying the reduced-dimensionality matrix $[C']$ by the *l*th row of the transformation matrix $[T]'$.

$$\overline{C_l} = T'_l[C'] \quad [1.12]$$

The goal of target transformations is to find a transformation vector T_l calculated by Equation [1.11] that produces a test vector $\overline{\overline{C_l}}$ that best matches the predicted vector $\overline{C_l}$. If a test vector is a real factor of the data matrix, then the predicted vector $\overline{C_l}$ will be similar to the test vector $\overline{\overline{C_l}}$.[17] The degree of similarity between a test vector and predicted vector was calculated based on the Pearson correlation.

Pearson Correlation

The method of least squares was used to minimize the deviation from the test vector and the predicted vector. The correlation coefficient was calculated to determine the similarity between the predicted vector $\overline{C_l}$ (related to the *m/z* variables from a sample TIS) and the test vector $\overline{\overline{C_l}}$ (related to the individual library ignitable liquid TIS). The Pearson product-moment correlation coefficient, calculated by Equation [1.13] is a measurement of the strength of linearity between the predicted vector and test vector, and was determined for each individual target transformation by the following equation:[18]

$$r = \frac{\sum(x - \overline{x})(y - \overline{y})}{\sqrt{\sum(x - \overline{x})^2 \sum(y - \overline{y})^2}} \qquad [1.13]$$

The values of *r* can range from 0 to 1. Values close to 0 indicate a lack of linearity between the two vectors, so the vectors would be considered uncorrelated.

Determination of Rank by Median Absolute Deviation

In the beginning stages of this research, the number of principal components retained was chosen based on a scree plot of the cumulative variance (see Figure 4), or the number of principal components was chosen based on the number of PC's corresponding to 95% of the variance of the data set. There was no consistent decision-making standard, which was problematic since using too many factors to reproduce the data set would result in the reproduction of the error.[17] Determining the number of PCs to retain was a significant problem since retaining too few would result in loss of relevant information, and retaining too many would reproduce signal

noise thus over-fitting the data.[9] The problem with choosing principal components based on scree plots alone is that there is not always a clear breaking point, see Figure 5. To overcome this problem, a more robust method proposed by Malinowski for determining the number of principal components to retain was used.[19]

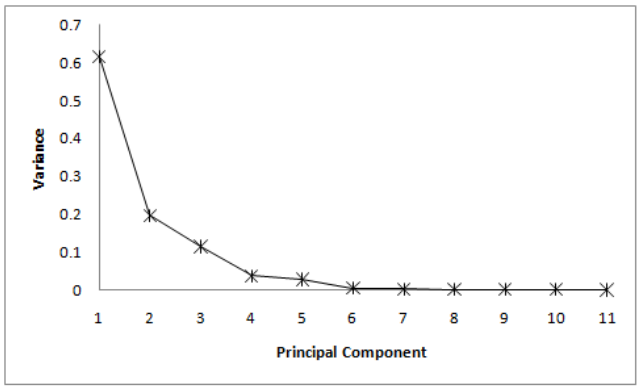

Figure 5: Scree Plot With No Definite Breaking Point

When trying to determine the number of principal components to retain, there are two general situations: when a reasonable estimation of the noise (the standard deviation of the measurements) is able to be determined prior to PCA, and when the noise of the data cannot be accurately estimated.

If the standard deviation of the measurements can be determined, then the residual standard deviation (RSD) can be calculated and used as an estimation of the rank of the data matrix. The RSD is calculated using the PCA eigenvalues and divides them into primary and secondary factors. Primary factors are those that account for the largest associated variation and secondary factors are considered to account for the noise and any "undesirable instrumental and experimental artifacts."[19] If the inherent noise in the data set can be sufficiently estimated, then the number of primary factors of a data set can be found at the point at which the noise

estimation (the standard deviation of the measurements) is closest to the RSD calculated from PCA. The RSD can be expressed in terms of the associated eigenvalues, see Equation [1.14], based on the relationship that the sum of the smallest set of eigenvalues is equivalent to the sum of the squares of the error in the data set, where *n* is the number of factors retained in PCA.[19]

$$\text{RSD} = \left(\frac{\sum_{j=n+1}^{s} \lambda_j}{(r-n)(c-n)} \right)^{1/2} \qquad [1.14]$$

When the standard deviation of measurements cannot be successfully estimated or calculated, outliers can be determined by the determination of rank by median absolute deviation (DRMAD) statistical method. The value of the median absolute deviation (MAD) is calculated based on Equation [1.15].

$$\text{MAD} = \text{median}\|x_i - \text{median}(x_i)\| \qquad [1.15]$$

A data point, x_i, is considered an outlier if the following equation is true[19]:

$$\frac{\|x_i - \text{median}(x_i)\|}{\text{MAD}} > 5 \qquad [1.16]$$

Using the DRMAD statistical approach, the set of secondary eigenvalues associated with the error can be determined since they are the smallest in comparison to primary factors, which would be considered outliers. If a primary factor was erroneously included in the set of secondary error eigenvalues, the calculated RSD from Equation [1.14] would increase

significantly in relation to the true RSD in such a way as to be considered an outlier by the DRMAD method.[19]

The DRMAD methodology was used with theoretical data sets by Malinowski to demonstrate the method's utility and robustness in comparison to other empirical, pseudo-statistical and statistical methods of the rank estimation of a matrix.[19] The DRMAD method identifies a factor as a PC by determining if the factor is an outlier of the data set. A factor is considered an outlier based on [1.16]. The DRMAD method of determining the number of principal components to retain before target transformations using TFA has been applied to other analytical data, including nuclear magnetic resonance data to determine the solvent effect of the formyl proton on chemical shifts of para-substituted benzaldehydes.[20]

Receiver Operating Characteristics

After the data set has been reduced by PCA and correlation values have been calculated from comparison of test and reference vectors by TFA, the rankings of correlation values for each ignitable liquid in a library can be plotted in a receiver operating characteristic (ROC) graph. A ROC curve graph is used to visually organize correlation values into classifications based on the ASTM IL class designation. A ROC graph is a plot of the true positive rate versus the false positive rate, see Figure 6. The true positive rate of a classifier is defined as the ratio of positive classifiers correctly classified to the number of total positive classifiers. The false positive rate is the ratio of negative classifiers incorrectly classified to total negative classifiers.

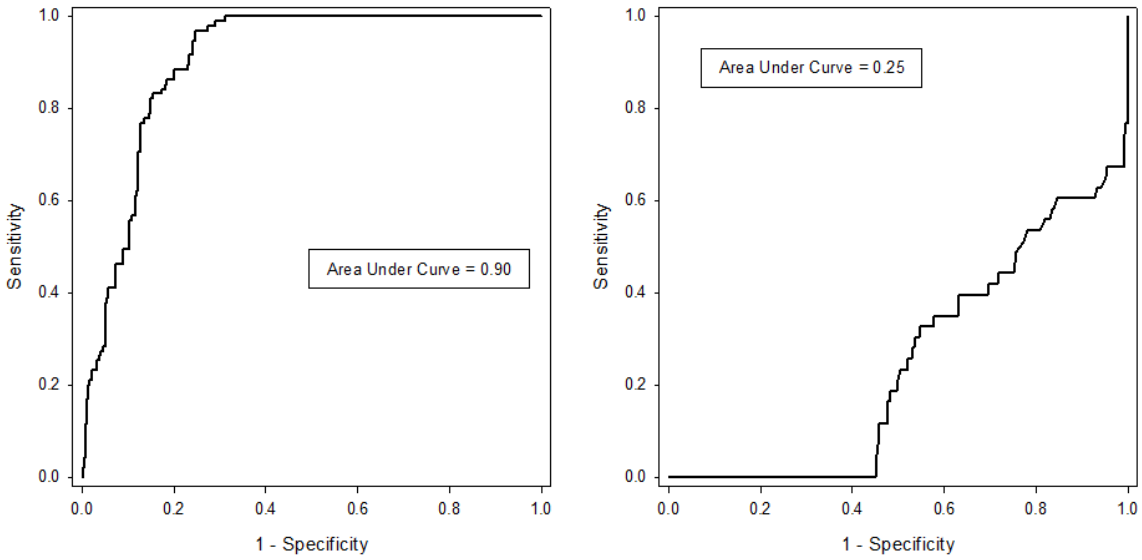

Figure 6: Example of ROC Curves

When interpreting a ROC graph, there are four main points or regions that are of value. The point at the origin is equivalent to a classification model that never assigned a positive (correct) classification. Such a model would never have any false positive errors, but also no true positive classifications. The opposite of this strategy occurs at the point (1,1). At this point on the ROC graph, the model indiscriminately assigns a positive classification. The point (0,1) corresponds to a model that always gives accurate classifications, and the line y=x signifies a classification model that is essentially randomly guessing a classification.[21]

Models that accurately classify positive and negative classifiers have an area under the curve (AUC) close to 1.0. An AUC value of 1.0 corresponds to a ROC curve with a perfect correlation since classifiers fall above the y=x line and close to the point (0,1), as shown in the left figure in Figure 6 . The same principle applies to classifiers that fall below the y=x line, meaning the model "performs worse than random guessing," and would be considered a poor classification, as shown in the right figure in Figure 6.[21] The AUC value can also be interpreted in terms of the

distribution of the correct and incorrect data sets, and whether the distribution of the correct and incorrect classification events was statistically distinguishable. Because a normal distribution cannot be assumed in relation to correlation values determined by TFA, the non-parametric test comparable to a two-sample *t*-test, the Wilcoxon rank sum test or the equivalent Mann-Whitney *U* test can be employed.[22]

For the purposes of this research, correlation values were used as the data subjected to the technique of ROC analysis. Two vectors were generated, one for the correlation values corresponding to the ignitable liquids of the "correct" class, and a second vector for the correlation values corresponding to the remaining ignitable liquids from all other ASTM IL classes. The correlation values were stepped through sequentially in decreasing order. For every correct correlation value, the ROC curve steps up by a proportion of the correct matrix, and for every incorrect correlation value, the ROC curve steps over by a proportion of the incorrect matrix.

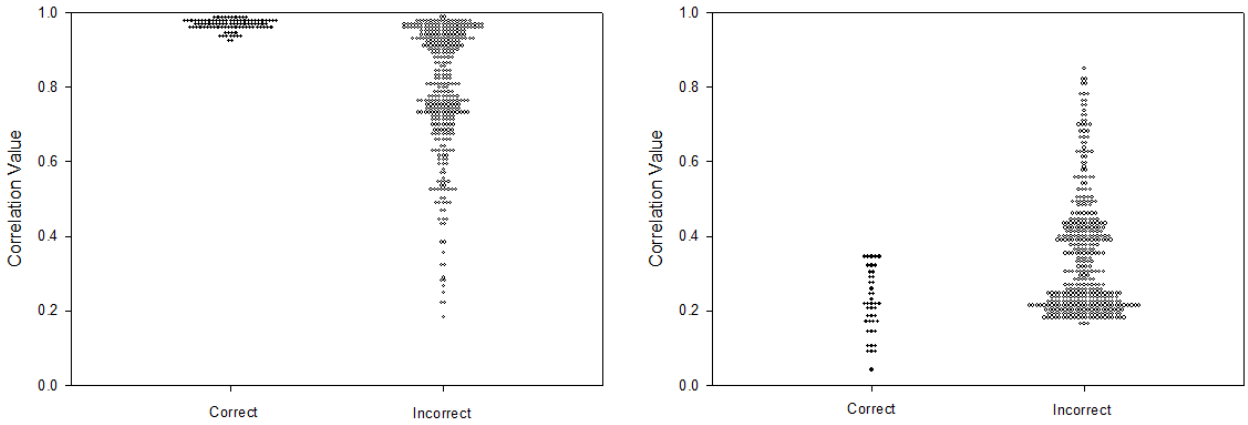

Figure 7: Example of Histograms of Correlation Values for ROC Curves

When the correlation values for the correct and incorrect matrices are displayed in a histogram plot, see Figure 7, a better understanding of how a ROC curve is generated is possible. The

histogram on the left and right represent the matrices used to generate the corresponding ROC curves in Figure 6. When stepping through the correlation values from high to low in the left example in Figure 7, all of the correct correlations are high meaning that they will be counted first with respect to the majority of incorrect values. This results in a ROC curve that initially steps up significantly, then steps across for the remaining distance as all of the incorrect values are counted, as seen in the left ROC curve in Figure 6.

Wilcoxon Rank Sum Test

The value of the AUC of a given ROC curve is equivalent to the non-parametric test, the Wilcoxon test.[22] The Wilcoxon rank sum test determines if the median from a class has significantly shifted from a second class, which would indicate the two classes are from different populations rather than portions of the same population. The test determines a rank sum value, *R*, for each class based on a ranking value which is used in place of the true data values. The rank scores, 1,2,3…*n* are assigned to each data value in increasing order of magnitude in both classes being compared, with *n* being equal to the total number of data points in both populations.[23] By summing the rankings for a class, a rank sum statistic, *R*, is determined, which is then used to calculate the Mann-Whitney U test statistic, *U*. To convert the rank sum statistic *R* to *U*, the following formula was used:

$$U_a = n_a n_b + \frac{n_a(n_a - 1)}{2} - \sum R_a \qquad [1.17]$$

where $\sum R_a$ is equal to *R*, the rank sum statistic of class a.

$$U_b = n_a n_b + \frac{n_b(n_b - 1)}{2} - \sum R_b \quad [1.18]$$

The same equation, Equation [1.17] can be modified to calculate the *U* statistic for class *b*, as in Equation [1.18] which also uses the rank sum statistic of population *b*, with the relationship between U_a and U_b shown in the following equation.[24]

$$n_a n_b = U_a + U_b \quad [1.19]$$

For comparisons between an ignitable liquid class and the rest of the library, population *a* corresponds to the ignitable liquid class and population *b* corresponds to all other classes.

The *U* value corresponding to the correct ignitable liquid class, population *a*, was converted to a Wilcoxon *W*-value using the following equation:

$$W_a = \frac{U_a}{n_a n_b} \quad [1.20]$$

where the value of *W* is equivalent to the area under the ROC curve.[25]

The *W* value calculated using Equation [1.20] corresponds to population *a*, but if the *W* value for population *b* is desired, then Equation [1.19] can be algebraically converted into Equation [1.21].

$$W_a + W_b = 1 \quad [1.21]$$

Bayesian Decision Theory

Bayesian decision theory is a supervised technique, meaning that prior knowledge of the data is required, for example the knowledge of classification groupings for data points or probability density functions (PDFs).[9, 26] The advantage of the Bayes method is that as the number of results increases, the prediction model improves since it takes into account prior information (prior probability) when calculating the posterior probability. The posterior probability from the Bayes equation is given by the following equation:

$$P(\omega_j|x) = \frac{p(x|\omega_j)P(\omega_j)}{\sum p(x|\omega_j)\,P(\omega_j)} \quad [1.22]$$

where $P(\omega_j)$ is the prior estimated probability and $p(x|\omega_j)$ is the conditional probability density of a specific class ω_j.[26] The term in the denominator is a normalization factor so that the sum of all posterior probabilities, $P(\omega_j|x)$, sum to 1. The posterior probability represents the probability that given a vector, *x*, the classification of *x* belongs to class ω_j.[26] The prior estimated probabilities, $P(\omega_j)$, would represent the prior knowledge of the probability of identifying a specific ASTM class over another. For example, if normal alkanes were never identified by a laboratory, they could be given a lower weight, or prior probability, to take into account the low probability of a normal alkane being present in the fire debris samples. Prior probabilities for each of the classes were not known so they were set equal when calculating posterior probabilities for each ASTM class. The conditional probability density $p(x|\omega_j)$ is a likelihood term that is given by any probability density function (PDF). For the purposes of this research, the kernel method was used to estimate the probability density function for the likelihood term.

The kernel method is an estimation of PDF of a set of values, and is calculated by the following equation:

$$f_n(x) = \frac{1}{nh}\sum K\left(\frac{x - X_j}{h}\right) \quad [1.23]$$

where K is the kernel function, *h* is the bandwidth, and X_j is a unique sample from the unknown density *f*.[27] The bandwidth is related to the degree of smoothing for the estimated PDF. If *h* is too small, then the estimated PDF will not be significantly smooth, but if *h* is too large then the data will be too smoothed.[18] The bandwidth *h* can be estimated by the following equation:

$$h = \frac{1.06}{n^{1/5}}s \quad [1.24]$$

where s is the standard deviation.[18] For normal distributions, the standard deviation is approximately 1.483*MAD, so it is possible to estimate the ideal bandwidth by converting Equation [1.24] into following form:[9]

$$h = \frac{1.57}{n^{1/5}} * MAD \quad [1.25]$$

If for each correlation value from a given class a Gaussian probability density function is graphed, then when summing the intensities of each of the values in the PDF, a broader curve is generated called the kernel density. The median correlation value within the kernel density must be within 3 standard deviations from 1, the value corresponding to a perfect correlation between the test and resultant vectors from TFA. This is equivalent to saying that at a given α-value, the

kernel density of the correct class should have a median value within 3 standard deviations from 1, and is determined by Equation [1.26].

$$\frac{\|1 - \text{median}(x_i)\|}{\text{MAD}} < 5 \qquad [1.26]$$

If the value calculated in Equation [1.26] is less than 5, then it can be assumed that the ideal correlation value (r=1) is within the 99% confidence interval for the PDF determined by the kernel method, and that there is only a 1% chance that the ideal correlation is an outlier**.** If the value calculated in Equation [1.26] is greater than 5, then 1 would be an outlier, indicating the PDF calculated by the kernel method falls too far away from r=1 to have a posterior probability calculated. Only classes with a PDF having the idea correlation value within 3 standard deviations of the class mean will have a posterior probability calculated.

Proposed Research

This research aimed to develop a method of detection and classification of ILRs present in fire debris samples using the total ion spectrum. The proposed classification method uses PCA to extract latent variables from a fire debris sample set of TIS. These latent variables are then compared to individual TIS in a reference library by TFA and sorted based on their correlation values. The correlation values and corresponding IL classes were then used to calculate the posterior probability value for each class. Posterior probability values were calculated for only those classes having a value of $\frac{\|1-\text{median}(x_i)\|}{\text{MAD}}$ less than 5. The class with the highest posterior probability was identified as the IL class present. This method was applied to large scale

experimental burns as well as laboratory test burns to determine an overall rate of correctly classifying the IL class present.

CHAPTER 2
EXPERIMENTAL METHODS

Computer Simulation Models

Large scale experimental burns and laboratory test burns provide an opportunity for sample collection of realistic representations of structure fires and large scale fires. However, it is not feasible to perform numerous experimental laboratory burns, especially large scale experimental burns, so an alternative method of generating data that can be used for statistical analysis was required. Computer model simulation allows for user-controlled sample generation. The conditions affecting a sample are able to be manipulated, which allows for a greater range of testing. By using a computer model, the TIS of a substrate can be combined with the TIS of an ignitable liquid, to generate a fire debris sample that has a certain percentage of known ignitable liquid. This allows for a greater degree of control, since the generated sample and TIS are not subject to environmental or laboratory factors. The amount of ignitable liquid present in a computer-generated TIS can be designated by the user so that low limits of ignitable liquid contributions can be achieved. This has previously not been possible due to the experimental setup of the large scale burns. The opportunity for known percent contributions of ILs in the data set could be used to determine if the classification method was successful in correctly classifying ILs, even when present in low concentrations in a fire debris sample.

A simulation code was written for the program MATLAB in which a variety of parameters could be adjusted including the specific IL or IL class, the percent contribution of IL per sample, and

the number of samples with an IL contribution. By adjusting these parameters, a sample set of artificial TIS equivalent to the sample set obtained from the large scale experimental burns can be generated and prepared for statistical analysis, being treated like all other large scale burn sample sets. The percent contribution of IL in a sample was especially important in the computer simulation models since it is a parameter that could be difficult to control in a large scale burn setting.

Individual ignitable liquid tests indicate the classification accuracy only for a specific ignitable liquid. While the IL chosen may be a good representation of the ASTM class to which it belongs, not all classes have uniform ignitable liquid samples. As a result, it may be hard to find only one IL that can be considered a representation of the entire class. In order to observe any trends in classification accuracy rates, one IL per simulation would be insufficient to make a generalization for an entire class. To determine how an individual IL class performs, it was necessary to run simulations using different ILs for each simulation.

Computer Model Design

For each ASTM-defined ignitable liquid class, a series of experiments were performed to determine an approximate limit of detection and determine the rate of correct classifications at varying IL contributions. With this model, an ignitable liquid class could be selected and the corresponding TIS generated would be a combination of a percentage of a randomly chosen IL spectrum from the selected class and a randomly chosen substrate TIS. This would generate one TIS, and the process was repeated for the total number of TIS desired to make up the data set. Comparisons to library reference TIS were performed by TFA of the generated data sets.

The experiment was set up to include 12 computer-generated TIS to be analyzed by TFA against a reference library. In designing how the TIS for each TFA data set would be generated, it did not seem realistic to include an ignitable liquid contribution in all 12 samples. The aim was to represent a data set from an actual fire scene or suspected arson investigation. There is a low probability of all collected samples having an ignitable liquid present, which was taken into account when justifying an ignitable liquid contribution for only a portion of the 12 samples per TFA test.

A series of experiments were run using code written for MATLAB. The code generated 12 TIS representing samples collected from a suspected arson scene by using a combination of IL and substrate TIS from a reference library. Each spectrum was composed of the appropriate percentage of IL spectrum and a randomly chosen substrate spectrum from a reference library of total ion spectra. The number of spectra of the 12 total spectra containing an IL contribution was varied from 1 to 12. At each number of spectra containing and IL contribution, the percentage of IL contribution towards the generated spectrum was varied across a range of percent contributions established by user-specified parameters. At each percentage of spectra with an IL contribution and at each percent of IL contribution per spectra, the parameters were repeated n-times with each n^{th}-iteration using a new IL from the user-selected IL class as the contributing IL. For each n^{th}-iteration using a new IL, each of the 12 generated spectra contained contributions from a randomly selected substrate spectrum at the appropriate percent contribution. For each of the n-number of simulations at the percent IL contribution and at the number of samples with an IL contribution, TFA was performed on the data set of the 12

generated spectra. The 12 total samples were then analyzed against a reference library and the average correlation values, ROC AUC values, Wilcoxon rank sum values and p-values were calculated. The n-number of correlation values, ROC AUC values, Wilcoxon rank sum values and corresponding p-values for each percent IL contribution at each percent of samples with IL contributions were then averaged and graphed.

By using different substrate TIS for each of the generated TIS spectra, it is possible for simulations to contain more factors than spectra. Under these conditions, the method would fail to detect the ignitable liquid classes present in the sample set if the contribution of IL was low. In these instances, the computer simulations act as a worst case scenario showing how the detection and classification model performs under conditions where there are more factors than spectra.

Each class of IL (AR, Gasoline, HPD, MPD LPD, ISO, NAL, NP, OXY and MISC) was analyzed using the computer simulation model that calculated the average correlation values, ROC AUC values, Wilcoxon rank sum and p-values.

Large Scale Experimental Burns

Large scale experimental burns were set up to test the multivariate statistical method of ignitable liquid detection and classification by using samples collected from a setting that is more representative of a structure fire. The large scale burns used an 8’ x 20’ x 8’ Konex steel container, see Figure 8, with the interior built-out to resemble a home or apartment, see Figure 9

and Figure 10. Each container had a set of doors at one end and a window cut out from the back wall. The doors and window allowed ventilation during the burn. The floor of the containers was covered with a variety of flooring materials including wood laminate, vinyl tile, and carpet and padding. Each container had living room and bedroom furniture and accessories.

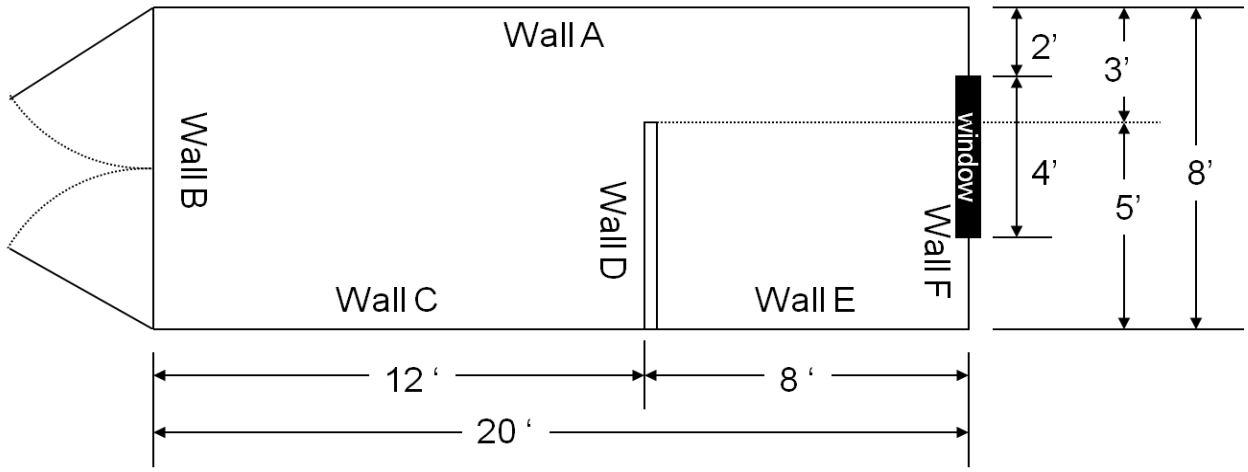

Figure 8: Schematic of Large Scale Burn Container

Figure 9: Building Arrangement of Container

Figure 10: Window Cut From Container Wall

After the samples were collected they were transported back to the National Center for Forensic Science (NCFS) at the University of Central Florida. For laboratory analysis, an activated charcoal strip (ACS) (Albrayco Technologies, Cromwell, CN) was suspended in the headspace above the fire debris sample and sealed in the can. Any volatiles in the fire debris sample were extracted and adsorbed onto the ACS when the can and ACS were placed in an oven set to 66°C for 6-18 hours. At the end of the 16-18 hour period, the can and ACS were removed and the ACS was divided in half. One half was archived and the other half was used for analysis. To the half used for analysis, 1 mL of CS_2 was added to the autosampler vial to desorb any components off the ACS. Ignitable liquid residues and other volatiles in the sample were then analyzed by

GC-MS to identify what, if any, compounds were present in the fire debris sample in order to identify and classify the ignitable liquid used in the large-scale burn.

Container Design

The containers were built out using 2”x4” pieces of pine wood as a frame, and sheetrock walls. Plywood was used as the subflooring, with carpet and padding used as the main type of floor covering. Some containers contained wood laminate or other flooring materials. The furniture inside each container was purchased from a local furniture warehouse. Four large scale burns had been done prior to this work, so to continue with the naming convention, all subsequent containers were numbered starting with 5.

Container 5

The carpet was a nylon carpet purchased from a local home improvement store. Wood laminate flooring was also included in the container, and placed in the entry way to the back room. Based on results from previously burned containers, additional items were added to the containers in an effort to increase the fuel load and to also make the burn more realistic to a domestic fire. Items added included curtains, clothing, shoes, magazines, and miscellaneous items in the trash.

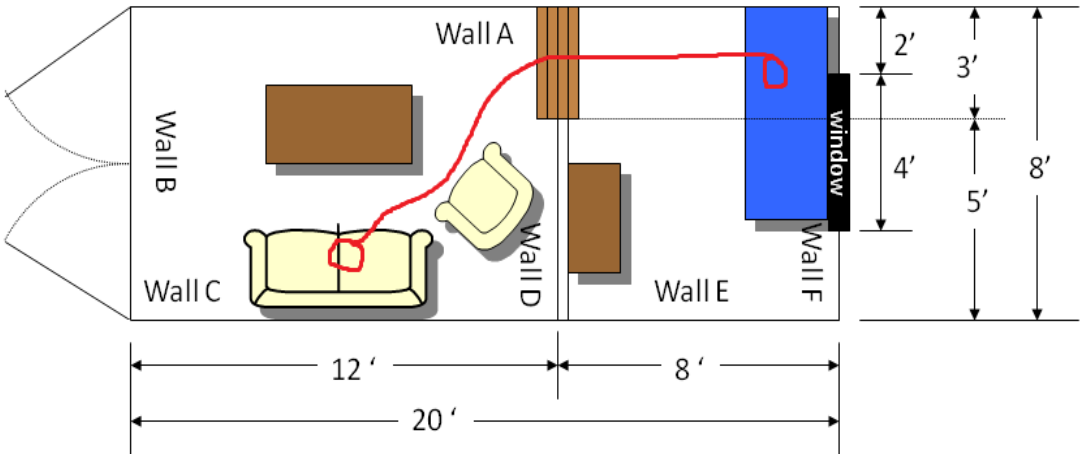

Figure 11: Pour Pattern in Container 5

The container was burned with approximately 500 mL of gasoline as the ignitable liquid. For a reference TIC and TIS, see Appendix A. The gasoline was trailed from the couch, through the front room (Room 1), across the back room (Room 2), and stopped on the mattress, see Figure 11. The temperatures at various locations inside the container were monitored and recorded by a series of thermocouples placed throughout the inside of the container. The locations of the thermocouples are shown in Figure 12 and Table 2.

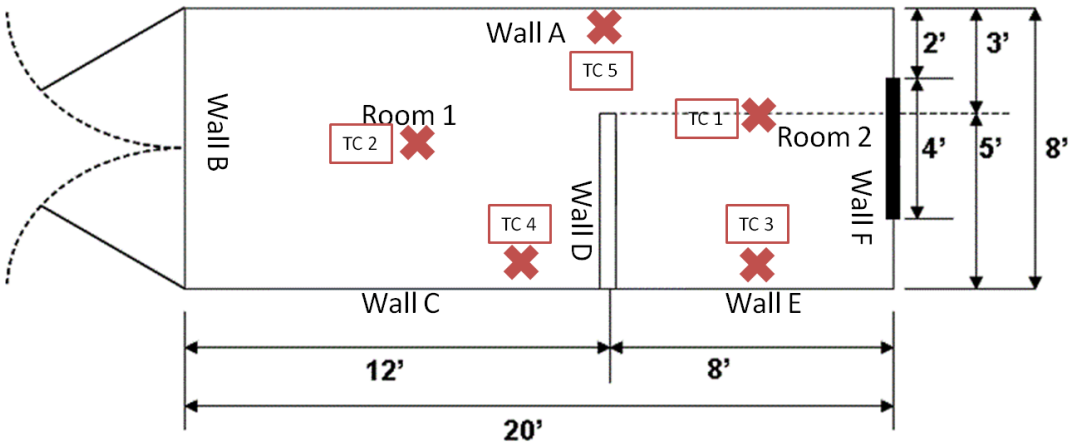

Figure 12: Thermocouple Layout Container 5

Table 2: Thermocouple Locations Container 5

TC	Room	Wall Location Measured From Wall	Height
1	2	A: 36"	Ceiling
2	1	A: 40"	Ceiling
3	2	D: 25"	12"
4	1	D: 46"	12"
5	2	F: 96"	90"

The temperatures were monitored and recorded for the duration of the burn, which allowed for the determination of the maximum temperatures inside each room. At the end of the burn, the container was extinguished with water by personnel at the Florida State Fire College.

Once the container was sufficiently cooled, locations were marked and samples were collected from the locations according to Figure 13 and placed individually into gallon-sized metal cans. The locations of the samples were measured using two different walls as points of reference.

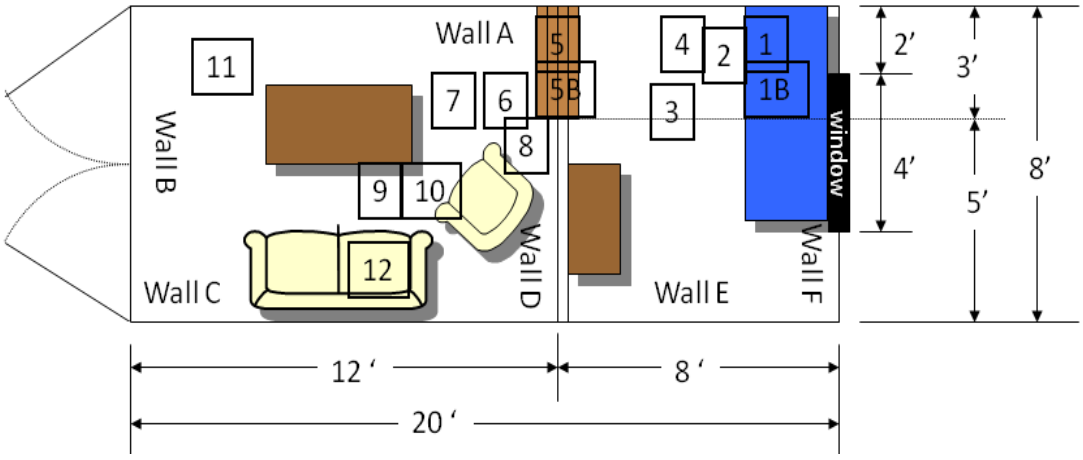

Figure 13: Sample Locations in Container 5

Container 6

Container 6 was arranged as a duplicate to Container 5. The furniture was identical, and the miscellaneous items such as clothing were arranged in a nearly identical manner.

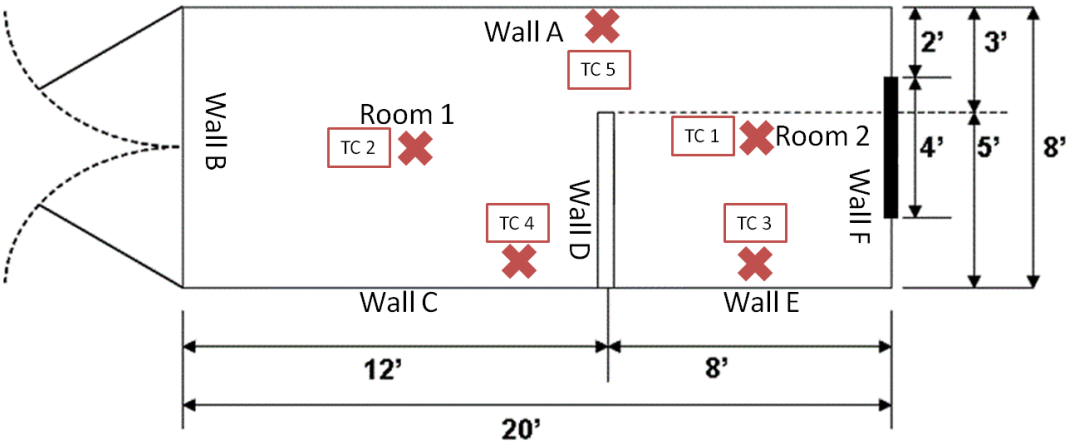

Figure 14: Thermocouple Layout Container 6

Table 3: Thermocouple Locations Container 6

TC	Room	Wall Location Measured From Wall	Height
1	2	A: 45"	Ceiling
2	1	A: 42"	Ceiling
3	2	D: 25"	6"
4	1	D: 41"	12"
5	2	F: 96"	90"

The same ignitable liquid was used, but the volume was reduced to 250 mL. After ignition, the fire did not spread along the ignitable liquid trail to the back room, and so was extinguished. A fresh 500 mL sample of gasoline was poured on a new trail through the container, corresponding to the green line in Figure 15.

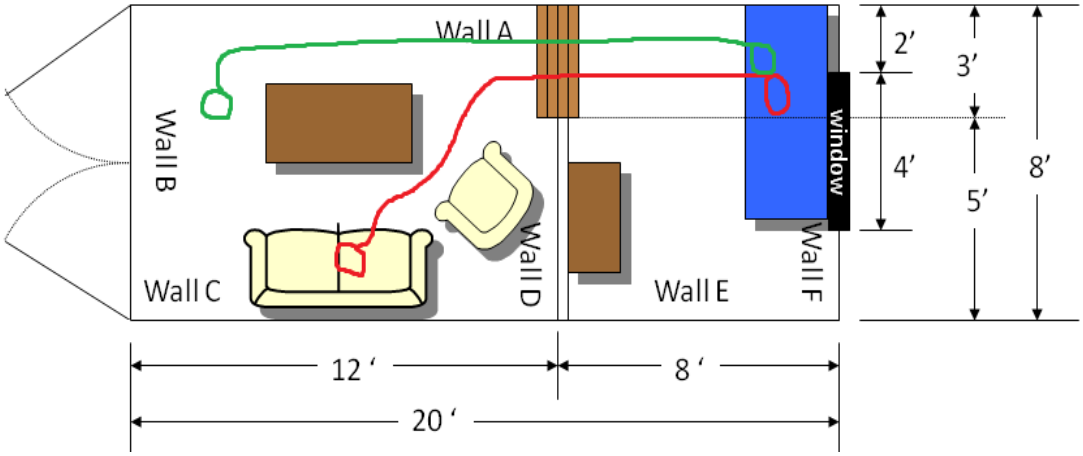

Figure 15: Pour Patterns in Container 6

The container was burned for 5.5 minutes and extinguished with water. After the container had cooled, sample markers were placed at the locations according to Figure 16 and samples were collected into gallon-sized metal cans. The fire debris samples were analyzed using the method previously described.

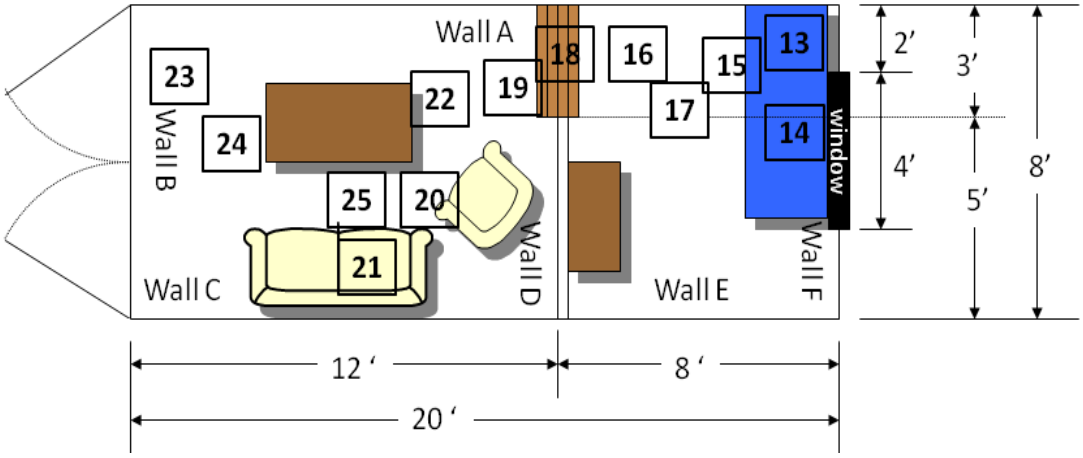

Figure 16: Sample Locations in Container 6

Container 7

For previous experiments, only single ignitable liquid tests had been performed. Container 7 was burned to address the question of whether using multiple ignitable liquids would result in

samples having signatures from each ignitable liquid and if the data analysis method would be able to identify both ignitable liquids as being present in the container. To test this, Container 7 was burned using two individual ignitable liquids, a gasoline and a medium petroleum distillate (MPD). For the TIC and TIS of these ignitable liquids, see Appendix C. The two ignitable liquids were poured in separate trails, see Figure 17, where the purple line corresponds to the trail of gasoline, and the green line corresponds to the trail of the MPD. The volume of each ignitable liquid used was 500 mL.

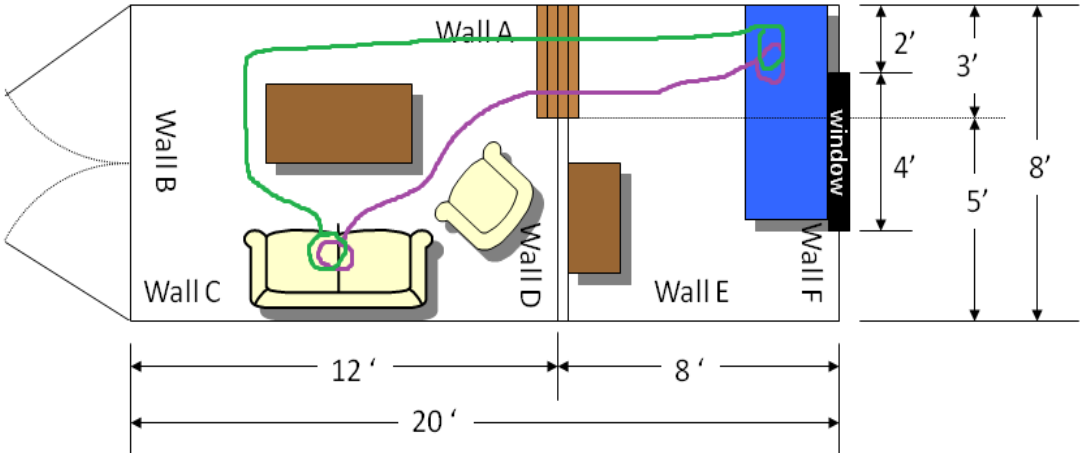

Figure 17: Pour Pattern in Container 7

Both ignitable liquid trails began on the couch in Room 1 and ended on the bed in the back room, Room 2. The ignition point was on the couch and the container was burned for approximately 8 minutes. Temperatures were monitored using thermocouples connected to a computer system to record the temperatures. The thermocouples were placed in the container at the locations as shown in Figure 18 and Table 4.

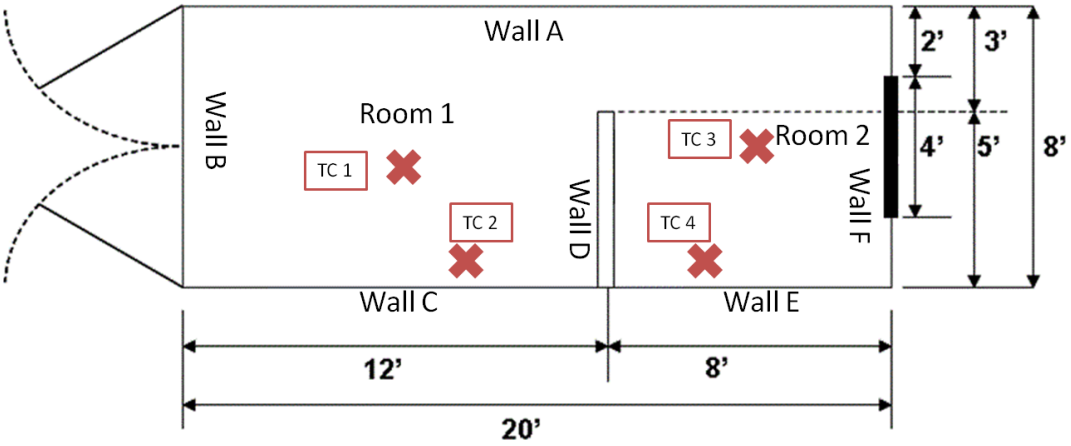

Figure 18: Thermocouple Layout Container 7

Table 4: Thermocouple Locations Container 7

TC	Room	Wall Location Measured From Wall	Height
1	1	C: 43"	Ceiling
2	1	D: 39"	2"
3	2	E: 45"	Ceiling
4	2	D: 36"	8"

Samples were collected along both ignitable liquid trails, see Figure 19, and placed into gallon-sized metal cans and transported to the laboratory at NCFS for analysis based on the previously used method of analysis for samples from past containers.

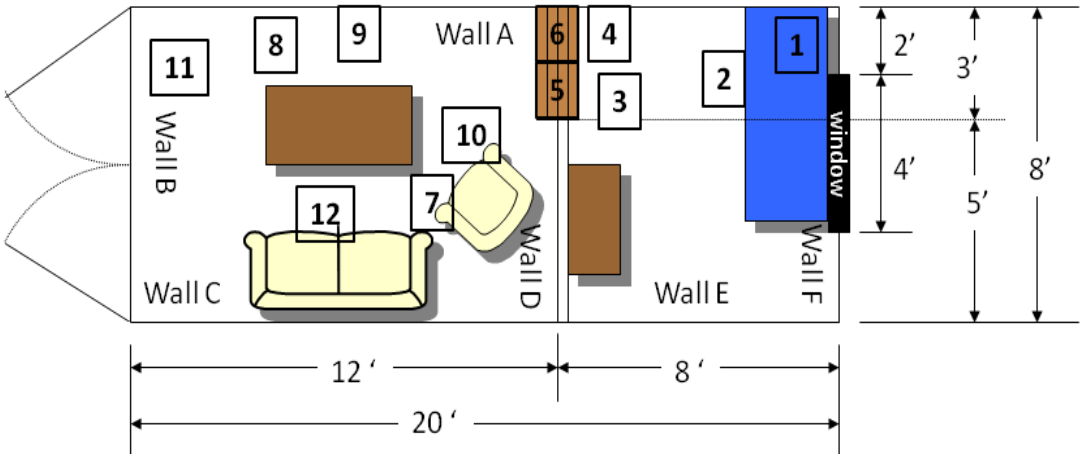

Figure 19: Sample Locations in Container 7

Container 8

Container 8 was set up to replicate the conditions in Container 7 for the same purpose of trying to determine whether the detection and classification model could identify and correctly classify both classes of ignitable liquids present. The same gasoline (purple line in Figure 20) and MPD (green line in Figure 20) were used and the same volumes of ignitable liquids were used, 500 mL of both. The trail began at the couch in Room 1 and ended on the bed in Room 2, with ignition occurring at the couch.

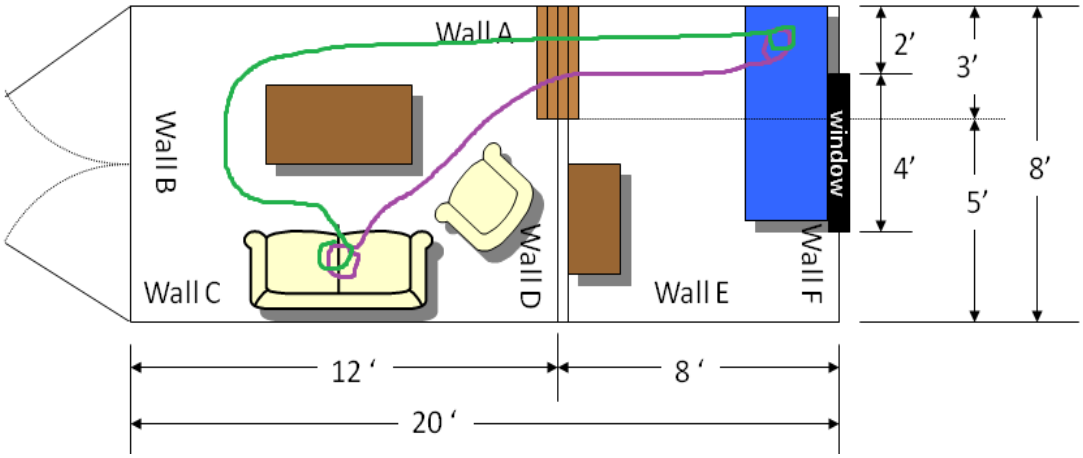

Figure 20: Pour Patterns in Container 8

Thermocouples, arranged according to Figure 21 and Table 5, were connected to a computer to record the temperature data for the duration of the burn. The container was burned for approximately 8 minutes before being extinguished with water.

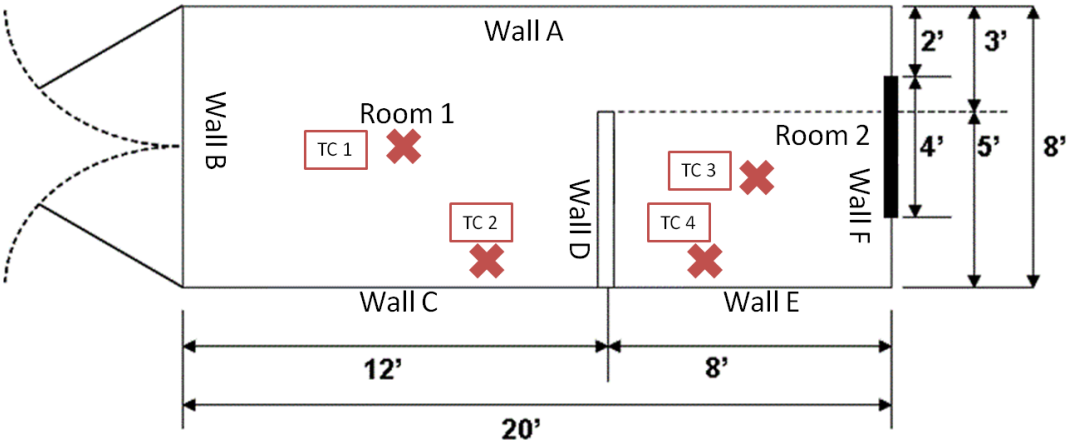

Figure 21: Thermocouple Layout Container 8

Table 5: Thermocouple Locations Container 8

TC	Room	Wall Location Measured From Wall	Height
1	1	C: 45"	Ceiling
2	1	D: 35"	2"
3	2	E: 38"	Ceiling
4	2	D: 34"	8"

Once the container had time to cool, sample identification markers were placed on or near the pour trail to indicate the location of samples to be collected. The samples were then collected and placed into individual metal cans then transported back to the laboratory for testing using the same method used for the sampling and instrumental analysis of samples collected from previous containers.

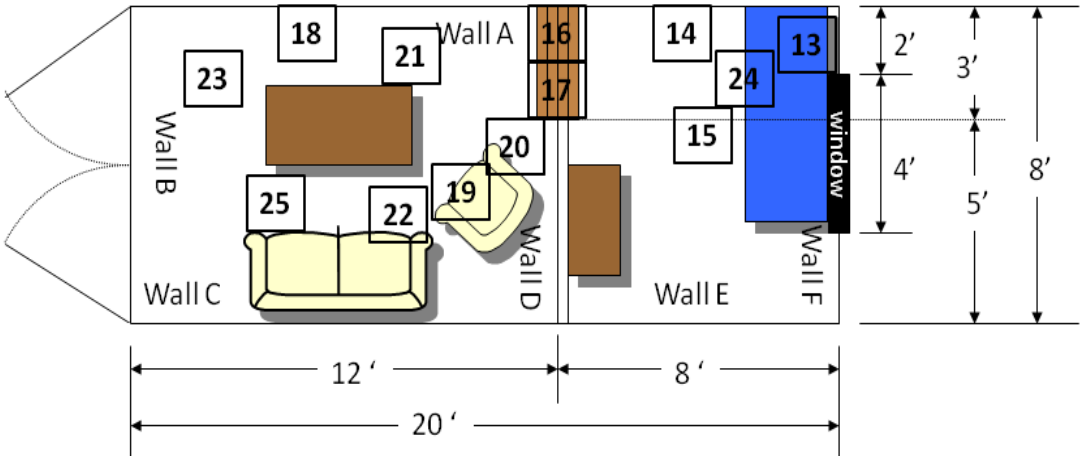

Figure 22: Sample Locations in Container 8

Container 9

Previous containers used a gasoline, a medium petroleum distillate, or a mixture of both as the ignitable liquid. If the remaining containers continued to use gasoline and PD ILs, a classification method that should be applicable to all ASTM IL classes would be based on results from only these 2 classes. Therefore, Containers 9-12 were burned using other ASTM classes of ignitable liquids to determine the accuracy of the classification method established.

Container 9 was furnished with items purchased from a local furniture warehouse, so were identical to those in Containers 10-12. No additional clothing or shoes were placed in the container like previous containers, but magazines were placed on the bed, dresser, chair, couch, coffee table, and inside the trash can. A wood vinyl flooring was used in the back room, and the front room was covered with an olefin carpet and padding. All flooring substrates were purchased from a local home improvement store. In addition, a series of stone tiles were placed in the container, to determine what, if any, would be the ignitable liquid residues retained by the tiles. The tiles were fixed onto pieces of plywood, and then grout was applied. After the grout

had set, one of the two tile pieces was sealed with a tile and grout sealant purchased from a local home improvement store. This was done to replicate the conditions that may be found in a residential fire, since depending on the location and homeowner preference, tile used in the home may or may not be sealed. The tiles were placed in the container so that they would be in the line of the pour pattern, see Figure 23.

Figure 23: Pour Pattern Across Flooring in Container 9

The ignitable liquid used was a 50:50 mixture of gasoline and diesel fuel, a heavy petroleum distillate (HPD). Containers 7 and 8 were burned with two ignitable liquids being present, but they were poured along two separate trails. In Container 9 however, the gasoline and HPD were mixed prior to pouring the ignitable liquids in the containers. Therefore, as seen in Figure 24, the red line is the pour pattern of a 50:50 mixture of Gas:HPD.

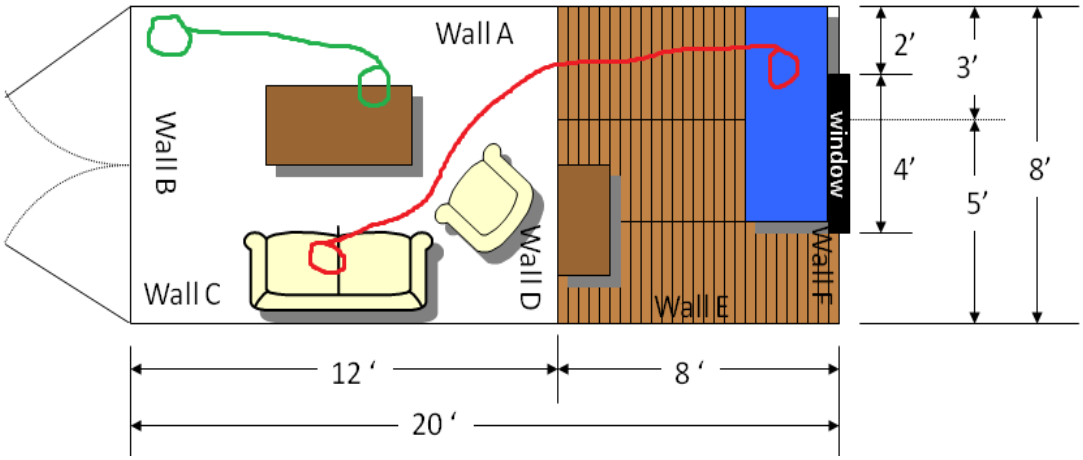

Figure 24: Pour Pattern in Container 9

The green line in Figure 24 shows the trail for an experiment testing the possible sources of contamination at the scene of a fire. The experiment tested the possibility of recovering and identifying from fire debris samples an IL that had been introduced to the scene by walking through an IL then transferring it to the carpet. To test this, new athletic shoes were worn while walking through the front room of the container after being exposed to fresh gasoline poured into a disposable aluminum pan, see Figure 25 and Figure 26. The shoes were then removed at the end of the coffee table in the front room and left in the container for the remainder of the burn.

Figure 25: Gasoline Contamination Experiment 1

Figure 26: Gasoline Contamination Experiment 2

Thermocouples were placed in the locations according to Figure 27 and Table 6 and connected to a computer to monitor and record temperatures throughout the container for the duration of the burn, approximately 6 minutes.

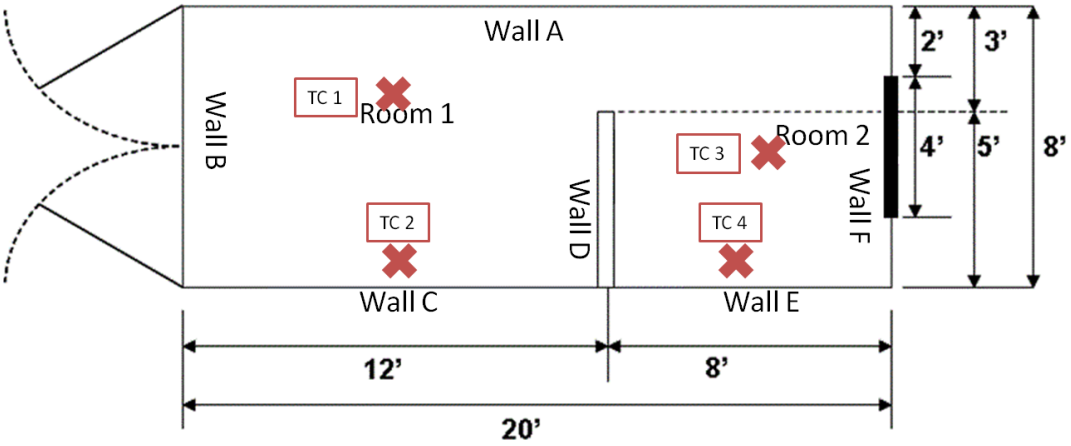

Figure 27: Thermocouple Layout Container 9

Table 6: Thermocouple Locations Container 9

TC	Room	Wall Location Measured From Wall	Height
1	1	A: 36"	Ceiling
2	1	D: 68"	42"
3	2	E: 38"	Ceiling
4	2	D: 42"	45"

After the fire was extinguished, the container was cooled and samples were collected from the approximate locations as seen in Figure 28. The samples were placed into individual gallon-sized metal cans and transported back to the laboratory at the National Center for Forensic Science (NCFS). Analysis of the fire debris samples was performed the same as previous burns.

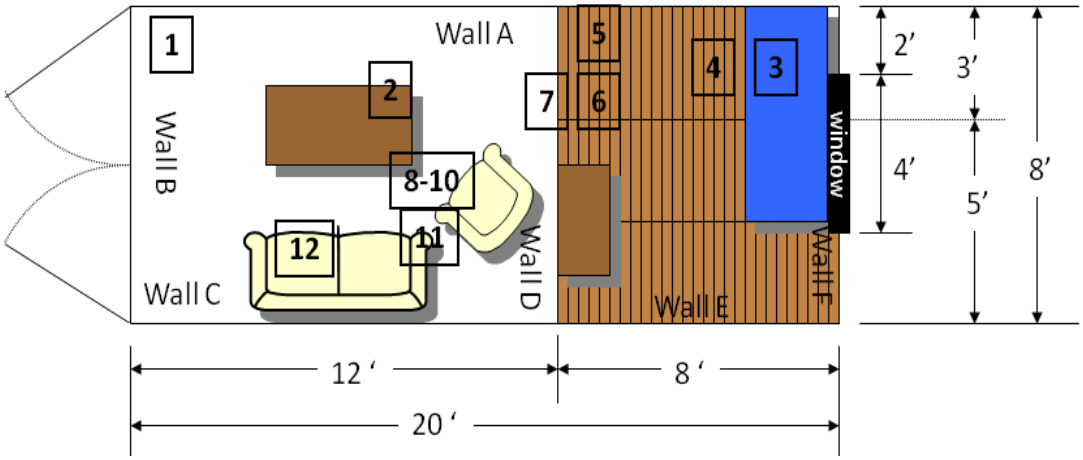

Figure 28: Sample Locations in Container 9

Container 10

Container 10 was furnished with items purchased from a local furniture warehouse store. The furnishings were identical to those used in Container 9 and arranged in approximately the same manner, as shown in Figure 29. Magazines were added throughout the container to increase the fuel load, and were placed on the bed, dresser, chair, couch, coffee table, and inside the trash can. Wood vinyl flooring was used in the back room, and the front room was covered with an olefin carpet with the same padding used in previous containers. All flooring substrates were purchased from a local home improvement store. In addition, a series of stone tiles were placed in the container along the pour pattern (red line in Figure 29) for the same purpose as in Container 9.

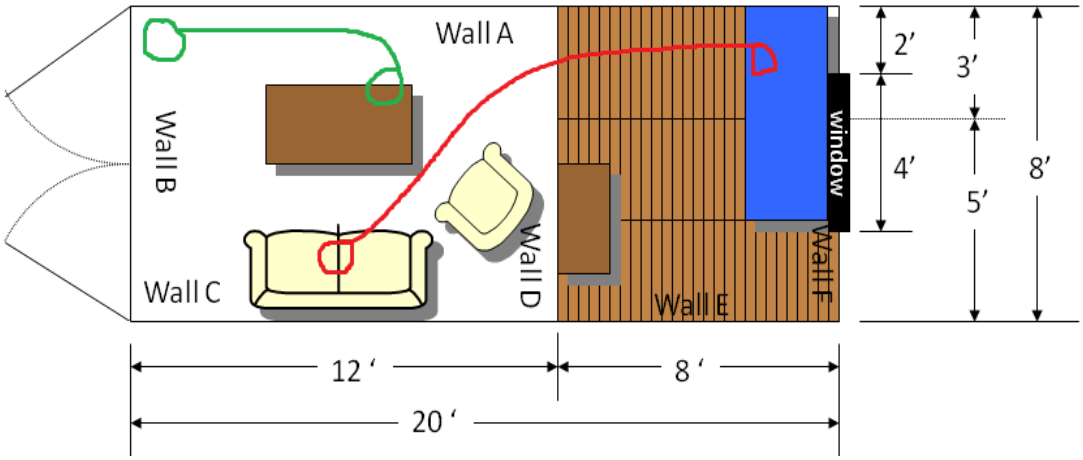

Figure 29: Pour Pattern in Container 10

The ignitable liquid used in Container 10 was 500 mL of a camp fuel classified as a light petroleum distillate (LPD) purchased from a local home improvement store. The LPD was trailed starting at the bed and ending on the couch, along the path of the red line in Figure 29. The green line in Figure 29 shows the trail of the gasoline-covered athletic shoes. The same process used in Container 9 was repeated: new athletic shoes were worn while walking through the front room of the container after being exposed to fresh gasoline poured into a disposable aluminum pan, see Figure 25 and Figure 26 from Container 9. The shoes were then removed at the end of the coffee table in the front room and left in the container during the burn.

Thermocouples were used to monitor and record the temperatures in both rooms of the container. The thermocouples were placed throughout the container according to Figure 30 and Table 7 and were connected to a computer to record the temperatures.

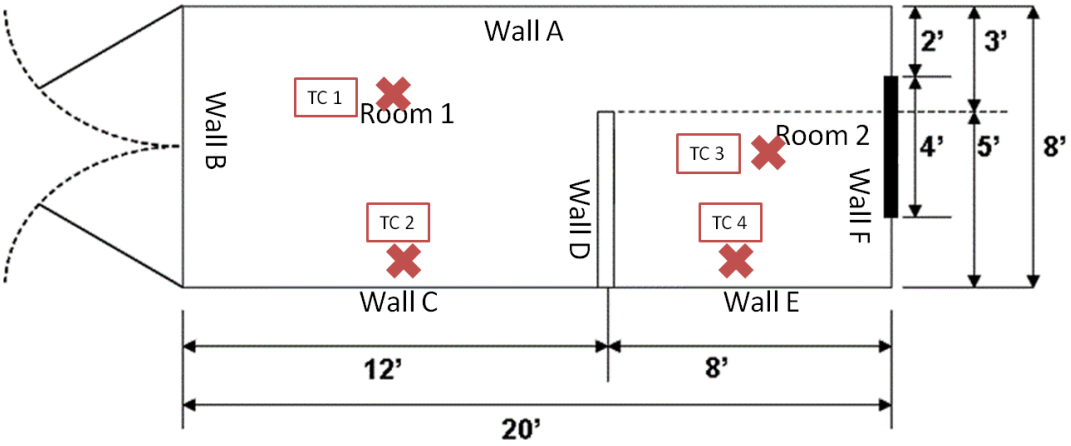

Figure 30: Thermocouple Layout Container 10

Table 7: Thermocouple Locations Container 10

TC	Room	Wall Location Measured From Wall	Height
1	1	A: 35"	Ceiling
2	1	D: 64"	49"
3	2	E: 40"	Ceiling
4	2	D: 42"	48"

The container burned for approximately 6 minutes. After the fire was extinguished, the container was cooled and samples were collected from the approximate locations as seen in Figure 31. Once the samples were collected from the container, they were placed into individual gallon-sized metal cans and sealed with a lid. The samples were then analyzed using the previously described method identical to past burns.

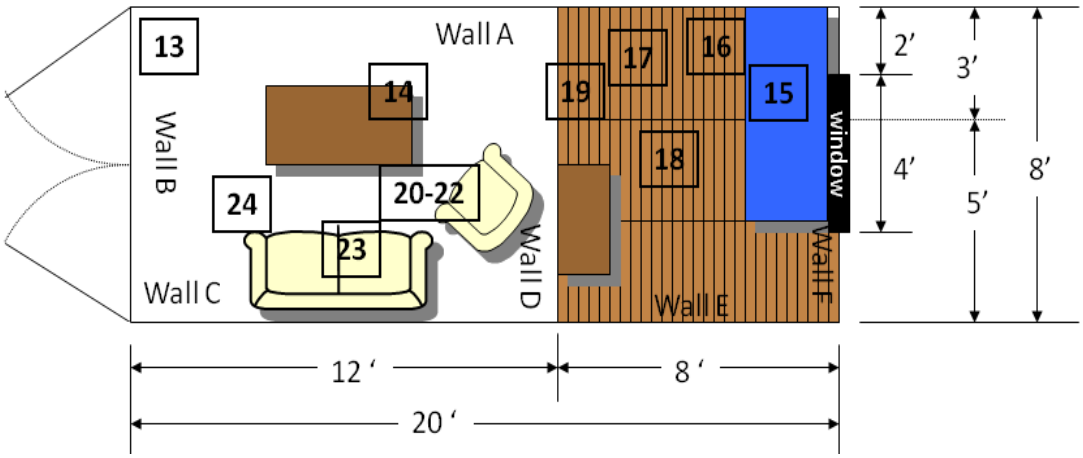

Figure 31: Sample Locations in Container 10

Container 11

Container 11 was furnished with items purchased from a local furniture warehouse store. The furnishings were identical to those used in the two previous containers and arranged in approximately the same way for consistency. Magazines were added throughout the container to increase the fuel load, and were placed on the bed, dresser, chair, couch, coffee table, and inside the trash can. The flooring in the back room was wood vinyl flooring, and the front room was covered with an olefin carpet and padding, all of which were purchased from a local home improvement store. In addition, a series of stone tiles were placed in the container along the pour pattern (red line in Figure 32) for the same purpose as in Container 9 and Container 10. This was done to replicate the conditions that may be found in a residential fire.

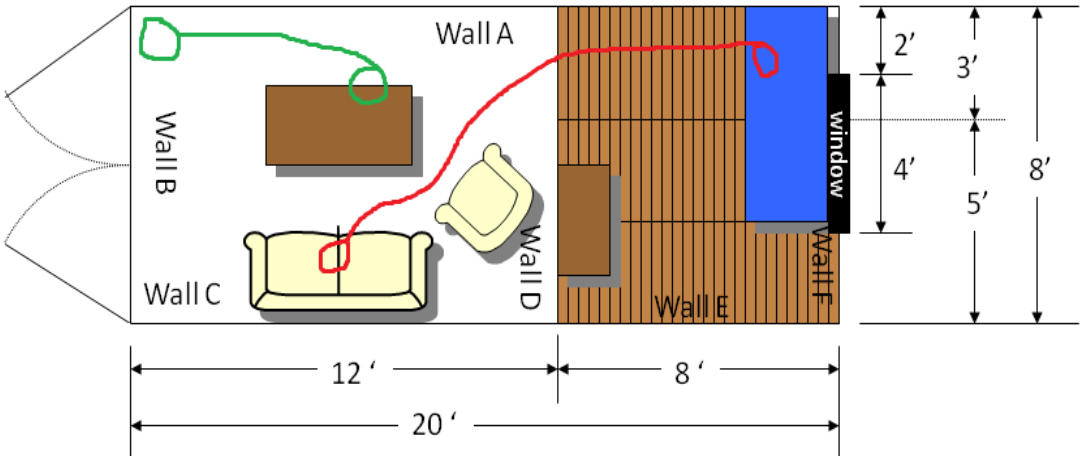

Figure 32: Pour Pattern in Container 11

The ignitable liquid used in Container 11 was 500 mL of a torch fuel classified as a naphthenic-paraffinic product (NP). The NP was trailed starting at the bed and ending on the couch, along the path of the red line in Figure 32. The green line in Figure 32 shows the trail of the gasoline-covered athletic shoes. The same process used in Container 9 and Container 10 was repeated, new athletic shoes were worn while walking through the front room of the container after the soles were covered in fresh gasoline that had been poured into a disposable aluminum pan, see Figure 25. The shoes were then removed at the end of the coffee table in the front room and left in the container during the burn, see Figure 26.

Thermocouples were used to monitor and record the temperatures in both rooms of the container and recorded by a computer. The thermocouples were placed throughout the container according to Figure 33 and Table 8, similar in location to previous containers.

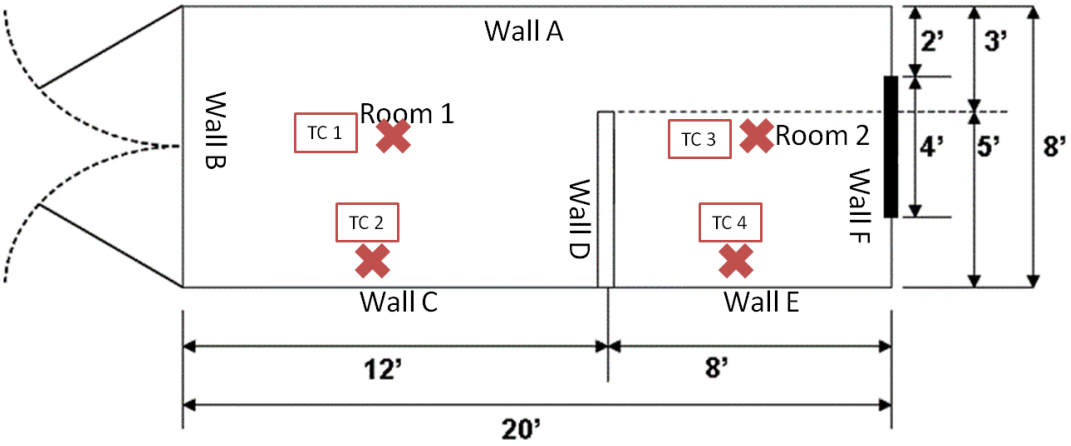

Figure 33: Thermocouple Layout Container 11

Table 8: Thermocouple Locations Container 11

TC	Room	Wall Location Measured From Wall	Height
1	1	A: 41"	Ceiling
2	1	D: 68"	50"
3	2	E: 45"	Ceiling
4	2	D: 45"	54"

The burn was initiated at the couch and the container was burned for approximately 6 minutes. After the fire was extinguished and the container cooled, samples were collected at the approximate locations as seen in Figure 34. The samples were placed into individual gallon-sized metal cans and transported back to the laboratory at the National Center for Forensic Science. Samples were analyzed using the previously described method of volatile extraction and analysis.

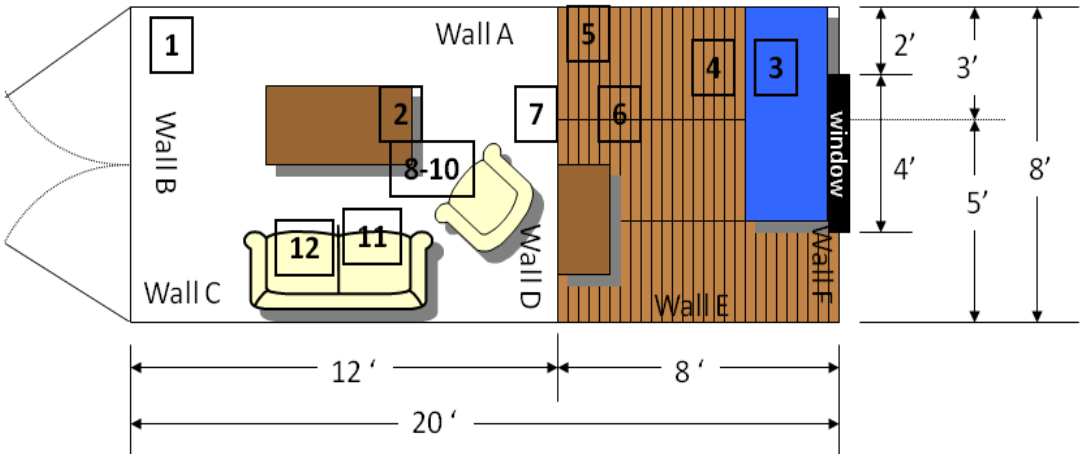

Figure 34: Sample Locations in Container 11

Container 12

Container 12 was furnished with items purchased from a local furniture warehouse store identical to those in Container 9, Container 10, and Container 11 and arranged in approximately the same manner. The magazines added throughout the container to increase the fuel load were placed on the bed, dresser, chair, couch, coffee table, and inside the trash can. The two types of flooring used were identical to the previous three containers, which consisted of wood vinyl flooring in the back room and olefin carpet with padding in the front room. All flooring substrates were purchased from a local home improvement store. As in the previous three containers, two sets of stone tiles were placed in the container along the pour pattern indicated by the red line in Figure 35.

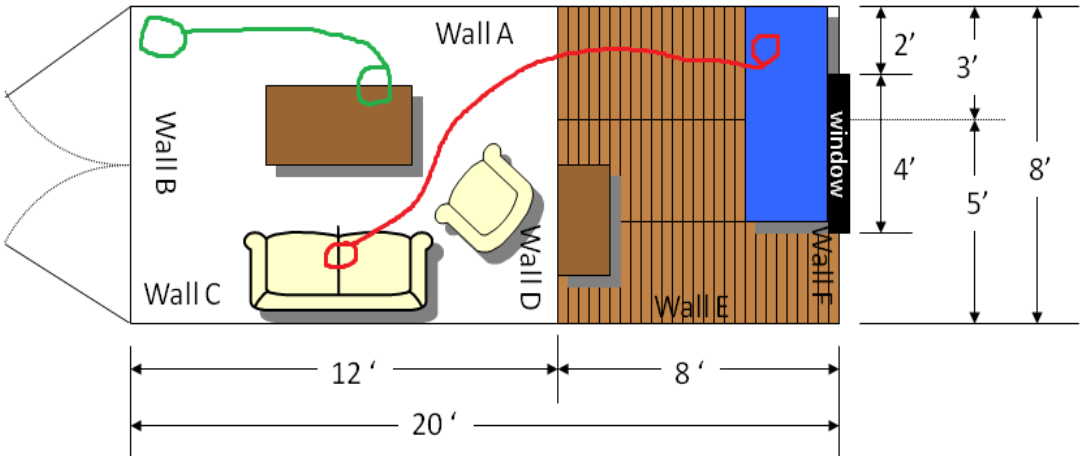

Figure 35: Pour Pattern in Container 12

The ignitable liquid used in Container 12 was 500 mL of a charcoal starter fluid classified as an isoparaffinic product (ISO) purchased from a local home improvement store. The ISO was trailed starting at the bed and ending on the couch, see red-line trail in Figure 35. The green line shows the trail of the gasoline-covered athletic shoes. As done in the previous three containers, the soles of a new pair of athletic shoes were covered in gasoline then worn while walking through the front room of the container, see Figure 25. The shoes were then removed at the end of the coffee table in the front room and left in the container during the burn, see Figure 26.

Thermocouples placed according to Figure 36 and Table 9 were used to monitor the temperatures in both rooms of the container. The thermocouples were connected to a computer to record the temperatures in order to graph the temperatures.

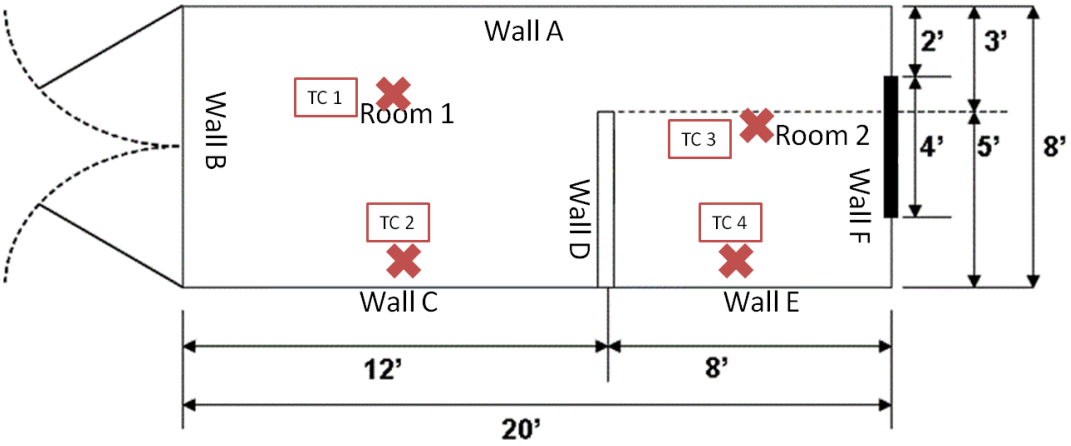

Figure 36: Thermocouple Layout Container 12

Table 9: Thermocouple Locations Container 12

TC	Room	Wall Location Measured From Wall	Height
1	1	A: 36"	Ceiling
2	1	D: 60"	55"
3	2	E: 52"	Ceiling
4	2	D: 44"	52"

The container burned for approximately 10 minutes before being extinguished. The container then cooled and samples were collected from the approximate locations seen in Figure 37. The samples were placed into individual gallon-sized metal cans and transported back to the laboratory at the National Center for Forensic Science for analysis using the same method as previous burns.

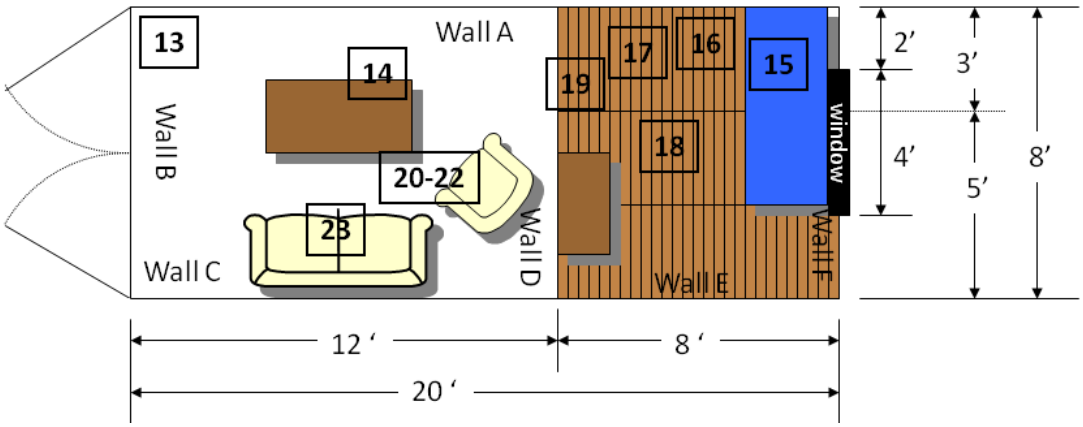

Figure 37: Sample Locations in Container 12

Laboratory Burn Method

Laboratory analysis of fire debris samples was based on a method developed by the State of Florida Bureau of Forensic Fire and Explosive Analysis.[28] For test samples burned in the laboratory, approximately 4.0 grams of the sample material was placed into an unlined pint-sized metal can with a compression seal. Because the can would be heated from the bottom, samples were positioned so that the top of the substrate (the part that would be exposed in an actual fire) was facing the bottom of the can. By doing this, the samples were in same orientation with respect to the heat source in both the laboratory burn and in a fire. The ignitable liquid was added to the sample substrate and a vented lid with a series of 7 puncture holes was placed on top. The can was then placed on a ring stand assembly approximately 4.0 cm above a propane torch. The propane torch was ignited, and the can was heated from the bottom for two minutes after the presence of smoke was observed from the vented lid. After two minutes, the propane torch was turned off and the sample was removed from the ring stand. The vented lid was then replaced with a solid lid to prevent any vapors from the sample substrate and/or the ignitable liquid escaping.

Once the can cooled, any ILRs present were extracted using passive headspace sampling based on the ASTM E1412 guideline. The lid was removed and an ACS was suspended in the headspace of the sample. The lid was then replaced to seal the ACS inside the can, and the can was placed into an oven set at 66°C for 16-18 hours to adsorb any volatiles from the sample onto the charcoal strip. After the 16-18 hour heating period, the can was removed from the oven and the ACS was divided in half. One half was placed in a glass autosampler vial to be retained for archiving purposes, and the other half was placed into a glass autosampler vial with 1.0 mL of CS_2 to desorb the volatile components on the charcoal strip into the solvent. The autosampler vials were then sealed using an autosampler cap with a Teflon septum. The vial used for analysis containing the ACS in CS_2 was then placed on the autosampler tray of the GC-MS.

Instrumental Parameters

For sample analysis, an Agilent 6890 Gas Chromatograph coupled to an Agilent 5973 Mass Spectrometer was used. The injector of the gas chromatograph was run in split mode with a 50:1 split ratio at 250°C. The GC oven temperature was initially set to 50°C for 3 minutes, then increased to 280°C at a rate of 10°C/min and held at 280°C for 4 minutes. The GC column used was a methyl-siloxane HP-1 column having the following dimensions: 0.2 mm internal diameter, 25 m length, and 0.5µm film thickness. The transfer line between the GC and MS was set to 280°C and the source temperature was 230°C. The mass analyzer scanned the mass range from 30-350 at a rate of 2-3 scans/second after a 2 minute solvent delay.[28]

Statistical Analysis

The 3-dimensional data produced by GC-MS analysis was converted into a total ion spectrum as mentioned previously in the New Methods for Data Analysis section of Chapter 1. The total ion spectrum of each sample was combined into a composite data set for each container. The multiple TIS that made up a container data set were then analyzed by principal components analysis and target factor analysis to determine correlation values between the data set as a whole and individual ignitable liquids in a reference library maintained by the National Center for Forensic Science.

Statistical analysis was performed using the software package MATLAB. A program code similar to the computer model simulation code was written to perform a singular value decomposition of the entire data set of the TIS from the fire debris samples, and then PCA was preformed prior to TFA. The correlation values obtained from TFA between the data set and each of the ignitable liquids in the reference library were sorted in decreasing order. The correlation values and ASTM IL class were then used in the statistical program R, which calculated the median, average, standard deviation and posterior probabilities by the kernel density function of the correlation values for each of the ignitable liquid classes: Aromatics (subclassified into light, medium and heavy), Gasoline, Isoparaffinic Products, Naphthenic-Paraffinic Products, Normal Alkanes, Oxygenated Solvents, Petroleum Distillates (subclassified into light, medium and heavy), and Miscellaneous. Posterior probabilities for classes with a value of $\frac{\|1-\text{median}(x_i)\|}{\text{MAD}}$ that was greater than 5 were not calculated and the corresponding classes were eliminated as possible classes when determining the ignitable liquid class present in the

sample. Only classes with a value of $\frac{\|1-\text{median}(x_i)\|}{\text{MAD}}$ that was less than 5 had the posterior probability calculated. When determining the posterior probabilities, a value of 1/n (n=number of total classes) was used as the prior probability for each class and the probability density function for each class was estimated by the kernel distribution method. The class with the highest posterior probability was assigned as the correct class. This was the basis for the classification method established based on previous laboratory burns and large scale burns. Previous data sets were then used to evaluate the classification method and determine the classification method's accuracy.

CHAPTER 3
RESULTS

Computer Simulation Models

Each class was tested using a program written in house for the statistical analysis of computer generated TIS data sets using TFA to calculate correlation values that were used in a Bayesian analysis to calculate posterior probabilities. The series of trials varied the percentage of IL contribution per TIS, and the total number of spectra with an IL contribution. Each class (AR, Gas, HPD, MPD LPD, ISO, NAL, NP, OXY and MISC) was tested across a range of IL contribution from 0-95% for samples ranging from 1-11 of the 12 total TIS. The resulting identification of the class was assigned a 0 value if the classification method incorrectly identified the class of ignitable liquid used, and a value of 1 was assigned for correct classifications. The classification tables for each class are presented below. The posterior probabilities of the correctly identified class of IL present have also been graphed for each class, with a color scale ranging from red to blue for correct to incorrect classifications, respectively.

Table 10: AR Classification Matrix

% IL Contribution	Number of Spectra with IL Contribution										
	1	**2**	**3**	**4**	**5**	**6**	**7**	**8**	**9**	**10**	**11**
0	0	0	0	0	0	0	0	0	0	0	0
5	0	0	0	0	0	0	0	0	0	0	0
10	0	0	0	0	0	0	0	0	0	0	0
15	0	0	0	0	0	0	0	0	0	0	0
20	0	0	0	0	0	0	0	0	0	0	0
25	0	0	0	0	0	0	0	0	0	0	0
30	0	0	0	0	0	0	0	0	0	0	0
35	0	0	0	0	0	0	0	0	0	0	0
40	0	0	0	0	0	0	0	0	0	0	0
45	0	0	0	0	0	0	0	0	0	0	0
50	0	0	0	0	0	0	0	0	0	0	0
55	0	0	0	0	0	0	0	0	0	0	0
60	0	0	0	0	0	0	0	0	0	0	0
65	0	0	0	0	0	0	0	0	0	0	0
70	0	0	0	0	0	0	0	0	0	0	0
75	0	0	0	0	0	0	0	0	0	0	0
80	0	0	0	0	0	0	0	0	0	0	1
85	0	0	0	0	0	0	0	0	0	1	1
90	0	0	0	0	0	0	0	0	0	0	1
95	0	0	0	0	0	0	0	1	1	1	1

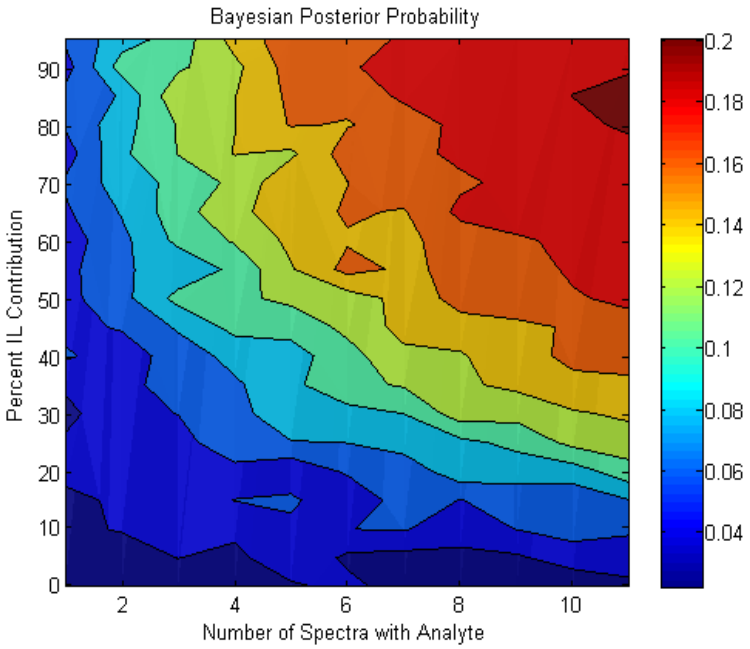

Figure 38: AR Bayesian Probability Plot

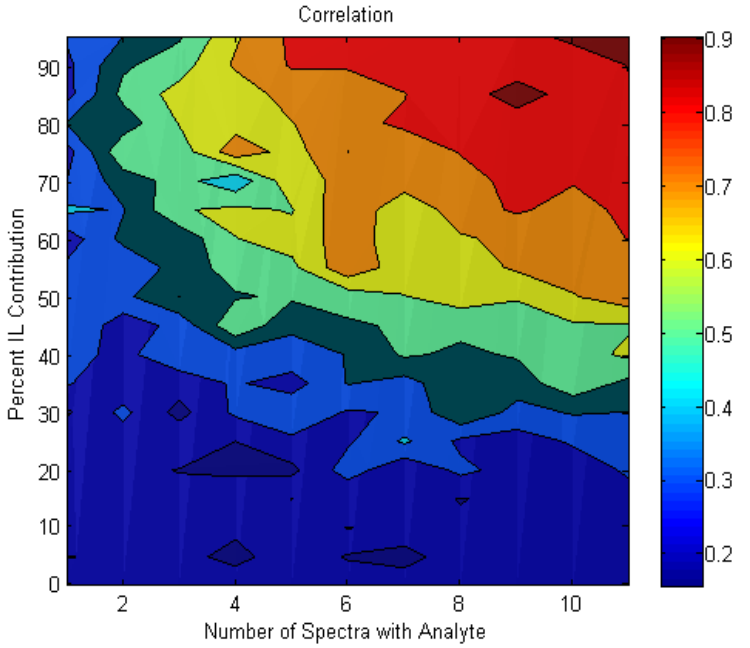

Figure 39: AR Correlation Value Plot

Table 11: Gas Classification Matrix

% IL Contribution	Number of Spectra with IL Contribution										
	1	**2**	**3**	**4**	**5**	**6**	**7**	**8**	**9**	**10**	**11**
0	0	0	0	0	0	1	0	0	0	0	0
5	0	0	1	0	1	0	0	0	1	1	1
10	0	1	1	1	1	1	1	1	1	1	1
15	0	1	1	1	1	0	1	1	1	1	1
20	1	1	0	1	1	1	1	1	1	1	1
25	0	1	1	1	1	1	1	1	1	1	1
30	0	1	1	1	1	1	1	1	1	1	1
35	1	1	1	1	1	1	1	1	1	1	1
40	1	1	1	1	1	1	1	1	1	1	1
45	1	0	1	1	1	1	1	1	1	1	1
50	1	1	1	1	1	1	1	1	1	1	1
55	1	1	1	1	1	1	1	1	1	1	1
60	1	1	1	1	1	1	1	1	1	1	1
65	1	1	1	1	1	1	1	1	1	1	1
70	1	1	1	1	1	1	1	1	1	1	1
75	1	1	1	1	1	1	1	1	1	1	1
80	1	1	1	1	1	1	1	1	1	1	1
85	1	1	1	1	1	1	1	1	1	1	1
90	1	1	1	1	1	1	1	1	1	1	1
95	1	1	1	1	1	1	1	1	1	1	1

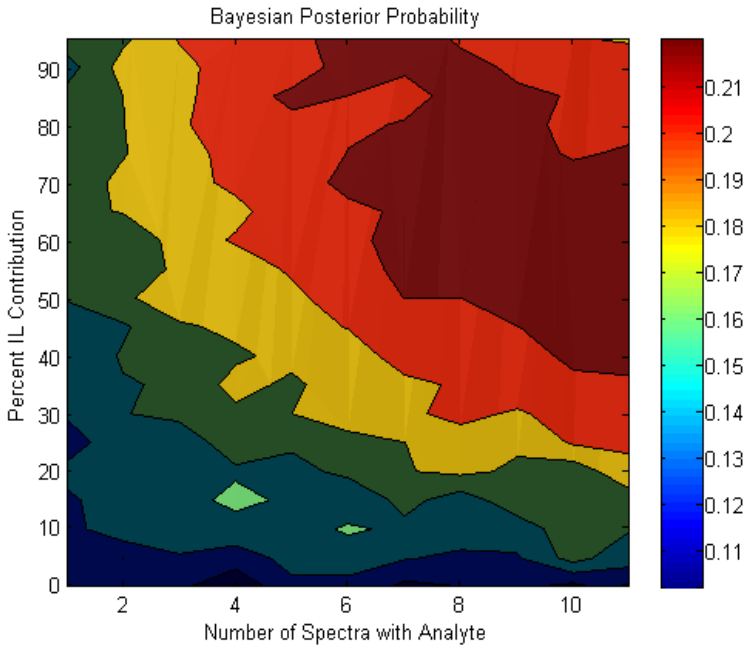

Figure 40: Gas Bayesian Probability Plot

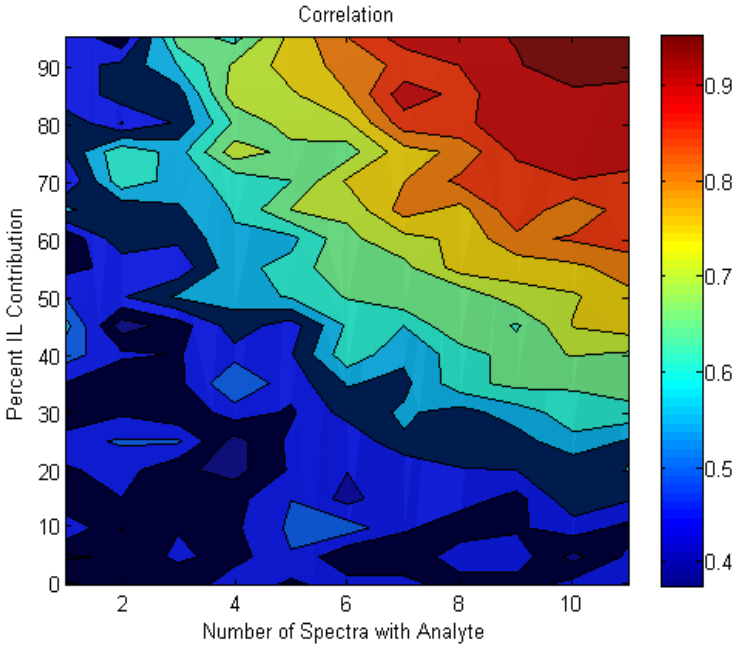

Figure 41: Gas Correlation Value Plot

Table 12: HPD Classification Matrix

% IL Contribution	Number of Spectra with IL Contribution										
	1	**2**	**3**	**4**	**5**	**6**	**7**	**8**	**9**	**10**	**11**
0	0	0	0	0	0	0	0	0	0	0	0
5	0	0	0	0	0	0	0	0	0	0	0
10	0	0	0	0	0	0	0	1	0	0	0
15	0	0	0	1	0	0	0	0	0	0	0
20	0	1	0	0	0	0	0	1	0	1	1
25	0	0	1	1	0	1	1	1	0	1	0
30	0	0	0	1	0	1	0	0	1	1	1
35	0	0	1	0	1	1	1	1	1	1	1
40	1	0	0	0	1	1	1	1	1	1	1
45	0	1	0	1	1	1	1	1	1	1	1
50	0	1	1	1	1	1	1	1	1	1	1
55	0	1	1	1	1	1	1	1	1	1	1
60	0	1	1	1	1	1	1	1	1	1	1
65	0	0	1	1	1	1	1	1	1	1	1
70	0	1	1	1	1	1	1	1	1	1	1
75	1	1	1	1	1	1	1	1	1	1	1
80	1	1	1	1	1	1	1	1	1	1	1
85	0	1	1	1	1	1	1	1	1	1	1
90	1	1	1	1	1	1	1	1	1	1	1
95	1	1	1	1	1	1	1	1	1	1	1

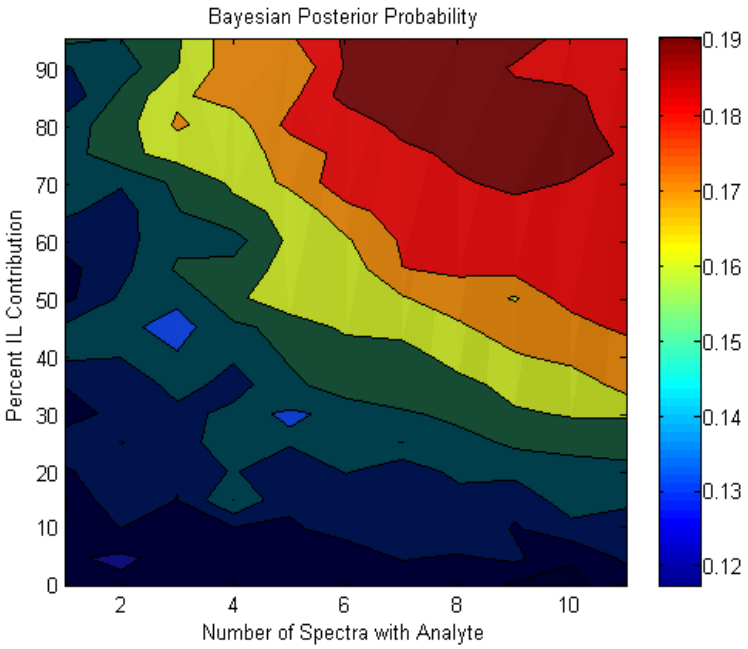

Figure 42: HPD Bayesian Probability Plot

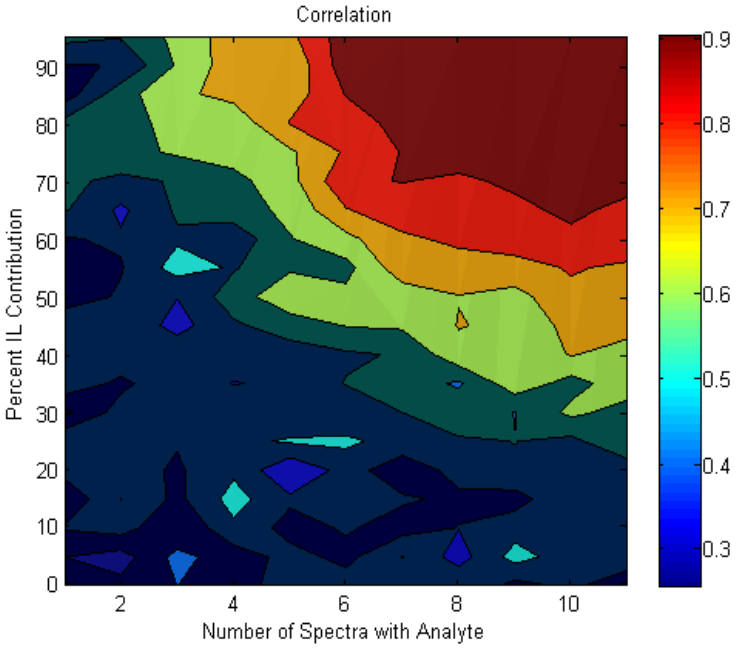

Figure 43: HPD Correlation Value Plot

Table 13: MPD Classification Matrix

% IL Contribution	Number of Spectra with IL Contribution										
	1	**2**	**3**	**4**	**5**	**6**	**7**	**8**	**9**	**10**	**11**
0	1	0	0	1	0	0	1	0	0	1	0
5	0	1	1	0	0	0	0	1	1	0	1
10	1	0	0	1	1	1	1	0	0	1	1
15	1	1	1	1	1	0	1	1	1	1	1
20	1	1	1	0	1	1	1	1	1	1	1
25	1	1	1	0	1	1	1	1	1	1	1
30	0	1	1	1	1	1	1	1	1	1	1
35	1	1	1	1	1	1	1	1	1	1	1
40	1	1	1	1	1	1	1	1	1	1	1
45	1	1	1	1	1	1	1	1	1	1	1
50	1	1	1	1	1	1	1	1	1	1	1
55	1	1	1	1	1	1	1	1	1	1	1
60	0	1	1	1	1	1	1	1	1	1	1
65	1	1	1	1	1	1	1	1	1	1	1
70	1	1	1	1	1	1	1	1	1	1	1
75	1	1	1	1	1	1	1	1	1	1	1
80	1	1	1	1	1	1	1	1	1	1	1
85	1	1	1	1	1	1	1	1	1	1	1
90	1	1	1	1	1	1	1	1	1	1	1
95	1	1	1	1	1	1	1	1	1	1	1

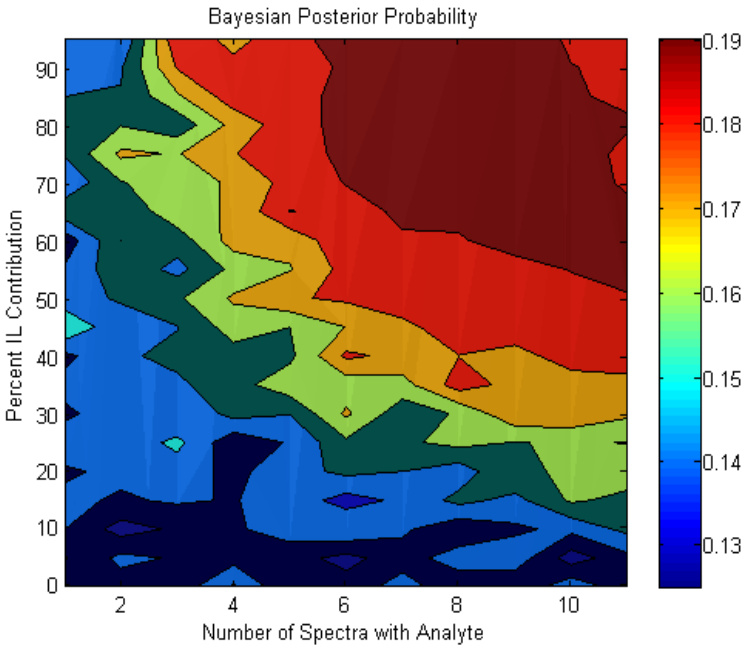

Figure 44: MPD Bayesian Probability Plot

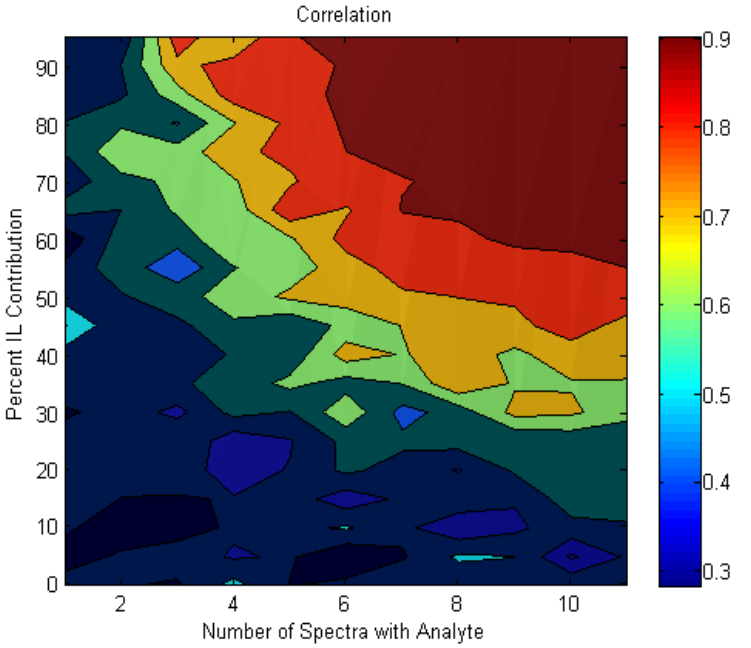

Figure 45: MPD Correlation Value Plot

Table 14: LPD Classification Matrix

% IL Contribution	Number of Spectra with IL Contribution										
	1	**2**	**3**	**4**	**5**	**6**	**7**	**8**	**9**	**10**	**11**
0	0	0	0	0	0	0	0	0	0	0	0
5	0	0	0	0	0	0	0	0	0	0	0
10	0	0	0	0	0	0	0	0	0	0	0
15	0	0	0	0	0	0	0	0	1	0	0
20	0	0	1	0	0	1	0	0	0	0	0
25	0	0	0	0	0	0	0	0	1	0	1
30	0	0	0	0	0	0	0	1	0	1	1
35	0	0	0	0	1	1	1	1	0	1	1
40	0	0	0	0	1	0	1	1	1	1	1
45	0	1	0	1	1	1	1	0	1	1	1
50	0	0	1	1	1	1	1	1	1	1	1
55	0	1	0	1	1	1	1	1	1	1	1
60	0	0	1	1	1	1	1	1	1	1	1
65	0	0	1	1	1	1	1	1	1	1	1
70	0	1	1	1	1	1	1	1	1	1	1
75	0	1	1	1	1	1	1	1	1	1	1
80	1	0	1	1	1	1	1	1	1	1	1
85	0	1	1	1	1	1	1	1	1	1	1
90	0	1	1	1	1	1	1	1	1	1	1
95	0	1	1	1	1	1	1	1	1	1	1

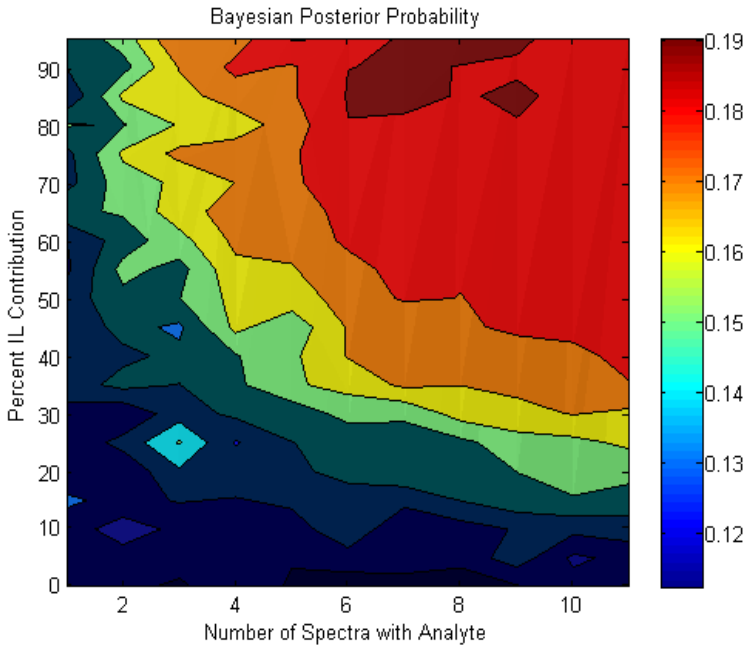

Figure 46: LPD Bayesian Probability Plot

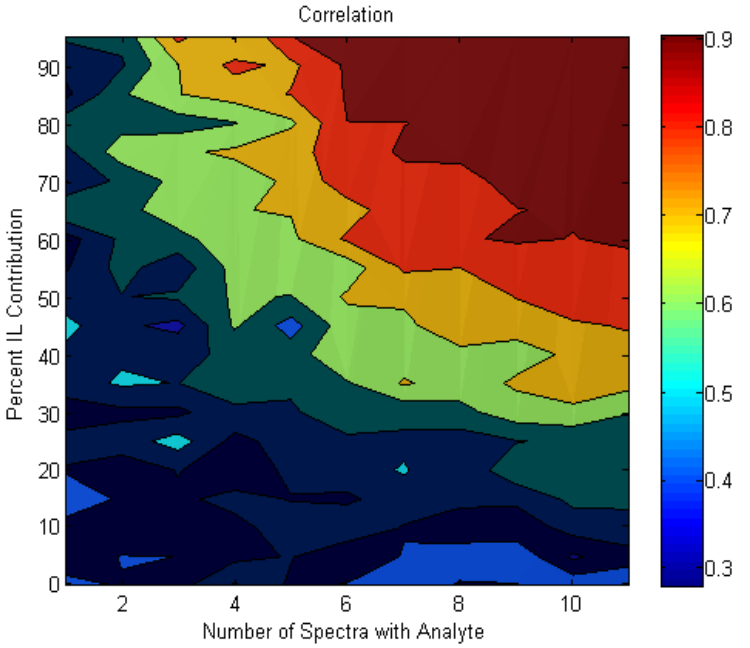

Figure 47: LPD Correlation Value Plot

Table 15: ISO Classification Matrix

% IL Contribution	Number of Spectra with IL Contribution										
	1	2	3	4	5	6	7	8	9	10	11
0	0	0	0	0	0	0	0	0	0	0	0
5	0	0	0	0	0	0	0	0	0	0	0
10	0	0	0	0	0	0	0	0	0	0	0
15	0	0	0	0	0	0	0	0	0	0	0
20	0	0	0	0	0	0	0	0	0	0	0
25	0	0	0	0	0	0	0	0	0	0	0
30	0	0	0	0	0	0	0	0	0	0	0
35	0	0	0	0	0	0	0	0	0	1	1
40	0	0	0	0	0	0	0	1	1	1	1
45	0	0	0	0	0	1	1	0	1	1	1
50	0	0	0	0	0	0	1	1	1	1	1
55	0	0	0	0	1	0	1	1	1	1	1
60	0	0	0	1	0	1	1	1	1	1	1
65	0	0	0	0	0	1	1	1	1	1	1
70	0	0	1	0	1	1	1	1	1	1	1
75	0	1	1	0	1	1	1	1	1	1	1
80	0	0	1	0	1	1	1	1	1	1	1
85	0	0	1	1	1	1	1	1	1	1	1
90	0	0	1	1	1	1	1	1	1	1	1
95	0	1	1	1	1	1	1	1	1	1	1

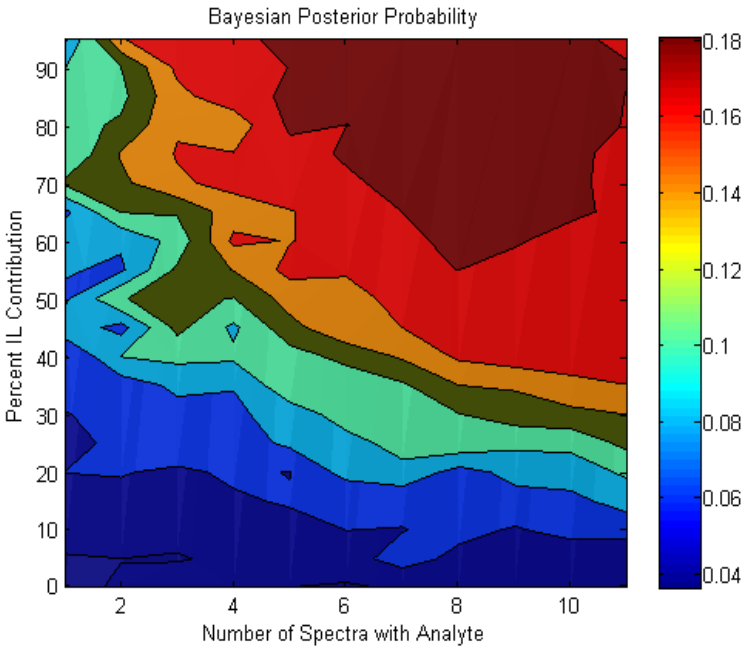

Figure 48: ISO Bayesian Probability Plot

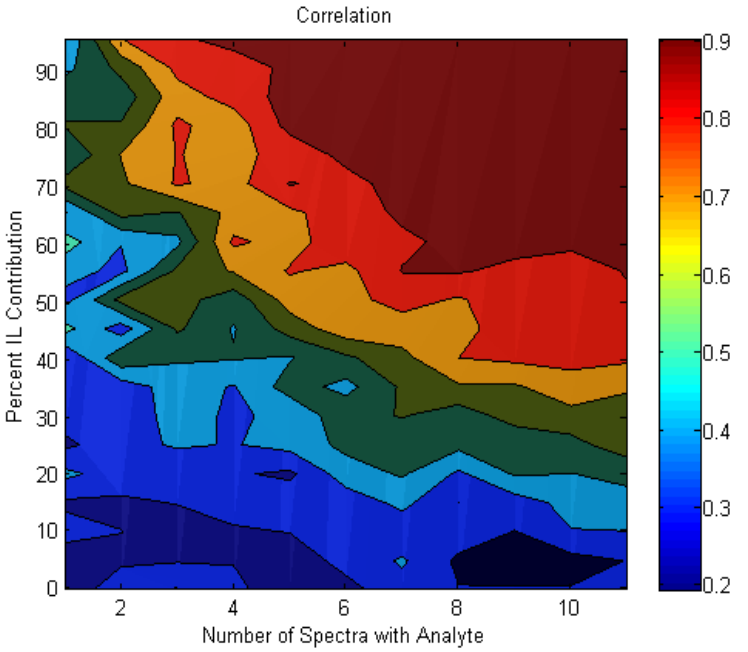

Figure 49: ISO Correlation Value Plot

Table 16: NAL Classification Matrix

% IL Contribution	Number of Spectra with IL Contribution										
	1	**2**	**3**	**4**	**5**	**6**	**7**	**8**	**9**	**10**	**11**
0	0	0	0	0	0	0	0	0	0	0	0
5	0	0	0	0	0	0	0	0	0	0	0
10	0	0	0	0	0	0	0	0	0	0	0
15	0	0	0	0	0	0	0	0	0	0	0
20	0	0	0	0	0	0	0	0	0	0	0
25	0	0	0	0	0	0	0	0	0	0	0
30	0	0	0	0	0	0	0	0	1	0	1
35	0	0	0	0	0	0	1	1	1	1	1
40	0	0	0	0	1	1	1	1	1	1	1
45	0	1	0	1	1	1	1	1	1	1	1
50	0	0	1	1	1	1	1	1	1	1	1
55	0	1	0	1	1	1	1	1	1	1	1
60	0	0	1	1	1	1	1	1	1	1	1
65	0	0	1	1	1	1	1	1	1	1	1
70	0	0	1	1	1	1	1	1	1	1	1
75	0	1	1	1	1	1	1	1	1	1	1
80	1	1	1	1	1	1	1	1	1	1	1
85	0	1	1	1	1	1	1	1	1	1	1
90	0	0	1	1	1	1	1	1	1	1	1
95	1	1	1	1	1	1	1	1	1	1	1

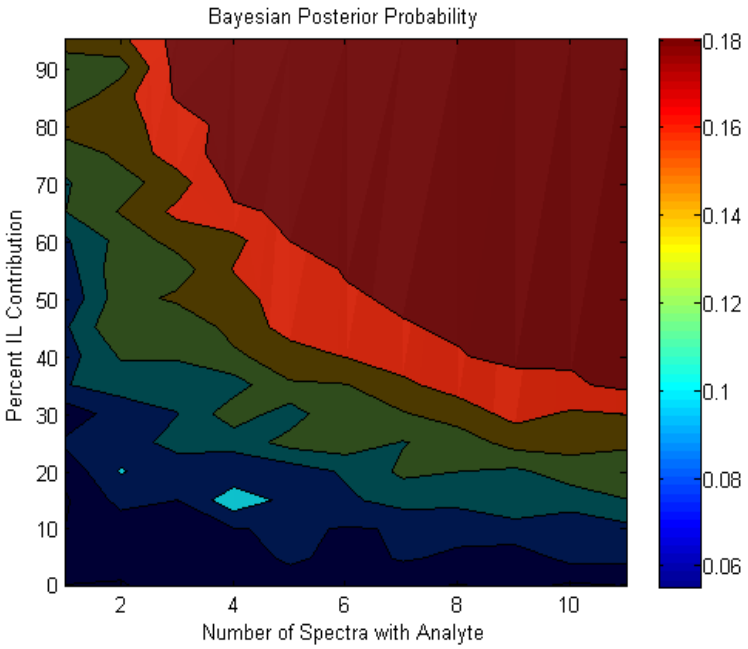

Figure 50: NAL Bayesian Probability Plot

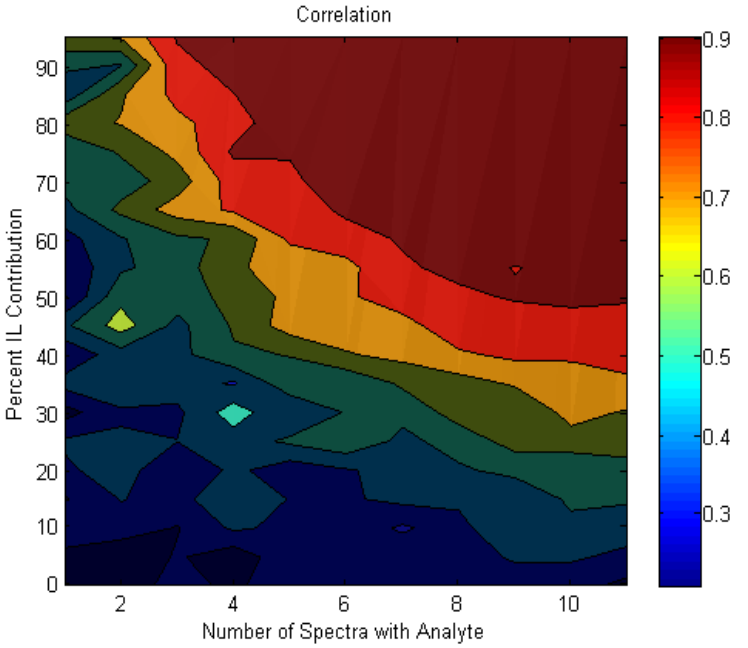

Figure 51: NAL Correlation Value Plot

Table 17: NP Classification Matrix

% IL Contribution	Number of Spectra with IL Contribution										
	1	2	3	4	5	6	7	8	9	10	11
0	0	0	0	0	0	0	0	0	0	0	0
5	0	0	0	0	0	0	0	0	0	0	0
10	0	0	0	0	0	0	0	0	0	0	0
15	0	0	0	0	0	0	0	0	0	0	0
20	0	0	0	0	0	0	0	0	0	0	0
25	0	0	0	0	0	0	0	1	0	0	0
30	0	0	0	0	0	0	0	0	1	0	1
35	0	0	0	0	0	1	1	1	1	1	1
40	0	0	0	0	1	1	1	1	1	1	1
45	0	0	0	0	1	0	1	1	1	1	1
50	0	1	1	1	1	1	1	1	1	1	1
55	0	0	0	0	1	1	1	1	1	1	1
60	0	0	0	0	0	1	1	1	1	1	1
65	0	0	1	1	1	1	1	1	1	1	1
70	0	1	1	1	1	1	1	1	1	1	1
75	0	1	1	1	1	1	1	1	1	1	1
80	1	1	1	1	1	1	1	1	1	1	1
85	0	0	0	1	1	1	1	1	1	1	1
90	0	1	1	1	1	1	1	1	1	1	1
95	0	0	1	1	1	1	1	1	1	1	1

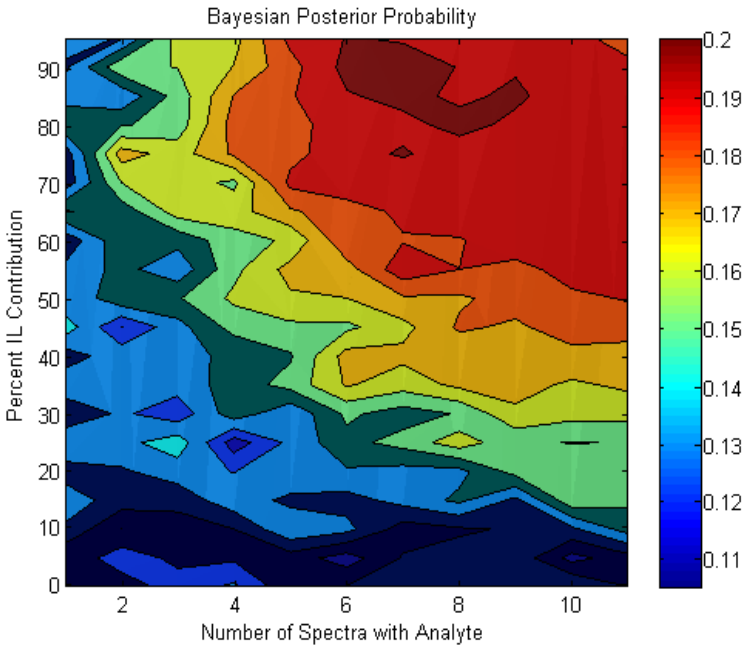

Figure 52: NP Bayesian Probability Plot

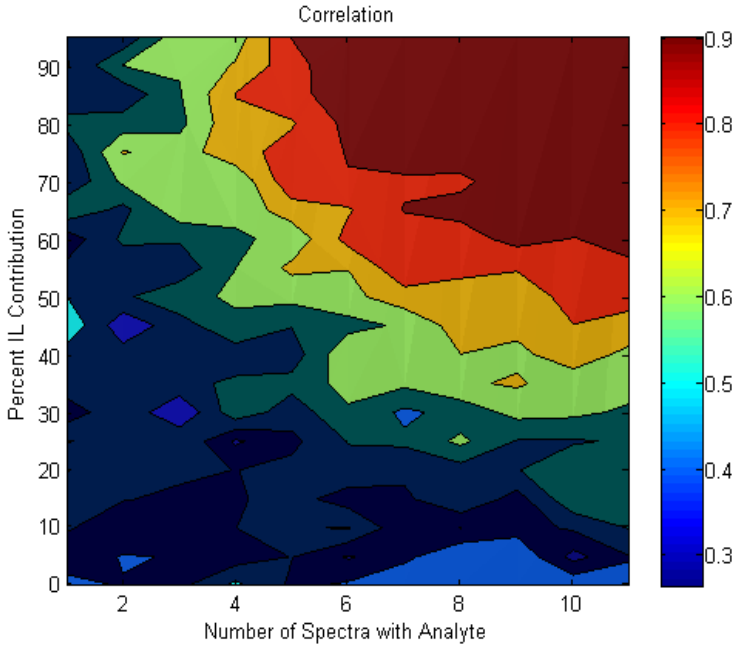

Figure 53: NP Correlation Value Plot

Table 18: OXY Classification Matrix

% IL Contribution	Number of Spectra with IL Contribution										
	1	**2**	**3**	**4**	**5**	**6**	**7**	**8**	**9**	**10**	**11**
0	0	1	1	0	1	0	0	1	1	0	1
5	1	0	1	1	0	1	1	1	1	1	1
10	0	1	1	1	1	0	1	1	1	1	1
15	0	1	1	0	0	1	1	1	1	1	1
20	0	0	1	1	1	1	1	1	1	1	1
25	1	1	1	1	1	1	1	1	1	1	1
30	1	1	1	1	1	1	1	1	1	1	1
35	0	0	1	1	1	1	1	1	1	1	1
40	1	1	1	1	1	1	1	1	1	1	1
45	0	1	1	1	1	1	0	1	1	1	1
50	0	1	0	1	1	1	1	1	1	1	1
55	1	1	1	1	1	1	1	1	1	1	1
60	1	1	0	0	1	1	1	1	1	1	1
65	0	1	0	1	1	0	0	1	0	1	1
70	1	1	1	1	1	1	1	1	1	0	0
75	1	0	1	1	1	1	1	0	0	0	1
80	0	1	1	1	1	0	1	1	1	0	1
85	1	1	0	1	1	0	0	0	0	1	1
90	0	1	1	0	1	0	0	0	0	0	1
95	1	1	1	0	0	0	0	0	0	0	0

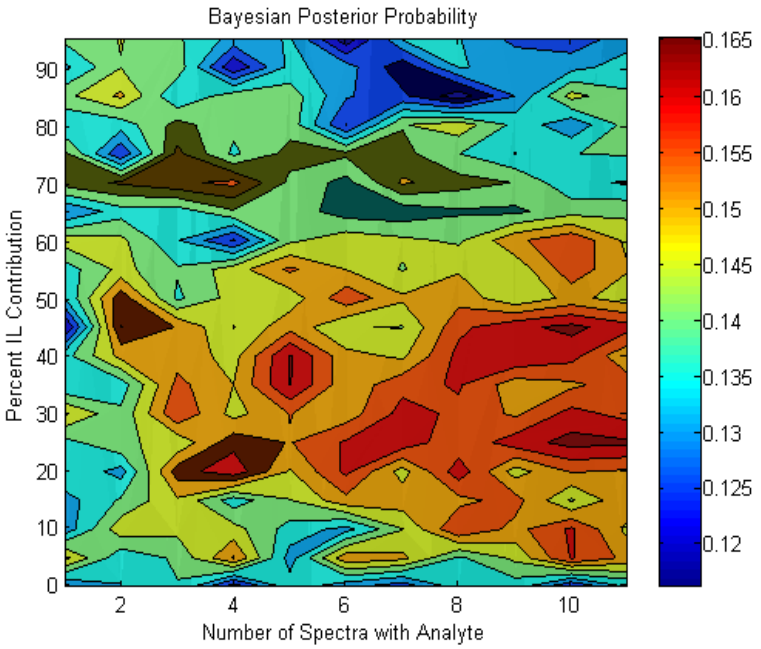

Figure 54: OXY Bayesian Probability Plot

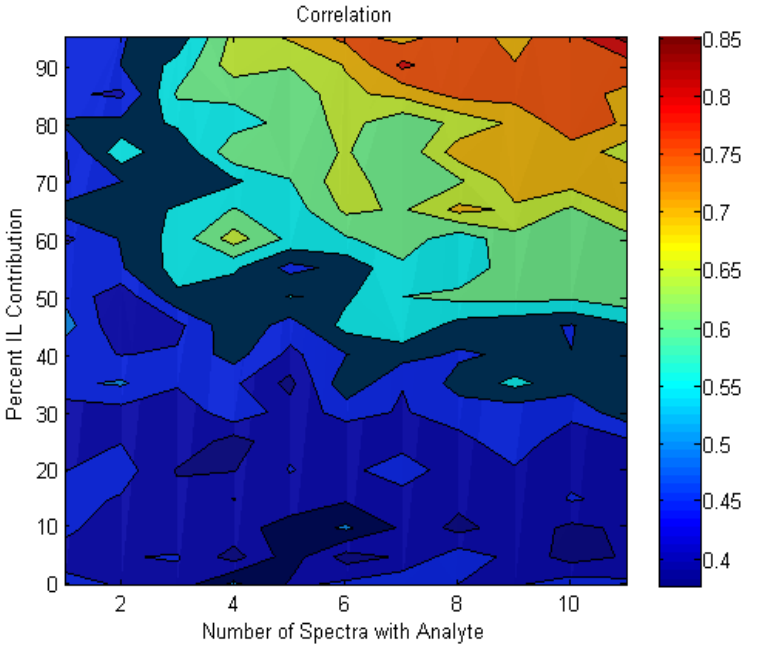

Figure 55: OXY Correlation Value Plot

Table 19: MISC Classification Matrix

% IL Contribution	Number of Spectra with IL Contribution										
	1	2	3	4	5	6	7	8	9	10	11
0	0	0	0	0	0	0	0	0	0	0	0
5	0	0	0	0	0	0	0	0	0	0	0
10	0	0	0	0	0	0	0	0	0	0	0
15	0	0	0	0	0	0	0	0	0	0	0
20	0	0	0	0	0	0	0	0	0	0	0
25	0	0	0	0	0	0	0	0	0	0	0
30	0	0	0	0	0	0	0	0	0	0	0
35	0	0	0	0	0	0	0	0	0	0	0
40	0	0	0	0	0	0	0	0	0	0	0
45	0	0	0	0	0	0	0	0	0	0	0
50	0	0	0	0	0	0	0	0	0	0	0
55	0	0	0	0	0	0	0	0	0	0	0
60	0	0	0	0	0	0	0	0	0	0	0
65	0	0	0	0	0	0	0	0	0	0	0
70	0	0	0	0	0	0	0	0	0	0	0
75	0	0	0	0	0	0	0	0	0	0	0
80	0	0	0	0	0	0	0	0	0	0	0
85	0	0	0	0	0	0	0	0	0	0	0
90	0	0	0	0	0	0	0	0	0	0	0
95	0	0	0	0	0	0	0	0	0	0	0

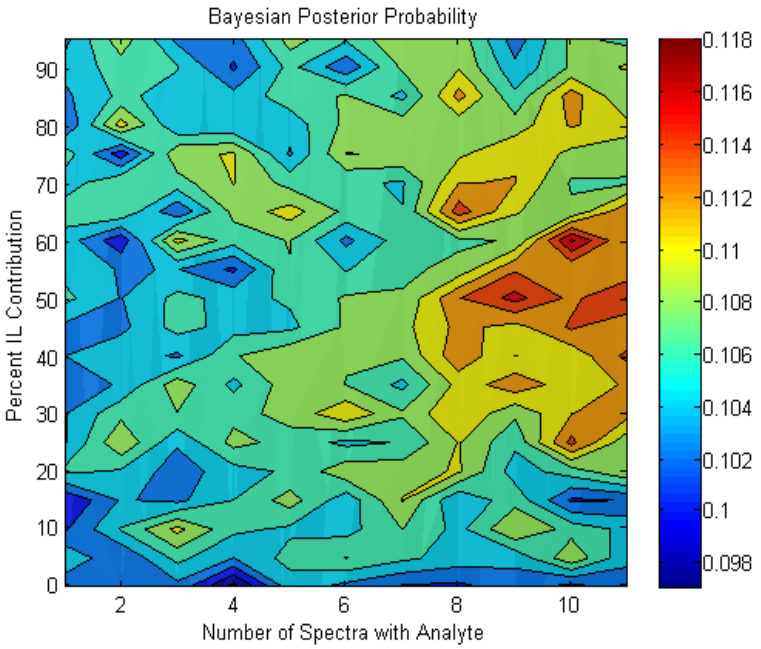

Figure 56: MISC Bayesian Probability Plot

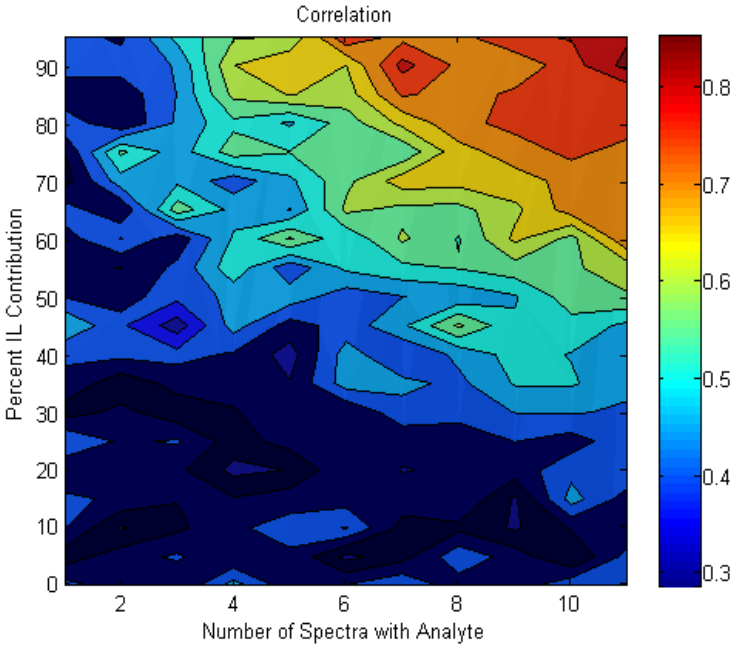

Figure 57: MISC Correlation Value Plot

Large Scale Experimental Burns

The large scale burns allowed for the collection of samples from conditions that more closely resembled a structure fire than laboratory conditions would allow. Containers were arranged to resemble a residential structure, complete with furniture, bedding, and miscellaneous items such as clothing, shoes, curtains, and magazines.

In total, 13 containers were burned however only Containers 5-12 were burned during the course of this research. The TFA results from each container were analyzed to identify whether an IL class was present. The IL class was identified based on a comparison of the posterior probabilities. The class with the highest posterior probability value was considered to be the IL class present. This classification system was then applied to the previously burned laboratory tests and Containers 1-4 to determine the accuracy of the method. The class median and average correlation values from the analysis of the large scale burns are compiled in Table 20 and Table 21. The calculated posterior probabilities are compiled in Table 22, and the results of the IL class identified in each container are summarized in Table 23.

Table 20: Median Correlation Values for Containers 5-12

Container	IL Used	IL Identified											
		Gas	HAR	HPD	ISO	LAR	LPD	MAR	MISC	MPD	NAL	NP	OXY
C5	Gas	0.849	0.010	0.387	0.205	0.519	0.267	0.809	0.366	0.274	0.211	0.250	0.408
C6	Gas	0.858	0.113	0.395	0.248	0.588	0.327	0.807	0.408	0.332	0.259	0.310	0.448
C7	Gas & MPD	0.781	0.014	0.816	0.562	0.286	0.641	0.555	0.660	0.695	0.574	0.675	0.522
C8	Gas & MPD	0.629	-0.022	0.794	0.592	0.192	0.741	0.328	0.670	0.751	0.637	0.704	0.629
C9	Gas & HPD	0.970	0.485	0.984	0.859	0.814	0.939	0.916	0.906	0.977	0.849	0.988	0.819
C10	LPD	0.590	-0.051	0.900	0.777	0.379	0.936	0.190	0.802	0.936	0.819	0.892	0.694
C11	NP	0.493	-0.062	0.923	0.722	0.095	0.888	0.060	0.739	0.946	0.741	0.956	0.528
C12	ISO	0.955	0.018	0.885	0.992	0.742	0.864	0.834	0.890	0.886	0.935	0.811	0.773

Table 21: Average Correlation Values for Containers 5-12

Container	IL Used	IL Identified											
		Gas	HAR	HPD	ISO	LAR	LPD	MAR	MISC	MPD	NAL	NP	OXY
C5	Gas	0.842	0.034	0.378	0.210	0.451	0.262	0.786	0.424	0.340	0.213	0.257	0.436
C6	Gas	0.849	0.117	0.392	0.254	0.525	0.317	0.763	0.445	0.375	0.261	0.313	0.461
C7	Gas & MPD	0.777	0.042	0.801	0.567	0.250	0.617	0.535	0.630	0.748	0.573	0.682	0.540
C8	Gas & MPD	0.632	0.013	0.789	0.604	0.181	0.724	0.335	0.619	0.773	0.643	0.703	0.606
C9	Gas & HPD	0.966	0.489	0.979	0.867	0.811	0.924	0.868	0.887	0.977	0.849	0.986	0.799
C10	LPD	0.549	0.005	0.893	0.788	0.419	0.915	0.223	0.759	0.928	0.820	0.889	0.676
C11	NP	0.472	-0.007	0.921	0.734	0.105	0.856	0.085	0.685	0.941	0.741	0.953	0.535
C12	ISO	0.927	0.032	0.884	0.970	0.789	0.858	0.821	0.831	0.886	0.937	0.808	0.703

Table 22: Posterior Probabilities for Containers 5-12

Container	IL Used	IL Identified											
		Gas	HAR	HPD	ISO	LAR	LPD	MAR	MISC	MPD	NAL	NP	OXY
C1	Gas	0.945	0.000	0.012	0.000	0.000	0.001	0.000	0.010	0.020	0.000	0.012	0.001
C2	Gas	0.998	0.000	0.000	0.000	0.000	0.000	0.002	0.001	0.000	0.000	0.000	0.000
C2	MPD	0.146	0.000	0.187	0.000	0.000	0.010	0.000	0.068	0.308	0.000	0.270	0.010
C3	MPD	0.000	0.000	0.467	0.000	0.000	0.000	0.000	0.101	0.364	0.000	0.051	0.016
C4	OXY	0.000	0.000	0.476	0.000	0.000	0.002	0.000	0.087	0.383	0.000	0.041	0.012
C5	Gas	0.977	0.000	0.000	0.000	0.000	0.000	0.001	0.003	0.000	0.000	0.000	0.019
C6	Gas	0.982	0.000	0.000	0.000	0.000	0.000	0.000	0.000	0.000	0.000	0.000	0.018
C7	Gas & MPD	0.000	0.000	0.024	0.000	0.000	0.000	0.000	0.433	0.537	0.000	0.000	0.005
C8	Gas & MPD	0.000	0.000	0.012	0.000	0.000	0.000	0.000	0.237	0.056	0.000	0.000	0.695
C9	Gas & HPD	0.166	0.000	0.220	0.002	0.000	0.038	0.017	0.076	0.211	0.000	0.254	0.016
C10	LPD	0.000	0.000	0.034	0.000	0.000	0.396	0.000	0.187	0.330	0.000	0.013	0.040
C11	NP	0.000	0.000	0.135	0.000	0.000	0.005	0.000	0.093	0.323	0.000	0.432	0.013
C12	ISO	0.250	0.000	0.011	0.499	0.000	0.002	0.009	0.077	0.027	0.098	0.000	0.027

Table 23: Summary of Classification Results for Large Scale Burns

Container	IL Present	IL Identified
5	Gas	Gas
6	Gas	Gas
7	Gas/MPD	MPD
8	Gas/MPD	OXY
9	Gas & HPD	NP
10	LPD	LPD
11	NP	NP
12	ISO	ISO

Container 5

Container 5 was burned with 500 mL of gasoline which when lit, trailed from the couch through the front room and to the bed in the back room, see Figure 58. The container doors were closed approximately 4 inches and the container was burned for about 4.5 minutes, see Figure 59. Ventilation through Container 5 was limited through the back window, which was open 2 inches. This affected the intensity of the fire since it limited the supply of oxygen and air flow in the container. Near the 4 minute mark, the temperatures in the container began to decrease as seen in the temperature plots of the thermocouple data in Figure 61. Because the fire in the container was dying, the doors to the container were open in order to extinguish the fire. When the doors were opened the fire quickly increased as seen in sharp increase around 4.5 minutes in the graph of thermocouple temperatures, Figure 61. After the fire increased in intensity so quickly, it was allowed to continue burning for about another 1.5 minutes during which time it reached temperatures of about 900 °C. After a total burn time of 6 minutes, the fire was extinguished and the damage and condition of the container was documented, Figure 60. The back room sustained minimal damage (see Figure 63) most likely because the fire had significantly self-extinguished during the first 4.5 minutes of the burn.

Figure 58: Container 5 Ignition

Figure 59: Container 5 Burning

Figure 60: Container 5 Post-Burn

The temperature read-outs on the thermocouples in Container 5, see Figure 12, were manually recorded every 30 seconds. The recorded temperatures were then graphed for comparison, see Figure 61.

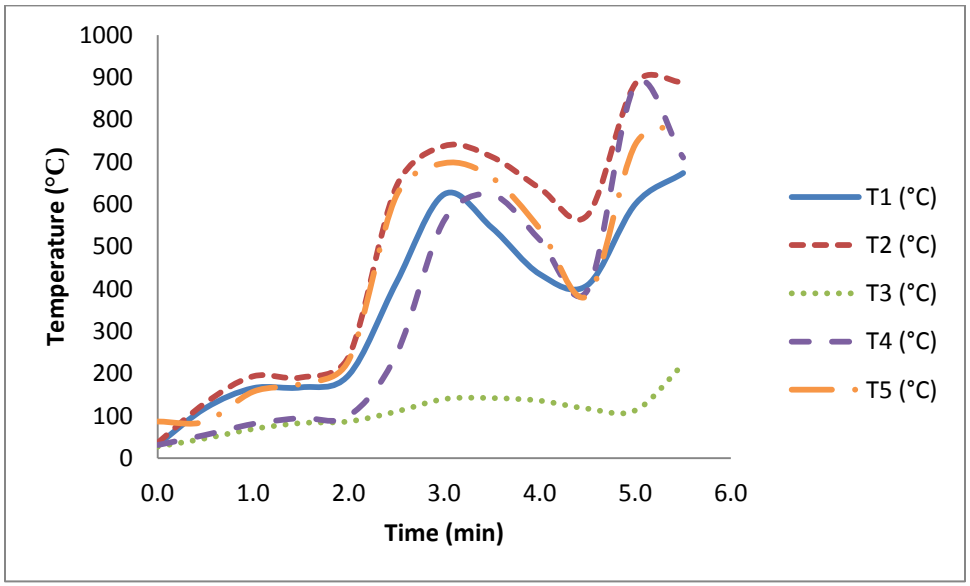

Figure 61: Temperature Plots of Container 5

The front room sustained a greater degree of damage compared to the back room, as seen in a comparison between Figure 62 and Figure 63. This was most likely due to the increased air flow when the doors were opened wider at about 4.5 minutes.

Figure 62: Container 5 Front Room Post-Burn

Figure 63: Container 5 Back Room Post-Burn

After the fire was extinguished, samples were collected as depicted in Figure 13 and Figure 64. The substrates collected in Container 5 are summarized in Table 24. Samples 1 and 5 were collected as two individual samples, A and B. Both A and B samples of Sample 5 were pieces of the wood laminate flooring placed in the hallway area between the front and back rooms, however 5 was the center part of one of the laminate boards, and Sample 5B consisted of parts from the connection seam between two wood laminate boards.

Figure 64: Container 5 with Sample ID Markers

Table 24: Container 5 Sample Identifications

Sample	Location	Material
1	Bed on pour	Bedding
1B	Under sample 1	Sheet
2	Floor on pour	Carpet & padding
3	2" – 4" off pour	Carpet & padding
4	Slightly off pour	Carpet, padding, and clothing
5	On pour	Laminate
5B	On pour	Seam of laminate
6	On pour	Carpet & padding
7	Edge of pour	Carpet & padding
8	Off pour	Trash can?
9	Edge of pour	Table, carpet & padding
10	Off pour between chair and couch	Shoe, carpet, & padding
11	Off pour	Carpet & padding
12	On pour	Couch padding & clothes

Table 25: Container 5 Samples IL Identification

Sample	IL
1	Gas
1B	Gas
2	Gas
3	Gas
4	None
5	None
5B	Gas
6	Gas
7	None
8	None
9	None
10	None
11	None
12	None

The TIS was generated for each sample and combined to form the data set for TFA. The correlation values between the data set and each ignitable liquid in a reference library were

calculated by TFA and sorted in decreasing order. These correlation values were then used with the Bayesian method to determine the class of ignitable liquid present. The results of the posterior probabilities are summarized in Table 22. The values highlighted in yellow are the highest posterior probability values and correspond to the identified IL class present in the debris samples. Based on the calculated posterior probabilities, the class that was identified by the method as present in the sample was gasoline, which was a correct classification. The second highest class was the aromatic class (medium aromatic subclass) which share many target compounds and therefore characteristic ions in the TIS as gasoline.

Container 6

Based on the temperature and fire intensity pattern observed in Container 5, the doors and window in Container 6 were opened 4-6 inches rather than 2 inches.

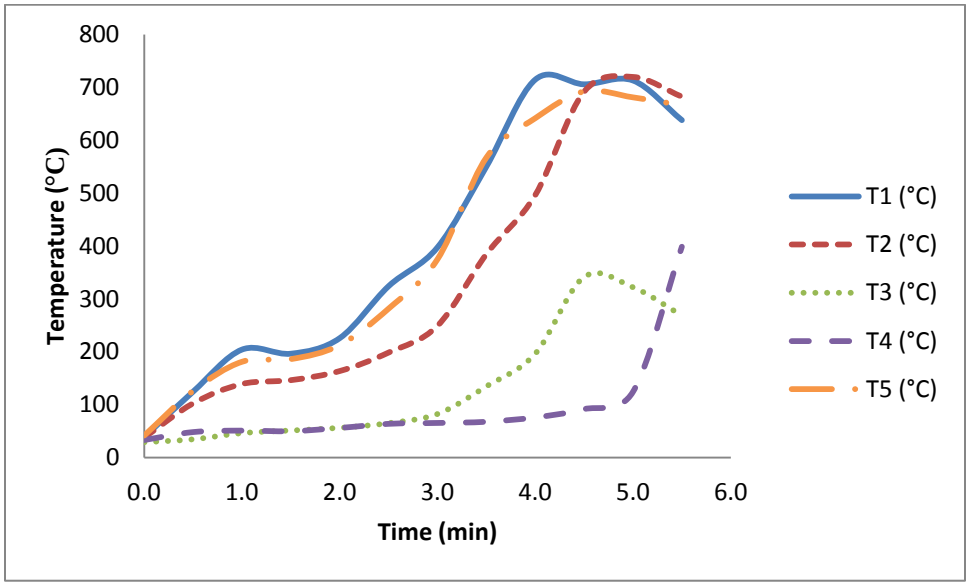

Figure 65: Temperature Plots of Container 6

Initially, 250 mL of gasoline was poured from the bed to the couch, see Figure 66, and then lit. The volume of ignitable liquid was not substantial enough to allow the fire to spread to the back room, so it was extinguished by stomping it out, see Figure 67 and Figure 68 for the weak trailing and subsequent extinguishing.

Figure 66: Container 6 Trial 1 IL Pour

Figure 67: Container 6 Trial 1 Ignition

Figure 68: Container 6 Trial 1 Extinguishment

An additional 500 mL of gasoline was then trailed along a different path (see Figure 15) starting on the bed and ending near the front of the container, see Figure 69. This second trail was then lit (Figure 70) and the fire quickly spread, as expected.

Figure 69: Container 6 Trial 2 IL Pour

Figure 70: Container 6 Trial 2 Ignition

After the second time igniting the IL trail, the container was burned for approximately 6 minutes. The thermocouples placed at the top of the container recorded temperatures over 700 °C during the course of the burn. After the fire was extinguished, the damage and condition of the container were documented, see Figure 71.

Figure 71: Container 6 Front Room Post Burn

After the container had sufficiently cooled, sample identification markers were placed throughout the container to identify the locations of samples to be collected. Samples were collected and placed into gallon-sized metal cans and sealed until ready for analysis in the laboratory. The sample locations can be seen in Figure 16 and Figure 72, and the types of materials collected for each sample are tabulated in Table 26.

Figure 72: Container 6 with Sample ID Markers

Samples were collected on and off the pour in order to have samples with no ignitable liquid as part of the data set, and their TICs could serve as a background spectrum for the pyrolysis products found in the container. The TIC for each sample was analyzed using the ASTM E1618 guidelines to determine if an IL could be identified. These results are tabulated in Table 27.

Table 26: Container 6 Sample Identifications

Sample	Location	Material
13	Bed on pour	Bedding
14	Bed on pour	Mattress
15	On pour	Carpet, padding, & clothes
16	on pour	Carpet & padding
17	Edge of pour	Debris
18	On pour	Laminate
19	Between both trails	Carpet, padding & drywall
20	On pour - site of stomping (NCFS)	Carpet & padding
21	Couch on pour	Couch foam
22	Edge of both pours (closer to second)	Carpet & padding
23	Off the pour	Carpet & padding
24	on pour	Carpet & padding
25	On pour - site of manual extinguish	Carpet & padding

Table 27: Container 6 Samples IL Identification

Sample	IL
13	None
14	Gas
15	Gas
16	Gas
17	None
18	Gas
19	None
20	Gas
21	Possible
22	None
23	None
24	Gas
25	Gas

TFA was applied to the compiled data set of all total ion spectra from Container 6. The median and average correlation values determined by TFA are tabulated in Table 20 and Table 21. The posterior probabilities based on the correlation values from TFA are tabulated in Table 22.

Container 7

The temperatures recorded from the thermocouples in Container 7 are displayed in Figure 76. The front portion of the ceiling in the front room fell down during the burn, which may account for the low temperature readings by Thermocouple 2, see Figure 76. Also, the back room sustained little damage, as seen in the background of Figure 74, compared the damage in the front room, see Figure 73. The furniture in the front room was consumed in the fire, and by the end of the almost 8 minute burn, 3 ceiling panels had fallen. The back room however remained largely unaffected, with only minimal damage to the lamp on the dresser, see Figure 75. It appears that the fire did not trail to the back room, explaining the low temperatures on

Thermocouple 3 and 4, see Figure 76. The front room may have had a more intense fire due to the increased airflow since both doors were open approximately 6 inches, and the window in the back was open 4-6 inches.

Figure 73: Container 7 Fallen Ceiling Post Burn

Figure 74: Container 7 Post Burn

Figure 75: Container 7 Back Room Post Burn

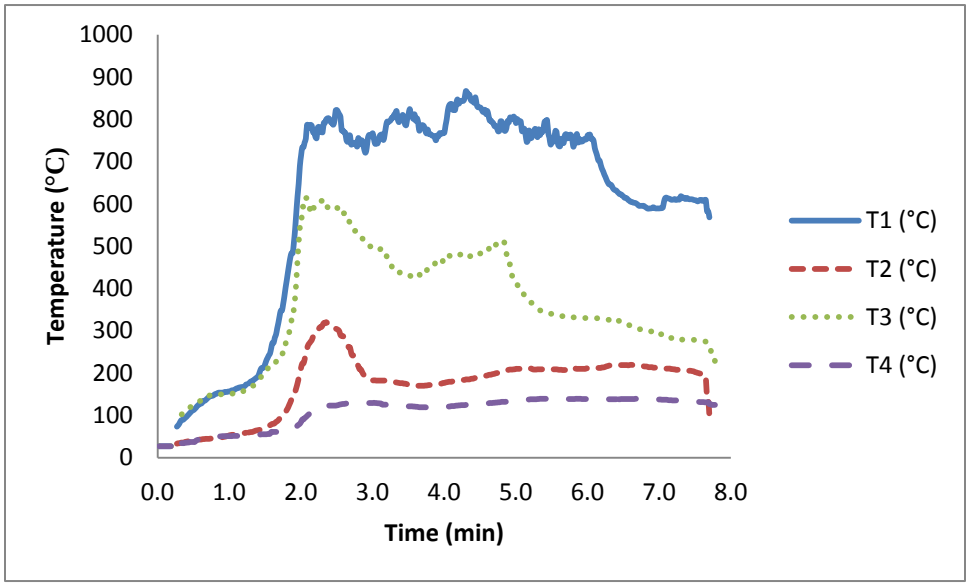

Figure 76: Temperature Plots of Container 7

After the container had sufficiently cooled, samples were collected. The debris collected for each sample and the approximate location in the container relative to the ignitable liquid trail are summarized in Table 28.

Table 28: Container 7 Sample Identifications

Sample	Location	Material
1	Pour on bed	Bedding
2	Pour on floor	Carpet, padding & clothes
3	On pour	Carpet & padding
4	On pour	Carpet & padding
5	On pour	Laminate
6	On pour	Laminate
7	On pour	Concrete
8	On pour	Concrete
9	Around pour	Debris
10	Around pour	Debris
11	On or near pour	Debris
12	On or near pour	Table & debris

After analyzing the samples using the previously established laboratory method, pattern recognition and target compound identification were used to visually determine if an ignitable liquid was present in each sample. The results of identification and classification of ILRs present based on the ASTM E1618 guidelines are summarized in Table 29.

Table 29: Container 7 Samples IL Identification

Sample	IL
1	None
2	Gas
3	Gas
4	MPD
5	Gas & MPD
6	MPD
7	Gas
8	MPD
9	MPD
10	Gas
11	None
12	None

The dataset of compiled TIS were analyzed by TFA to calculate correlation values between the data set and each reference IL in a library. The median correlation values calculated by TFA were then used to calculate the posterior probabilities for each class to determine the probability of a specific class as being present in the fire debris. The posterior probabilities are summarized in Table 22.

Container 8

Container 7 did not burn evenly throughout the entire container, most likely due to the increased airflow in the front room as a result of both doors being open about 6 inches unlike the previous containers, which only had 1 door open and the second door was kept completely closed. In Container 8, only one door was open about 6 inches and the back window was open about 8 inches. This increased the airflow through the back room, which may have helped the fire spread. Both the front and back rooms received considerable damage over the course of the 8 minute burn, see Figure 77 and Figure 78, with large portions of the ceiling falling down in both rooms.

Figure 77: Container 8 Front Room Post Burn

Figure 78: Container 8 Back Room Post Burn

The temperatures measured by the thermocouples have been graphed, see Figure 79. Because there are gaps in recorded data, the maximum temperature reached inside the container can only be estimated as about 800 °C.

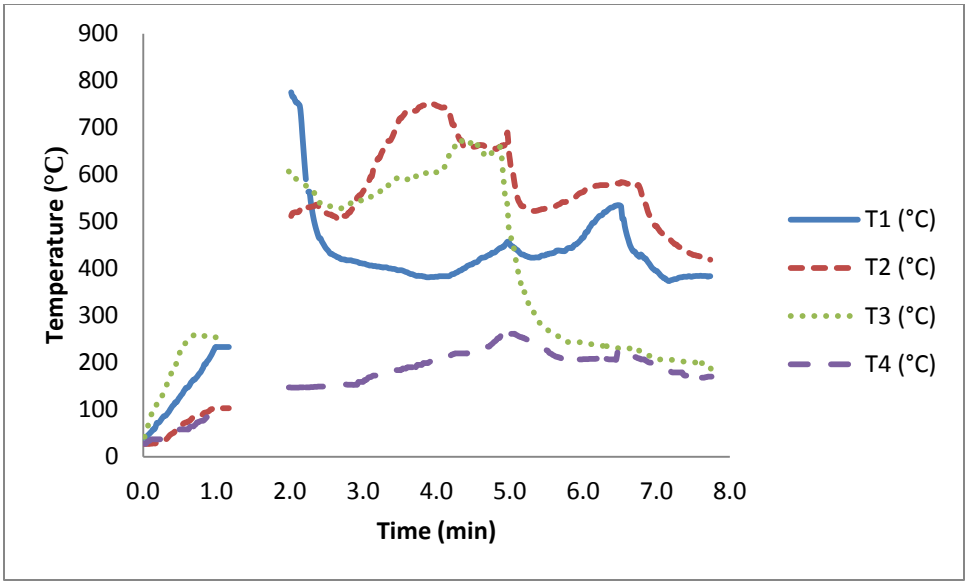

Figure 79: Temperature Plots of Container 8

The type of debris collected from Container 8 and the approximate location of the sample within the container with respect to the IL trail are compiled in Table 30. During previous burns it was observed that samples taken too far from the IL trail showed no IL pattern in the TIC, so only samples on or near the pour were collected for analysis.

Table 30: Container 8 Sample Identifications

Sample	Location	Material
13	Bed on pour	Bedding
14	On or near pour	Carpet & padding
15	On pour	Carpet & padding
16	On pour	Laminate
17	On pour	Laminate
18	On pour	Concrete
19	On pour	Concrete
20	Near trash can	Debris
21	On or near pour	Debris
22	Front of couch	Carpet & padding
23	Pour area	Debris & subfloor
24	Front of bed	Carpet & padding
25	Front of couch	Carpet, padding & subfloor

The TICs from each sample were analyzed using ASTM E1618 guidelines to identify the class, if any, of ignitable liquid present in each sample. The results of the pattern recognition and target compound identification are summarized in Table 31.

Table 31: Container 8 Samples IL Identification

Sample	IL
13	None
14	None
15	Gas
16	None
17	None
18	None
19	Gas
20	Gas
21	None
22	None
23	None
24	MPD
25	None

The correlation values obtained after TFA analysis of the data set with ignitable liquids in a reference library are summarized based on median and average correlations per class, see Table 20 and Table 21. The correlation values were then analyzed by the Bayesian method to calculate posterior probabilities, summarized in Table 22, which were used to classify the ignitable liquid present in the fire debris samples. The class of ignitable liquid identified was oxygenated solvents, which does not match either the gasoline or MPD classes used.

Container 9

Container 9 used a pre-mixed 50:50 mixture of diesel fuel (in the HPD subclass) and gasoline. The temperatures recorded by the thermocouples were graphed, see Figure 80. Temperatures during the course of the 6 minute burn reached over 800 °C.

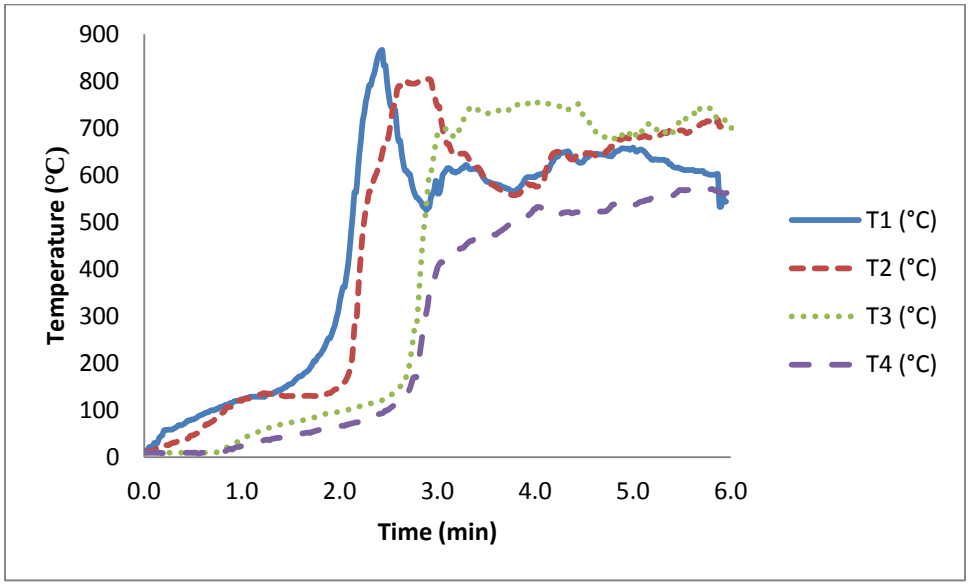

Figure 80: Temperature Plots of Container 9

There was considerable damage throughout the entire container, with portions of the ceiling falling in both rooms, see Figure 81. Over the course of the burn, the ceiling fell which coincides with the decrease in temperatures around 3 minutes, as shown in the temperature graph in Figure 80.

Figure 81: Container 9 Post Burn

The location and materials collected for each sample were recorded, see Figure 82 and Table 32.

The samples were sealed in gallon-sized metal cans until analysis at the laboratory.

Figure 82: Container 9 with Sample ID Markers

Table 32: Container 9 Sample Identifications

Sample	Location	Material
1	First step in shoe experiment	Debris
2	Underneath table	Shoes
2B	Underneath table	Carpet on shoes
3	On pour	Bedding
4	On pour	Vinyl flooring & rug
5	On pour	Vinyl flooring
6	Off pour	Vinyl flooring
7	On pour	Carpet & padding
8	On pour	Unsealed tiles
9	On pour	Sealed tiles
10	Underneath tiles	Carpet & padding
11	On pour	Remnants of the couch arm
12	Area of pour	Couch

The TICs were analyzed following ASTM E1618 guidelines in order to identify the presence of an ignitable liquid by using visual pattern recognition and target compound identification. The results of the ignitable liquid classification from the TICs by ASTM E1618 guidelines are summarized in Table 33. In some samples, the TIC appeared to have a combination of both gasoline and HPD. The TIC of samples 3, 4, 8, 9, and 10 all have a Gaussian distribution of n-alkane peaks, as well as target compounds of gasoline.

The TICs of the sealed tile, unsealed tile, and carpet and padding samples have been combined for easier comparison of the sample TIC patterns, see Figure 83.

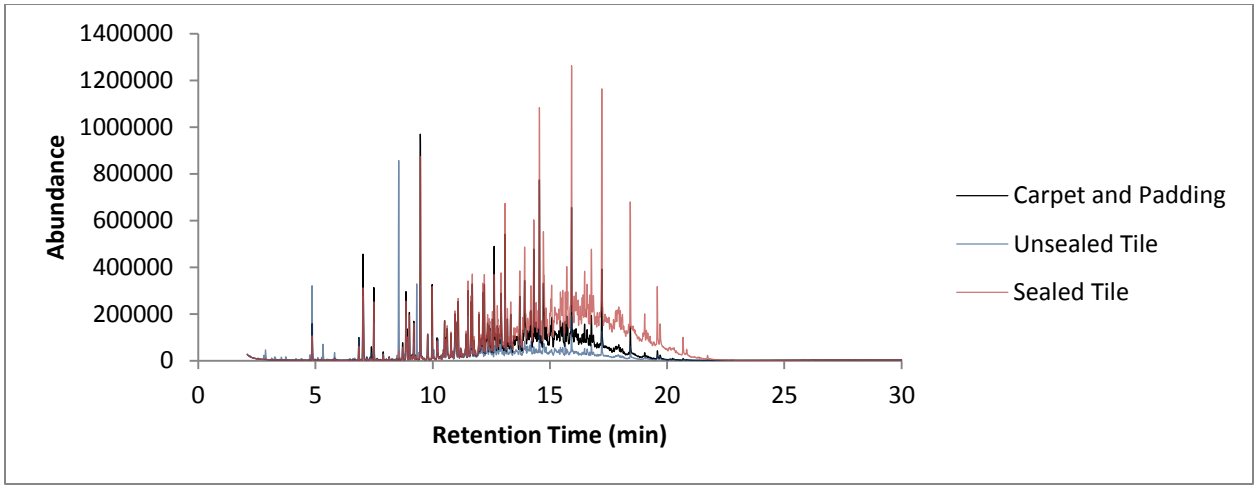

Figure 83: Container 9 Tile TIC Overlays

Figure 84: Container 9 Unsealed Tile Sample

Table 33: Container 9 Samples IL Identification

Sample	IL
1	None
2	Gas
2B	Gas
3	Gas/HPD
4	Gas/HPD
5	None
6	None
7	None
8	Gas/HPD
9	Gas/HPD
10	Gas/HPD
11	None
12	None

The correlation values calculated after TFA are summarized as part of Table 20 and Table 21. The correlation values were then used to calculate the posterior probability of a class as being present in the fire debris samples. The posterior probabilities are summarized in Table 22, with the highest posterior probability value corresponding to the NP class.

Container 10

Container 10 was burned for 6 minutes using a camp fuel which was classified as an LPD. There was significant damage to the entire container, see Figure 85, with a large portion of the ceiling falling in both the front and back rooms. The ceiling fell mid-way through the burn, corresponding to the same time as the dramatic drop in temperatures around the 3 minute mark for the thermocouple T1, Figure 86.

Figure 85: Container 10 Post Burn

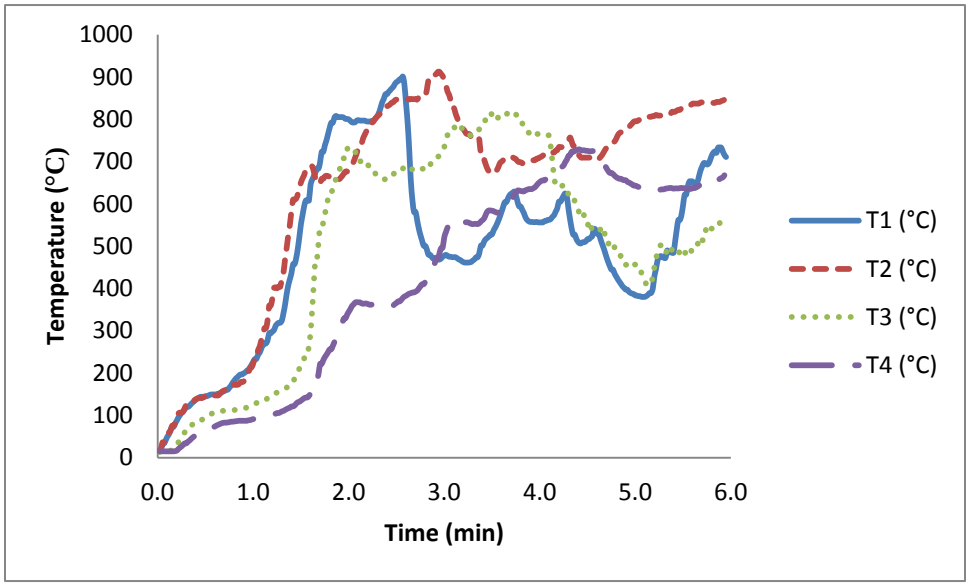

Figure 86: Temperature Plots of Container 10

The samples collected, were sealed in gallon-sized metal cans for transport back to the laboratory, see Figure 87. The debris material collected and the location relative within the container have been summarized in Table 34.

Figure 87: Container 10 Samples with ID Markers

Table 34: Container 10 Sample Identifications

Sample	Location	Material
13	First step in shoe experiment	Debris
14	Underneath table	Shoe & subfloor
15	On pour	Bedding
16	On pour	Vinyl flooring & rug
17	On pour	Vinyl flooring
18	Off pour	Vinyl flooring
19	On pour	Carpet, padding & debris
20	On pour	Unsealed tiles
21	On pour	Sealed tiles
22	Underneath tiles	Carpet & padding
23	On pour	Couch & magazines
24	On pour	Debris in front of couch

The TIC from each sample was analyzed by visual pattern recognition and target compound identification to identify the presence of an IL. The results of the IL identification are summarized in Table 35.

Table 35: Container 10 Samples IL Identification

Sample	IL
13	None
14	None
15	None
16	None
17	None
18	None
19	LPD
20	LPD
21	None
22	None
23	None
24	None

The results of the tile experiment, samples 20-22, were analyzed to determine what effect that sealant on tile and grout has on the ability to recover ILRs from fire debris samples. The samples, see Figure 88, were collected and the TIC of each collected sample, see Figure 89, were visually compared. Figure 90 is the same TIC as Figure 89 only focused on the lower-abundance patterns from sealed tile and carpet and padding. For easier comparison of the sample TIC patterns, the TICs of the unsealed tile, sealed tile, and carpet and padding have been stacked, see Figure 91.

Figure 88: Container 10 Tile Samples

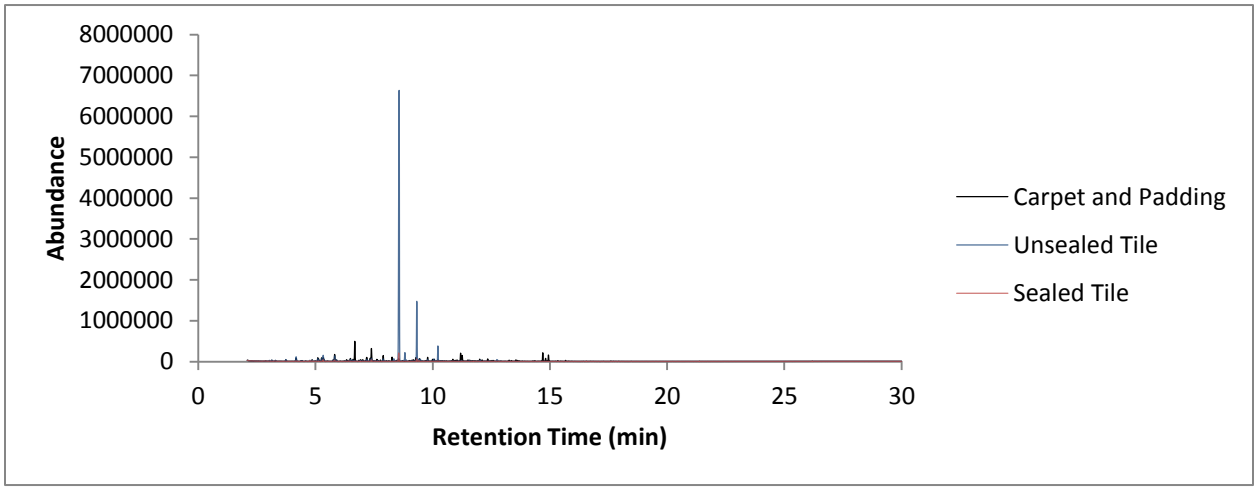

Figure 89: Container 10 Tile TIC Overlay

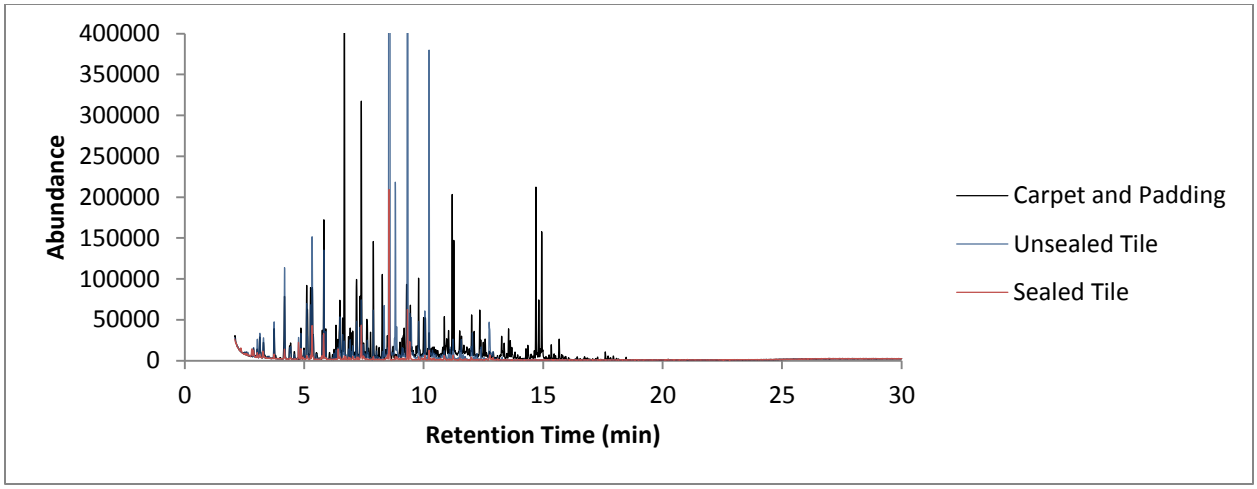

Figure 90: Container 10 Tile TIC Overlay Zoom

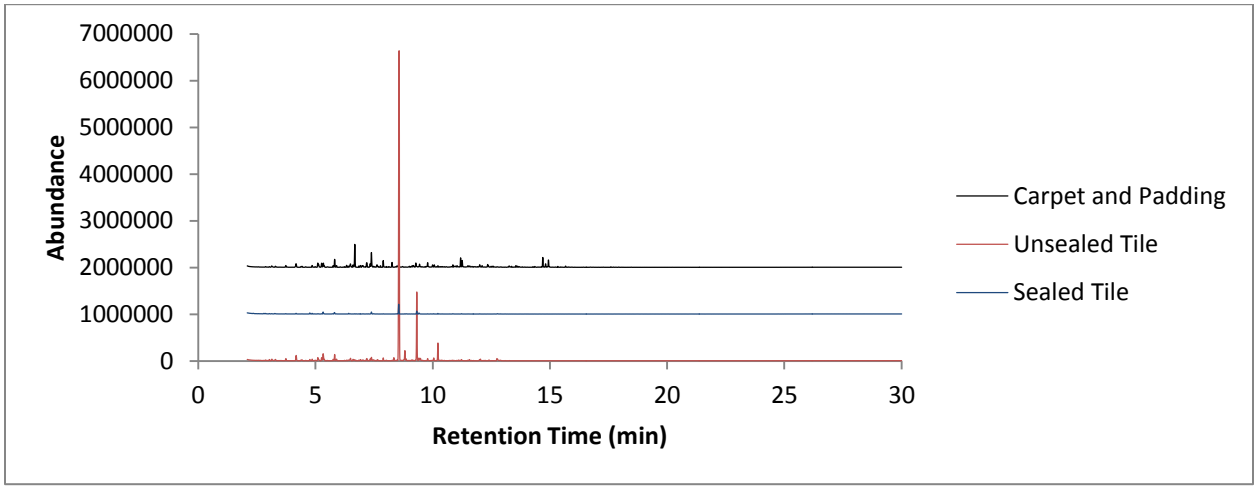

Figure 91: Container 10 Tile TIC Stacked Overlay

The correlation values calculated from TFA of the data set of compiled TIS from each sample were then used to calculate the posterior probability for the ASTM IL classes. The median and average TFA correlation results are tabulated in Table 20 and Table 21, respectively. The posterior probabilities calculated are summarized in Table 22. The class identified based on the calculated posterior probabilities was a light petroleum distillate (LPD).

Container 11

Container 11 used a torch fuel that was classified as a naphthenic-paraffinic (NP) ignitable liquid. As in previous containers, significant damage occurred in both rooms, including portions of the ceiling falling during the course of the 6 minute burn, see Figure 92 and Figure 93.

Figure 92: Container 11 Front Room Post Burn

Figure 93: Container 11 Back Room Post Burn

The temperatures recorded by the thermocouples are graphed in Figure 94. The drop in temperatures around 2.5 minutes coincided with the ceiling falling.

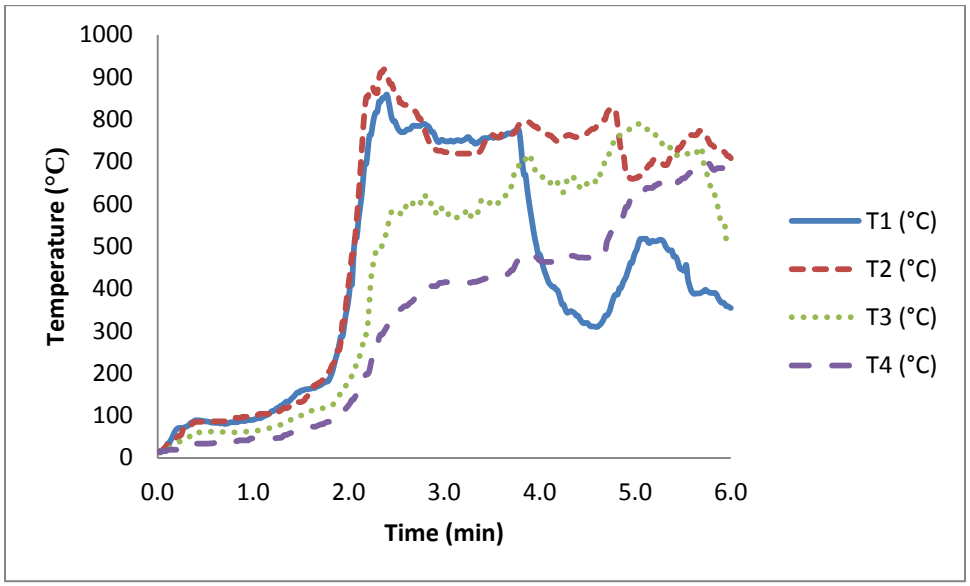

Figure 94: Temperature Plots of Container 11

The samples were collected, Figure 95, and placed into gallon-sized metal cans until the ignitable liquid residues could be extracted at the laboratory. The debris material collected and the location of each sample relative to the ignitable liquid trail are summarized in Table 36.

Figure 95: Container 11 Samples with ID Markers

Table 36: Container 11 Sample Identifications

Sample	Location	Material
1	First step in shoe experiment	Debris
2	Underneath table	Shoes
3	On pour	Bedding
4	On pour	Vinyl flooring & rug
5	On pour	Vinyl flooring
6	Off pour	Vinyl flooring
7	On pour	Carpet, padding & debris
8	On pour	Unsealed tiles
9	On pour	Sealed tiles
10	Underneath tiles	Carpet & padding
11	On pour	Magazines & debris
12	On pour	Couch

The TICs for each sample were analyzed based on the guidelines established in ASTM E1618. Identification and classification by this ASTM standard is based on visual pattern recognition and target compound analysis, and the results of the detection of ignitable liquids present in each TIC are summarized in Table 37.

Table 37: Container 11 Samples IL Identification

Sample	IL
1	None
2	Possible
3	NP
4	NP
5	None
6	None
7	None
8	Possible
9	NP
10	NP
11	None
12	None

The tile samples, see Figure 96, were collected as part of the experiment of the effect of sealant on ILR recovery. The overlays of the TICs of the unsealed tile, sealed tile, and carpet and padding are shown in Figure 97 and Figure 98.

Figure 96: Container 11 Tile Samples

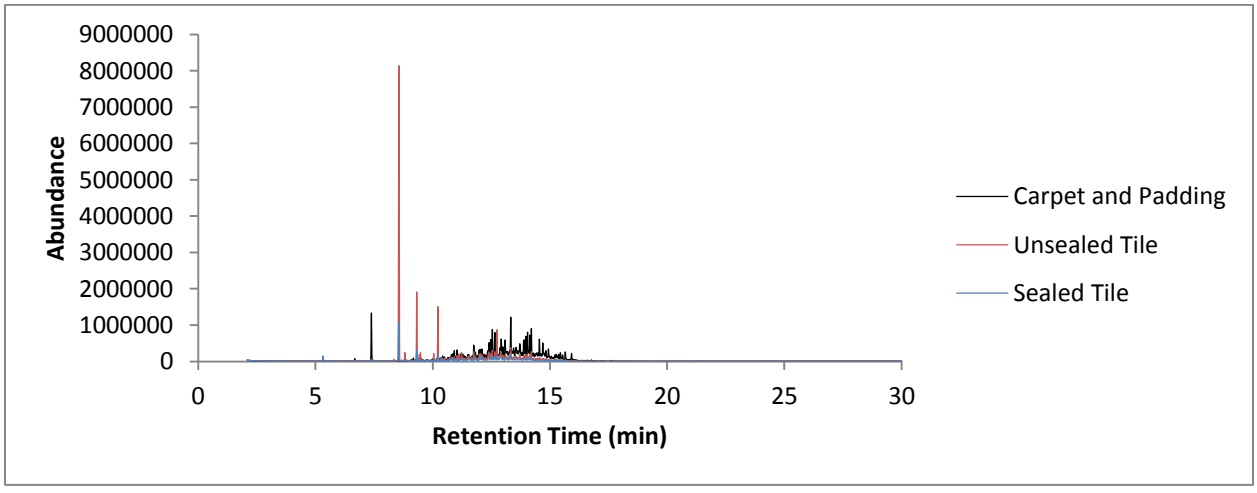

Figure 97: Container 11 Tile TIC Overlay

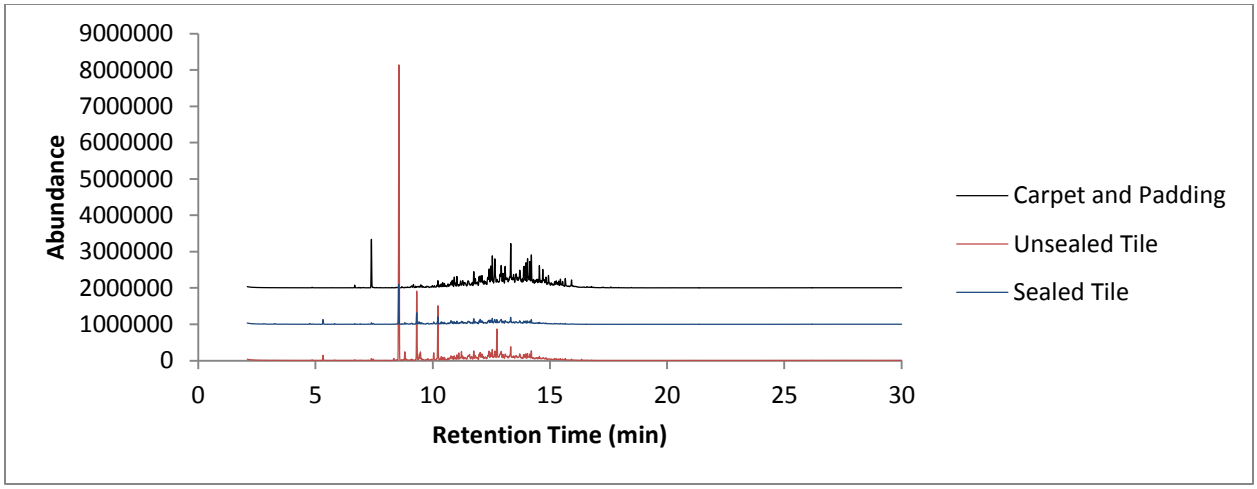

Figure 98: Container 11 Tile TIC Stacked Overlay

The median and average correlation values calculated by TFA of the TIS data set are summarized in Table 20 and Table 21, respectively, along with the posterior probabilities calculated using the correlation values, see Table 22. A correct classification was obtained with the identification of the NP class as being the ignitable liquid class present in the fire debris samples.

Container 12

Container 12 had a charcoal starter fluid classified as an isoparaffinic liquid (ISO) as the ignitable liquid for the burn. The container was burned for 6 minutes, and the temperatures are plotted in Figure 99.

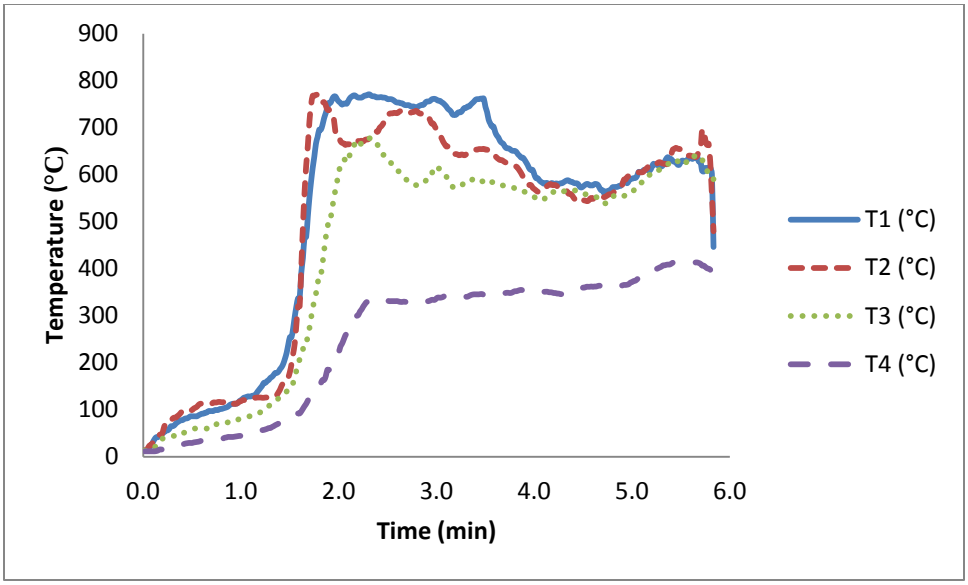

Figure 99: Temperature Plots of Container 12

The debris material collected for each sample (Figure 100) is summarized in Table 38 along with the location of each sample relative to the ignitable liquid pour trail.

Figure 100: Container 12 Samples with ID Markers

Table 38: Container 12 Sample Identifications

Sample	Location	Material
13	First step in shoe experiment	Debris
14	Underneath table	Shoes
14B	Underneath table	Carpet on shoes
15	On pour	Bedding
16	On pour	Vinyl flooring & rug
17	On pour	Vinyl flooring
18	Off pour	Vinyl flooring
19	On pour	Carpet & padding
20	On pour	Unsealed tiles
21	On pour	Sealed tiles
22	Underneath tiles	Carpet & padding
23	On pour	Couch

The TIC corresponding to each sample was analyzed by pattern recognition and target compound identification based on the guidelines in ASTM E1618. The results of the pattern recognition and target compound identification are summarized in Table 39.

Table 39: Container 12 Samples IL Identification

Sample	IL
13	None
14	Gas
14B	Gas
15	ISO
16	ISO
17	ISO
18	None
19	ISO
20	ISO
21	ISO
22	ISO
23	None

Figure 101 depicts an overlay of the TICs from the sealed tile, unsealed tile, and carpet and padding to compare the ILR recoveries in each sample.

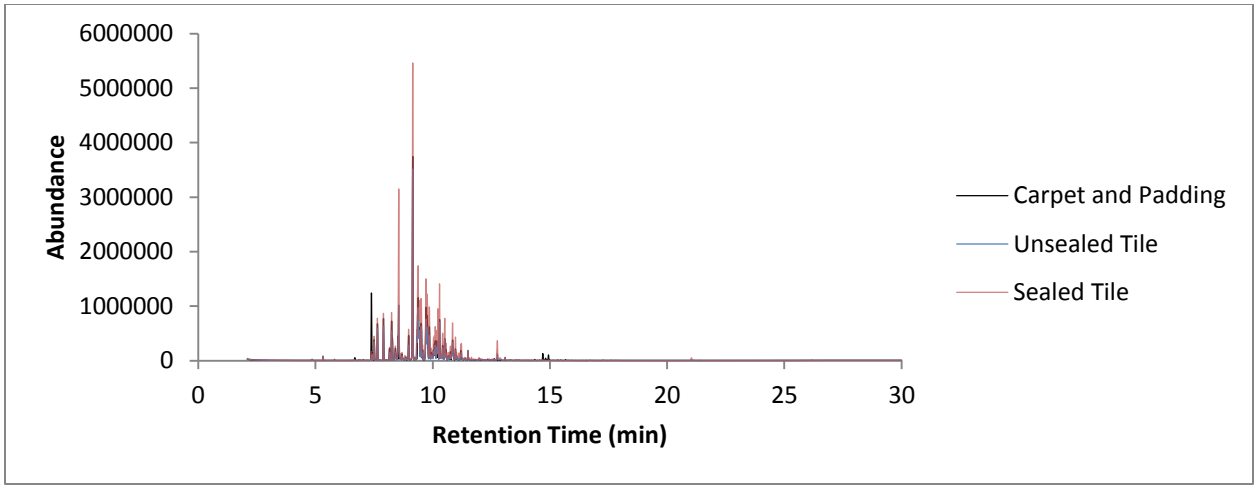

Figure 101: Container 12 Tile TIC Overlay

The correlation values obtained from the application of TFA of the data set of compiled TIS from each sample were used to calculate the posterior probabilities, which along with the median and average correlation values for each class, are summarized in Table 20, Table 21 and Table 22.

Application To Previous Experiments

Laboratory Test Burns

A series of laboratory burns were performed during previous research regarding the detection of IL from fire debris samples. The TIS from these fire debris samples for each test were combined and then TFA was performed on each test's data set. The correlation values were then used to calculate posterior probabilities in order to determine the class of ignitable liquid present. The results of the laboratory burns are compiled in Table 40, Table 41, and Table 42.

Table 43 summarizes the accuracy of each laboratory test burn.

Table 40: Median Correlation Values for Laboratory Test Burns

Test	IL Used	IL Identified											
		Gas	HAR	HPD	ISO	LAR	LPD	MAR	MISC	MPD	NAL	NP	OXY
T5	Gas	0.937	0.887	0.609	0.440	0.933	0.592	0.846	0.652	0.623	0.460	0.599	0.620
T6	LPD	0.623	0.044	0.461	0.265	0.319	0.369	0.478	0.407	0.389	0.292	0.366	0.337
T7	MPD	0.649	0.108	0.950	0.841	0.358	0.918	0.561	0.782	0.972	0.863	0.943	0.590
T8	OXY	0.566	0.449	0.881	0.873	0.444	0.862	0.265	0.792	0.920	0.800	0.921	0.738
T9	LAR	0.809	0.112	0.818	0.557	0.998	0.773	0.361	0.765	0.841	0.605	0.869	0.674
T10	NP	0.627	0.475	0.900	0.911	0.540	0.885	0.338	0.821	0.920	0.944	0.920	0.672
T11	HPD	0.664	0.841	0.945	0.763	0.285	0.780	0.566	0.759	0.876	0.797	0.884	0.523
T12	NAL	0.608	0.035	0.822	0.906	0.317	0.750	0.572	0.746	0.799	0.978	0.745	0.443
T13	NP	0.607	0.035	0.874	0.641	0.317	0.782	0.552	0.655	0.894	0.658	0.965	0.414
T14	MPD	0.601	-0.062	0.954	0.845	0.133	0.914	0.518	0.776	0.973	0.867	0.954	0.590
T15	NP	0.356	-0.028	0.820	0.958	0.038	0.825	-0.008	0.765	0.823	0.953	0.748	0.618
T16	LPD	0.647	-0.021	0.341	0.160	0.511	0.240	0.393	0.390	0.265	0.168	0.269	0.311
T17	MPD	0.492	-0.043	0.919	0.760	0.152	0.858	0.168	0.766	0.916	0.781	0.882	0.502
T18	HPD	0.503	0.539	0.705	0.496	0.193	0.509	0.235	0.531	0.580	0.527	0.571	0.346
T19	NAL	0.387	-0.026	0.843	0.900	0.079	0.754	0.068	0.771	0.807	0.959	0.757	0.468
T20	Gas	0.900	0.078	0.267	0.070	0.756	0.080	0.716	0.331	0.079	0.069	0.058	0.189
T21	NP	0.312	-0.077	0.912	0.701	0.038	0.847	-0.009	0.685	0.933	0.728	0.967	0.382
T22	OXY	0.450	-0.054	0.615	0.722	0.201	0.552	0.117	0.557	0.600	0.637	0.535	0.431
T23	NP	0.646	0.025	0.831	0.906	0.471	0.821	0.349	0.766	0.820	0.930	0.745	0.539
T24	MAR	0.812	-0.078	0.678	0.550	0.400	0.628	0.899	0.641	0.660	0.573	0.624	0.460
T25	Gas	0.890	0.094	0.256	0.059	0.723	0.051	0.737	0.300	0.052	0.053	0.029	0.121
T26	Gas	0.915	0.010	0.298	0.129	0.757	0.137	0.696	0.355	0.140	0.121	0.111	0.198
T27	Gas	0.858	0.000	0.283	0.121	0.834	0.145	0.542	0.357	0.153	0.115	0.146	0.226
T28	Gas	0.838	-0.024	0.286	0.144	0.789	0.173	0.524	0.367	0.174	0.141	0.162	0.284
T29	LPD	0.674	0.054	0.481	0.271	0.412	0.367	0.516	0.483	0.404	0.294	0.388	0.393
T30	MPD	0.583	-0.030	0.934	0.861	0.425	0.899	0.341	0.821	0.954	0.883	0.903	0.558
T31	MAR	0.739	-0.048	0.254	0.126	0.435	0.187	0.896	0.326	0.219	0.134	0.237	0.252

Test	IL Used	IL Identified											
		Gas	HAR	HPD	ISO	LAR	LPD	MAR	MISC	MPD	NAL	NP	OXY
T32	OXY	0.723	0.001	0.538	0.586	0.676	0.506	0.308	0.585	0.523	0.526	0.452	0.573
T33	NAL	0.352	-0.042	0.827	0.891	0.066	0.749	0.013	0.758	0.797	0.951	0.756	0.464
T34	NP	0.434	-0.072	0.880	0.690	0.116	0.800	0.125	0.694	0.885	0.719	0.900	0.436
T35	HPD	0.622	0.037	0.753	0.547	0.349	0.594	0.308	0.649	0.665	0.569	0.667	0.444
T36	Gas	0.937	0.029	0.275	0.158	0.874	0.220	0.864	0.370	0.199	0.177	0.162	0.593
T37	NONE	0.173	-0.020	0.178	0.143	0.043	0.199	0.005	0.175	0.185	0.174	0.173	0.252
T38	Gas	0.848	0.090	0.281	0.073	0.495	0.072	0.804	0.241	0.074	0.070	0.046	0.126
T39	Gas	0.875	0.141	0.338	0.120	0.562	0.122	0.785	0.302	0.126	0.121	0.097	0.167
T40	OXY	0.795	-0.046	0.752	0.620	0.538	0.646	0.362	0.696	0.681	0.636	0.627	0.561
T41	OXY	0.274	-0.067	0.692	0.539	-0.024	0.826	-0.039	0.577	0.771	0.569	0.713	0.374
T42	Gas	0.745	0.034	0.831	0.601	0.866	0.844	0.278	0.788	0.863	0.646	0.866	0.700
T43	Gas	0.883	0.202	0.894	0.803	0.727	0.808	0.701	0.810	0.876	0.798	0.825	0.610
T44	NP	0.801	0.002	0.907	0.818	0.831	0.895	0.363	0.847	0.921	0.851	0.886	0.710
T45	Gas & MPD	0.883	0.202	0.894	0.803	0.727	0.808	0.701	0.810	0.876	0.798	0.825	0.610

Table 41: Average Correlation Values for Laboratory Test Burns

Test	IL Used	IL Identified											
		Gas	HAR	HPD	ISO	LAR	LPD	MAR	MISC	MPD	NAL	NP	OXY
T5	Gas	0.937	0.887	0.609	0.440	0.933	0.592	0.846	0.652	0.623	0.460	0.599	0.620
T6	LPD	0.606	0.078	0.456	0.274	0.272	0.361	0.429	0.407	0.427	0.297	0.370	0.324
T7	MPD	0.649	0.141	0.940	0.846	0.297	0.888	0.488	0.728	0.967	0.862	0.938	0.619
T8	OXY	0.580	0.459	0.877	0.864	0.440	0.843	0.287	0.707	0.908	0.803	0.915	0.698
T9	LAR	0.756	0.164	0.815	0.578	0.902	0.737	0.392	0.708	0.839	0.609	0.865	0.618
T10	NP	0.639	0.488	0.902	0.915	0.528	0.880	0.362	0.740	0.915	0.945	0.911	0.663
T11	HPD	0.667	0.741	0.939	0.767	0.235	0.758	0.505	0.699	0.877	0.798	0.885	0.533
T12	NAL	0.606	0.047	0.831	0.897	0.257	0.743	0.503	0.644	0.795	0.974	0.741	0.449
T13	NP	0.612	0.064	0.871	0.658	0.262	0.752	0.488	0.651	0.892	0.664	0.959	0.456
T14	MPD	0.599	-0.029	0.947	0.849	0.108	0.881	0.518	0.709	0.968	0.867	0.949	0.610
T15	NP	0.366	0.000	0.827	0.947	0.048	0.809	0.043	0.606	0.815	0.956	0.748	0.586
T16	LPD	0.607	-0.011	0.340	0.165	0.520	0.240	0.389	0.424	0.297	0.170	0.274	0.326
T17	MPD	0.505	-0.039	0.912	0.767	0.154	0.829	0.179	0.686	0.916	0.782	0.879	0.477
T18	HPD	0.506	0.479	0.700	0.500	0.186	0.501	0.232	0.500	0.590	0.527	0.573	0.336
T19	NAL	0.393	-0.022	0.849	0.892	0.085	0.750	0.082	0.616	0.805	0.958	0.755	0.442
T20	Gas	0.868	0.075	0.246	0.071	0.695	0.086	0.702	0.358	0.164	0.070	0.070	0.271
T21	NP	0.332	-0.073	0.907	0.715	0.046	0.816	0.017	0.637	0.927	0.726	0.963	0.424
T22	OXY	0.438	-0.040	0.611	0.704	0.209	0.552	0.131	0.521	0.600	0.645	0.532	0.477
T23	NP	0.632	0.036	0.834	0.904	0.449	0.806	0.356	0.697	0.817	0.933	0.744	0.533
T24	MAR	0.789	-0.086	0.676	0.558	0.359	0.627	0.768	0.621	0.670	0.576	0.626	0.439
T25	Gas	0.861	0.088	0.232	0.057	0.653	0.057	0.733	0.329	0.142	0.054	0.044	0.234
T26	Gas	0.862	0.008	0.287	0.129	0.697	0.142	0.675	0.388	0.217	0.124	0.122	0.299
T27	Gas	0.796	-0.002	0.274	0.121	0.806	0.151	0.542	0.415	0.215	0.115	0.154	0.323
T28	Gas	0.779	-0.020	0.283	0.146	0.769	0.179	0.516	0.428	0.231	0.142	0.168	0.359
T29	LPD	0.653	0.077	0.477	0.282	0.411	0.357	0.473	0.493	0.443	0.297	0.392	0.363
T30	MPD	0.581	-0.013	0.926	0.864	0.437	0.884	0.330	0.765	0.947	0.882	0.900	0.552
T31	MAR	0.719	-0.042	0.265	0.131	0.433	0.187	0.751	0.400	0.249	0.135	0.238	0.281

Test	IL Used	IL Identified											
		Gas	HAR	HPD	ISO	LAR	LPD	MAR	MISC	MPD	NAL	NP	OXY
T32	OXY	0.686	0.007	0.537	0.574	0.693	0.508	0.336	0.615	0.527	0.531	0.453	0.524
T33	NAL	0.356	-0.044	0.834	0.884	0.083	0.745	0.041	0.611	0.794	0.950	0.753	0.442
T34	NP	0.433	-0.061	0.879	0.702	0.118	0.769	0.123	0.654	0.881	0.719	0.896	0.443
T35	HPD	0.616	0.034	0.744	0.552	0.352	0.582	0.313	0.626	0.682	0.570	0.669	0.432
T36	Gas	0.907	0.070	0.272	0.165	0.865	0.225	0.802	0.472	0.241	0.180	0.169	0.537
T37	NONE	0.231	0.018	0.184	0.152	0.052	0.201	0.038	0.193	0.191	0.180	0.171	0.347
T38	Gas	0.824	0.087	0.262	0.072	0.436	0.075	0.780	0.302	0.168	0.071	0.061	0.203
T39	Gas	0.850	0.132	0.316	0.120	0.497	0.125	0.740	0.348	0.215	0.121	0.113	0.245
T40	OXY	0.762	-0.040	0.746	0.621	0.547	0.643	0.384	0.665	0.705	0.637	0.630	0.527
T41	OXY	0.272	-0.067	0.686	0.564	-0.013	0.809	-0.017	0.504	0.757	0.575	0.707	0.420
T42	Gas	0.713	0.065	0.827	0.625	0.871	0.821	0.344	0.737	0.860	0.648	0.862	0.639
T43	Gas	0.869	0.198	0.895	0.799	0.691	0.799	0.653	0.765	0.883	0.799	0.828	0.566
T44	NP	0.746	0.015	0.895	0.829	0.830	0.887	0.395	0.782	0.916	0.853	0.885	0.636
T45	Gas & MPD	0.869	0.198	0.895	0.799	0.691	0.799	0.653	0.765	0.883	0.799	0.828	0.566

Table 42: Posterior Probabilities for Laboratory Test Burns

Test	IL Used	IL Identified											
		Gas	HAR	HPD	ISO	LAR	LPD	MAR	MISC	MPD	NAL	NP	OXY
T5	Gas	0.525	0.131	0.000	0.000	0.000	0.301	0.021	0.006	0.000	0.000	0.000	0.016
T6	LPD	0.000	0.000	0.000	0.000	0.000	0.000	1.000	0.000	0.000	0.000	0.000	0.000
T7	MPD	0.000	0.000	0.191	0.004	0.042	0.000	0.000	0.090	0.499	0.000	0.155	0.019
T8	OXY	0.008	0.000	0.012	0.013	0.002	0.000	0.000	0.045	0.242	0.000	0.260	0.418
T9	LAR	0.000	0.000	0.000	0.000	0.000	0.961	0.000	0.030	0.000	0.000	0.000	0.008
T10	NP	0.000	0.000	0.060	0.229	0.016	0.000	0.000	0.031	0.131	0.466	0.064	0.003
T11	HPD	0.062	0.002	0.778	0.000	0.000	0.000	0.000	0.070	0.008	0.000	0.066	0.015
T12	NAL	0.000	0.000	0.003	0.036	0.000	0.000	0.000	0.002	0.000	0.959	0.000	0.000
T13	NP	0.000	0.000	0.010	0.000	0.002	0.000	0.000	0.048	0.104	0.000	0.829	0.007
T14	MPD	0.000	0.000	0.215	0.004	0.019	0.000	0.000	0.085	0.440	0.000	0.221	0.017
T15	NP	0.000	0.000	0.002	0.480	0.003	0.000	0.000	0.024	0.002	0.485	0.000	0.005
T16	LPD	0.000	0.000	0.000	0.000	0.000	0.000	0.000	1.000	0.000	0.000	0.000	0.000
T17	MPD	0.000	0.000	0.369	0.000	0.001	0.000	0.000	0.143	0.447	0.000	0.026	0.014
T18	HPD	0.000	0.000	0.354	0.000	0.000	0.000	0.000	0.646	0.000	0.000	0.000	0.000
T19	NAL	0.000	0.000	0.009	0.035	0.000	0.000	0.000	0.006	0.000	0.950	0.000	0.000
T20	Gas	0.997	0.000	0.000	0.000	0.000	0.000	0.003	0.000	0.000	0.000	0.000	0.000
T21	NP	0.000	0.000	0.053	0.000	0.003	0.000	0.000	0.065	0.231	0.000	0.635	0.014
T22	OXY	0.000	0.000	0.000	0.000	0.000	0.000	0.000	0.000	0.000	0.000	0.000	1.000
T23	NP	0.000	0.000	0.001	0.408	0.012	0.000	0.000	0.007	0.001	0.570	0.000	0.000
T24	MAR	0.000	0.000	0.000	0.000	0.000	0.000	0.900	0.100	0.000	0.000	0.000	0.000
T25	Gas	0.998	0.000	0.000	0.000	0.000	0.000	0.002	0.000	0.000	0.000	0.000	0.000
T26	Gas	0.999	0.000	0.000	0.000	0.000	0.000	0.001	0.000	0.000	0.000	0.000	0.000
T27	Gas	1.000	0.000	0.000	0.000	0.000	0.000	0.000	0.000	0.000	0.000	0.000	0.000
T28	Gas	1.000	0.000	0.000	0.000	0.000	0.000	0.000	0.000	0.000	0.000	0.000	0.000
T29	LPD	0.000	0.000	0.000	0.000	0.000	0.000	0.000	1.000	0.000	0.000	0.000	0.000
T30	MPD	0.000	0.000	0.219	0.004	0.062	0.000	0.000	0.096	0.549	0.001	0.039	0.029
T31	MAR	0.000	0.000	0.000	0.000	0.000	0.000	1.000	0.000	0.000	0.000	0.000	0.000

Test	IL Used	IL Identified											
		Gas	HAR	HPD	ISO	LAR	LPD	MAR	MISC	MPD	NAL	NP	OXY
T32	OXY	0.000	0.000	0.000	0.000	0.000	0.000	0.000	0.994	0.000	0.000	0.000	0.005
T33	NAL	0.000	0.000	0.005	0.024	0.000	0.000	0.000	0.010	0.000	0.961	0.000	0.000
T34	NP	0.000	0.000	0.224	0.000	0.000	0.000	0.000	0.160	0.213	0.000	0.356	0.047
T35	HPD	0.000	0.000	0.003	0.000	0.000	0.000	0.000	0.997	0.000	0.000	0.000	0.000
T36	Gas	0.895	0.000	0.000	0.000	0.000	0.001	0.070	0.008	0.000	0.000	0.000	0.027
T37	NONE	0.000	0.000	0.000	0.000	0.000	0.000	0.000	0.000	0.000	0.000	0.000	0.000
T38	Gas	0.999	0.000	0.000	0.000	0.000	0.000	0.001	0.001	0.000	0.000	0.000	0.000
T39	Gas	1.000	0.000	0.000	0.000	0.000	0.000	0.000	0.000	0.000	0.000	0.000	0.000
T40	OXY	0.224	0.000	0.000	0.000	0.000	0.000	0.000	0.381	0.000	0.000	0.000	0.395
T41	OXY	0.000	0.000	0.000	0.000	0.000	0.000	0.000	0.000	0.000	0.000	0.000	1.000
T42	Gas	0.002	0.000	0.003	0.000	0.005	0.060	0.000	0.685	0.073	0.000	0.023	0.148
T43	Gas	0.090	0.000	0.283	0.000	0.000	0.000	0.000	0.157	0.457	0.000	0.009	0.004
T44	NP	0.001	0.000	0.134	0.004	0.186	0.000	0.000	0.106	0.503	0.000	0.043	0.023
T45	Gas & MPD	0.090	0.000	0.283	0.000	0.000	0.000	0.000	0.157	0.457	0.000	0.009	0.004

Table 43: Summary of Results for Laboratory Tests

Test	IL Present	IL Identified
5	Gas	Gas
6	LPD	MAR
7	MPD	MPD
8	OXY	OXY
9	LAR	LAR
10	NP	NAL
11	HPD	HPD
12	NAL	NAL
13	NP	NP
14	MPD	MPD
15	NP	NAL
16	LPD	MISC
17	MPD	MPD
18	HPD	MISC
19	NAL	NAL
20	Gas	Gas
21	NP	NP
22	OXY	OXY
23	NP	NAL
24	MAR	MAR
25	Gas	Gas
26	Gas	Gas
27	Gas	Gas
28	Gas	Gas
29	LPD	MISC
30	MPD	MPD
31	MAR	MAR
32	OXY	MISC
33	NAL	NAL
34	NP	NP
35	HPD	MISC
36	Gas	Gas
37	None	None
38	Gas	Gas
39	Gas	Gas
40	OXY	OXY
41	OXY	OXY
42	Gas	MISC
43	Gas	MPD
44	NP	MPD
45	MPD/Gas	MPD

Large Scale Experimental Burns

The method of determining the class of IL present by calculating posterior probabilities was applied to the initial set of 4 containers that were burned. The individual tables summarizing the median and average correlation values and the calculated posterior probabilities are tabulated in Table 44, Table 45 and Table 46, respectively. The IL class identification results are summarized in Table 47.

Table 44: Median Correlation Values for Previously Burned Containers

Container	IL Used	IL Identified											
		Gas	HAR	HPD	ISO	LPD	LAR	MAR	MISC	MPD	NAL	NP	OXY
C1	Gas	0.952	0.332	0.885	0.673	0.614	0.840	0.816	0.822	0.896	0.694	0.898	0.650
C2	Gas	0.880	0.348	0.759	0.549	0.592	0.693	0.849	0.704	0.731	0.598	0.714	0.545
C2	MPD	0.943	0.064	0.950	0.737	0.732	0.905	0.729	0.831	0.967	0.759	0.967	0.615
C3	MPD	0.714	-0.063	0.949	0.797	0.354	0.862	0.320	0.801	0.928	0.813	0.893	0.647
C4	OXY	0.665	-0.004	0.932	0.772	0.243	0.871	0.236	0.774	0.918	0.803	0.871	0.561

Table 45: Average Correlation Values for Previously Burned Containers

Container	IL Used	IL Identified											
		Gas	HAR	HPD	ISO	LAR	LPD	MAR	MISC	MPD	NAL	NP	OXY
C1	Gas	0.936	0.371	0.881	0.690	0.565	0.820	0.769	0.767	0.894	0.695	0.893	0.648
C2	Gas	0.859	0.325	0.748	0.561	0.492	0.675	0.795	0.657	0.737	0.604	0.712	0.528
C2	MPD	0.934	0.085	0.947	0.750	0.653	0.870	0.724	0.784	0.966	0.758	0.962	0.626
C3	MPD	0.680	0.000	0.948	0.803	0.337	0.845	0.330	0.730	0.939	0.814	0.896	0.645
C4	OXY	0.629	0.073	0.930	0.779	0.220	0.851	0.247	0.699	0.923	0.803	0.870	0.574

Table 46: Posterior Probabilities for Previously Burned Containers

Container	IL Used	IL Identified											
		Gas	HAR	HPD	ISO	LAR	LPD	MAR	MISC	MPD	NAL	NP	OXY
C1	Gas	0.945	0.000	0.012	0.000	0.000	0.000	0.000	0.000	0.020	0.000	0.012	0.001
C2	Gas	0.998	0.000	0.000	0.000	0.000	0.000	0.000	0.001	0.000	0.000	0.000	0.000
C2	MPD	0.146	0.000	0.187	0.000	0.000	0.010	0.000	0.000	0.308	0.000	0.270	0.000
C3	MPD	0.000	0.000	0.467	0.000	0.000	0.000	0.000	0.000	0.364	0.000	0.051	0.000
C4	OXY	0.000	0.000	0.476	0.000	0.000	0.002	0.000	0.000	0.383	0.000	0.041	0.000

Table 47: Summary of Classification Results for Containers 1-4

Container	IL Present	IL Identified
1	Gas	Gas
2 Burn 1	Gas	Gas
2 Burn 2	MPD	MPD
3	MPD	HPD
4	OXY	HPD

The results from the previous set of burns in combination with Containers 5 through Container 12 are summarized below, in Table 48. Overall, the classification system has a 69% accuracy rate for large scale laboratory burns.

Table 48: Summary of Classification Results for Containers 1-12

Container	IL Present	IL Identified
1	Gas	Gas
2 Burn 1	Gas	Gas
2 Burn 2	MPD	MPD
3	MPD	HPD
4	OXY	HPD
5	Gas	Gas
6	Gas	Gas
7	Gas/MPD	MPD
8	Gas/MPD	OXY
9	Gas & HPD	NP
10	LPD	LPD
11	NP	NP
12	ISO	ISO

Limited Sample Large Scale Experimental Burns

Certain sample TICs had a significant ignitable pattern identified after pattern recognition and target compound identification per the guidelines in ASTM E1618. Samples identified as having a strong ILR pattern based on the ASTM E1618 guidelines were omitted from the data set, as well as the corresponding TISs analyzed by TFA to calculate correlation values. The correlation

values obtained from TFA analysis of this reduced-sample data set were then used to calculate posterior probabilities for each class as being present in the fire debris. The samples omitted from the limited sample trials are tabulated in Table 49, based on those samples that had a significant IL pattern.

Table 49: List of Omitted Samples from Containers 5-12

Container	Omitted Samples
5*	1B, 5B, 6
6*	14, 18, 20, 24, 25
7*	2, 5, 7, 10
8*	24
9*	3, 4, 8, 9, 10
10*	19
11*	3, 4, 10
12*	15, 16, 17, 19

The class median and average correlation values from the analysis of the limited sample data sets from the large scale burns are compiled in Table 50 and Table 51, respectively. The calculated class posterior probabilities are compiled in Table 52.

Table 50: Median Values for Large Scale Burns with Limited Samples

Container	IL Used	IL Identified											
		Gas	HAR	HPD	ISO	LAR	LPD	MAR	MISC	MPD	NAL	NP	OXY
C5*	Gas	0.978	0.133	0.875	0.727	0.947	0.896	0.831	0.864	0.903	0.782	0.859	0.807
C6*	Gas	0.910	-0.004	0.392	0.213	0.531	0.274	0.815	0.381	0.280	0.218	0.257	0.411
C7*	Gas/MPD	0.939	0.072	0.974	0.898	0.589	0.925	0.835	0.897	0.990	0.922	0.990	0.699
C8*	Gas/MPD	0.965	0.608	0.866	0.629	0.848	0.888	0.925	0.875	0.907	0.688	0.905	0.849
C9*	Gas & HPD	0.832	0.036	0.791	0.617	0.542	0.826	0.652	0.747	0.812	0.651	0.751	0.627
C10*	LPD	0.555	-0.052	0.860	0.694	0.172	0.878	0.091	0.769	0.882	0.727	0.853	0.653
C11*	NP	0.140	-0.004	0.120	0.106	0.041	0.140	0.009	0.128	0.135	0.119	0.118	0.169
C12*	ISO	0.850	-0.019	0.884	0.982	0.489	0.823	0.648	0.818	0.873	0.932	0.791	0.561

Table 51: Average Correlation Values for Large Scale Burns with Limited Samples

Container	IL Used	IL Identified											
		Gas	HAR	HPD	ISO	LAR	LPD	MAR	MISC	MPD	NAL	NP	OXY
C5*	Gas	0.962	0.142	0.874	0.745	0.930	0.871	0.818	0.809	0.899	0.783	0.850	0.739
C6*	Gas	0.871	0.025	0.384	0.217	0.462	0.268	0.781	0.435	0.344	0.220	0.263	0.442
C7*	Gas/MPD	0.923	0.109	0.966	0.896	0.576	0.894	0.815	0.839	0.989	0.921	0.987	0.710
C8*	Gas/MPD	0.955	0.581	0.868	0.657	0.853	0.853	0.879	0.844	0.906	0.690	0.904	0.808
C9*	Gas & HPD	0.827	0.061	0.789	0.633	0.471	0.817	0.626	0.703	0.819	0.654	0.747	0.610
C10*	LPD	0.516	0.005	0.852	0.707	0.185	0.858	0.119	0.695	0.880	0.731	0.847	0.617
C11*	NP	0.207	0.043	0.128	0.110	0.047	0.145	0.032	0.146	0.139	0.124	0.119	0.235
C12*	ISO	0.832	-0.012	0.882	0.960	0.440	0.827	0.645	0.747	0.871	0.934	0.792	0.560

Table 52: Posterior Probabilities for Large Scale Burns with Limited Samples

Container	IL Used	IL Identified											
		Gas	HAR	HPD	ISO	LAR	LPD	MAR	MISC	MPD	NAL	NP	OXY
C5*	Gas	0.745	0.000	0.002	0.000	0.159	0.007	0.000	0.027	0.010	0.000	0.000	0.000
C6*	Gas	0.975	0.000	0.000	0.000	0.000	0.000	0.000	0.000	0.000	0.000	0.000	0.000
C7*	Gas/MPD	0.073	0.000	0.194	0.011	0.000	0.023	0.000	0.081	0.298	0.011	0.294	0.000
C8*	Gas/MPD	0.761	0.000	0.003	0.000	0.000	0.004	0.083	0.052	0.030	0.000	0.018	0.049
C9*	Gas & HPD	0.000	0.000	0.000	0.000	0.000	0.000	0.000	0.000	0.000	0.000	0.000	0.003
C10*	LPD	0.000	0.000	0.088	0.000	0.000	0.106	0.000	0.000	0.236	0.000	0.003	0.000
C11*	NP	0.000	0.000	0.000	0.000	0.000	0.000	0.000	0.000	0.000	0.000	0.000	0.000
C12*	ISO	0.001	0.000	0.015	0.756	0.000	0.001	0.000	0.000	0.026	0.143	0.000	0.000

The results of the limited sample tests are summarized in Table 53, and had an accuracy rate of 86% in identifying and classifying the class of ignitable liquid in fire debris samples using only a portion of the total samples collected.

Table 53: Summary of Classification Results for Large Scale Burns with Limited Samples

Container	IL Present	IL Identified
5*	Gas	Gas
6*	Gas	Gas
7*	Gas/MPD	MPD
8*	Gas/MPD	Gas
9*	Gas & HPD	Gas
10*	LPD	MISC
11*	NP	None
12*	ISO	ISO

Table 54 summarizes the results of tests from Containers 5-12, the limited-sample tests from Containers 5-12, and the previously burned Containers 1-4. The accuracy rate of these collective tests was 74% for the detection and correct classification of a class of ignitable liquid.

Table 54: Combined Summary of Results for Containers 1-12

Container	IL Present	IL Identified
1	Gas	Gas
2 Burn 1	Gas	Gas
2 Burn 2	MPD	MPD
3	MPD	HPD
4	OXY	HPD
5	Gas	Gas
5*	Gas	Gas
6	Gas	Gas
6*	Gas	Gas
7	Gas/MPD	MPD
7*	Gas/MPD	MPD
8	Gas/MPD	OXY
8*	Gas/MPD	Gas
9	Gas & HPD	NP
9*	Gas & HPD	Gas
10	LPD	LPD
10*	LPD	MISC
11	NP	NP
11*	NP	None
12	ISO	ISO
12*	ISO	ISO

* Test with limited samples.

CHAPTER 4
DISCUSSION

The detection and classification model was evaluated based on the results for the computer simulations and large scale burns. For instances resulting in an incorrect classification, the class of ignitable liquid identified was compared to the class of ignitable liquid present. The average TIS for each IL class was compared against the other ASTM-defined IL classes, and a Pearson correlation value was calculated. The correlation values for the average TIS for each class comparison are compiled in Table 55. The aromatic class was subclassified into light (LtAR), medium (MedAR) and heavy (HeAR) aromatics. The petroleum distillates and aromatic classes were compared as an entire combined class as well as based on the subclasses.

Table 55: IL Class Similarities of Average TIS

	Gas	HeAR	HPD	ISO	LPD	LtAR	MedAR	MPD	NAL	NP	OXY	AR
Gas												
HeAR	0.041											
HPD	0.433	-0.019										
ISO	0.284	-0.057	0.858									
LPD	0.311	-0.097	0.882	0.833								
LtAR	0.673	-0.014	0.049	-0.025	-0.017							
MedAR	0.836	0.015	0.144	-0.023	-0.030	0.398						
MPD	0.360	-0.095	0.970	0.843	0.936	0.003	0.057					
NAL	0.269	-0.046	0.870	0.953	0.823	-0.027	-0.027	0.837				
NP	0.251	-0.103	0.949	0.773	0.859	-0.029	-0.040	0.966	0.774			
OXY	0.572	-0.061	0.574	0.554	0.626	0.410	0.186	0.578	0.560	0.493		
AR	0.831	0.316	0.087	-0.045	-0.055	0.8676	0.695	-0.005	-0.046	-0.071	0.347	
PD	0.366	-0.079	0.964	0.863	0.972	0.0063	0.043	0.989	0.860	0.940	0.612	-0.003

Computer Simulation Models

The use of computer simulations allowed for fast analysis of data sets that were generated under specific parameters. Each IL class was tested individually over a range of percent IL contributions per sample, and total number of samples per data set that contained an IL contribution.

The aromatic product class (AR) had a narrow range of percent IL contribution and number of spectra with an IL contribution that resulted in a correct classification. Aromatic products are composed of aromatic and condensed ring aromatic compounds with no significant contributions from alkanes or cycloalkanes. Without subclassification, the aromatic class has a high degree of variation among ILs. Specifically, variation in carbon ranges among AR ILs results in TISs that are significantly different even though the TISs come from ILs within the same AR class. This may explain why correct classifications were only observed for simulations having at least an 80% IL contribution in 11 of the 12 samples, and simulations having a 95% contribution in 9 of 12 samples. The TIS of ignitable liquids in this class were grouped based on the carbon range to determine an average TIS for each of the subclassifications: light, medium and heavy. The average TIS for the subclasses were not highly correlated ($r<0.4$ for each subclass), which explains the need for a high percent contribution of ignitable liquid in the sample set to achieve a correct classification. Subclassification of AR ILs has been previously shown to improve correct classification rates.[29] In future classification tests, the AR class was subclassified based on the established carbon ranges in ASTM E1618.

In the gasoline simulations, gasoline was correctly identified in simulations with low percent IL contributions and when gasoline was in a small percentage of samples in the data set. Gasoline contains a blend of compounds including alkylbenzenes, naphthalenes, indanes and other aromatic and alkane products which is unlike other classes of ILs that go through additional refining processes, see Figure 1.[4] This makes the TIC and TIS profiles of gasoline ILs unique in comparison to ILs from other ASTM IL classes. Therefore, a correct classification for the gasoline class can be achieved with a relatively low percent IL contribution.

In the petroleum distillate subclass computer simulations, the HPD class could be correctly identified down to a 30% IL contribution in 4 of the 12 samples. It is possible that some incorrect classifications occurred when the classification model identified either LPD or MPD as the correct class rather than HPD. The MPD subclass simulations required only a small percent IL contribution in the spectra for a correct classification. Posterior probabilities indicated a correct classification in simulations with an MPD contribution down to 15% in 2 of the 12 samples. The LPD subclass was correctly identified in simulation trials down to an IL contribution of 45% in 3 of the 12 samples.

The results of the ISO class simulations indicated that as the percent IL contribution increased, the number of spectra with an IL contribution required for a correct classification decreased. The classification model correctly identified ISO in simulations having a 35% IL contribution in 10 of the 12 samples and in simulations having an 85% IL contribution in 3 of the 12 samples.

The NAL class simulations consistently resulted in correct classifications when a minimum of 3 samples of the 12 total contained at least a 45% IL contribution. Ignitable liquids in this class are composed mainly of normal-alkanes, with little contributions of branched-chain alkanes, cycloalkanes, and aromatic products. This produces a spectrum that is relatively unique in comparison to the other classes that have ignitable liquids containing these products.

Computer simulations using ILs from the NP class resulted in correct classifications in simulations that had a 40% IL contribution in 5 of the 12 samples. The TIC profile of an NP IL is characterized by the presence of isoalkanes and cycloalkanes, similar to a dearomatized PD TIC if the alkane peaks were absent. Even though ILs in the NP class are similar to each other in composition, the average TIS of the NP and PD classes are highly correlated, r=0.94.

The results of the simulations for the OXY class were inconsistent with expectations. When 5 to 11 of the 12 spectra have a 20 to 60% IL contribution, the classification method correctly identified the OXY class. However, when the percent IL contribution was 95% in 4 to 10 of the samples, an incorrect class was identified. Based on prior class simulations, incorrect classifications at this high of a percent IL contribution in that percentage of spectra were not expected. In simulations that had samples comprised of only substrates and no IL contribution, the classification method still identified the OXY class. This may be due to the broad range of correlation coefficients for OXY ILs. The OXY class includes a broad range ILs and their TIS patterns. Therefore, the range of correlation coefficients is also broad.

Further investigation into the subclassification or reclassification of OXY ILs may be necessary to lower the misclassification rate for the OXY class.

For the MISC group simulation test, no simulations resulted in a correct classification. This was most likely a result of the large variation among ILs within this group. There are no unique compounds or ions that could be used to distinguish a MISC IL from an IL in any other class. Also, there are no specific criteria for an IL to be classified in the MISC class. Therefore, the MISC class should not be treated as a class like the other ASTM-defined classes.

Large Scale Experimental Burns

From analysis of the large scale burns, the classification method had a 75% accuracy rate. This classification method may be advantageous since it eliminates the subjective nature of identification based on visual pattern recognition, which relies heavily on analyst discretion and experience.

Ignitable Liquid Detection and Classification

Gasoline was used as the ignitable liquid in Container 5. The gasoline class was correctly identified as the class of ignitable liquid present. It had the highest median and average class correlation values, and the highest posterior probability compared to the other IL classes, as well as the highest, see Table 20, Table 21, and Table 22.

The ignitable liquid used in Container 6 was gasoline. The gasoline class was correctly identified based on highest posterior probability value, see Table 22.

Container 7 contained two trails of ILs from different ignitable liquid classes, the MPD and gasoline classes. The MPD subclass had the highest posterior probability value. The highest median and average correlation values corresponded to the HPD subclass. HPD and MPD are subclasses of the PD class. The preferential loss of lighter components is possible given the high temperatures, over 800 °C, reached in the container during the burn. If an MPD loses some of the lighter components, the remaining heavier components may result in a chromatogram and TIS that is more indicative of an IL in the HPD subclass. This could account for the median and average correlation values in the HPD class being higher than the MPD class. The next two classes with the highest median and average correlation values were gasoline and MPD, which were both used as ignitable liquids in the burn.

The oxygenated solvent class was incorrectly identified as the IL present in Container 8. The classes of ILs used in this burn were gasoline and MPD. However, the highest median and average correlation values corresponded to the HPD subclass, see Table 20 and Table 21. Again, weathering could have caused an MPD ILR in the sample to resemble an HPD more than an MPD. Only a few samples had a strong IL pattern in the TICs, see Table 31, resulting in a limited contribution of IL to the total data set. This complicated the determination of the ignitable liquid class present and resulted in a misclassification. Comparing the median correlation values, none of the ignitable liquid classes had a median correlation value that was greater than 0.85. If a minimum median correlation value was

required for calculation of the posterior probability, the posterior probabilities for all of the IL classes in Container 8 would not have been calculated. The final classification would have been "undetermined" or "unable to classify", rather than the incorrect classification of OXY. The use of a median cutoff value should be explored in future work.

A 50:50 mixture of gasoline and an HPD was used as the ignitable liquid in Container 9; however the NP class was incorrectly identified. The NP class of ignitable liquids is comprised of cyclohexane-based products, charcoal starters, lamp oils, and insecticides. This class is characterized by predominant branched chain and cyclic alkanes, with a limited presence of aromatic and condensed ring aromatic products.[3] The similarities between the NP and PD classes (LPD, MPD, and HPD) include abundant alkanes and cycloalkanes. The average TIS from the NP and PD classes were highly similar, with a correlation value of r=0.94. Although the classification system identified the NP class as being present, it also calculated relatively high probabilities for gasoline and HPD. However, an analyst may also have encountered the same problem when looking at TICs of the samples collected, specifically samples 3, 4, 8, 9, and 10. Based on visual pattern recognition and target compound identification, an analyst identifying the IL class present may be hesitant to assign two IL classes. In this case, the analyst may identify one of the two classes, or a class like MISC which includes ignitable liquids that do not clearly fall into one of the 7 ASTM-defined classes.

In Container 10, the posterior probability correctly identified LPD as the class of ignitable liquid present. The median correlation also corresponded to an LPD.

Container 11 was burned using a NP ignitable liquid. This class had the highest median and average correlation values, as well as the highest posterior probability value, see Table 20, Table 21, and Table 22. The MPD class had the second highest posterior probability, median and average class correlation values. The average TIS from ignitable liquids in the NP and HPD classes had a correlation value of 0.95. This high degree of similarity between the TIS of ignitable liquids in these two classes explains the misclassification of Container 9 as containing a NP IL when it actually contained an HPD IL.

Container 12 contained an isoparaffinic ignitable liquid (ISO). The posterior probability and average and median correlation values identified isoparaffinic liquids as the correct class of IL present.

Gasoline Recovery

In Containers 9-12, an experiment was performed to test the ability to recover gasoline introduced to the scene by walking through each container after stepping in gasoline. The TIC profiles of the samples collected from each of the four containers as part of the gasoline recovery experiment showed no apparent gasoline pattern. Using ASTM E-1618 guidelines, gasoline was not detected from the fire debris samples collected at the site of gasoline exposure.

Sealant Effects

The effects of sealant on tile and grout were also tested in Containers 9-12. The experiment was designed to test the ability to recover ILs from tile and grout samples with and without a sealant. Tile that had been sealed should be resistant to the absorption of ignitable liquid into the pores of the tile. The recovery of ignitable liquids from sealed tile would most likely be limited since the ignitable liquid was not absorbed into the tile. In contrast, an IL poured on unsealed tile could have been absorbed into the pores of the tile and remain in the sample post burn. As a result, unsealed tile and grout may have a more abundant ILR concentration resulting in a stronger IL pattern in the TIC. The chromatograms of the tile from Container 9 have been combined, see Figure 83. Contrary to expectations, the TIC overlay for the tile samples in Container 9 showed that the sealed tile had a more abundant IL signature that the unsealed tile and the carpet and padding collected around and under the tile blocks. The ceiling fell on the samples during the course of the burn, possibly shielding the tile blocks from the fire. The TIC of the unsealed tile in Container 10, see Sample 10-22 in Figure 280, showed an ignitable liquid pattern consistent with an LPD. Figure 91 is an overlay of unsealed tile, sealed tile, and carpet and padding TICs that have been stacked to compare the TIC patterns. The TIC patterns in Figure 91 showed that the sealed tile does not have as intense of a pattern as the carpet and padding. This result is consistent with expectations since sealed tile would most likely not have had as much ignitable liquid absorbed into the pores of the tile, so there would be fewer ILRs to be extracted from the sample. The TIC of the sealed tile in Container 11 showed little to no ILR pattern. The TIC of the unsealed tile showed a greater abundance of ILRs similar to the carpet and padding sample than the sealed tile, see Figure 97 and Figure 98. The sealed tile in Container 12 retained more ILRs in

comparison to the unsealed tile and carpet and padding, see Figure 101. This may have been caused by fallen debris blocking the tile, or that the sealant was not effective at the high temperatures reached during the course of the burn.

Application to Previous Experiments

Laboratory Test Burns

Based on the results of the analysis of the previously burned laboratory samples, the classification method had a 70% accuracy rate in identifying the correct class of ignitable liquid. Test 37 had no ignitable liquid identified because none of the classes met the criteria for calculating a posterior probability. This result is important because the laboratory test burn for Test 37 used no ignitable liquid. The method of detection and classification correctly identified a situation in which no ignitable liquid was present. The results for Tests 6, 10, 15, 16, 18, 23, 29, 32, 35, 42, 43, and 44 were incorrectly classified. Of these, Tests 29, 32, 35, 42, 43, and 44 used volumes of ignitable liquid less than 100 µL. The reduced IL volume would result in a lower concentration of ILRs recoverable in the sample. The TIC and TIS patterns would therefore exhibit a low contribution of the IL and a relatively stronger contribution of the pyrolysis products, potentially contributing to an incorrect identification. Low volumes of an IL would present similar problems for the ability to correctly identify the IL class present when using the method of visual pattern recognition and target compound analysis as described in the ASTM E1618 guidelines.

Of the 7 total tests that used an NP IL, the NP class was misidentified as NAL for Tests 10, 15, and 23. An IL in the NP class may resemble a dearomatized PD TIC that had the spiking

n-alkane peaks removed.[4] The average TIS for the NP class was compared to the average TIS of ILs in the NAL class and the average TIS of ILs in the PD class. The correlation value between the average spectra from the NP class was 0.77 and 0.94 for NAL and PD, respectively. In addition, the average TIS of ILs from the NAL and PD classes have a correlation value of 0.86. The spectra from these IL classes are relatively similar because these classes have ILs with little to no aromatic compounds.

Large Scale Experimental Burns

Overall, the large scale experimental burn results (see Table 47) indicated a 60% classification accuracy rate. The MPD ignitable liquid in Container 2, Burn 2 was the same ignitable liquid used in Container 3. Despite being correctly identified in Container 2, Burn 2, the class HPD was incorrectly identified in Container 3. However, MPD was the second highest class identified in Container 3 by the posterior probability, average correlation and median correlation values. The identification of an HPD rather than MPD can be explained by multiple factors. The MPD and HPD classes are both subclasses of petroleum distillates that have an overlapping carbon range. The correlation value of the average TIS from ignitable liquids in the MPD and HPD classes was 0.97, indicating a strong correlation between the TIS from MPD and HPD ILs. The incorrect identification of the HPD subclass could also be a result of weathering. Weathering would effectively make the TIC pattern of the recovered MPD IL appear more like an HPD IL, which could also distort the TIS pattern.

Limited Sample Large Scale Burns

The results of the limited sample tests are summarized in Table 53, and had a correct classification rate of 86% in identifying and classifying the class of ignitable liquid in fire

debris samples. Table 54 summarized the results of the previously burned Containers 1-4 and the limited samples from Containers 5-12, and the original tests from Containers 5-12. The classification accuracy of the collective large scale burn tests is 74% for the identification and correct classification of a class of ignitable liquid.

Containers 5 and 6 used gasoline as the IL for the burns. Gasoline was the IL class identified in both containers in the limited sample analysis and in the original analysis using all collected samples.

Containers 7 and 8 were burned using two unique trails of gasoline and an MPD. The class of IL identified in both the limited and complete sample set trials for Container 7 was MPD. The identification of MPD which was one of the two classes present was considered a correct identification since the method is not designed to identify multiple IL classes. The IL class identified in Container 8 was originally OXY, which was an incorrect classification. When the data set from a limited number of samples, see Table 49, was analyzed to calculate posterior probabilities for each ASTM class, the IL class identified was gasoline. The use of a limited sample set changed the incorrect identification of the OXY class to a correct classification of gasoline. The limited sample set for Container 8 did not include sample 8-24. Sample 8-24 was the only sample identified as having an MPD contribution based on visual pattern recognition and target compound identification. When this sample was removed, the classification system identified gasoline. The identification of gasoline most likely resulted from the exclusion of the prominent ions from compounds in an MPD which

were not contributing to the overall ion intensities that previously resulted in the identification of the MPD subclass.

Container 9 was burned with a 50:50 mixture of gasoline and diesel fuel (HPD) however the classification method initially identified the NP class. When samples that had a TIC characteristic of both Gas and HPD were removed, gasoline was identified in the limited sample test. This was likely a result of the gasoline-related compounds in Samples 2 and 2B.

Originally, the class of IL identified in Container 10 was an LPD, which was a correct classification. When the limited sample test for Container 10 omitted Sample 19, the class of IL identified was MISC, which was an incorrect classification. This indicated that even though Sample 20 appeared to have an LPD contribution, it was not strong enough compared to the contribution of substrates and pyrolysis products from the other samples to result in a correct classification of LPD.

Container 11 omitted Samples 3, 4, and 10. The remaining samples had only weak characteristics of NP ILs. Initially, the IL class identified was correctly identified as the NP class. After the removal of samples, the data set contained 1 of 9 spectra with an IL contribution. The IL contribution was not abundant enough for the classification method to identify the presence of an IL class, and the result was that no IL was identified.

Container 12 omitted Samples 15, 16, 17, and 19. When these samples were omitted, the class identified was still the ISO class. Of the remaining samples, the prominent ions were

specific enough to other ISO ILs as to differentiate the data set between the ISO class and the other ASTM classes.

When considering the results of Containers 1-12 of the large scale burns, the tests using a limited number of samples from the large scale burns, and the laboratory tests, the classification method had a 72% accuracy rate. The method could be improved by several possibilities:

1. Redefining certain ASTM E1618 classes, specifically the OXY and MISC classes.
2. Implementing a median correlation cutoff value so misidentification of an IL based on poor correlation values could be avoided.
3. Examining the differences between the NAL and NP classes. Of the misclassified tests, NP was identified as NAL almost as many times as it was correctly identified as NP. Considering this, ions unique to NP may also be common to the NAL class. This is supported by the ASTM description of the NP class of ILs as having predominately branched chain and cyclic alkanes and the NAL class of ILs as having predominately straight-chain alkanes.

CHAPTER 5
FUTURE WORK

Identification and classification of fire debris is complicated by the presence of pyrolysis and combustion products that may cause incorrect classifications. The evaporation of volatile components during a fire changes the signature of ILRs recovered from fire debris samples.[30] This means the TIC from the fire debris sample used for visual pattern recognition is essentially incomplete in comparison to a neat IL sample, or could also contain pyrolysis products that may erroneously contribute to the ILR pattern.[4-5] To improve the correct classification rate, the ability to distinguish an ILR from pyrolysis products needs to improve. Isolation of ILRs from pyrolysis and combustion products produces a TIC with fewer background interferences, thus improving the probability of identifying the correct class of IL present in the sample.

Continuation of Current Work

The method of generating the TIS in the data sets for the computer simulation models contained more factors than spectra due to the number of substrate TIS that was used to generate the data set. Because of this, simulations with low contributions of ignitable liquids would result in incorrect classifications. For example, the aromatic class, see Table 10, only had correct classifications at the highest number of samples containing an IL contribution and at the highest percent contributions of the IL TIS. It may be possible to achieve correct classifications at lower IL contributions and in fewer spectra if the number of principal components had not exceeded the number of samples generated. For future simulations, the

method of generating a data set of TIS should be limited, in order to have a data set with more spectra than factors. This may improve the correct classification rate at lower percent contributions of ignitable liquids.

The classification accuracy rate could also improve with the implementation of a median correlation cutoff value. With the implementation of a median correlation cutoff value, the posterior probability of a class would not be calculated if the median correlation of that class was less than the cutoff value, 0.85. Therefore, only classes with a value of $\frac{\|1-\text{median}(x_i)\|}{\text{MAD}}$ less than 5 and with a median correlation value greater than 0.85 would have the posterior probability calculated. The implementation of a cutoff value may be justified in situations involving a class that has a low median correlation value but the value of $\frac{\|1-\text{median}(x_i)\|}{\text{MAD}}$ is less than 5. In this situation, the class would have a posterior probability calculated, which could be high relative to the posterior probabilities of other classes. Therefore, that class would be identified as being present despite the class having a low correlation value, $r < 0.85$. This would result in an incorrect classification. However, if the posterior probability for the class was not calculated because the median correlation value was less than the cutoff, the classification result would have been "not classified." A result of "not classified" or "not identified" is an improvement over an incorrect classification obtained without using the cutoff. Implementing a cutoff value of 0.85 for the minimum correlation value could improve the classification accuracy by reducing the rate of misclassifications of those classes with a highly diverse range of correlation values.

Determining the number of PCs to retain is critical to correctly identify the ignitable liquid class present in the sample. The DRMAD method determines the number of principal components to retain by determining if an eigenvalue is an outlier based on the MAD value. If an eigenvalue is an outlier then it is retained as a principal component. The next eigenvalue is evaluated in the same manner but the median value used is recalculated based on the reduced number of eigenvalues. Statistically, recalculating the median value for the MAD calculation to determine if an eigenvalue is an outlier may not be the preferred method to identify the number of PCs to retain. This method is problematic when the calculated MAD value is very large, resulting in a value of $\frac{\|1-\text{median}(x_i)\|}{\text{MAD}}$ that is greater than 5 and therefore retaining that value as a PC. Another option is to retain all of the variance. If only a portion of the variance is retained based on the scree plot method or DRMAD method, then the variance contributed from the IL could be excluded. If a sample set has a low volume of IL contributing towards the overall TIS signal, then the amount the IL signal contributes to the variance is also low. To avoid this possibility, retaining all of the variance ensures that any IL contribution towards the variance is included in subsequent calculations.

Subclassification of Oxygenated Solvents and Miscellaneous Classes

Currently, ignitable liquids are classified based on a hard classification system, which means that an ignitable liquid can only belong to one of the ASTM classes. This can make classification difficult since an ignitable liquid may have characteristics of multiple classes, see Figure 102.

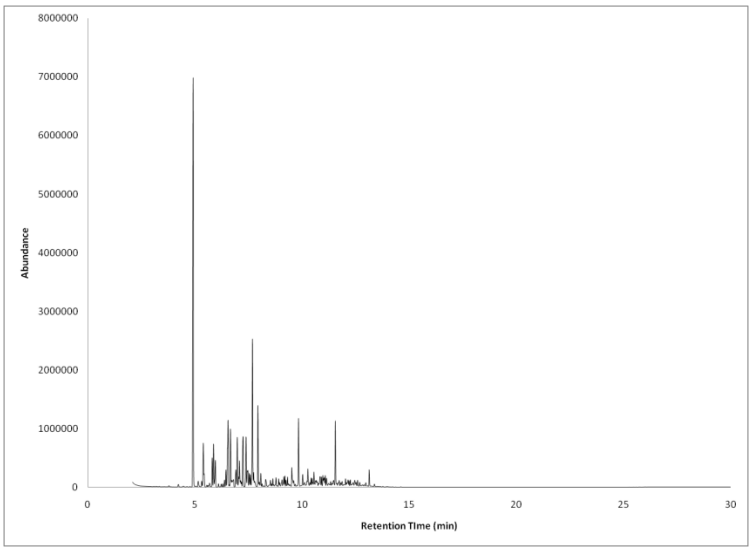

Figure 102: TIC of Oxygenated Solvent

The ignitable liquid in Figure 102 has a strong oxygenated product component however it also has a high correlation with the PD class**.** Classifying this IL in the OXY class may pose problems when trying to identify this IL from fire debris samples. In samples recovered from a fire, it is likely that the lighter, highly volatile oxygenated component would have been lost or consumed. This would result in the recovery of only the heavier, less volatile petroleum products when analyzing the fire debris samples. However, identifying MPD as the class of IL present would be incorrect since the IL is technically in the OXY class. Even if the oxygenated compound was not consumed during the fire and was able to be recovered, most analytical methods have difficulty recovering lower molecular weight compounds such as oxygenated compounds. Oxygenated compound ILRs are difficult to recover since they may be displaced on the activated charcoal strip by heavier compounds. Oxygenated compound ILRs can also be difficult to detect analytically if they elute near the solvent and prior to when the detector is turned on, or if the mass range being scanned was limited. The use of a soft classification system would allow the IL to be classified as both an MPD and an OXY.

Methods of Sample Analysis

Stauffer et al. propose a systematic approach to the analysis of fire debris samples in the presence of pyrolysis and/or combustion products. This approach involves identifying the sample and substrate, and estimating the typical compounds contributed from the substrates. Stauffer et al. suggest that having a reasonable assumption of the substrate and its components would allow for the prediction of pyrolysis products produced by the substrate based on knowledge of breakdown pathways. However, this approach relies on a large degree of estimation and assumption, as well as the experience of the analyst.[4]

Possible improved methods of analysis may involve changes to the treatment of data or the method of analysis of fire debris samples. For example, the application of differential mobility spectrometry has been used to classify ILRs from simulated fire debris samples based on a classification system developed using neat liquids. Despite a high accuracy rate (approximately 99%), matrix effects played a significant role in classifying the ILRs from fire debris samples when compared to neat liquids. Differences in sample treatment methods resulted in varying amounts of ILRs recovered from samples.[30] Another method of analyzing fire debris samples includes the use of isotope ratio mass spectrometry (IRMS) to identify the source of hydrocarbon products. If isotope ratios are unique to an IL, then a more specific ILR pattern would be generated that could be compared to reference ILs. This would facilitate the identification of the IL present and potential matching to an IL or group of ILs that have been manufactured in a similar geographic region. The additional information produced by GC-IRMS may not be enough to compare to ILs suspected of being present, but it could narrow down the possible ILs for investigators. Gas chromatography-isotope ratio

mass spectrometry has also been used with analysis of weathered samples, which have previously been problematic due to the loss of the lighter components. Isotope ratios however are not as affected by weathering, which makes it possible to link a weathered IL to the unweathered IL sample.[31]

Criminal Justice Applications

Arson is a difficult crime to prosecute due to the lack of physical evidence linking a suspect to the scene of the crime. Investigators would therefore benefit from the ability to compare ILRs identified from a fire scene to those obtained from the suspect's possession or person. While such specific ignitable liquid identification is not possible, even matching the IL class identified at the scene of a crime to a sample collected from the suspect may be enough to justify further investigation or compel a confession. Current research related to this involves the extraction of ILRs from the skin of volunteers using SPME and GC analysis.[32] The results indicated that as time progressed, the abundance of ILRs recovered by the SPME process decreased. In cases where the TIC pattern may not be readily identifiable based on ASTM E1618 guidelines for visual pattern recognition and target compound comparison, this research provides a statistically supported identification based on posterior probabilities calculated from correlation values obtained after PCA and TFA were performed on a data set to compare the TIS to individual IL spectra in a reference library.

APPENDIX A
CONTAINER 5

Ignitable Liquid TIC

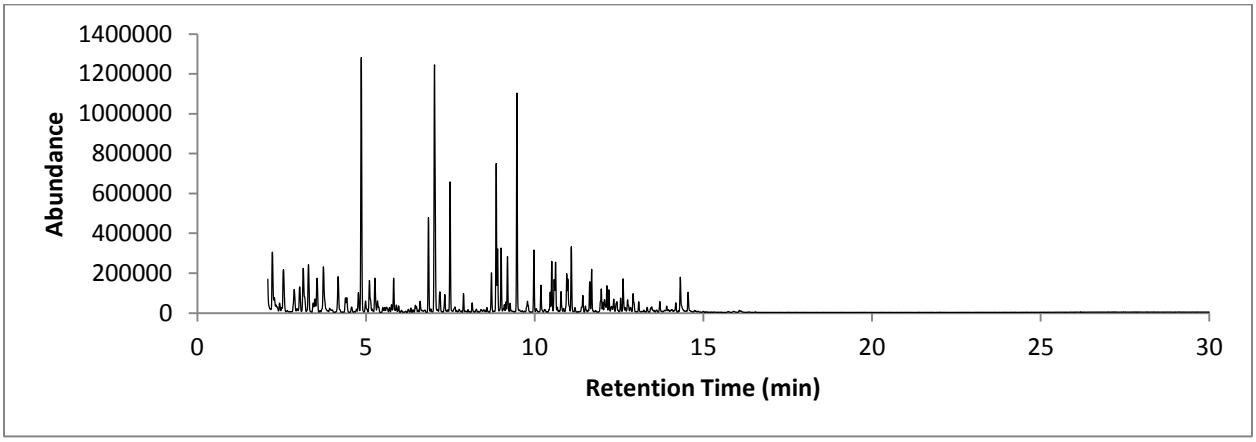

Figure 103: TIC C5-C6 Unweathered Gasoline

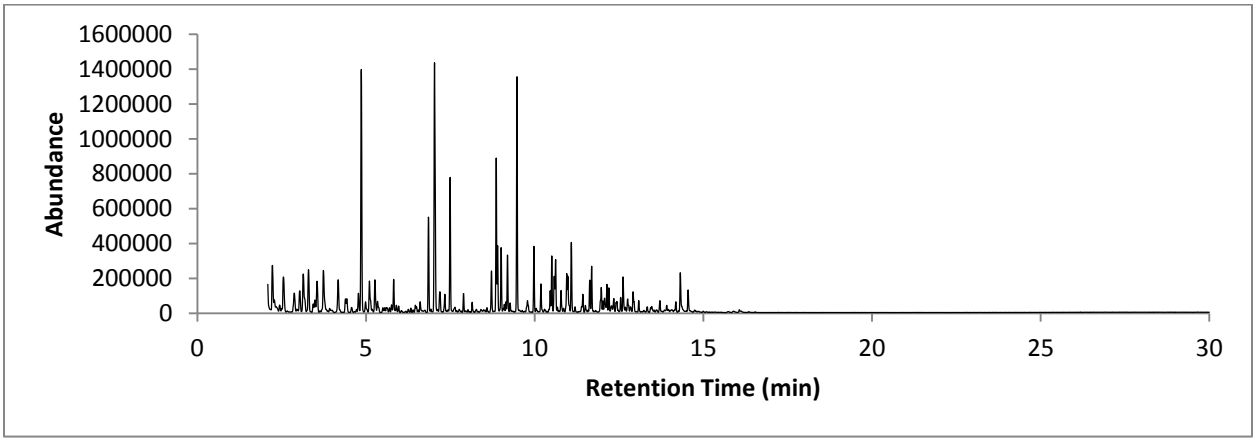

Figure 104: TIC C5-C6 25% Weathered Gasoline

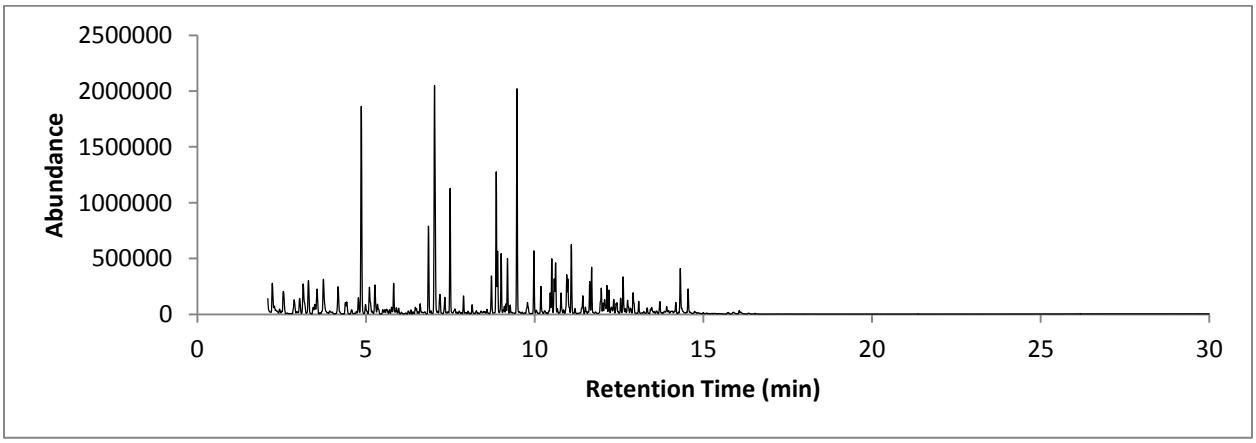

Figure 105: TIC C5-C6 50% Weathered Gasoline

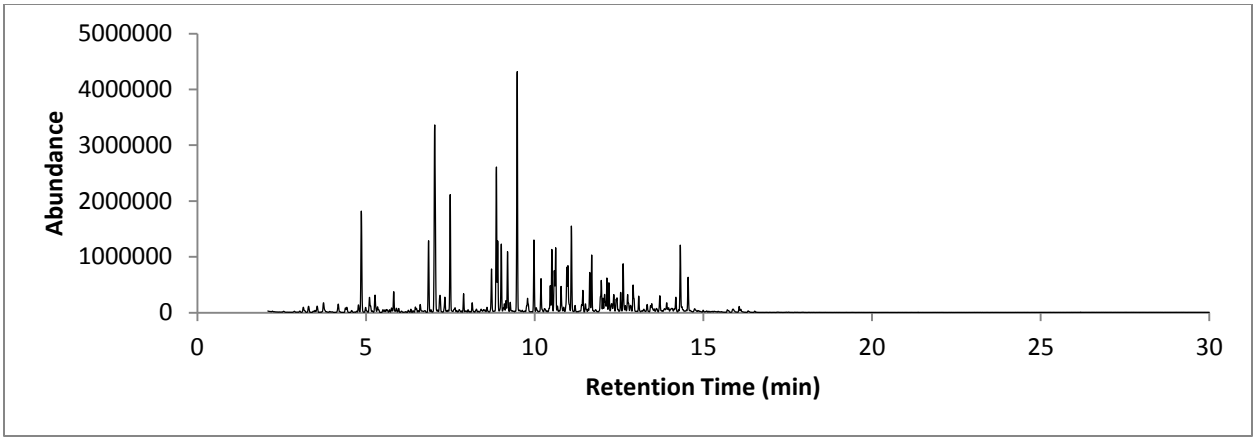

Figure 106: TIC C5-C6 75% Weathered Gasoline

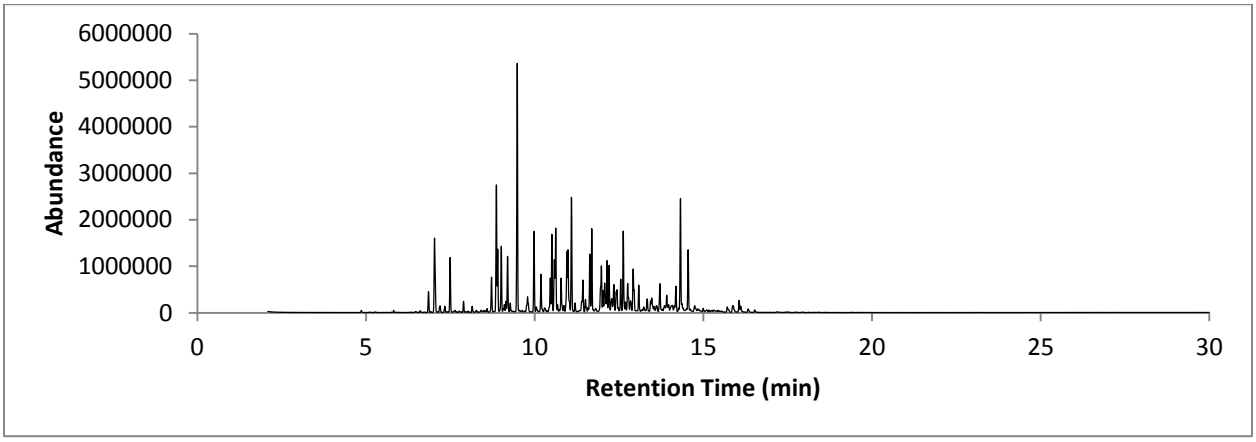

Figure 107: TIC C5-C6 90% Weathered Gasoline

Ignitable Liquid TIS

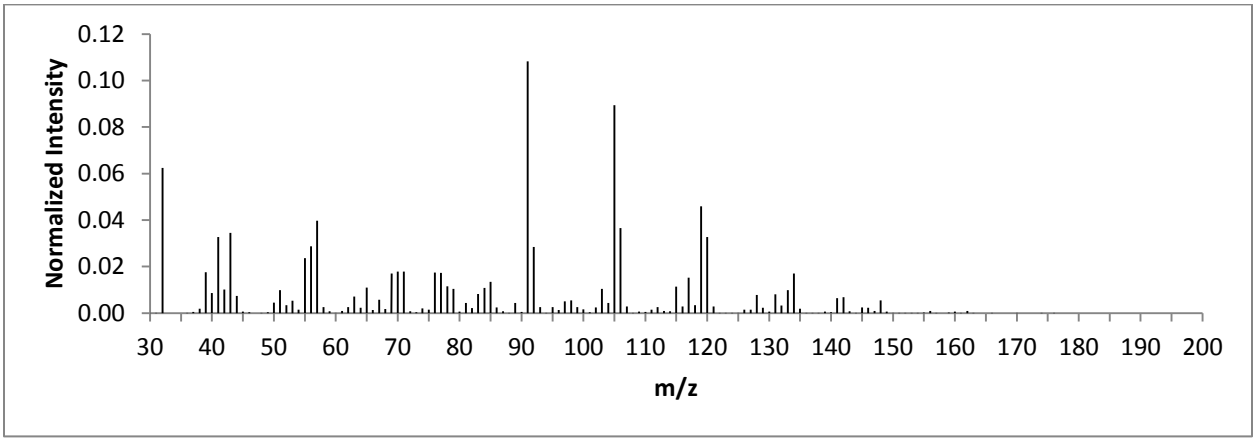

Figure 108: TIS C5-C6 Unweathered Gasoline

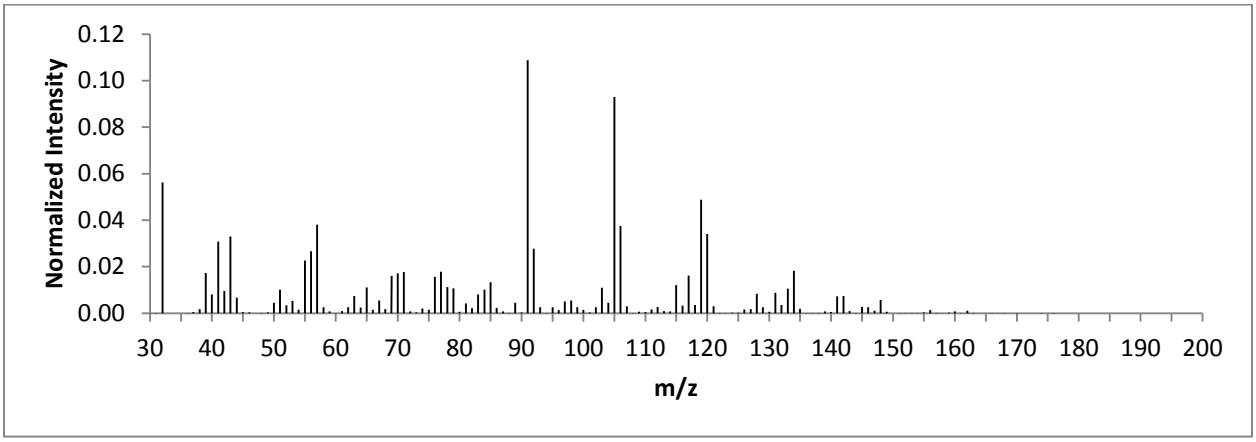

Figure 109: TIS C5-C6 25% Weathered Gasoline

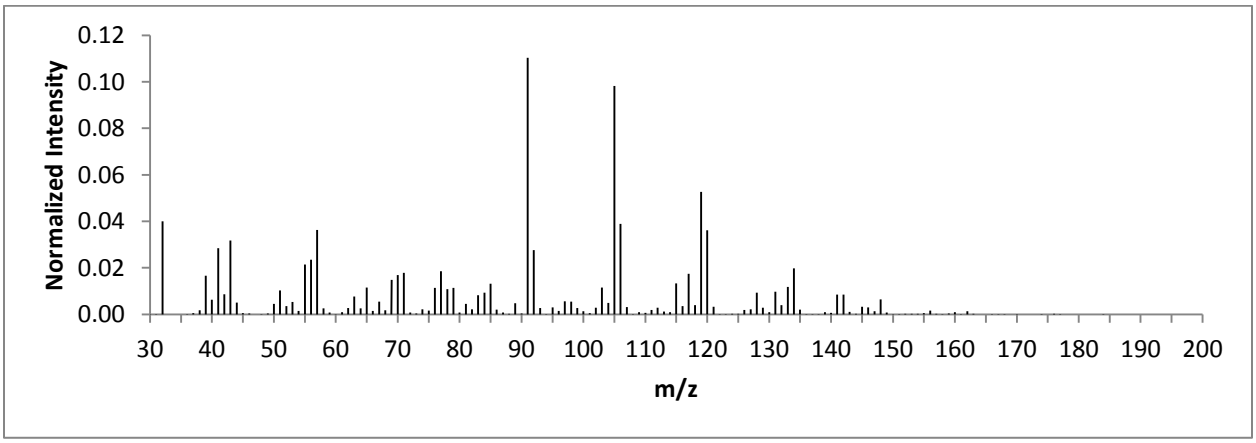

Figure 110: TIS C5-C6 50% Weathered Gasoline

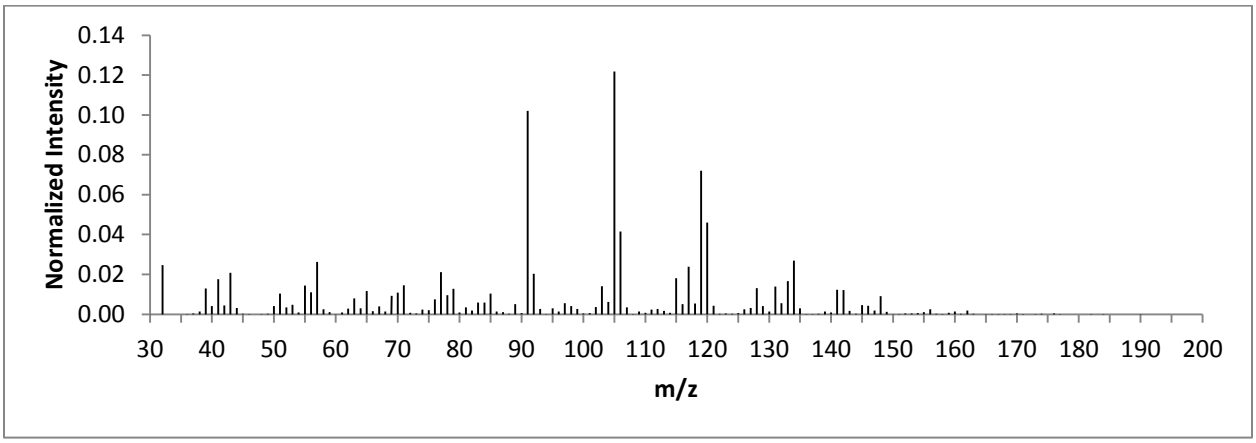

Figure 111: TIS C5-C6 75% Weathered Gasoline

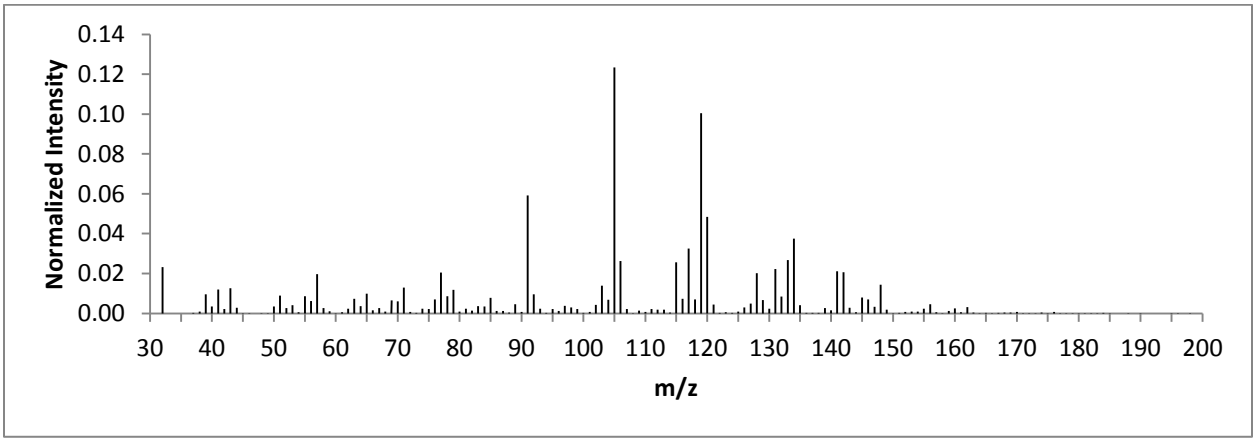

Figure 112: TIS C5-C6 90% Weathered Gasoline

Sample TIC

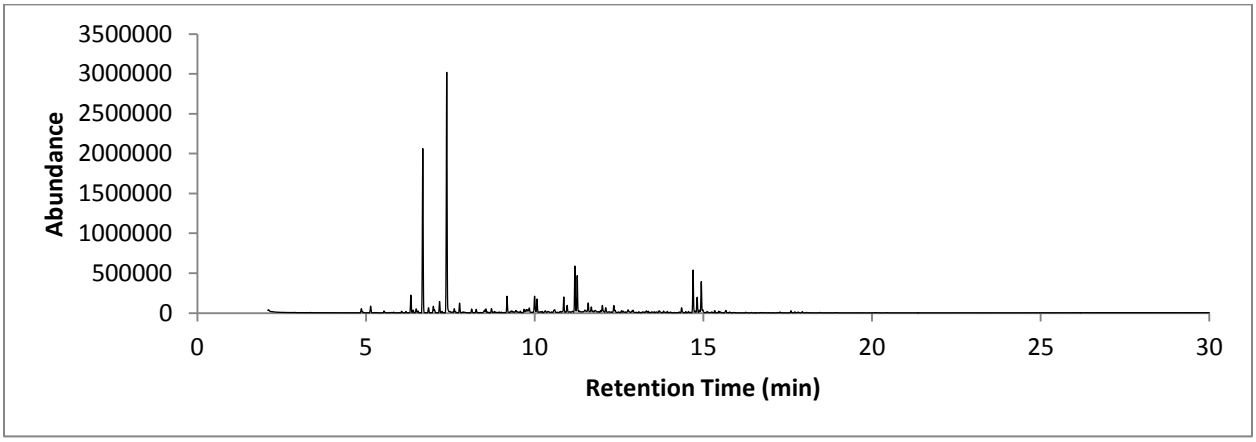

Figure 113: TIC C5-1

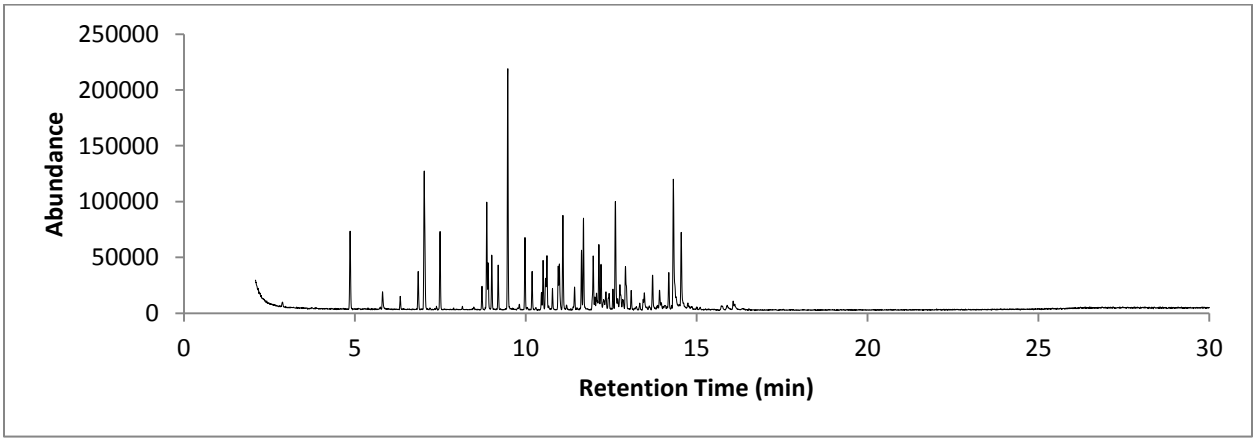

Figure 114: TIC C5-1B

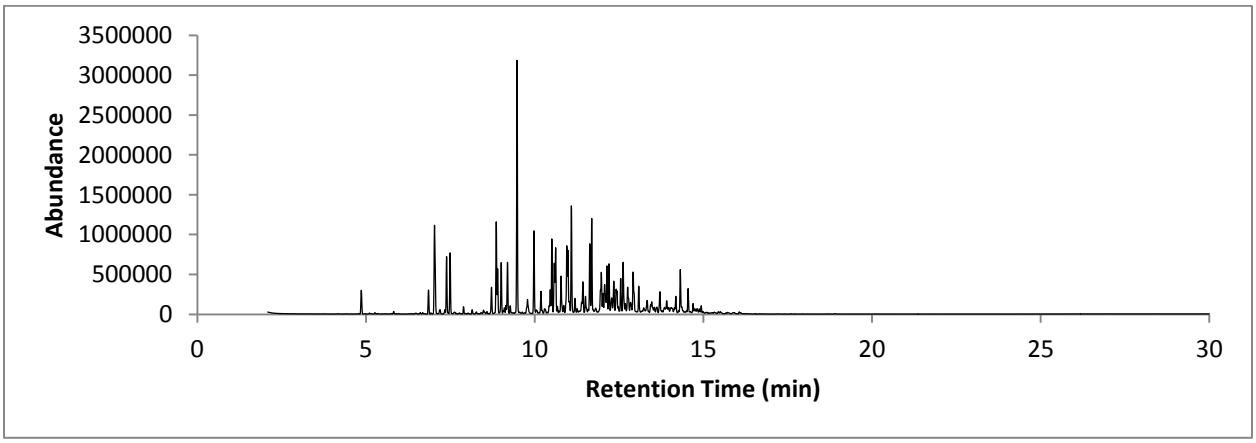

Figure 115: TIC C5-2

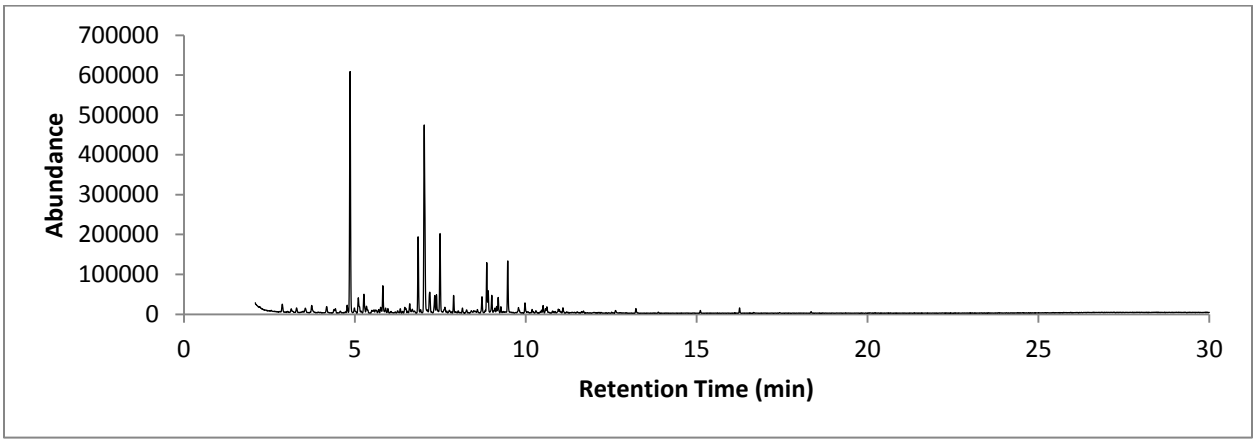

Figure 116: TIC C5-3

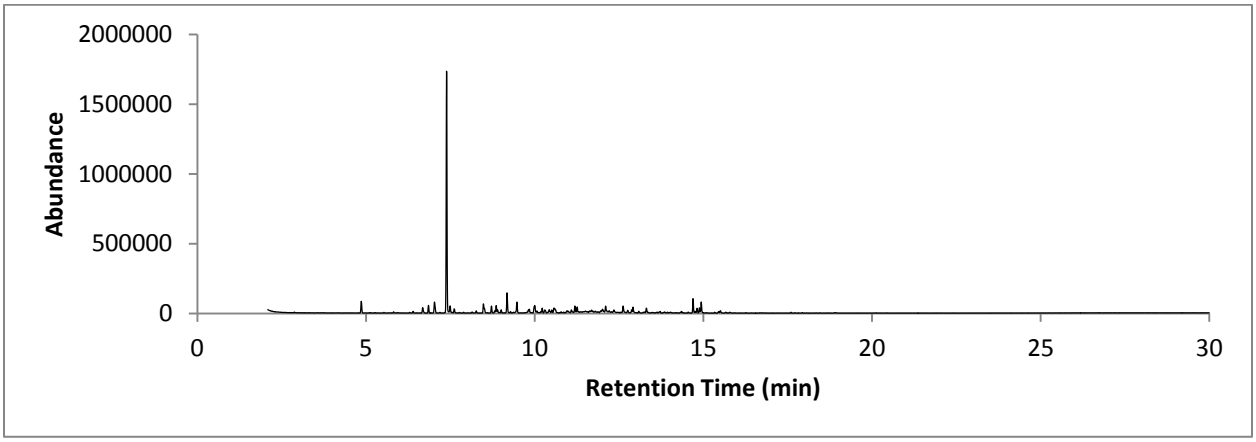

Figure 117: TIC C5-4

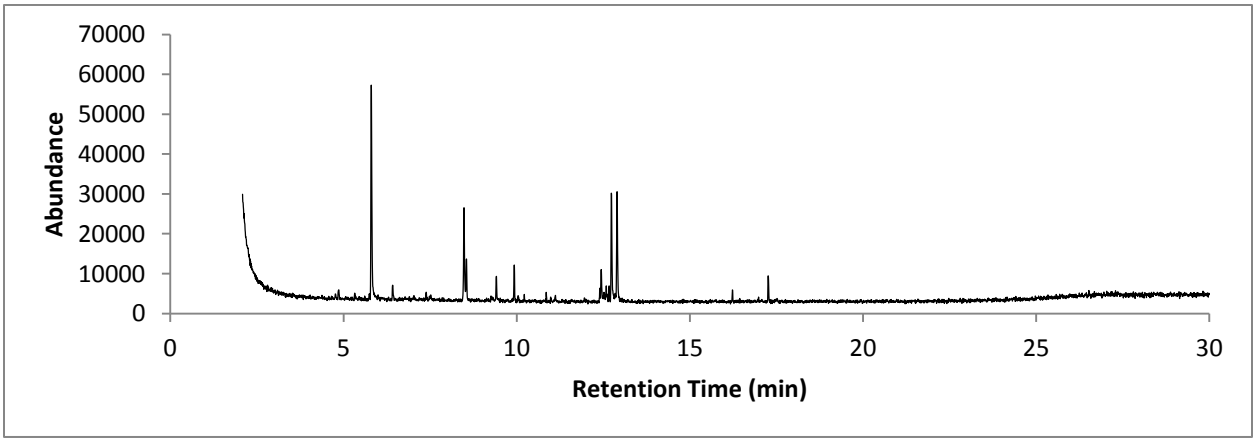

Figure 118: TIC C5-5

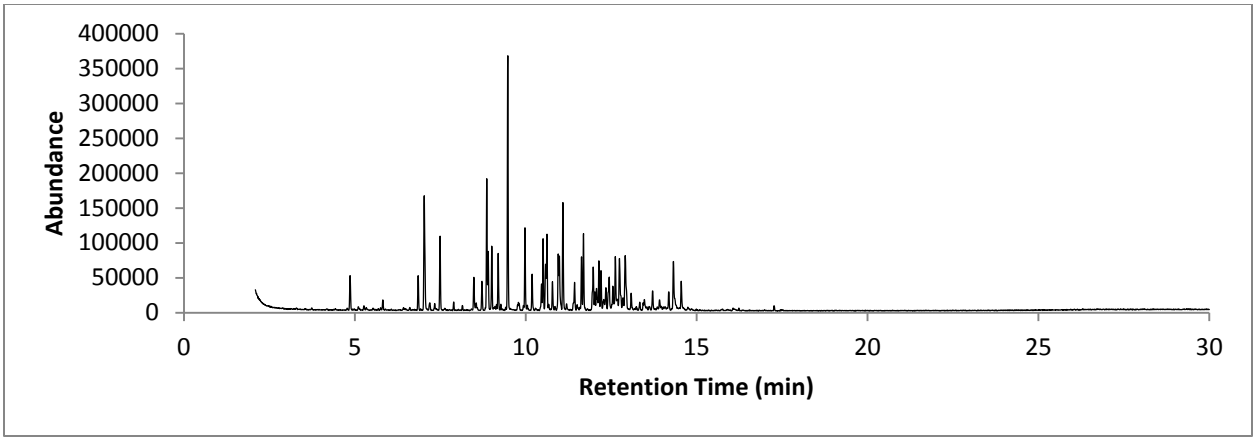

Figure 119: TIC C5-5B

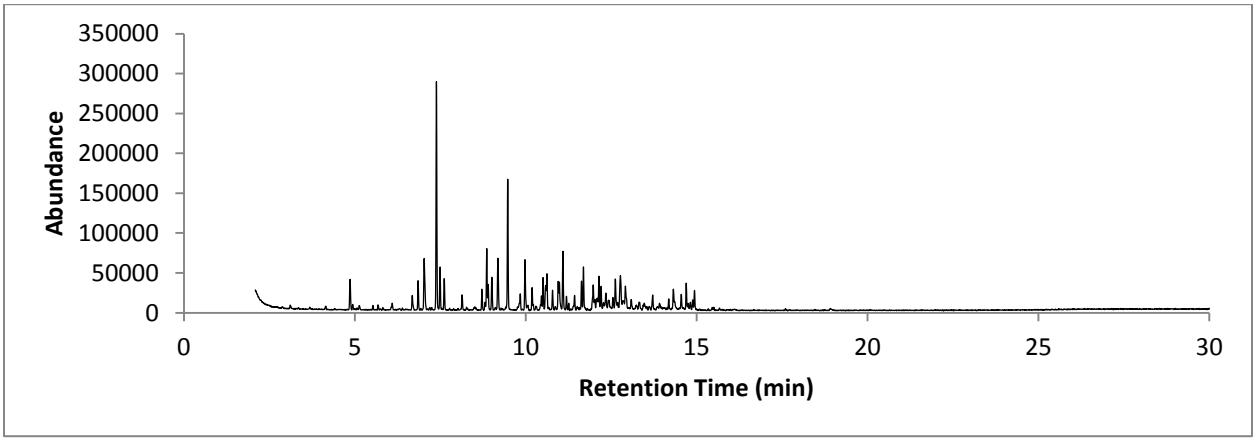

Figure 120: TIC C5-6

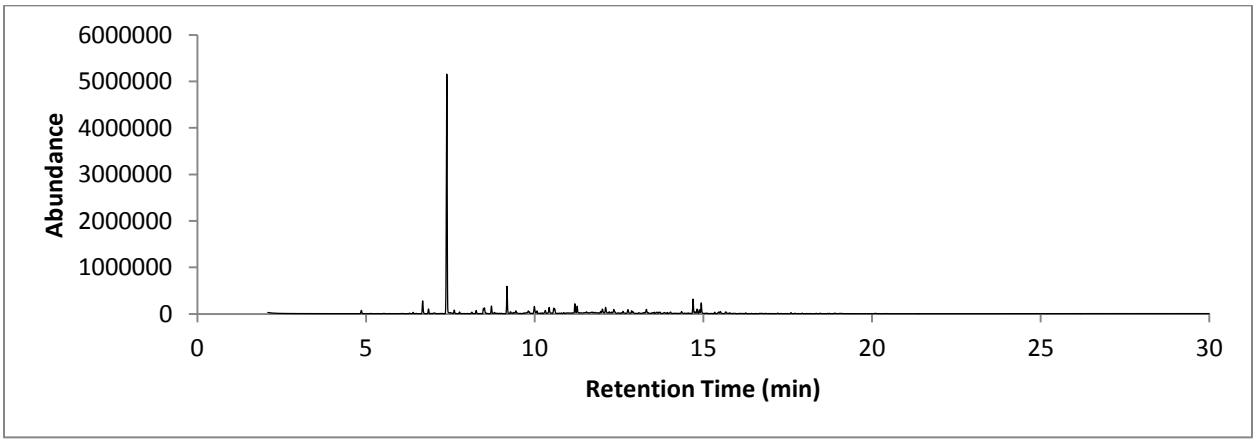

Figure 121: TIC C5-7

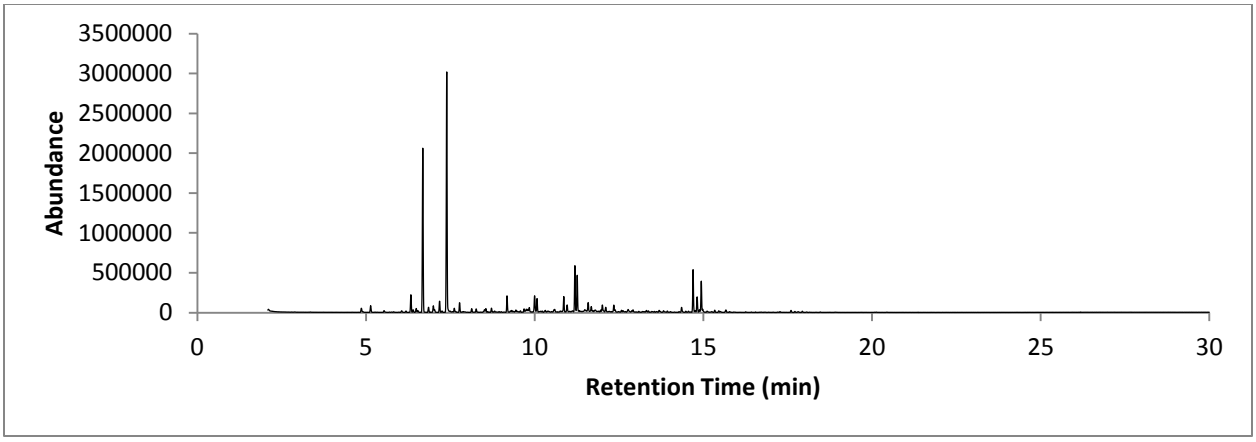

Figure 122: TIC C5-8

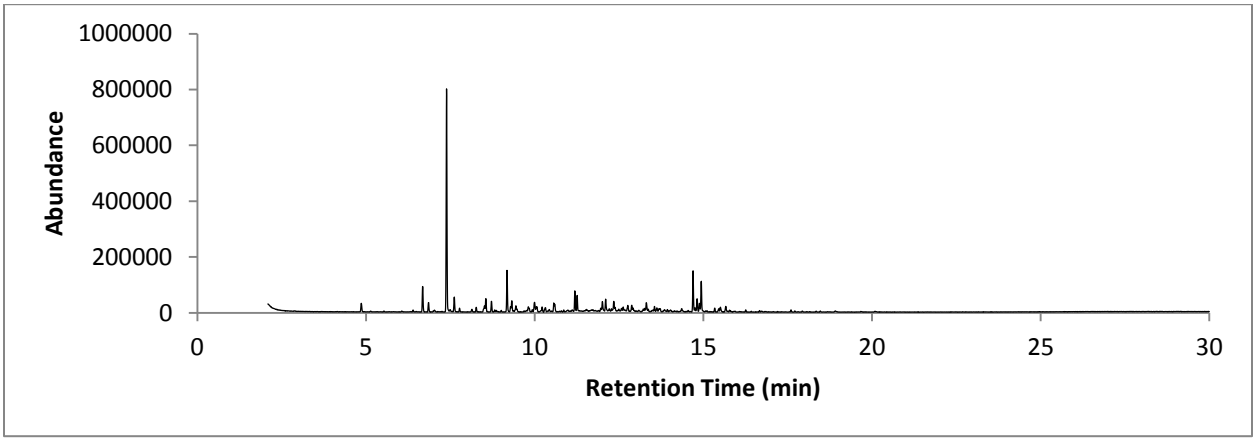

Figure 123: TIC C5-9

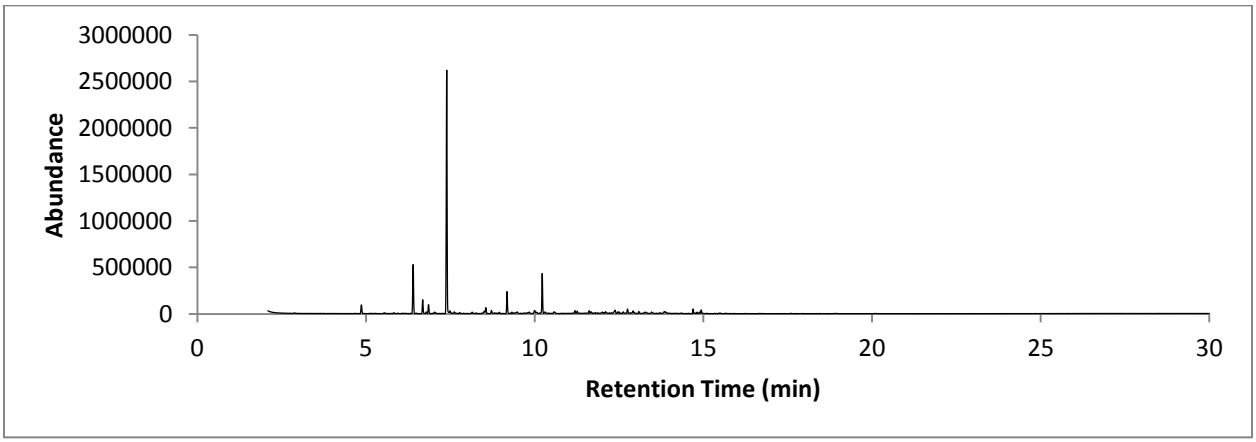

Figure 124: TIC C5-10

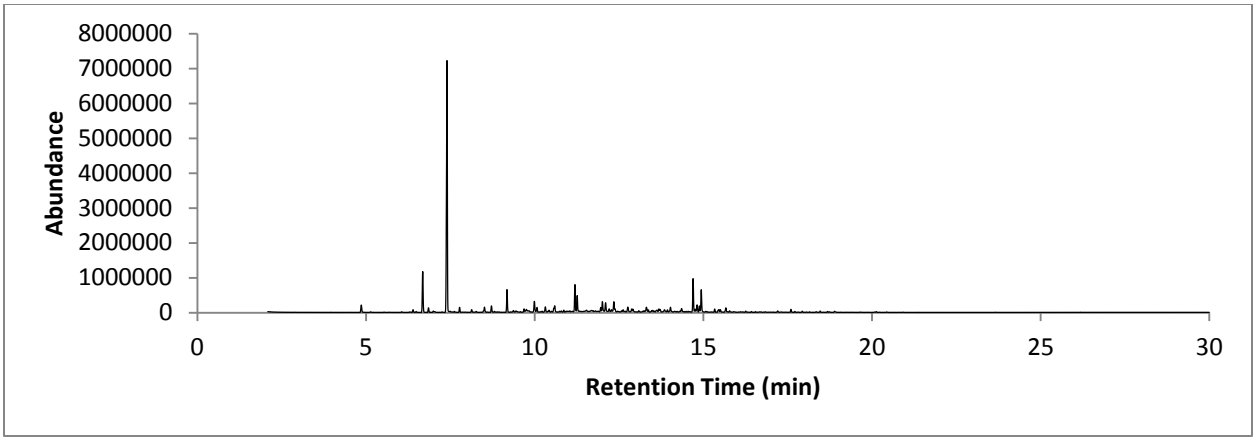

Figure 125: TIC C5-11

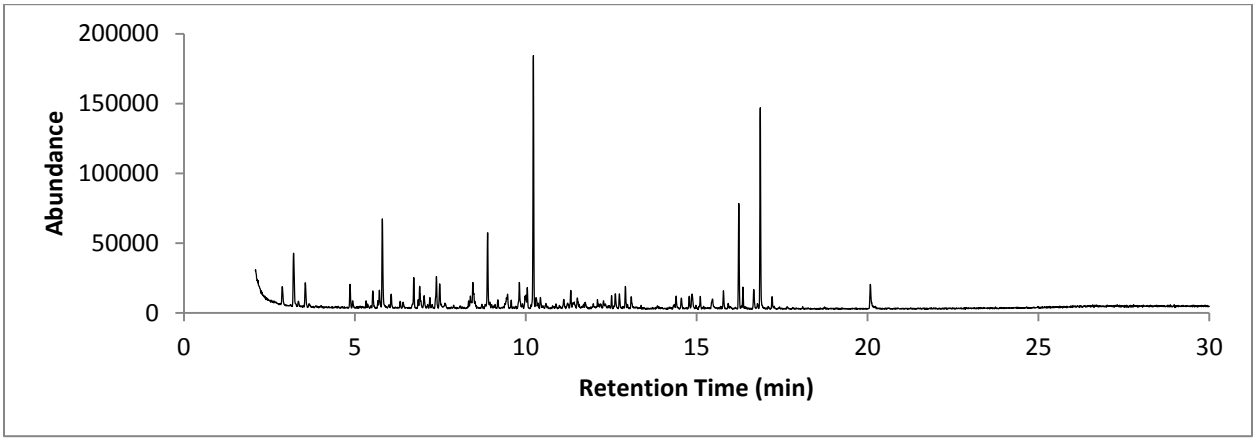

Figure 126: TIC C5-12

Sample TIS

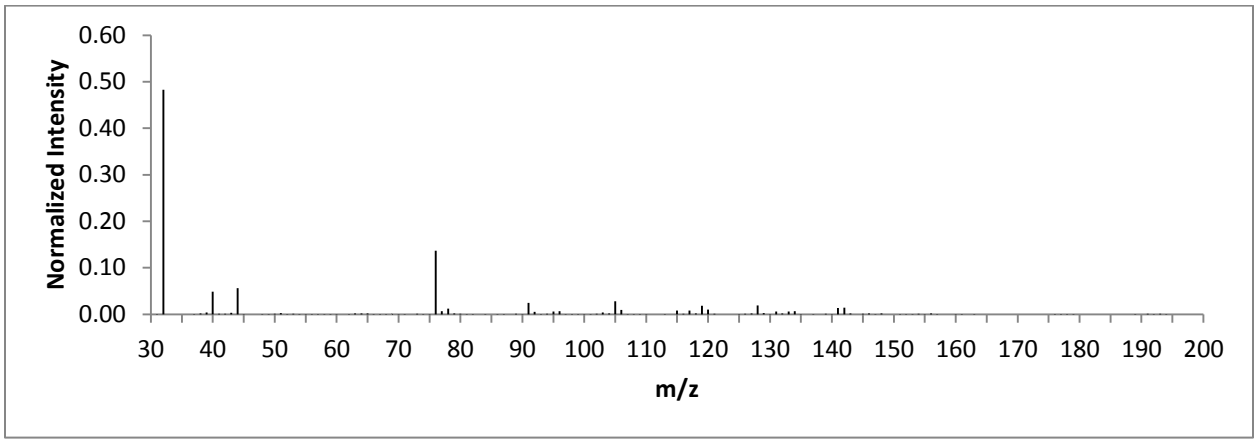

Figure 127: TIS C5-1

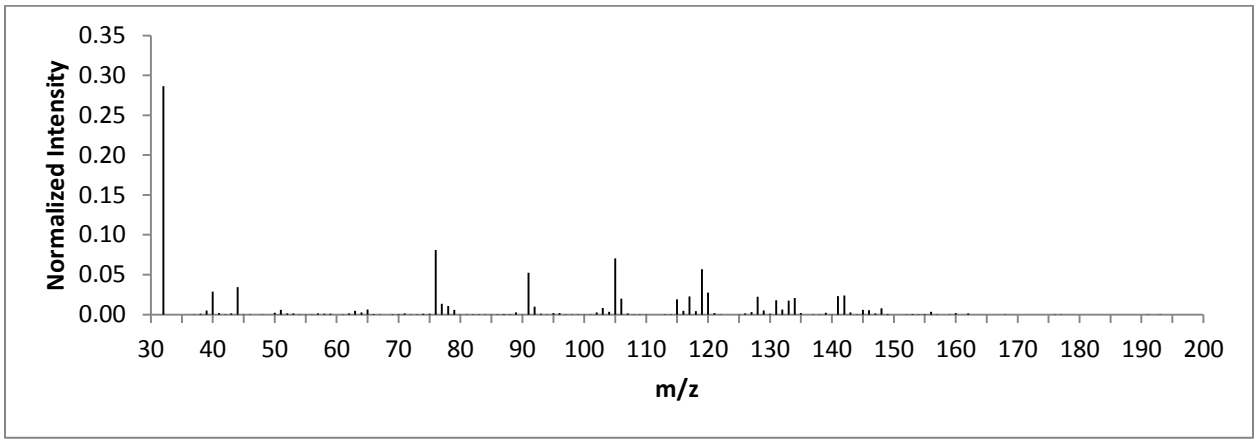

Figure 128: TIS C5-1B

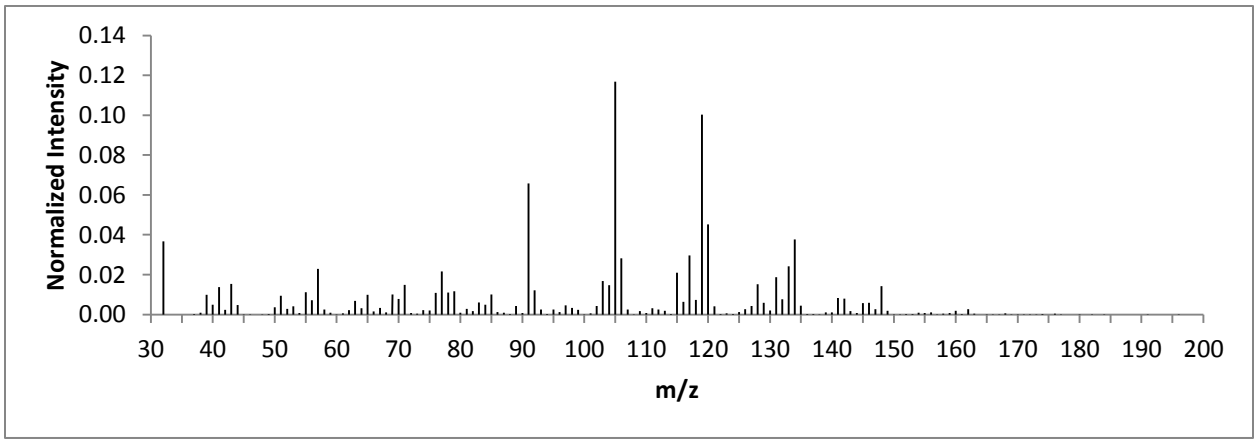

Figure 129: TIS C5-2

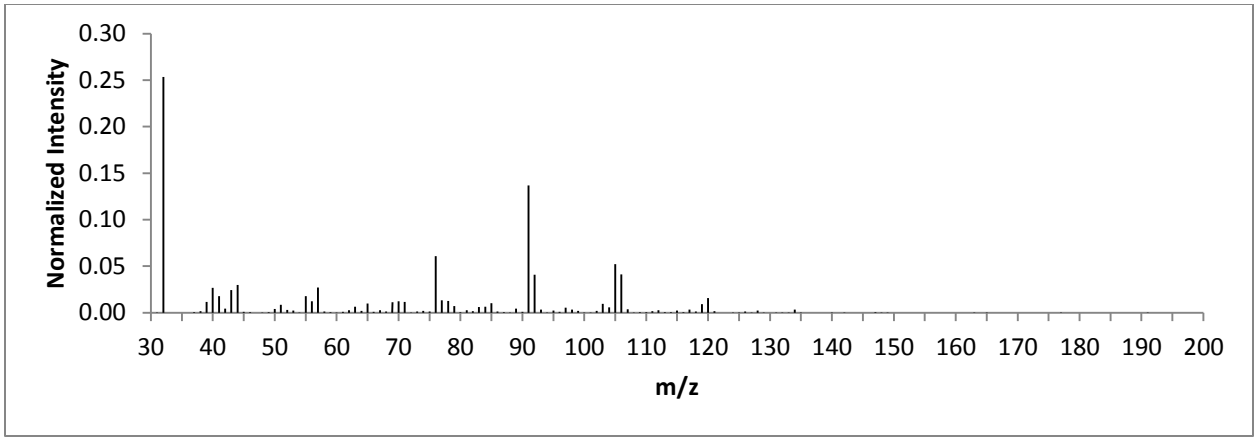

Figure 130: TIS C5-3

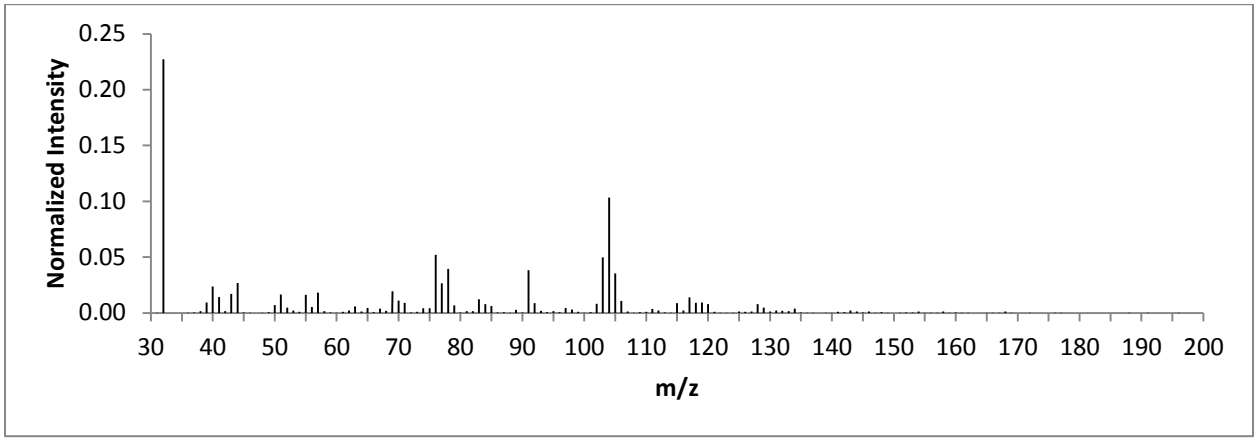

Figure 131: TIS C5-4

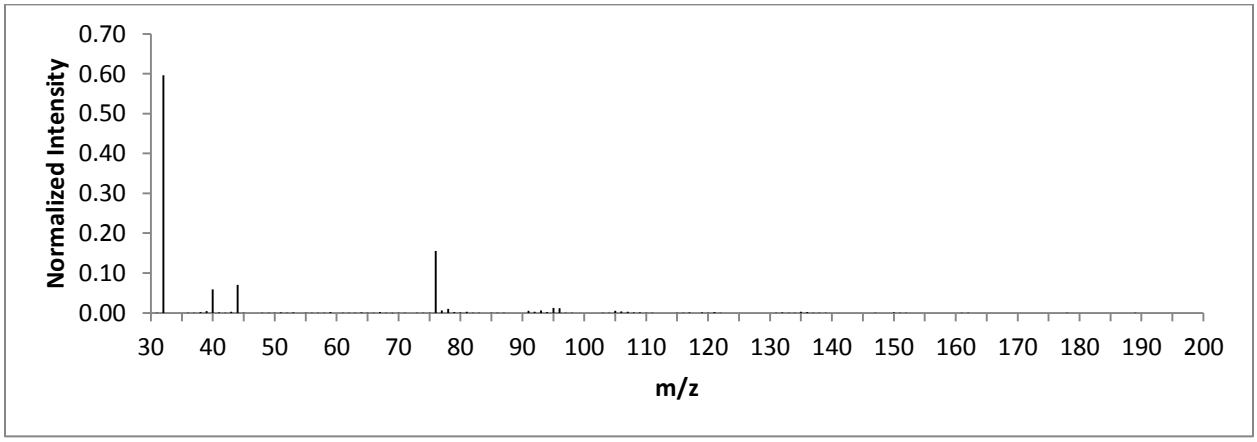

Figure 132: TIS C5-5

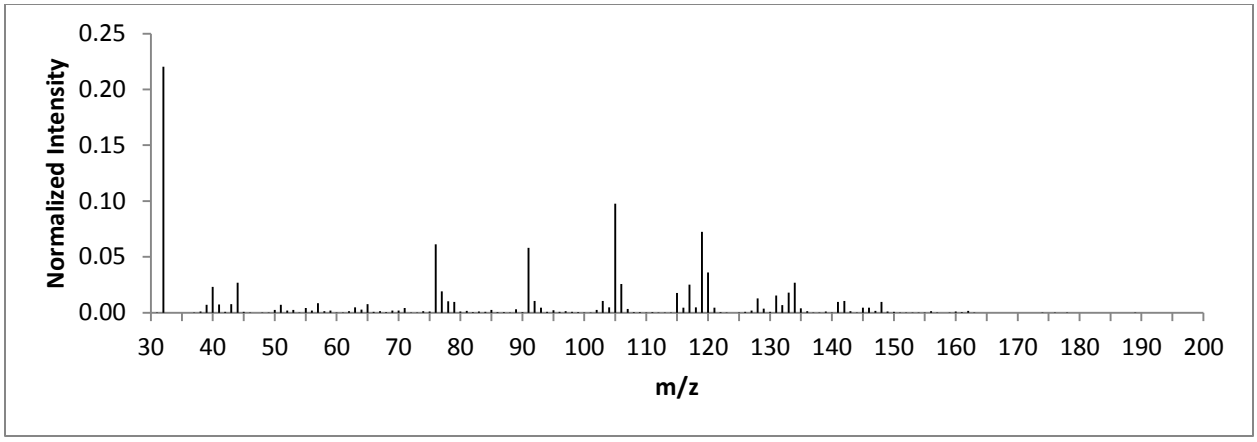

Figure 133: TIS C5-5B

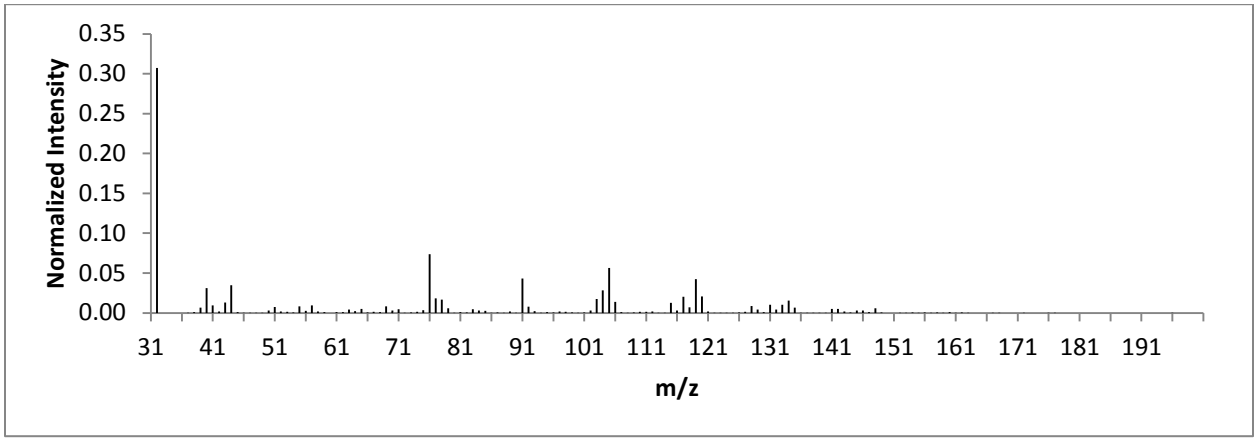

Figure 134: TIS C5-6

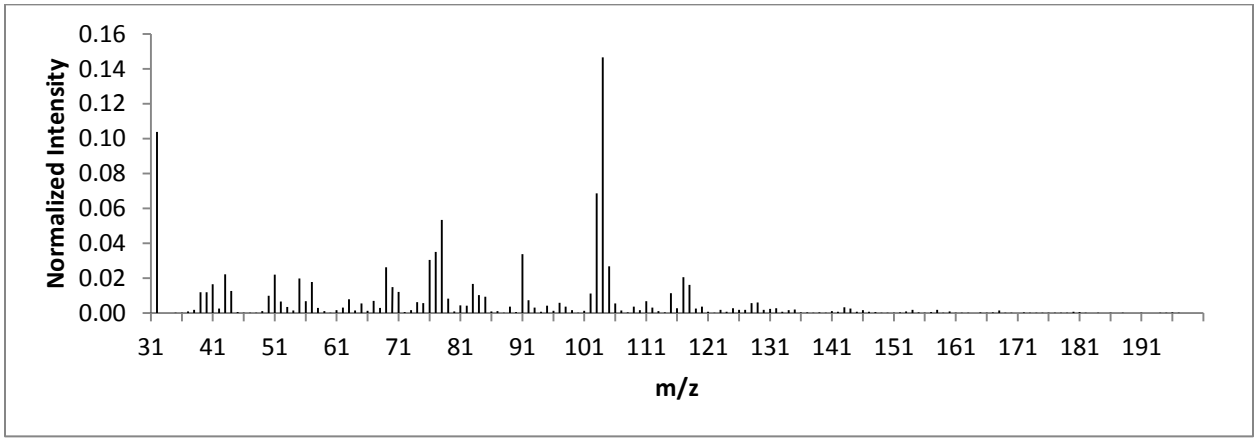

Figure 135: TIS C5-7

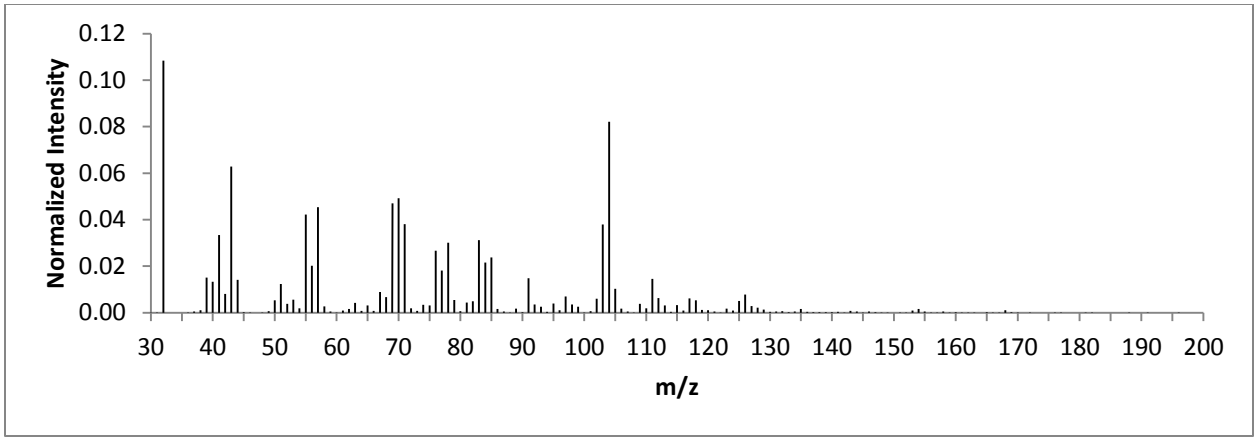

Figure 136: TIS C5-8

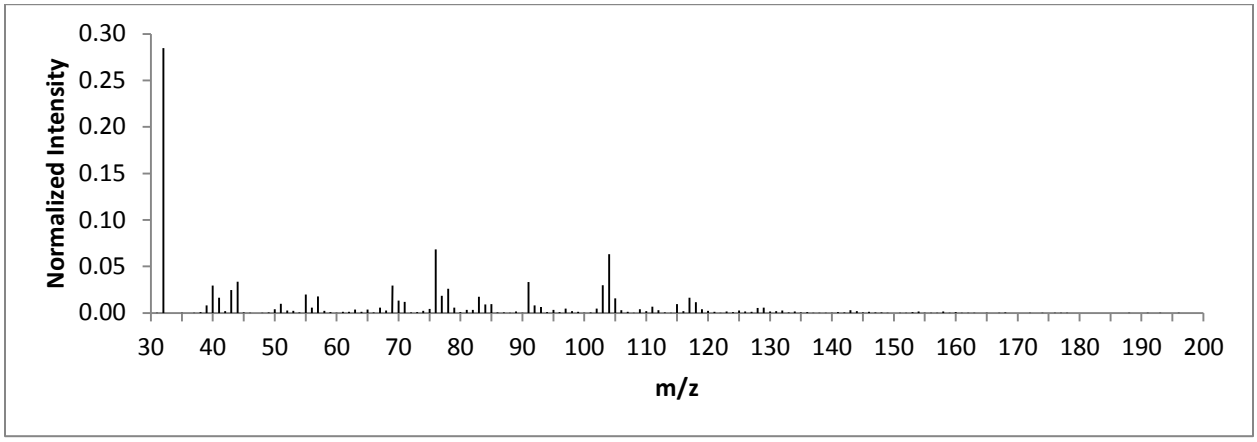

Figure 137: TIS C5-9

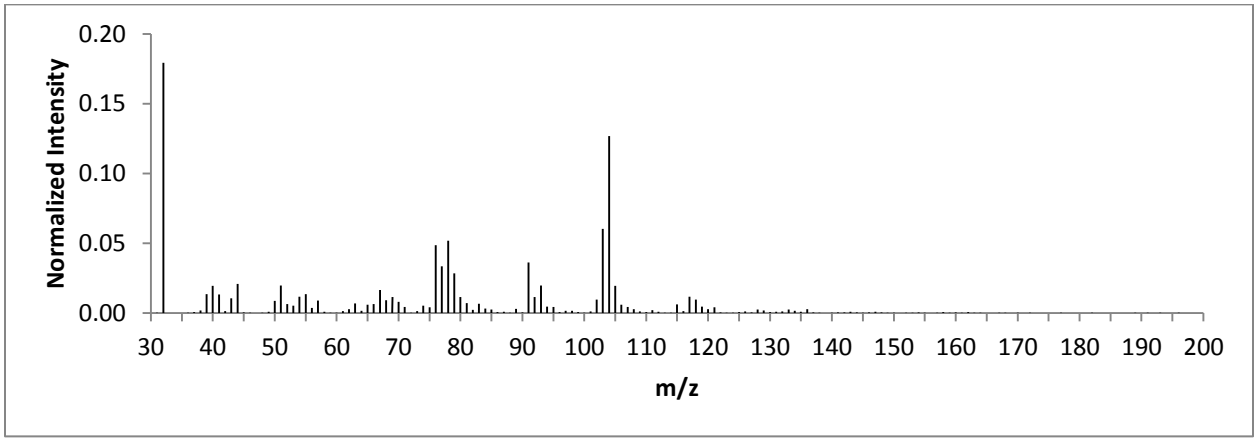

Figure 138: TIS C5-10

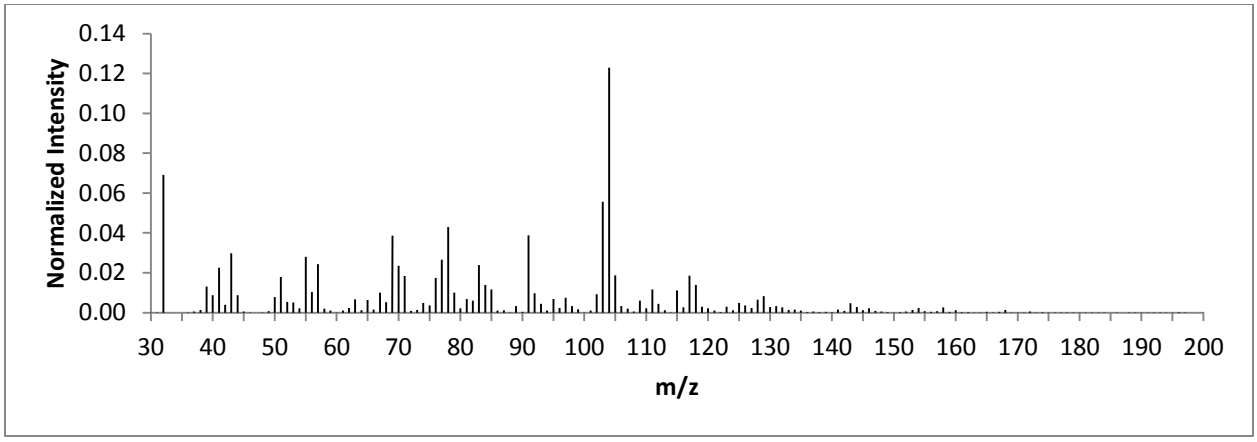

Figure 139: TIS C5-11

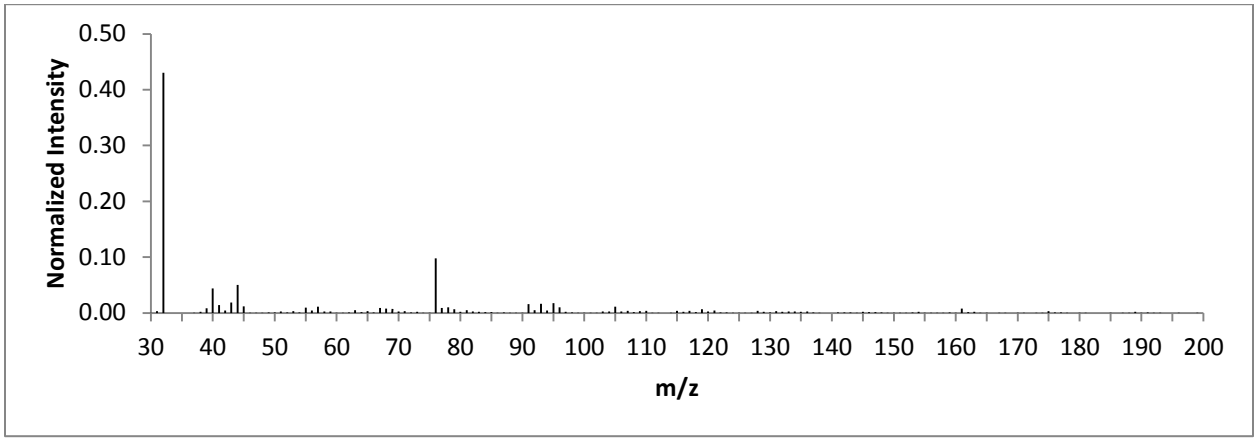

Figure 140: TIS C5-12

APPENDIX B
CONTAINER 6

Ignitable Liquid TIC

See Ignitable Liquid TIC in APPENDIX A.

Ignitable Liquid TIS

See Ignitable Liquid TIS in APPENDIX A.

Sample TIC

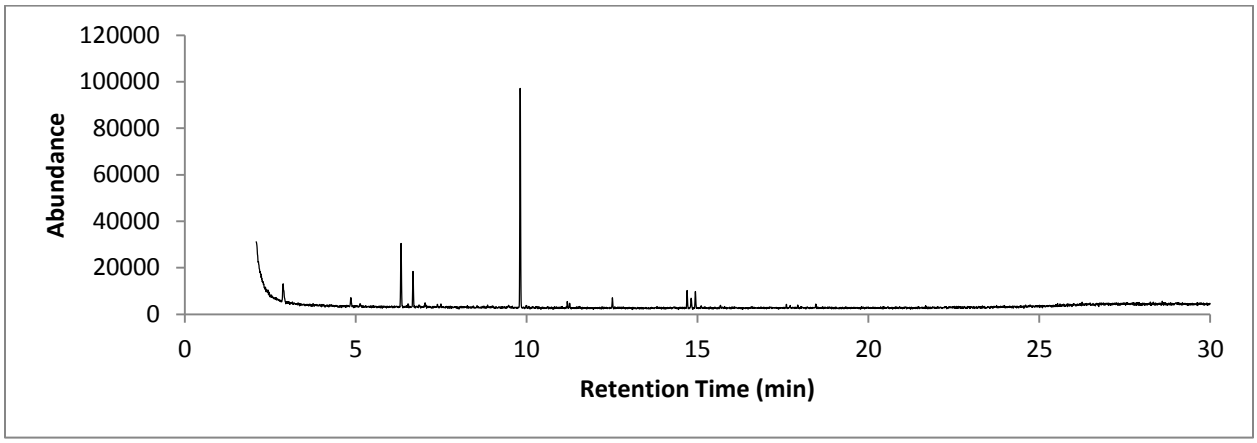

Figure 141: TIC C6-13

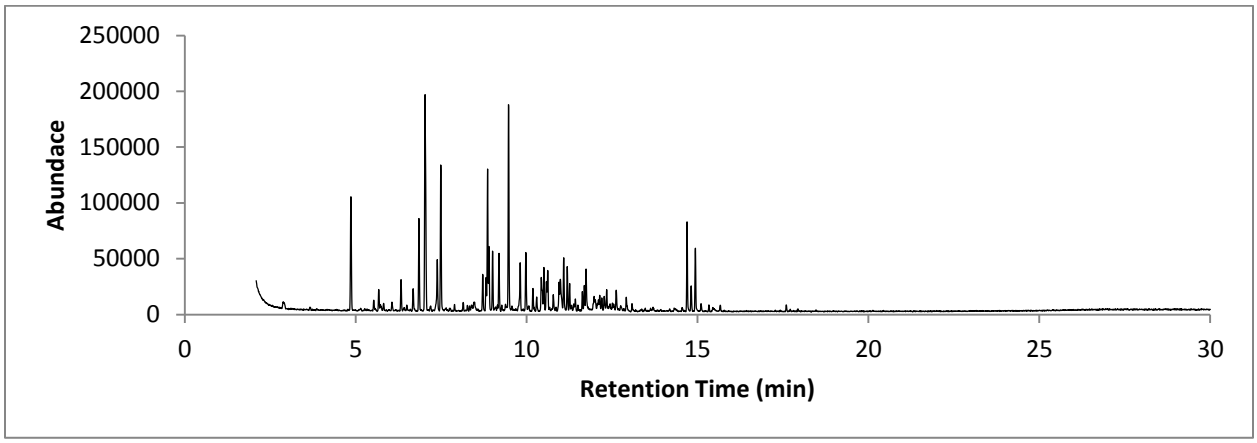

Figure 142: TIC C6-14

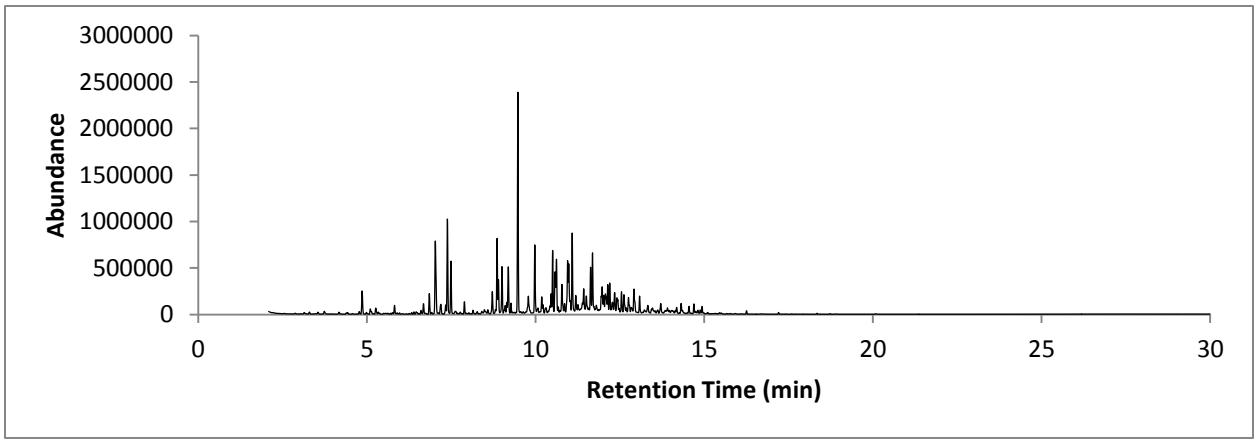

Figure 143: TIC C6-15

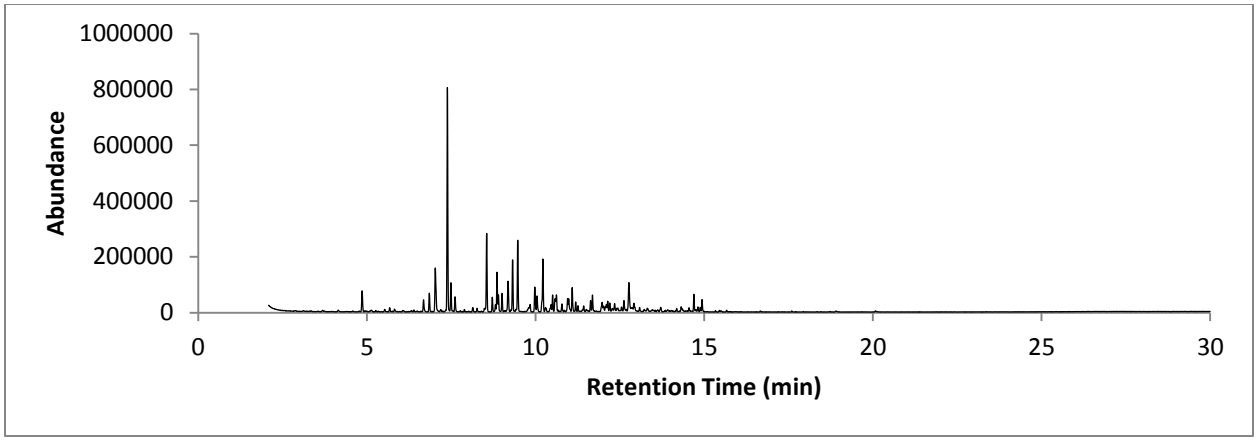

Figure 144: TIC C6-16

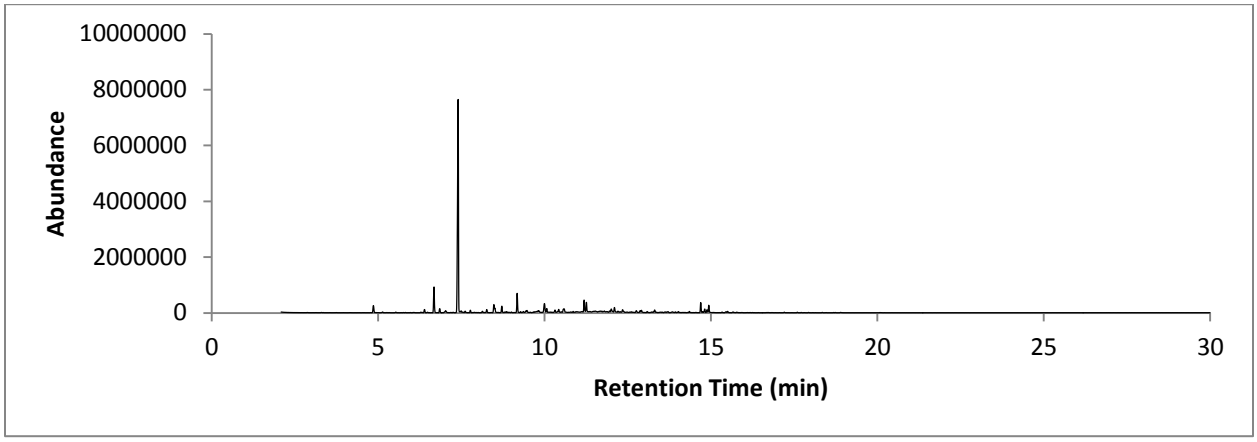

Figure 145: TIC C6-17

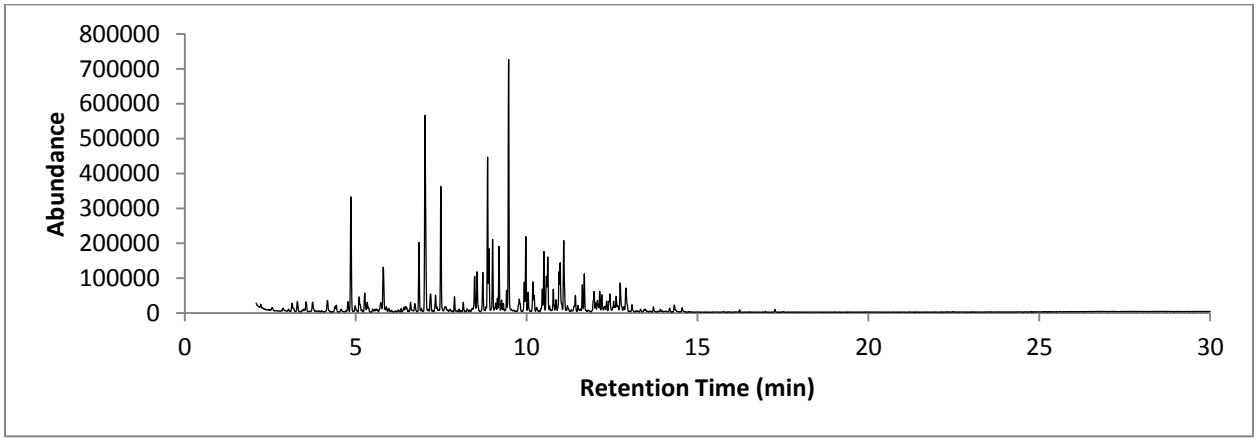

Figure 146: TIC C6-18

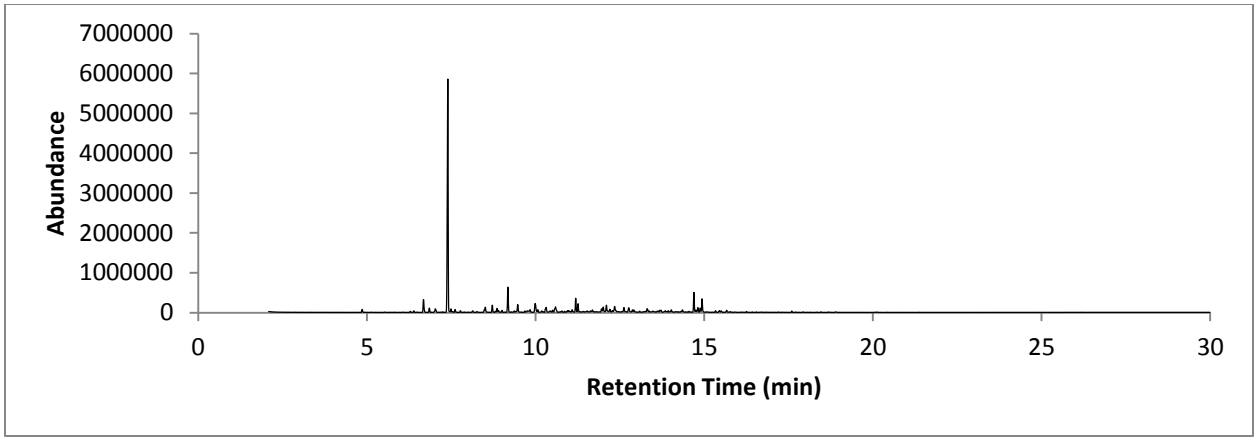

Figure 147: TIC C6-19

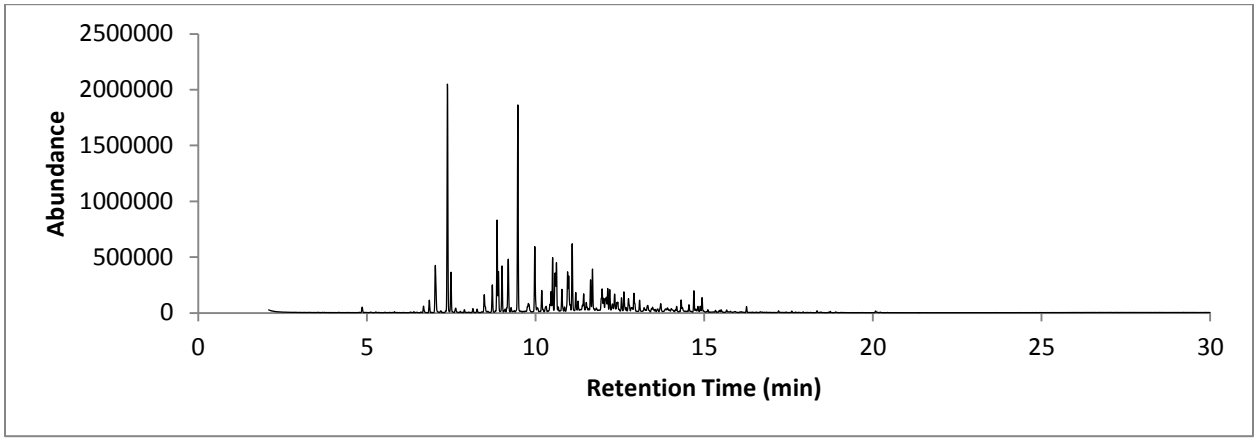

Figure 148: TIC C6-20

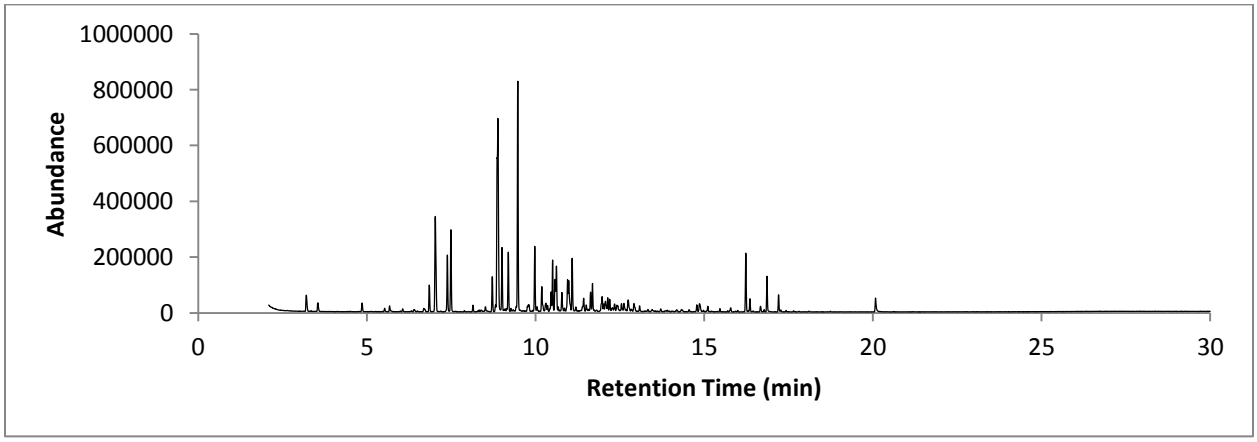

Figure 149: TIC C6-21

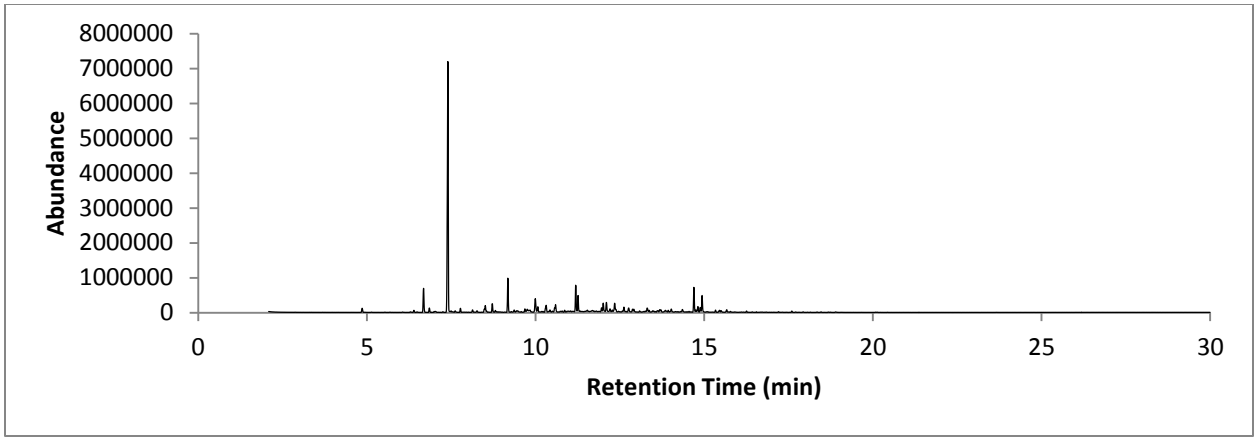

Figure 150: TIC C6-22

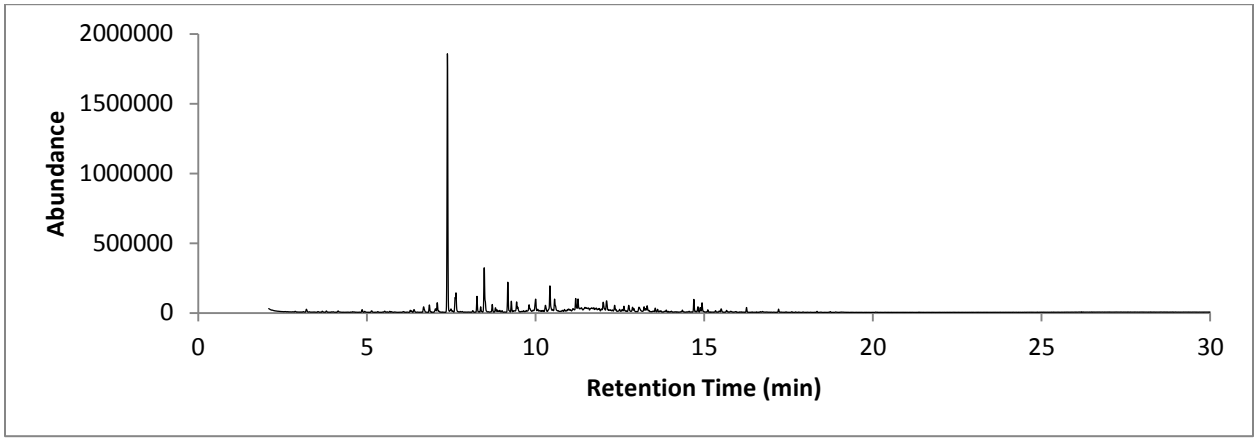

Figure 151: TIC C6-23

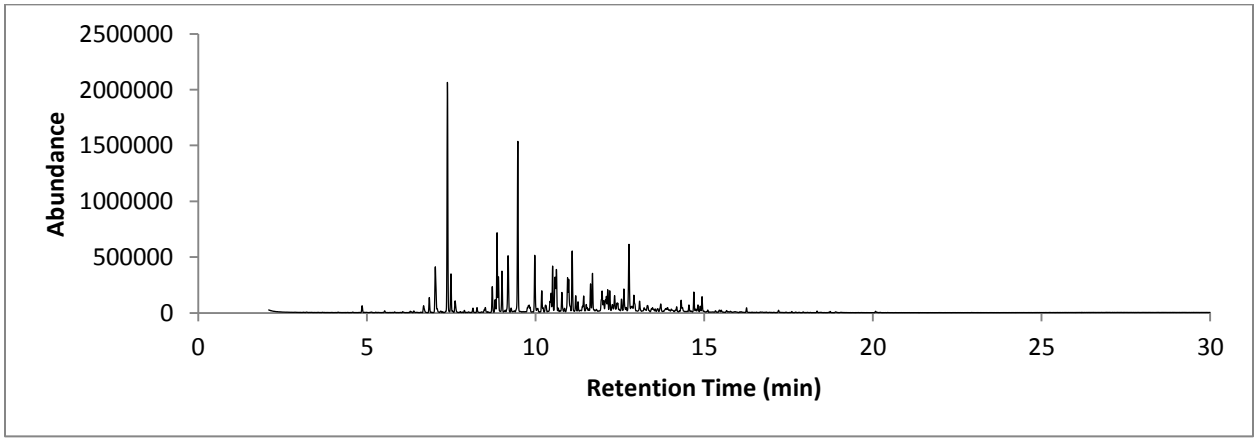

Figure 152: TIC C6-24

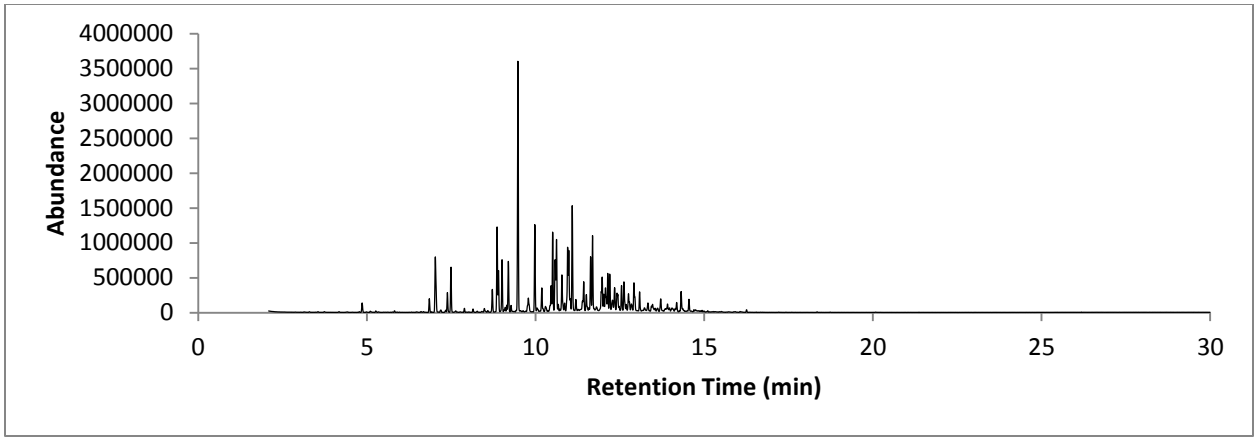

Figure 153: TIC C6-25

Sample TIS

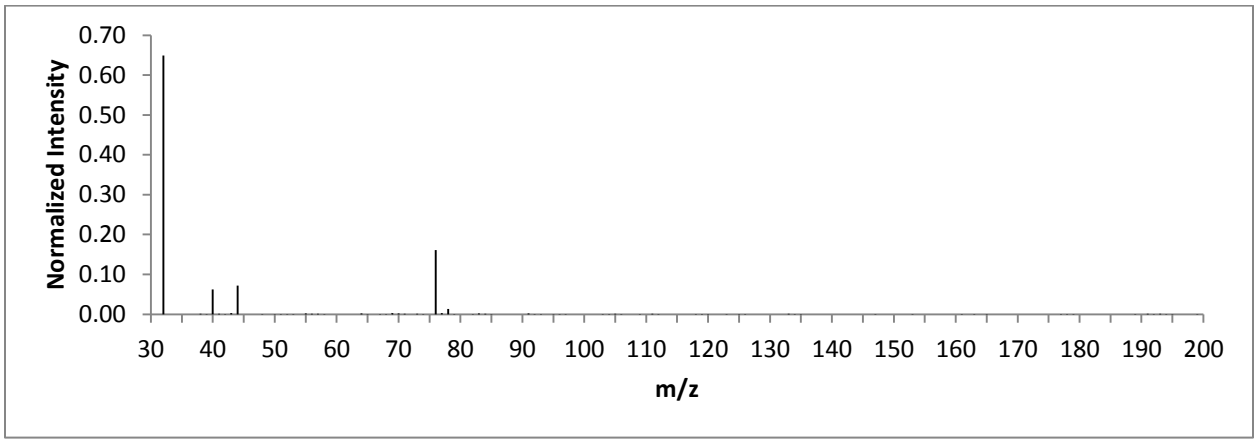

Figure 154: TIS C6-13

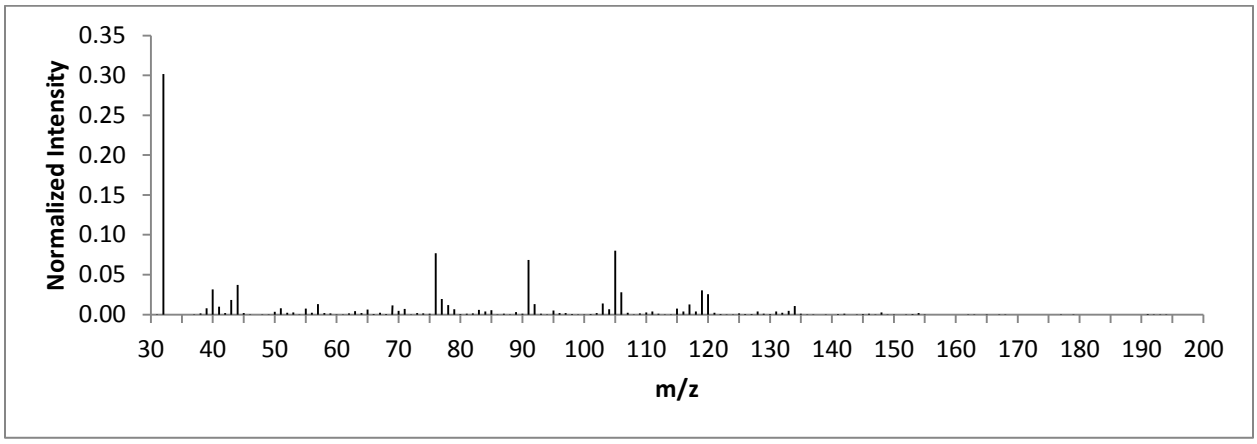

Figure 155: TIS C6-14

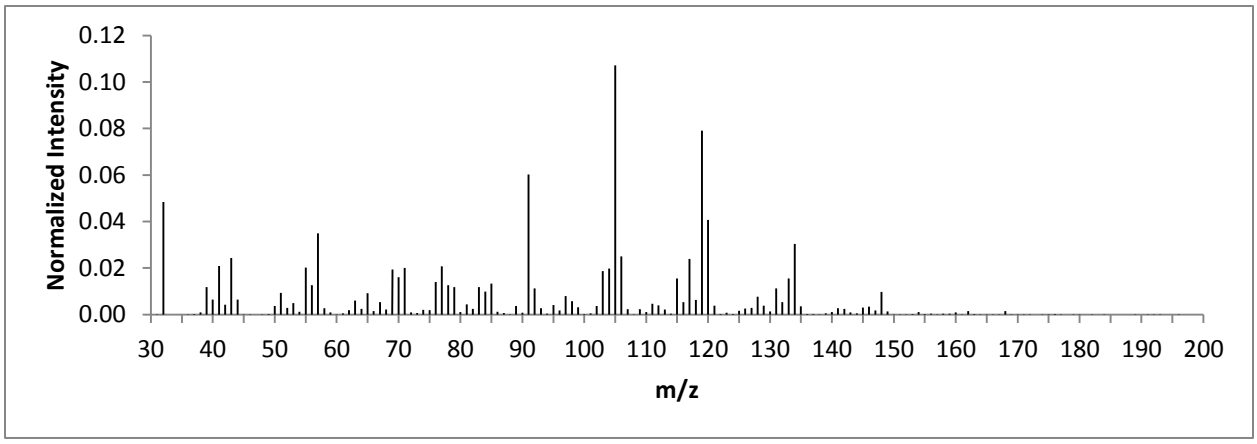

Figure 156: TIS C6-15

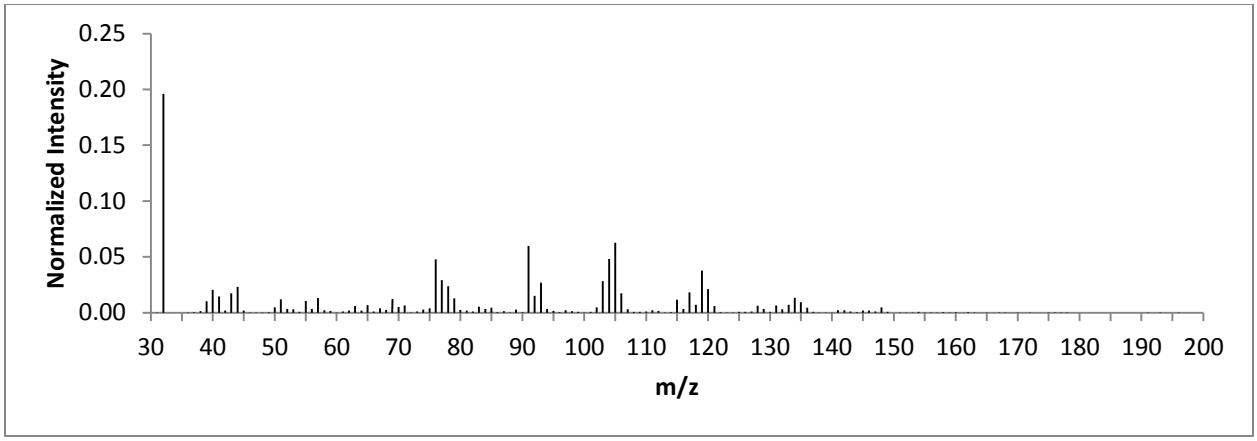

Figure 157: TIS C6-16

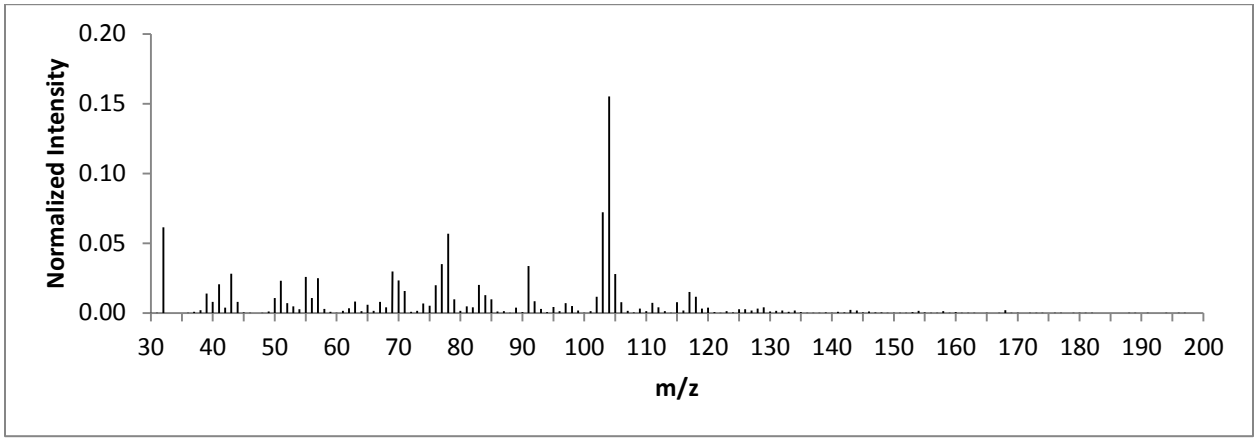

Figure 158: TIS C6-17

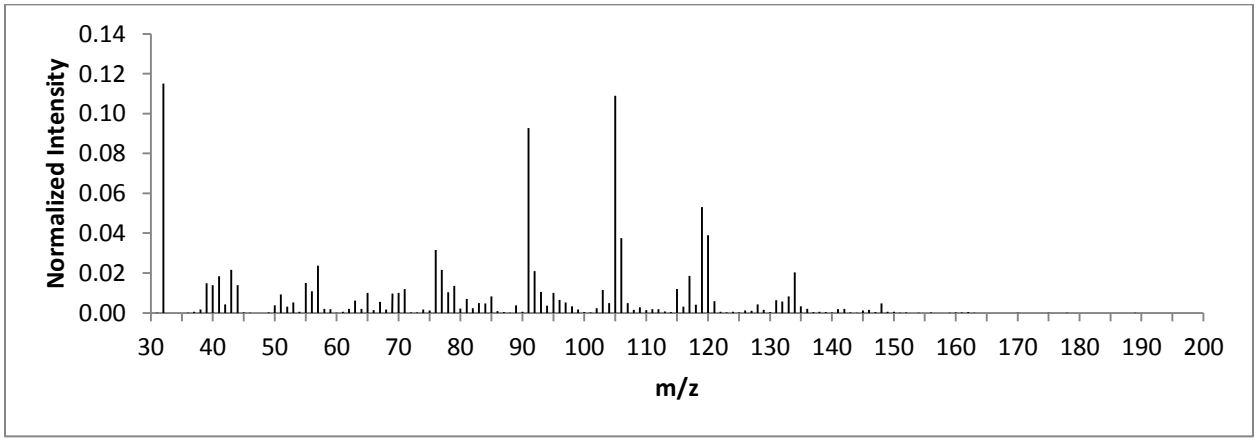

Figure 159: TIS C6-18

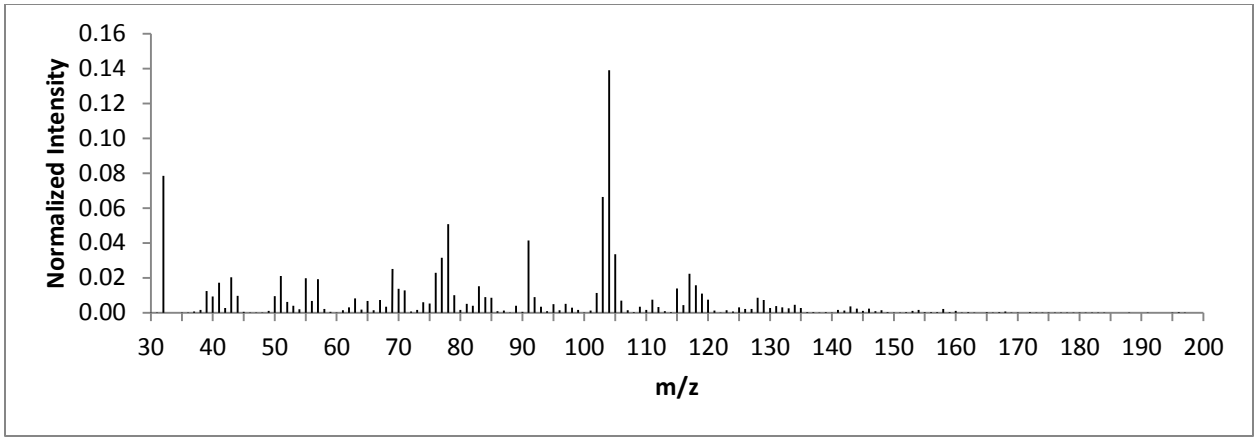

Figure 160: TIS C6-19

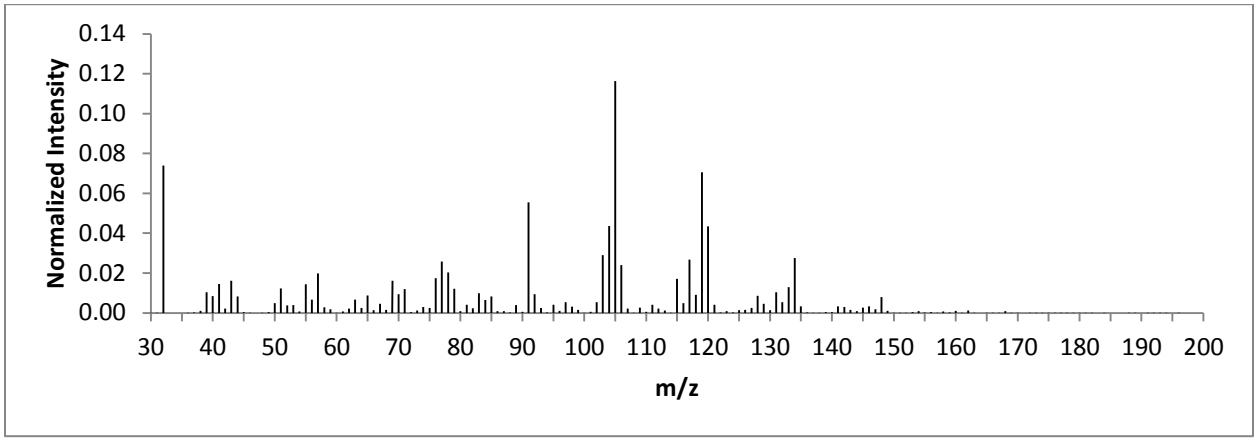

Figure 161: TIS C6-20

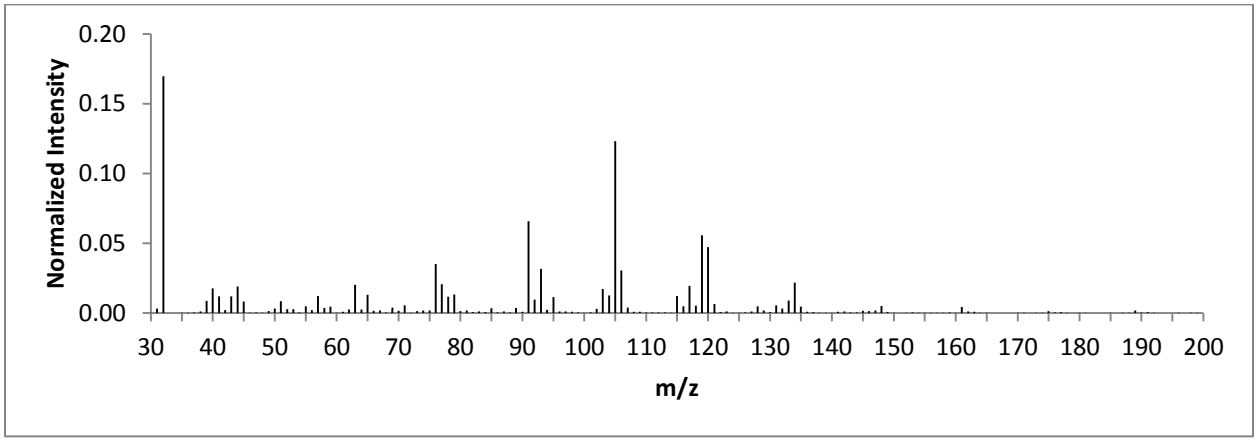

Figure 162: TIS C6-21

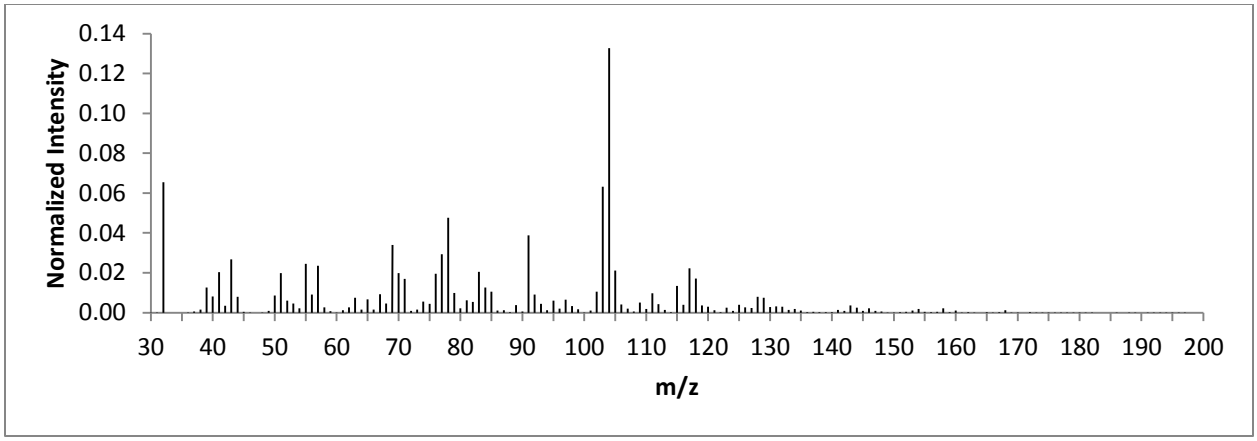

Figure 163: TIS C6-22

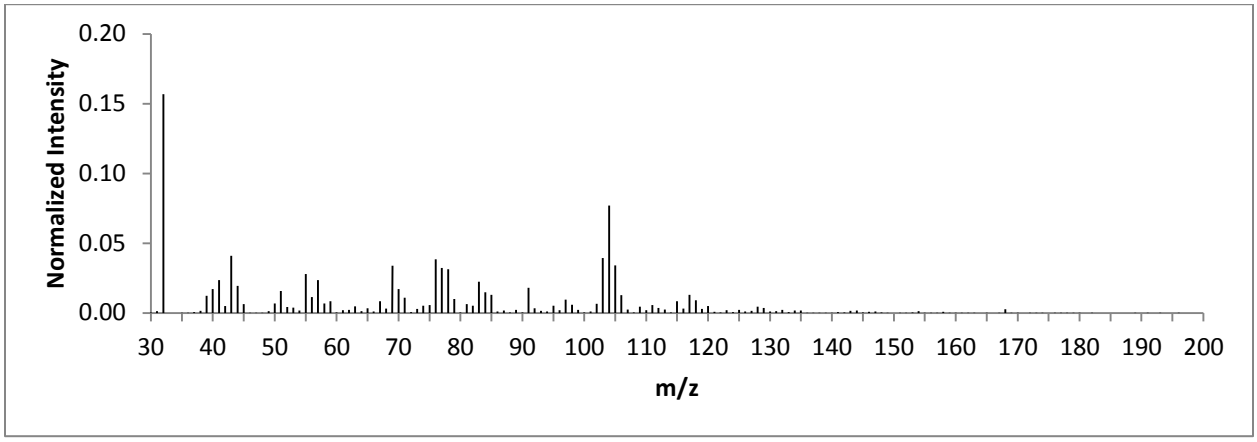

Figure 164: TIS C6-23

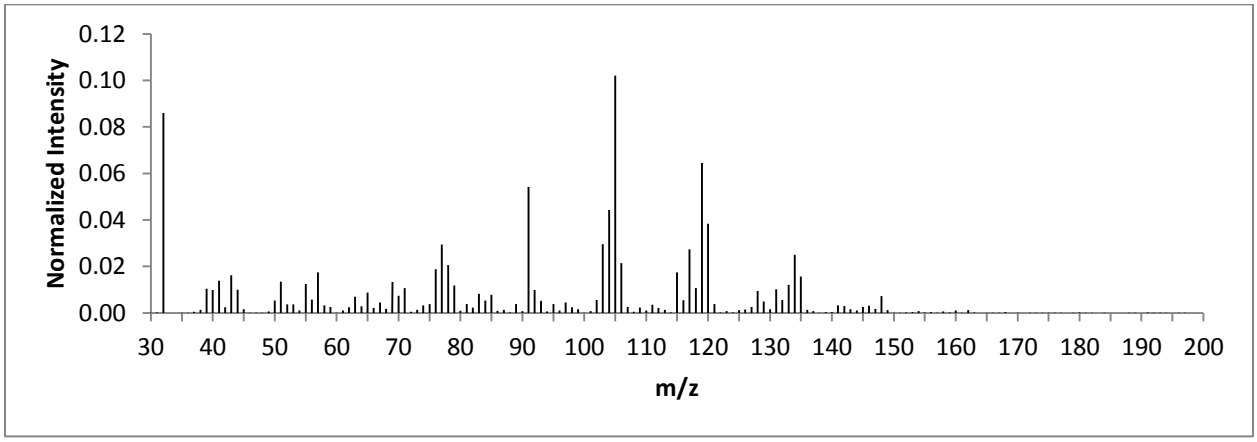

Figure 165: TIS C6-24

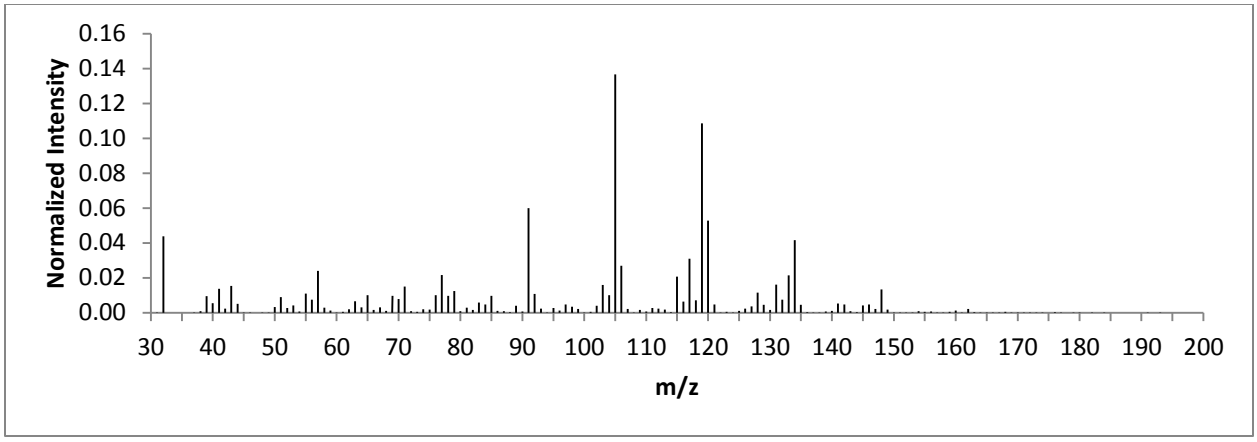

Figure 166: TIS C6-25

APPENDIX C
CONTAINER 7

Ignitable Liquid TIC

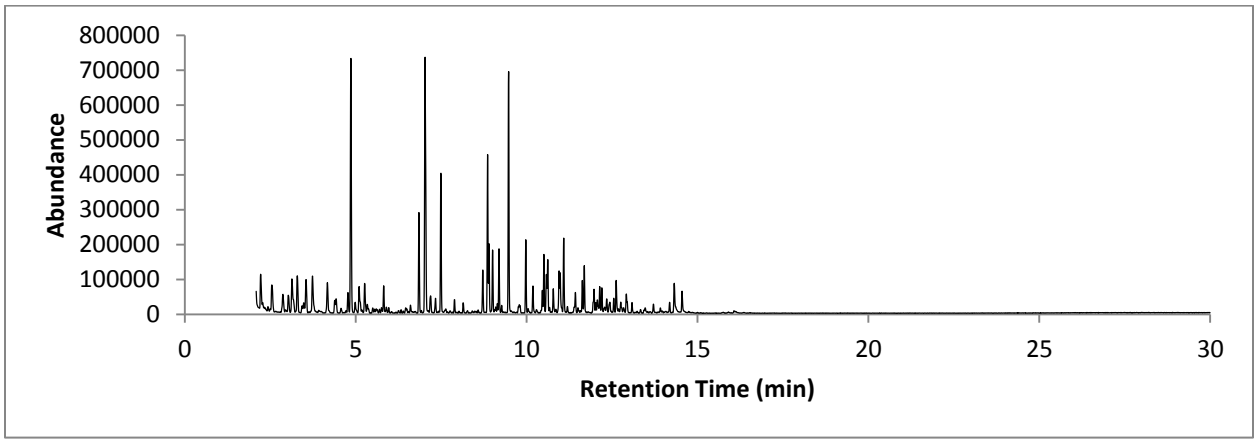

Figure 167: TIC C7-C8 Unweathered Gasoline

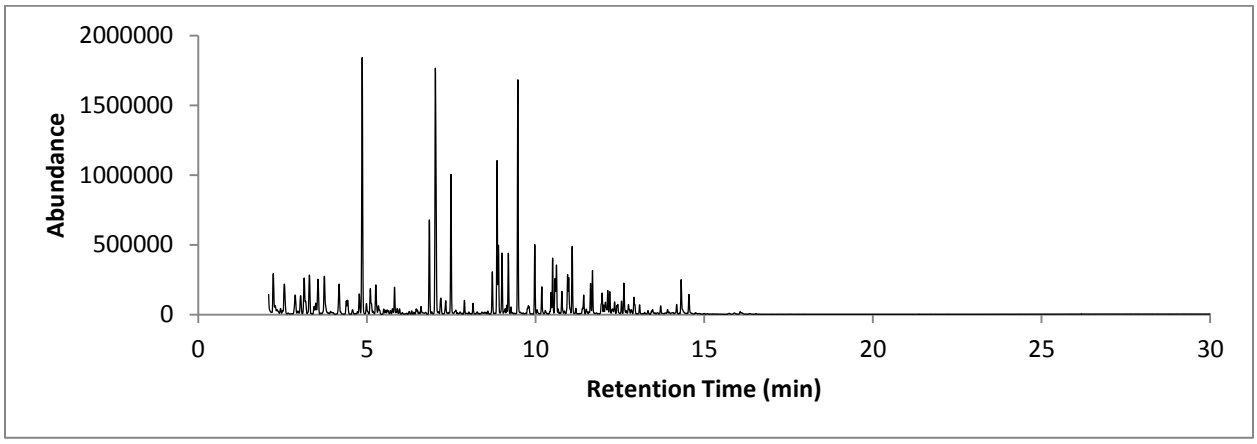

Figure 168: TIC C7-C8 25% Weathered Gasoline

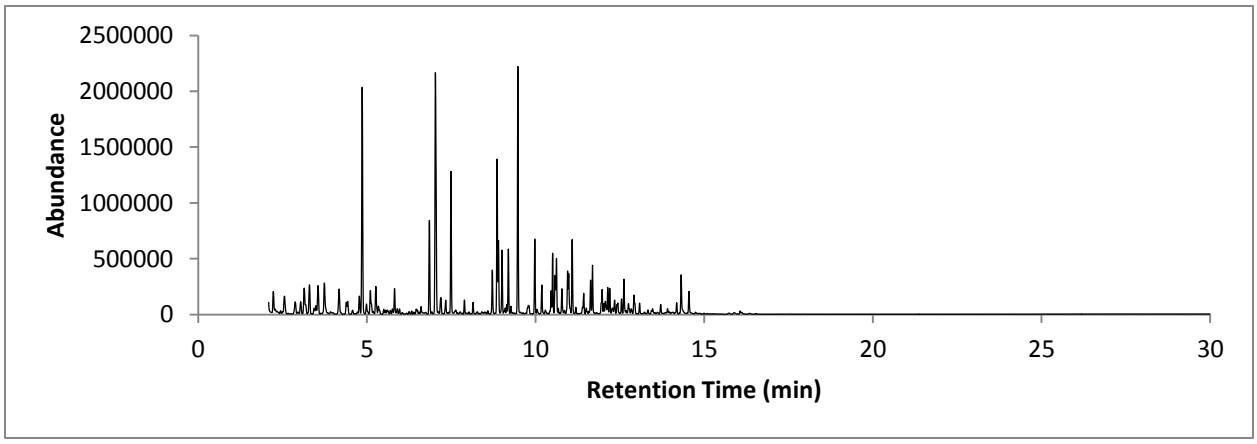

Figure 169: TIC C7-C8 50% Weathered Gasoline

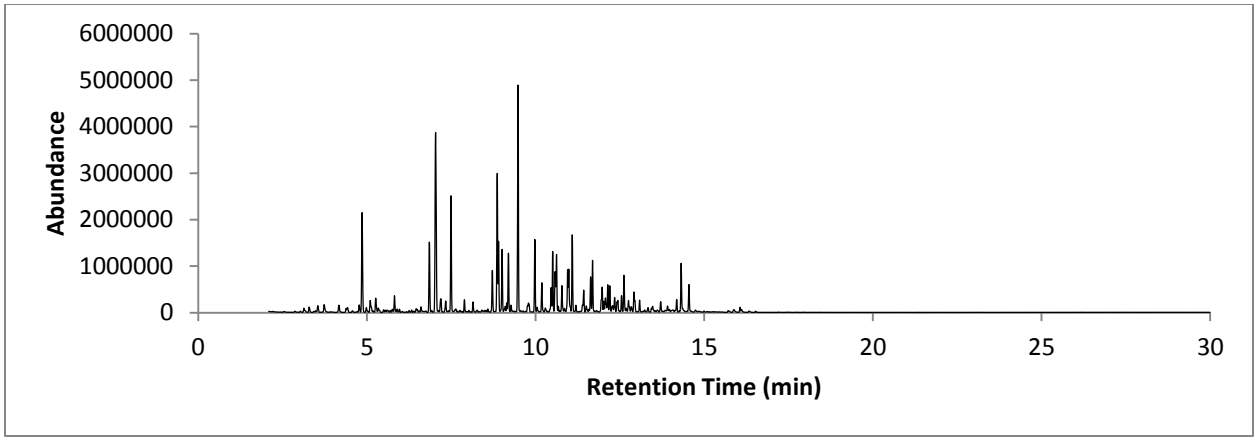

Figure 170: TIC C7-C8 75% Weathered Gasoline

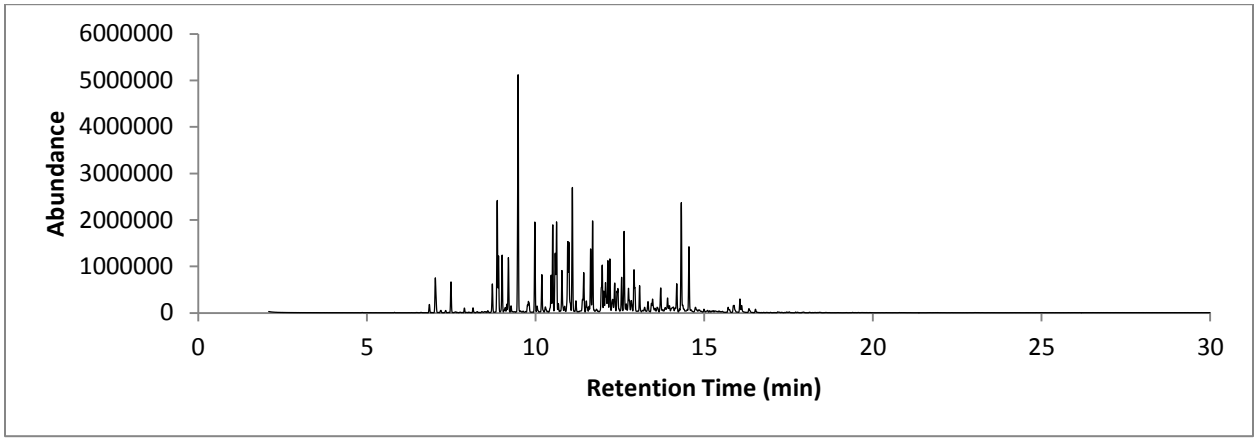

Figure 171: TIC C7-C8 90% Weathered Gasoline

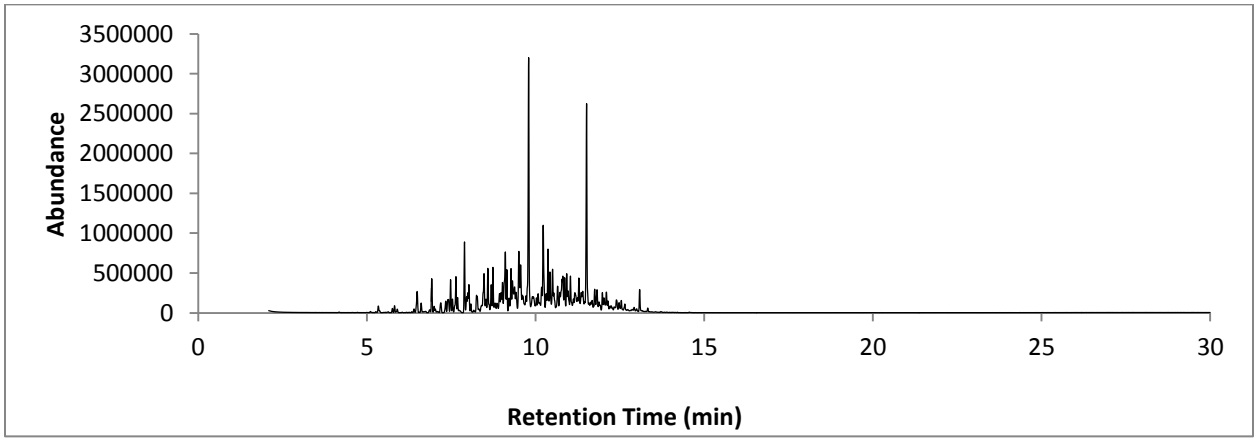

Figure 172: TIC C7-C8 Unweathered MPD

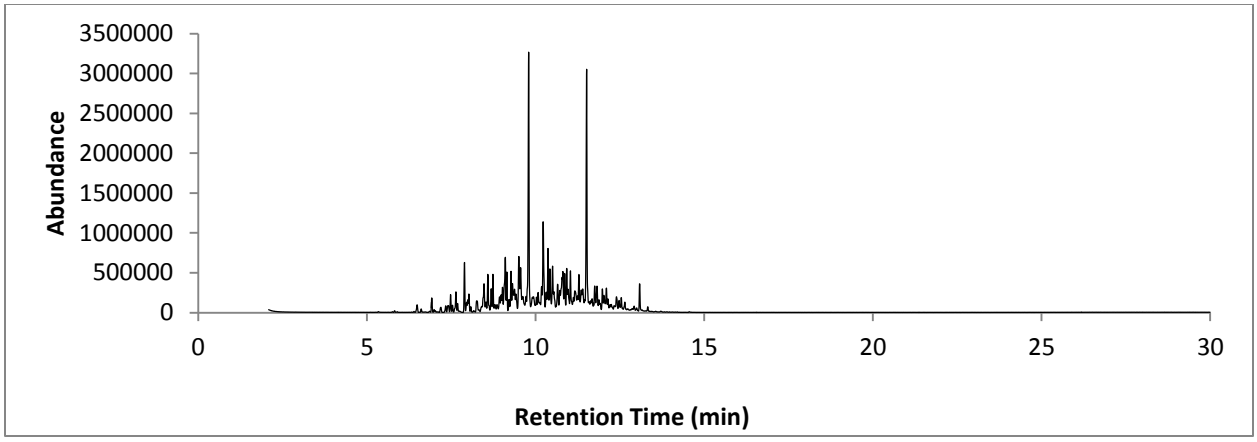

Figure 173: TIC C7-C8 25% Weathered MPD

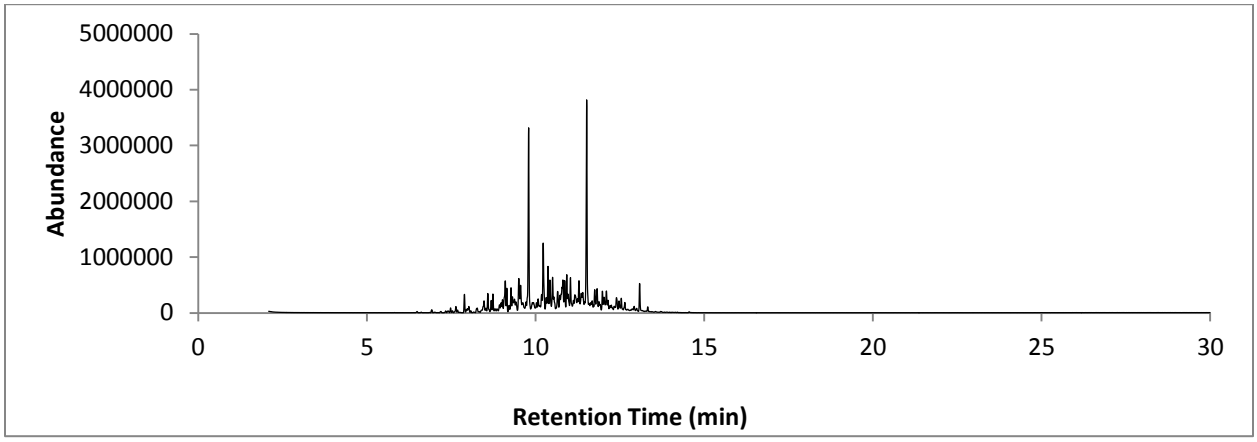

Figure 174: TIC C7-C8 50% Weathered MPD

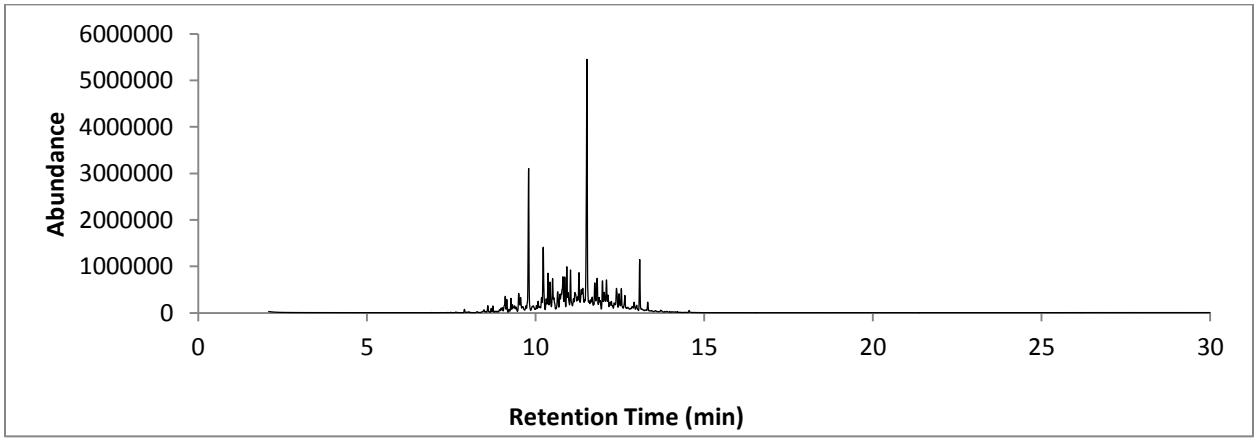

Figure 175: TIC C7-C8 75% Weathered MPD

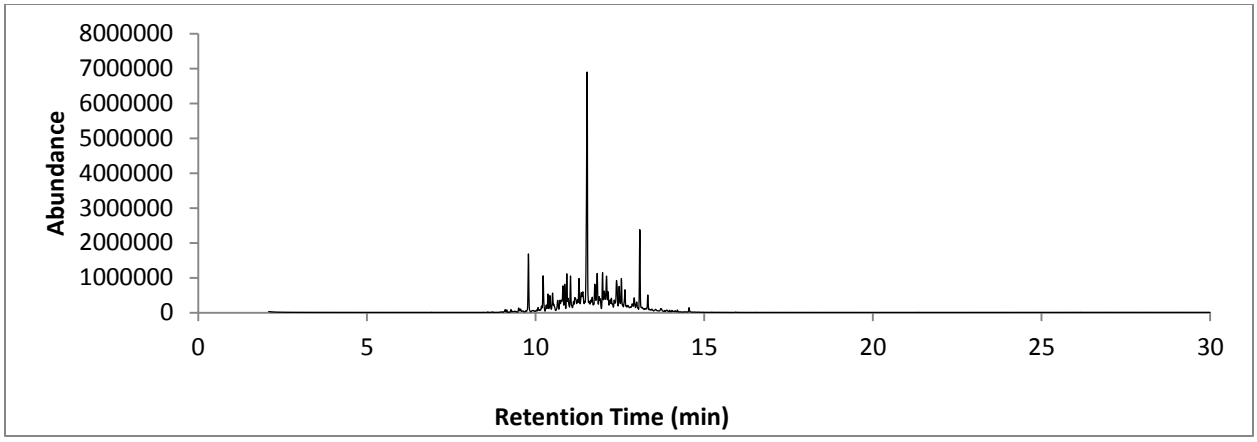

Figure 176: TIC C7-C8 90% Weathered MPD

Ignitable Liquid TIS

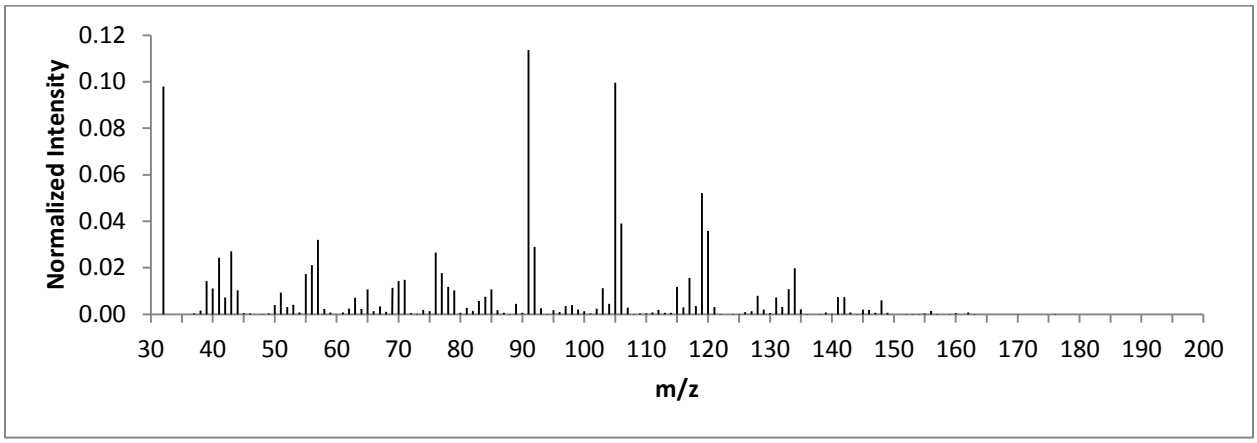

Figure 177: TIS C7-C8 Unweathered Gasoline

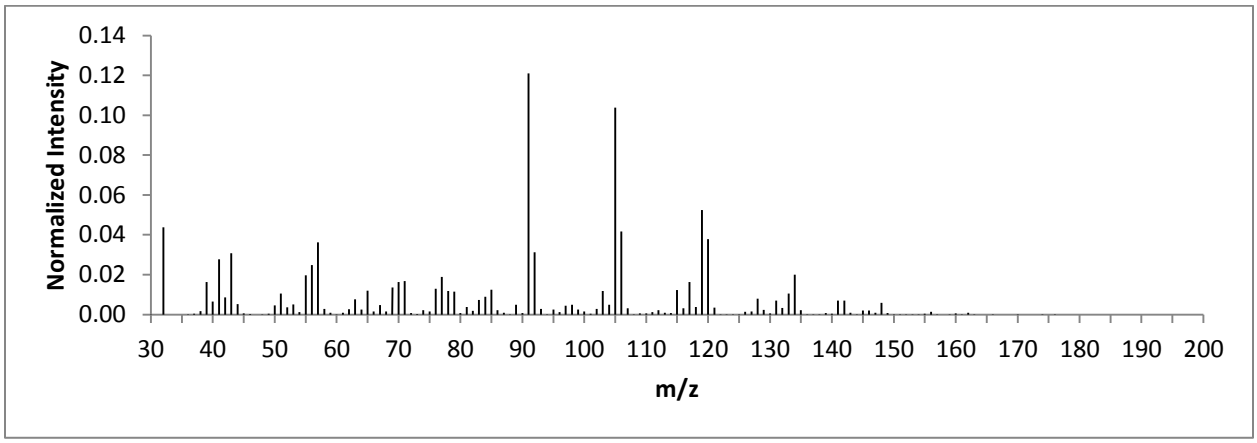

Figure 178: TIS C7-C8 25% Weathered Gasoline

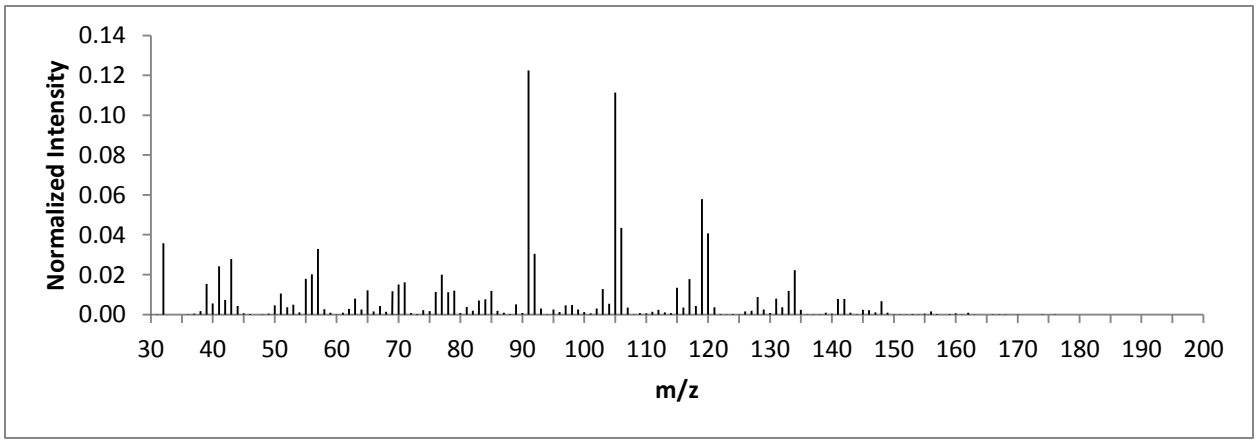

Figure 179: TIS C7-C8 50% Weathered Gasoline

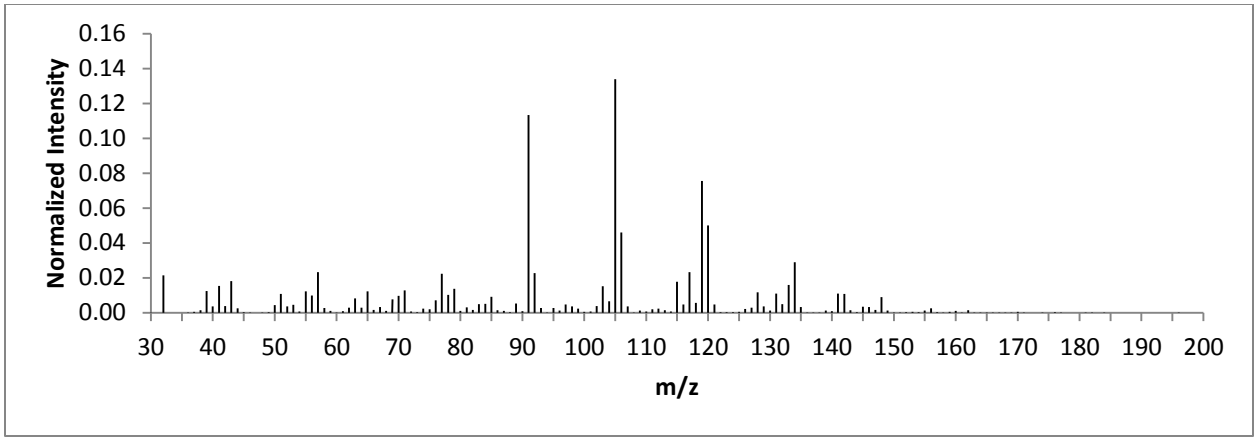

Figure 180: TIS C7-C8 75% Weathered Gasoline

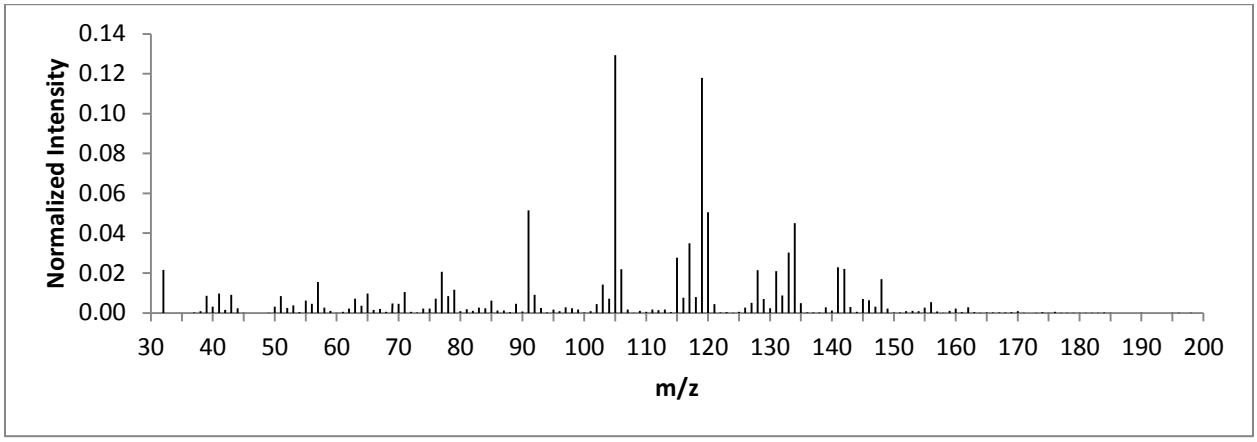

Figure 181: TIS C7-C8 90% Weathered Gasoline

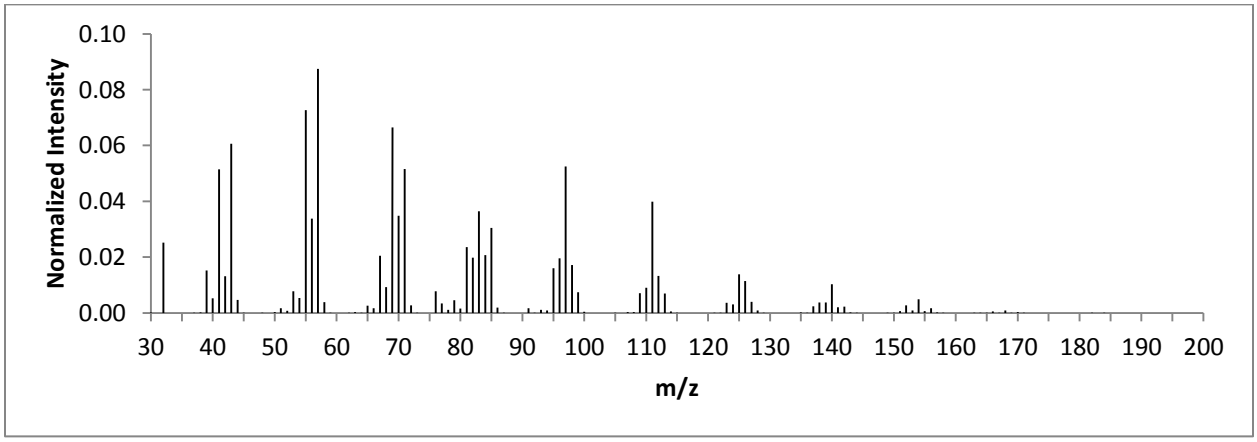

Figure 182: TIS C7-C8 Unweathered MPD

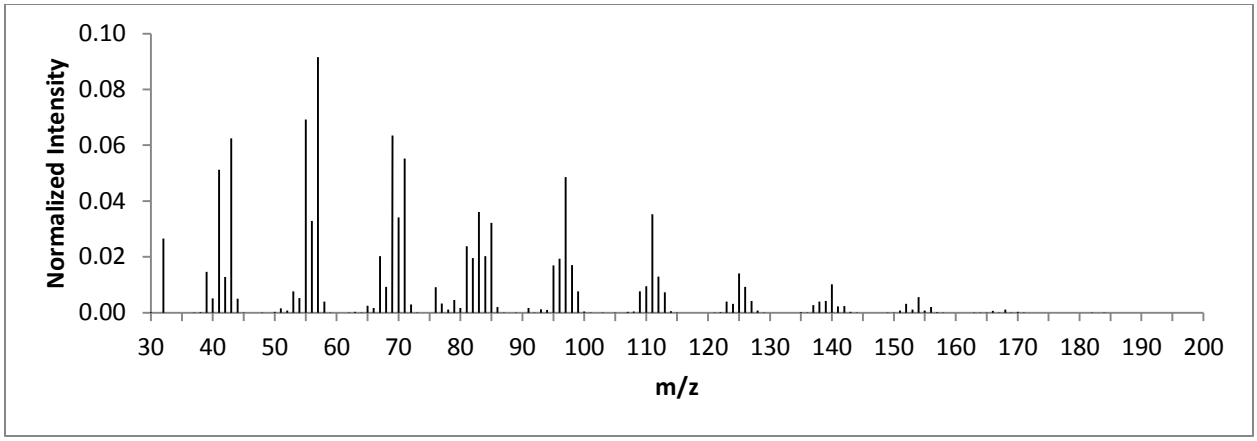

Figure 183: TIS C7-C8 25% Weathered MPD

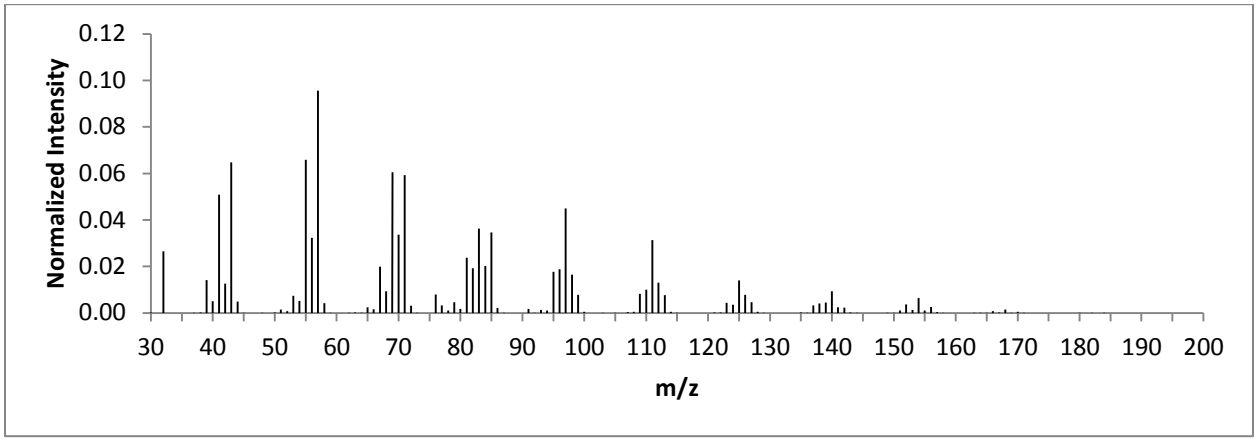

Figure 184: TIS C7-C8 50% Weathered MPD

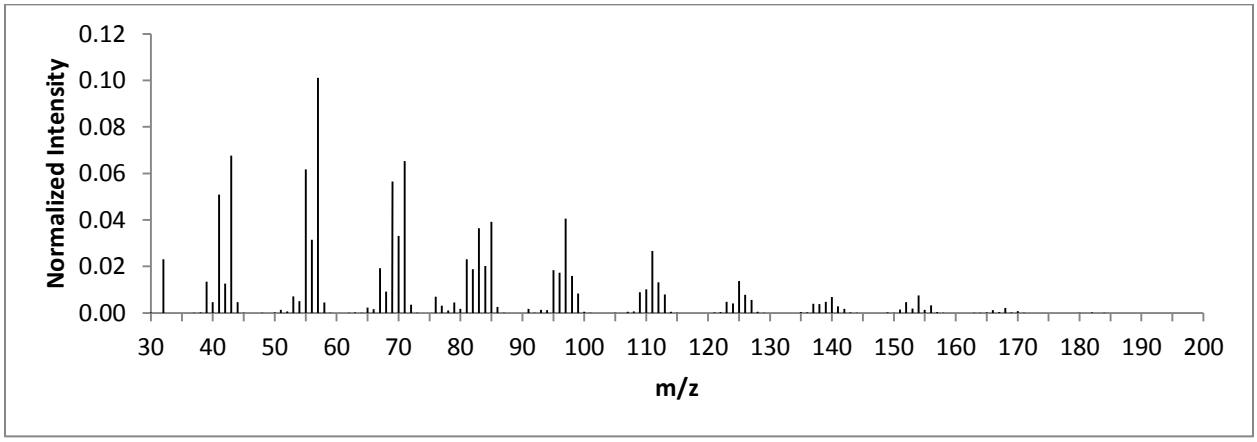

Figure 185: TIS C7-C8 75% Weathered MPD

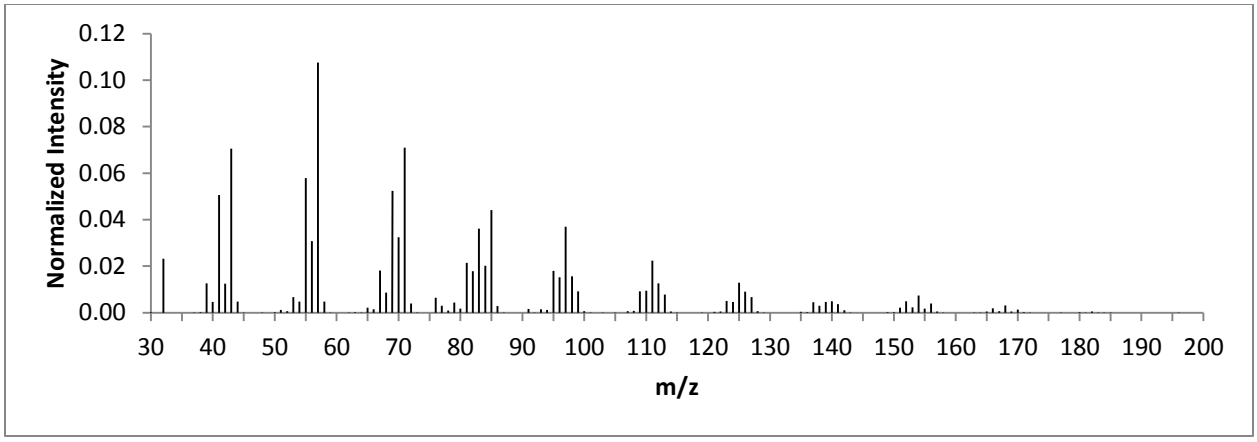

Figure 186: TIS C7-C8 90% Weathered MPD

Sample TIC

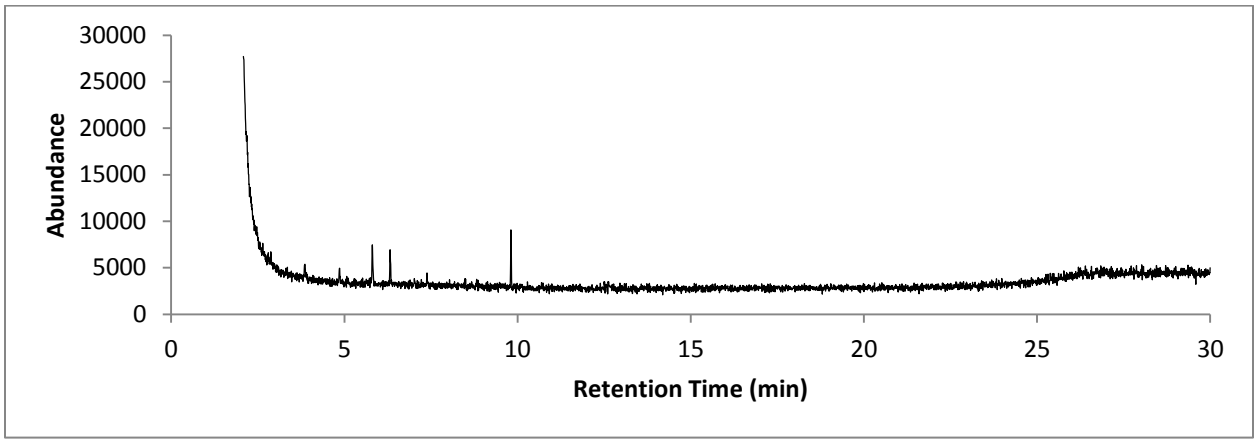

Figure 187: TIC C7-1

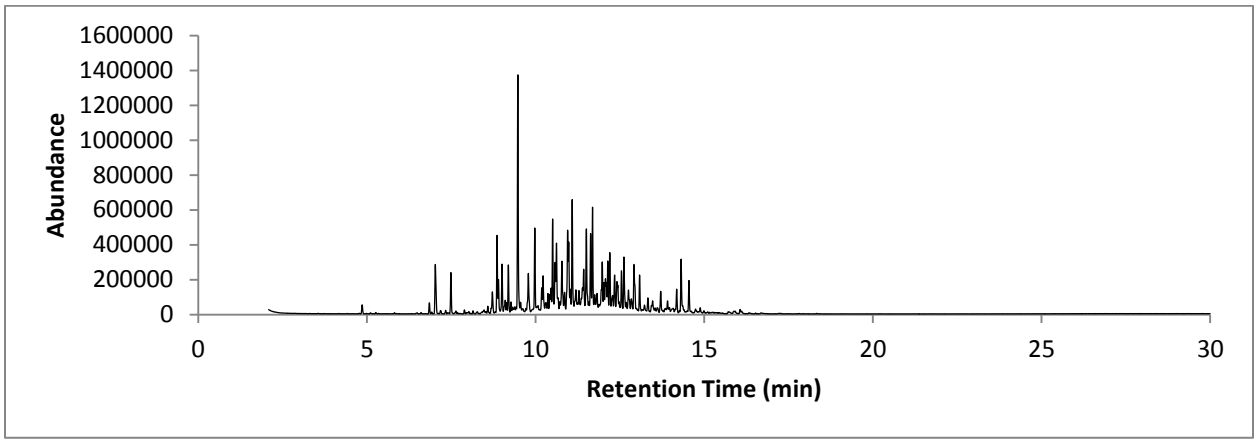

Figure 188: TIC C7-2

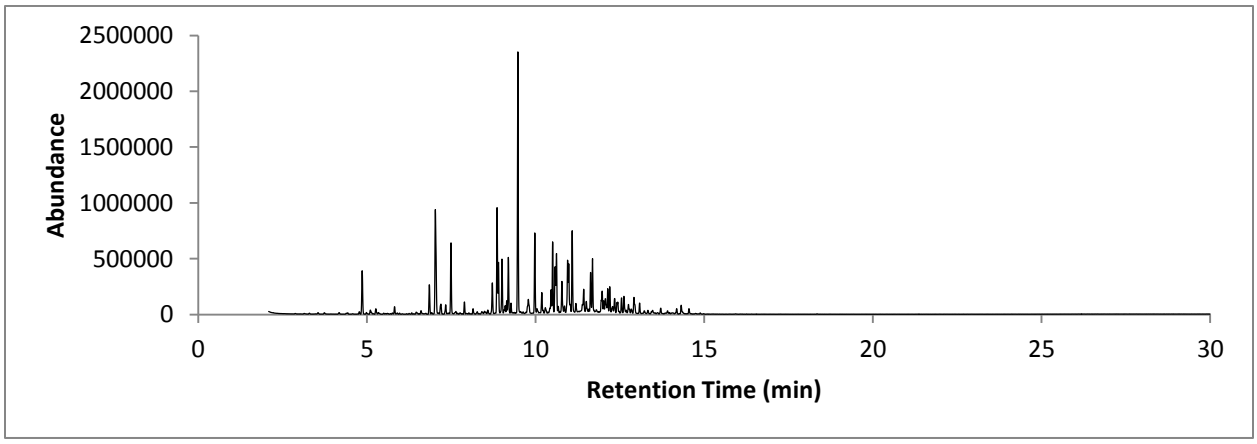

Figure 189: TIC C7-3

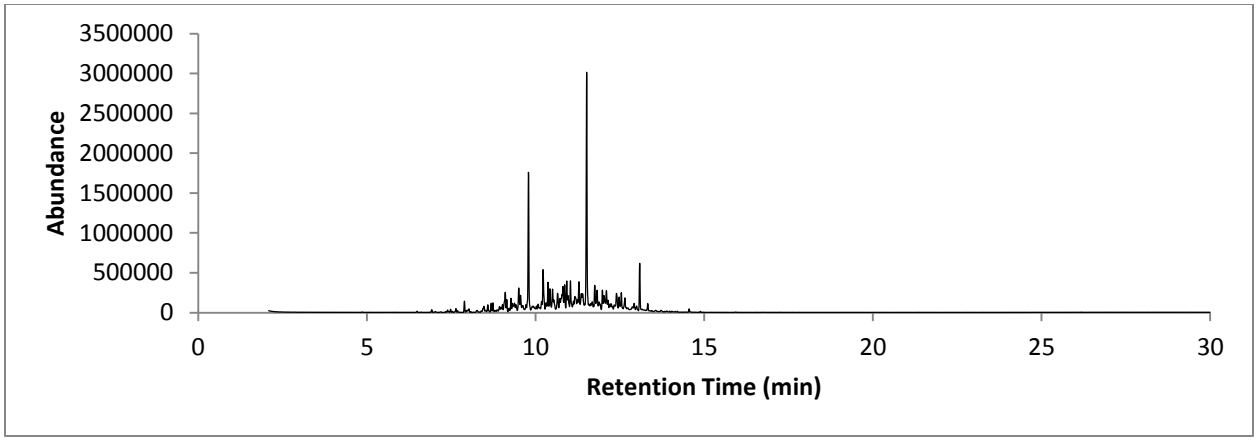

Figure 190: TIC C7-4

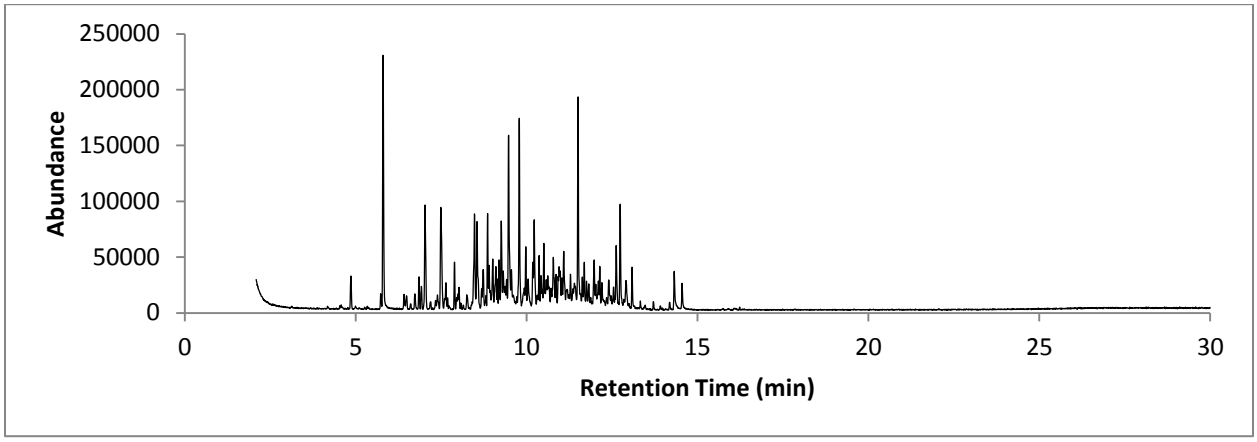

Figure 191: TIC C7-5

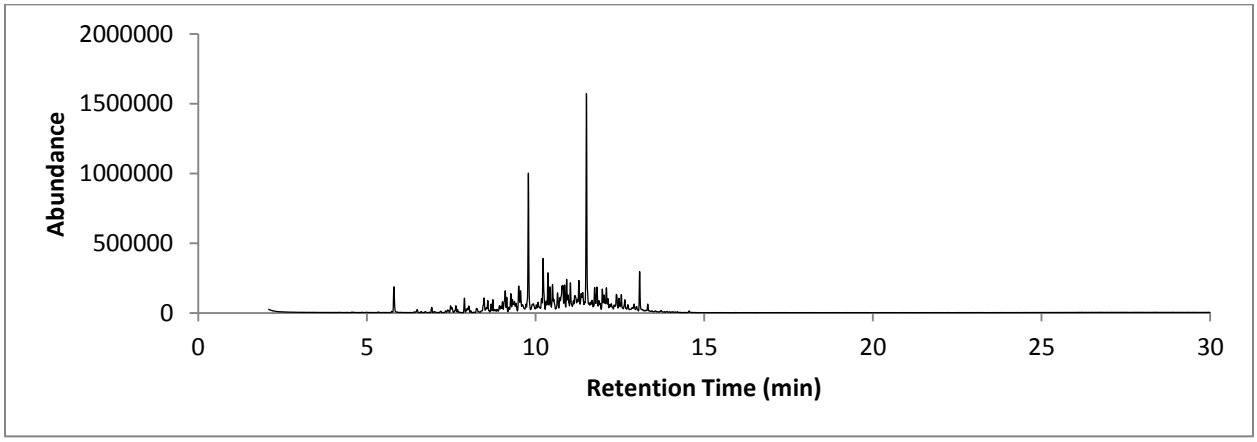

Figure 192: TIC C7-6

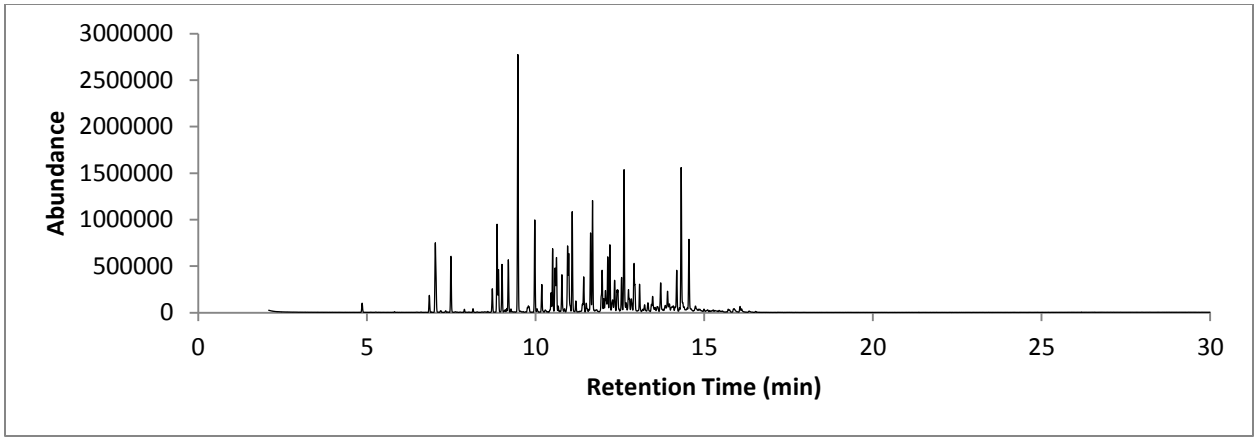

Figure 193: TIC C7-7

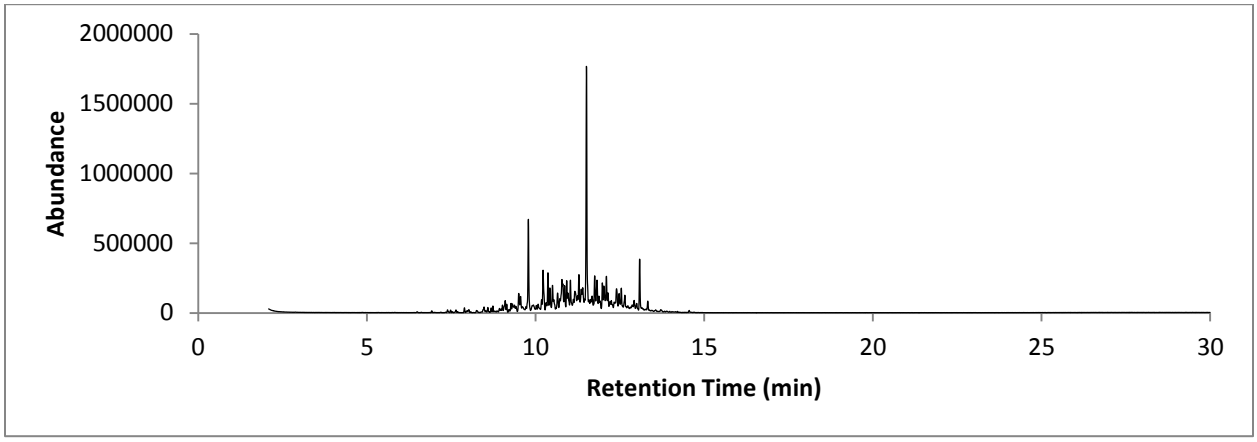

Figure 194: TIC C7-8

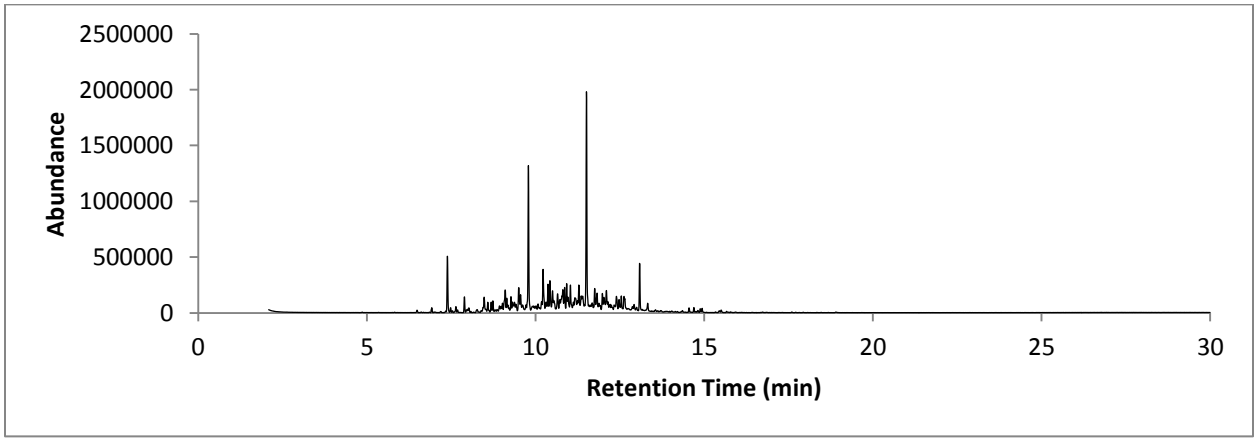

Figure 195: TIC C7-9

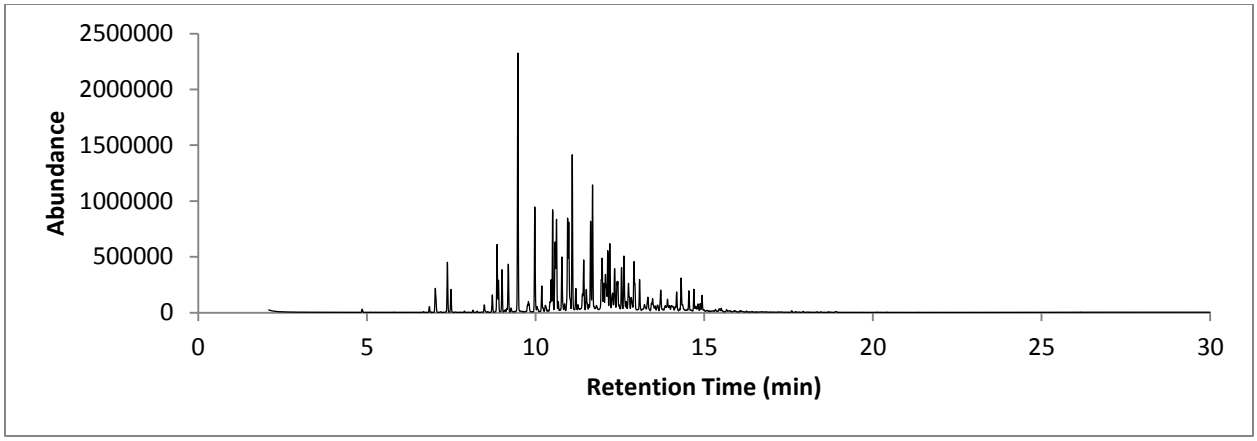

Figure 196: TIC C7-10

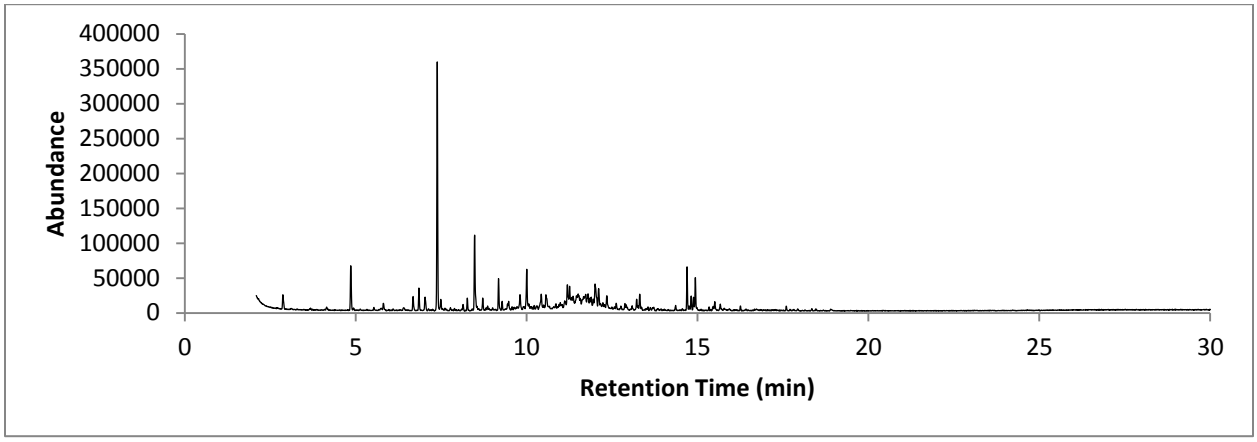

Figure 197: TIC C7-11

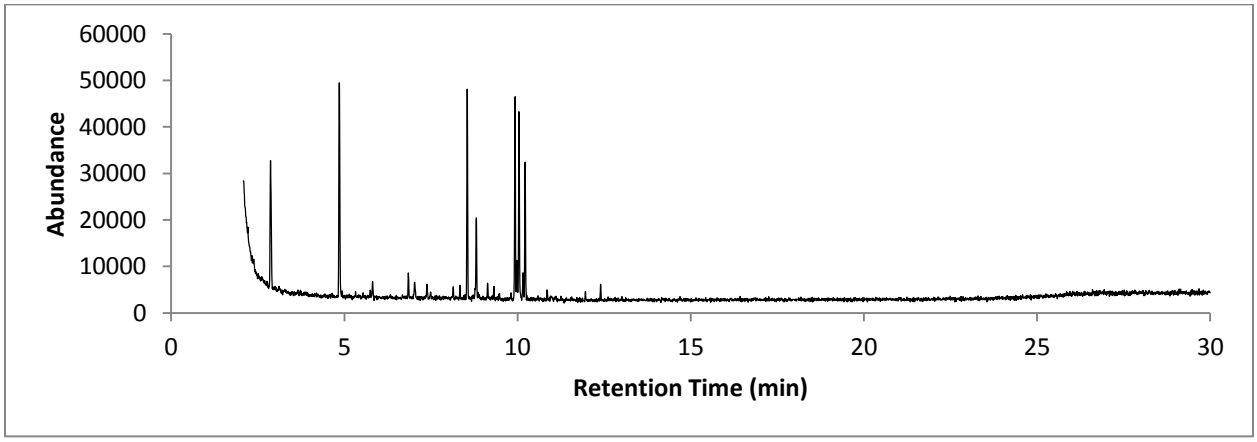

Figure 198: TIC C7-12

Sample TIS

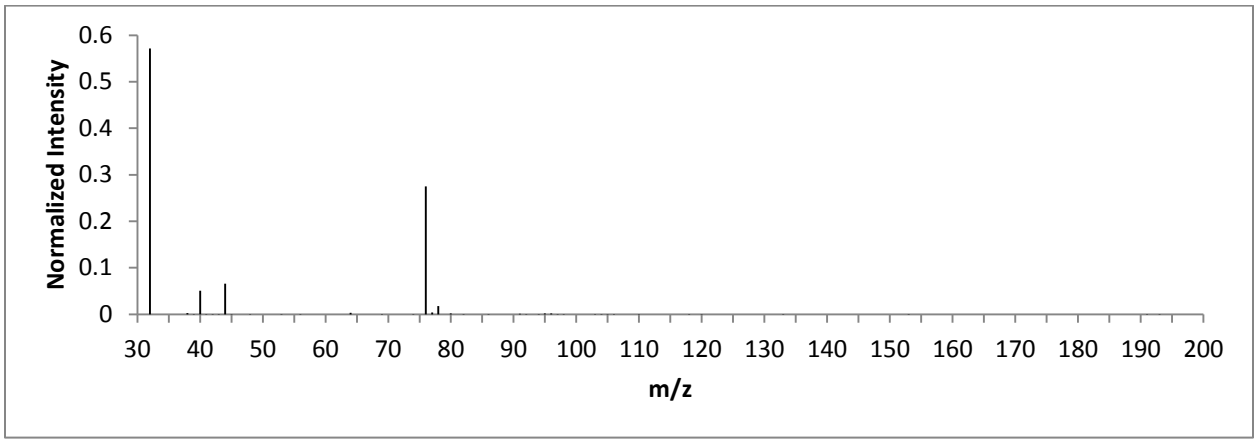

Figure 199: TIS C7-1

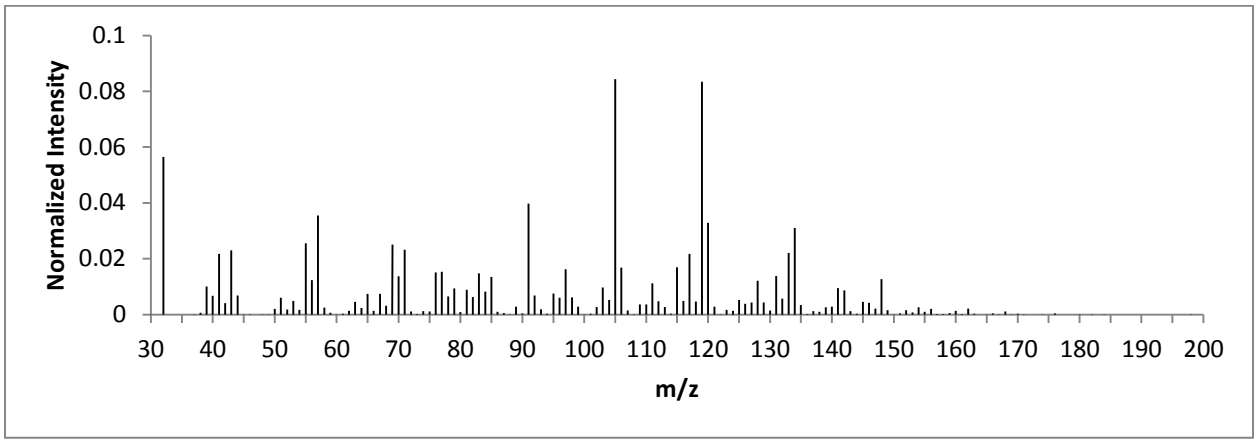

Figure 200: TIS C7-2

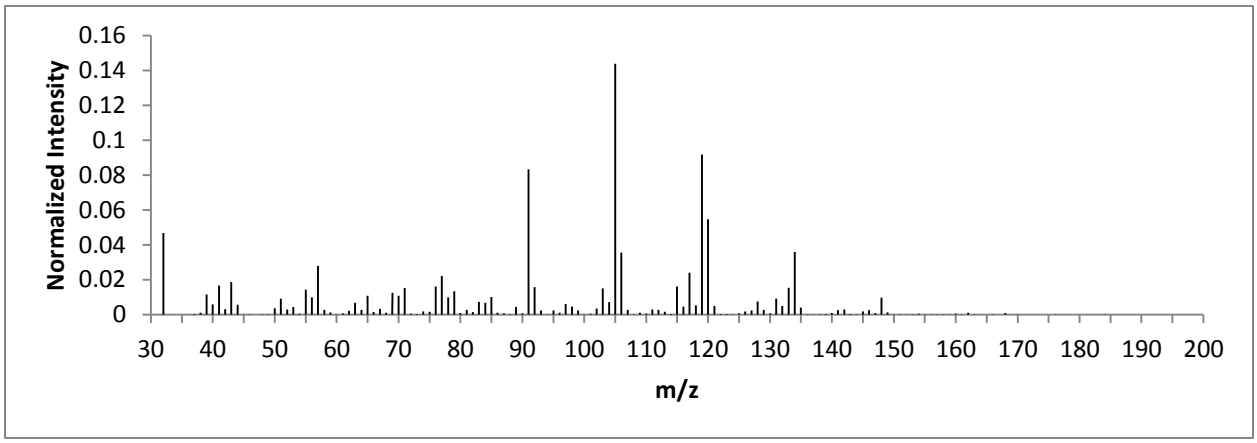

Figure 201: TIS C7-3

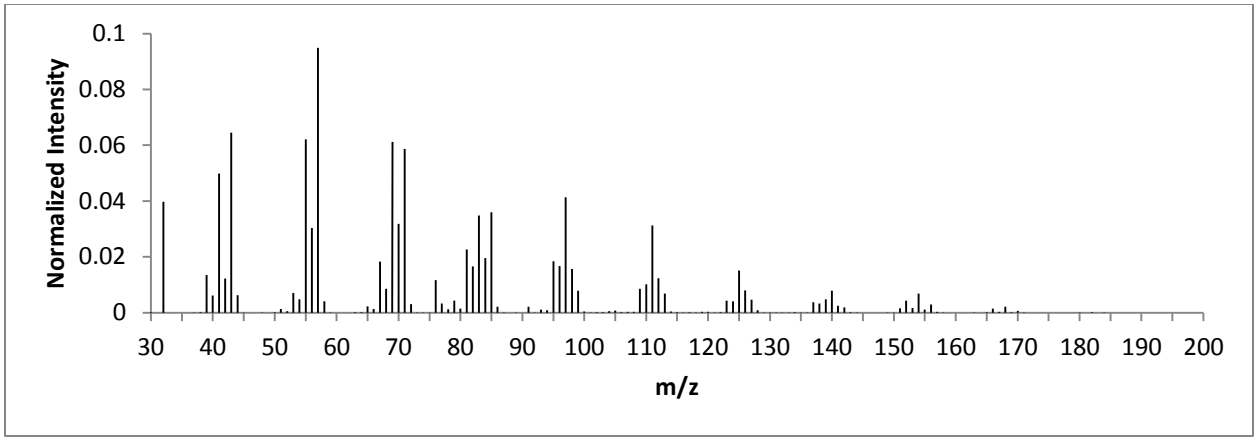

Figure 202: TIS C7-4

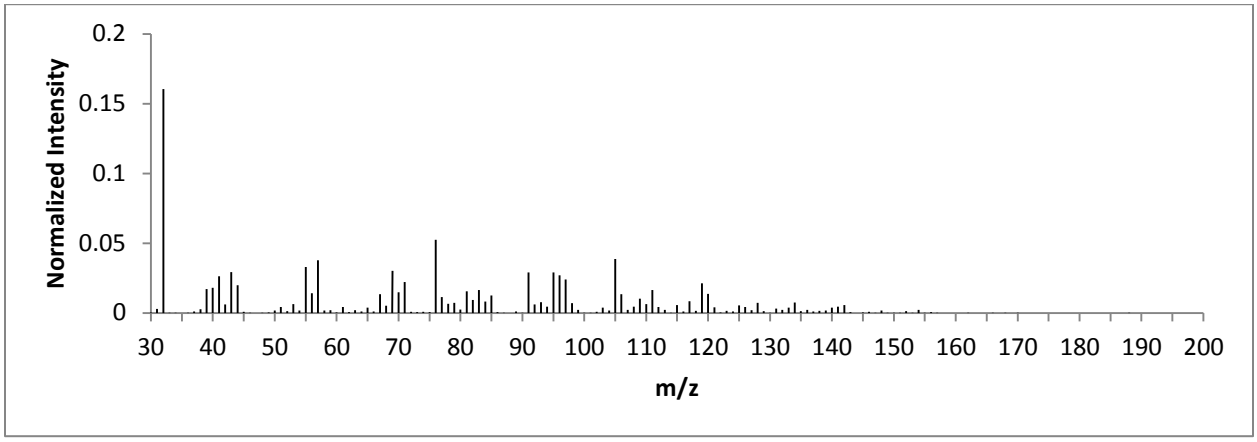

Figure 203: TIS C7-5

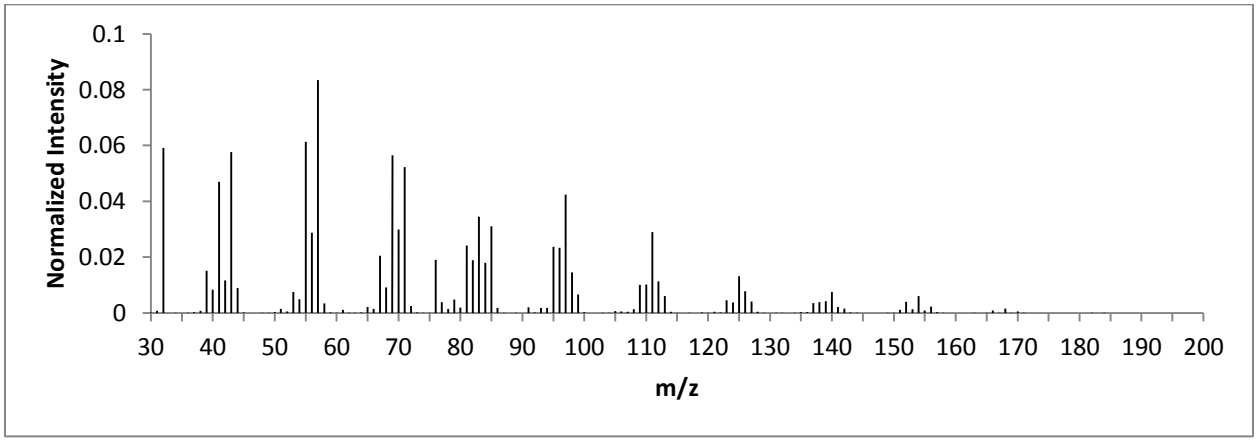

Figure 204: TIS C7-6

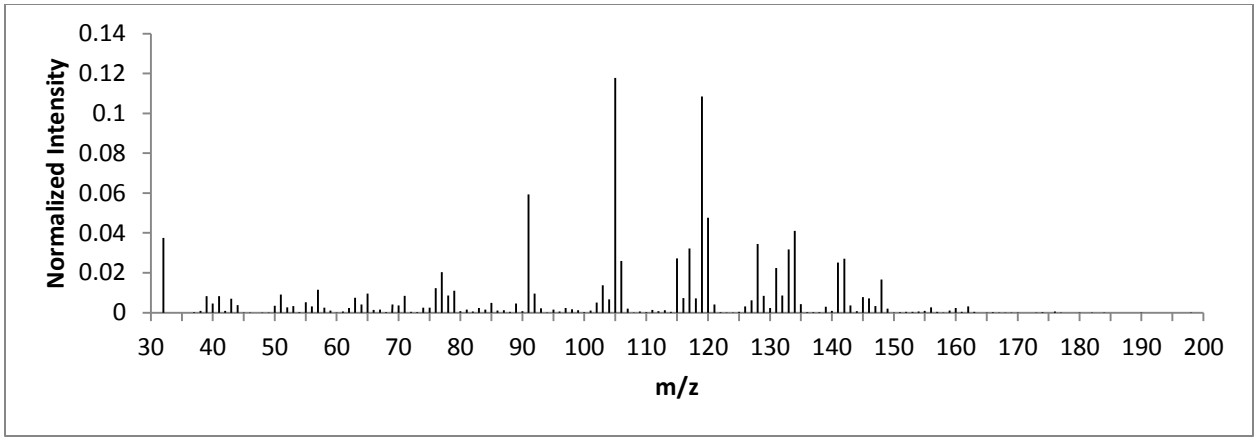

Figure 205: TIS C7-7

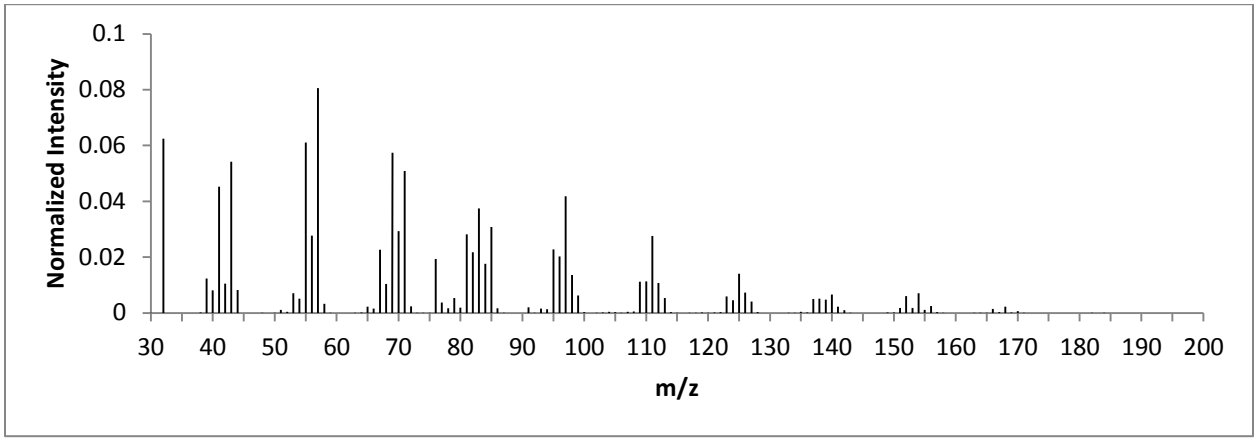

Figure 206: TIS C7-8

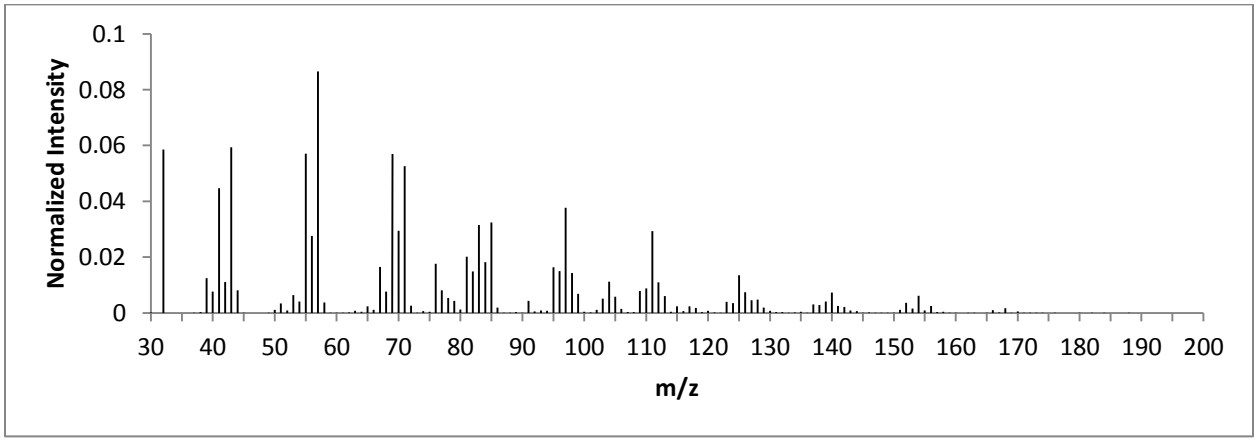

Figure 207: TIS C7-9

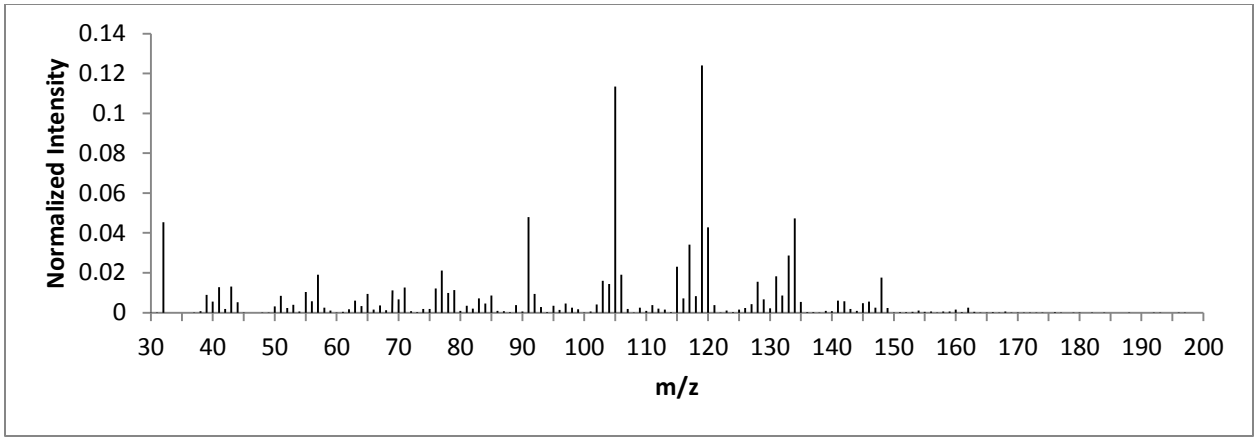

Figure 208: TIS C7-10

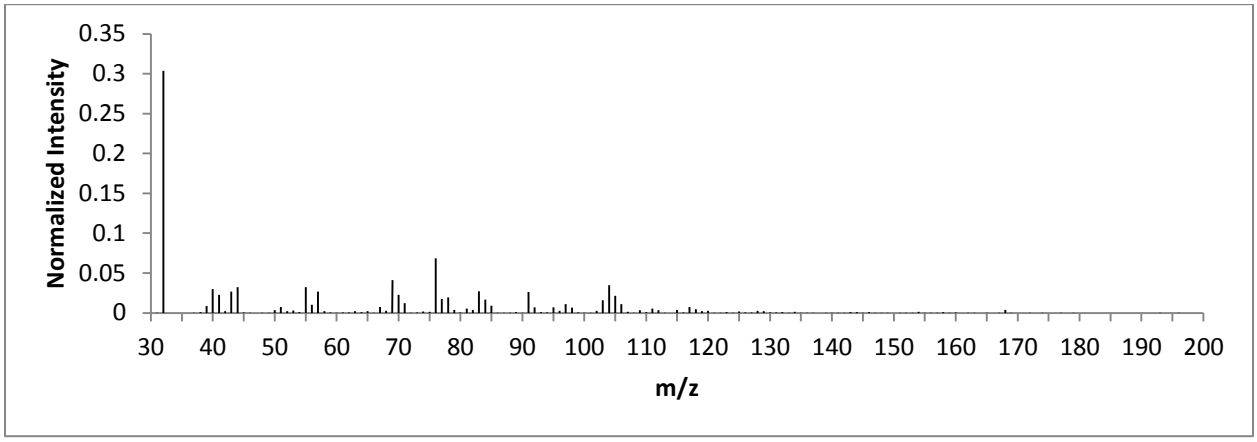

Figure 209: TIS C7-11

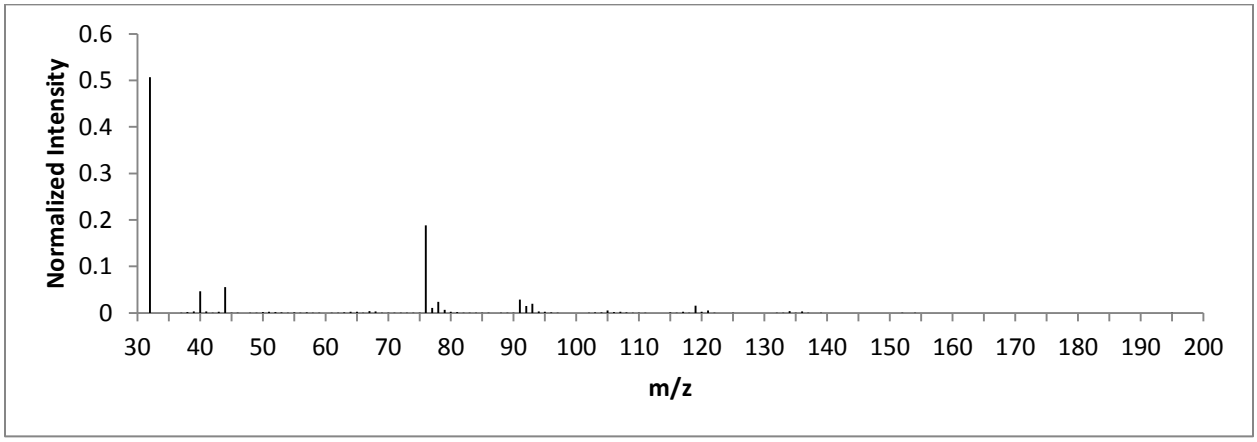

Figure 210: TIS C7-12

APPENDIX D
CONTAINER 8

Ignitable Liquid TIC

See Ignitable Liquid TIC in APPENDIX C.

Ignitable Liquid TIS

See Ignitable Liquid TIS in APPENDIX C.

Sample TIC

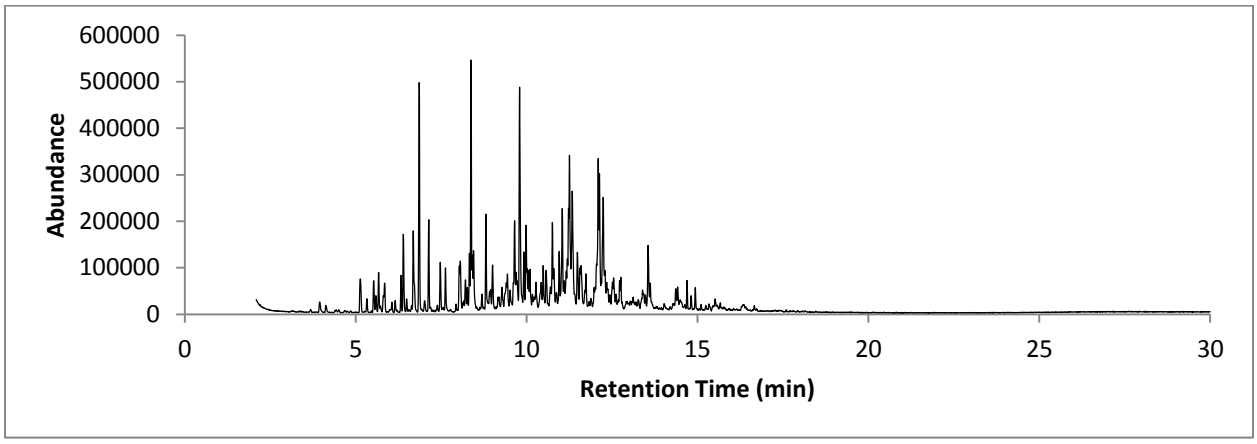

Figure 211: TIC C8-13

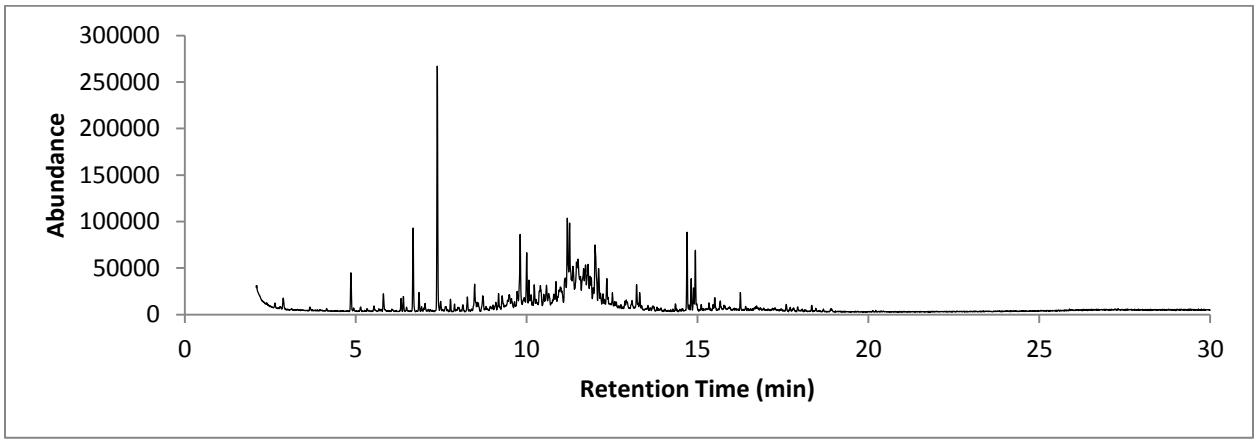

Figure 212: TIC C8-14

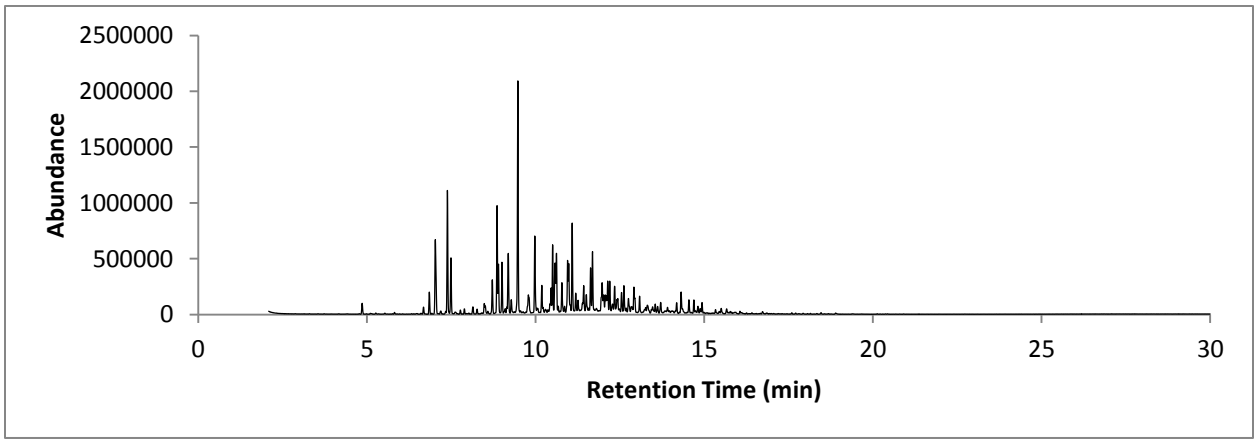

Figure 213: TIC C8-15

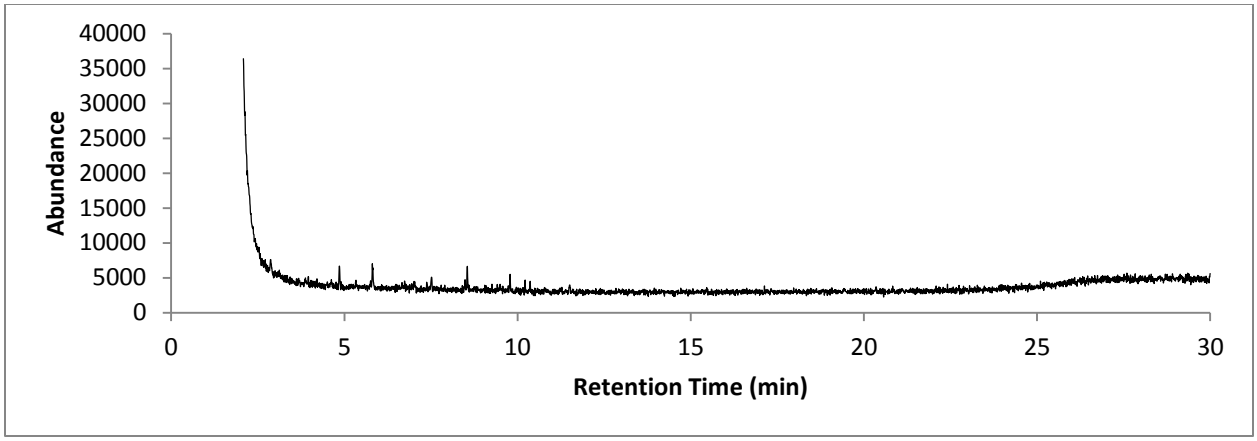

Figure 214: TIC C8-16

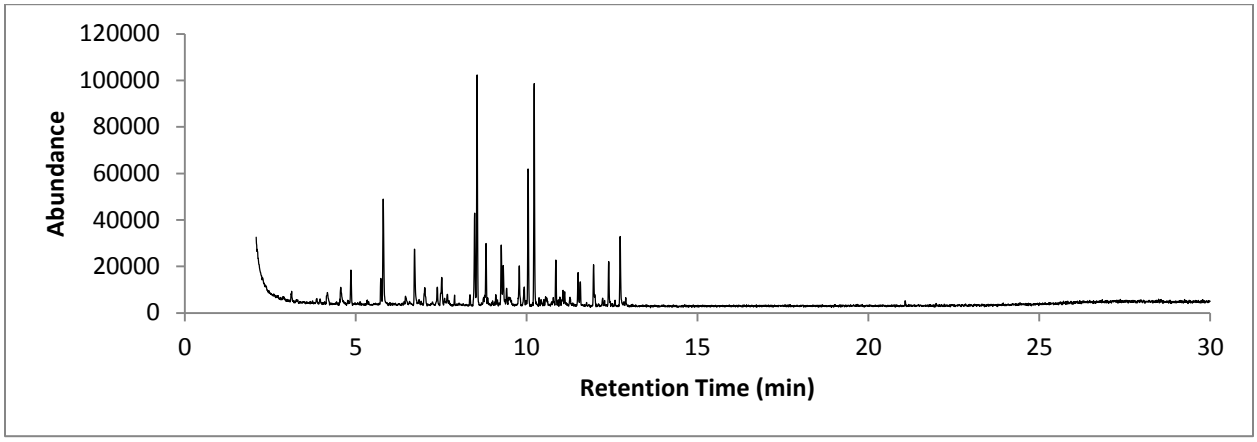

Figure 215: TIC C8-17

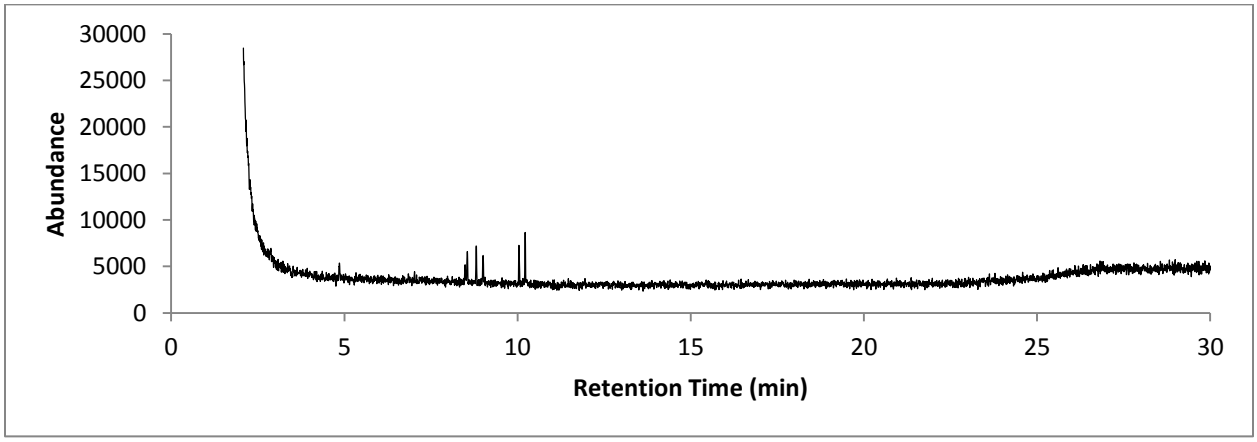

Figure 216: TIC C8-18

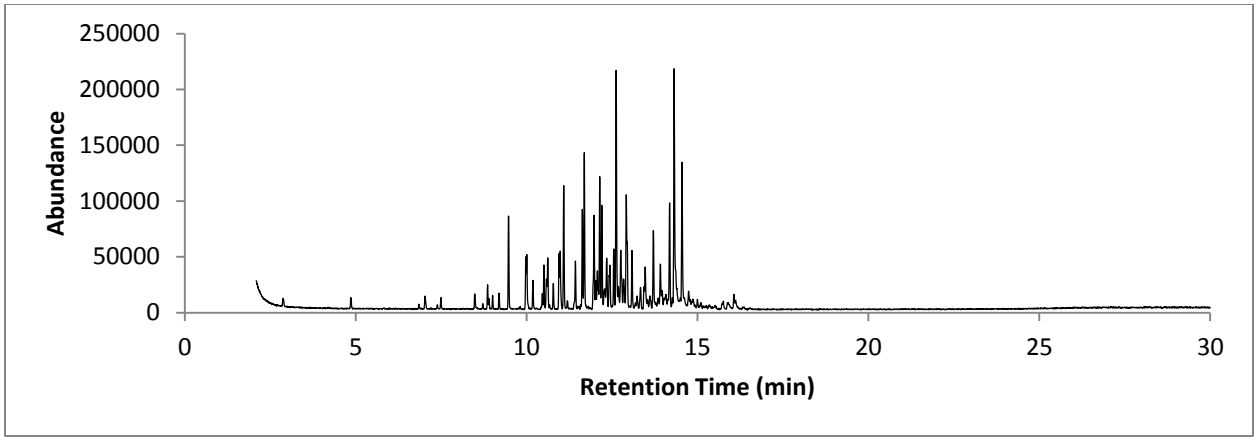

Figure 217: TIC C8-19

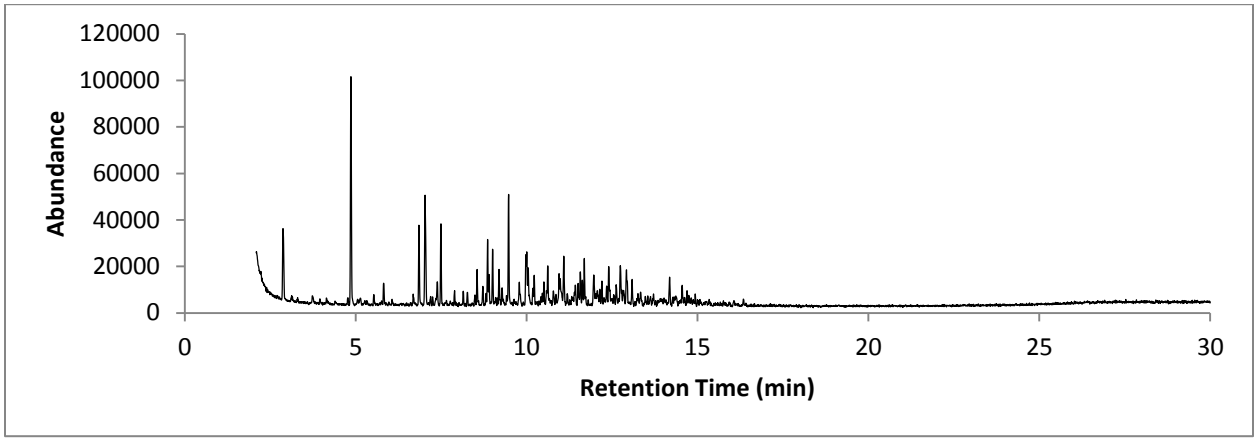

Figure 218: TIC C8-20

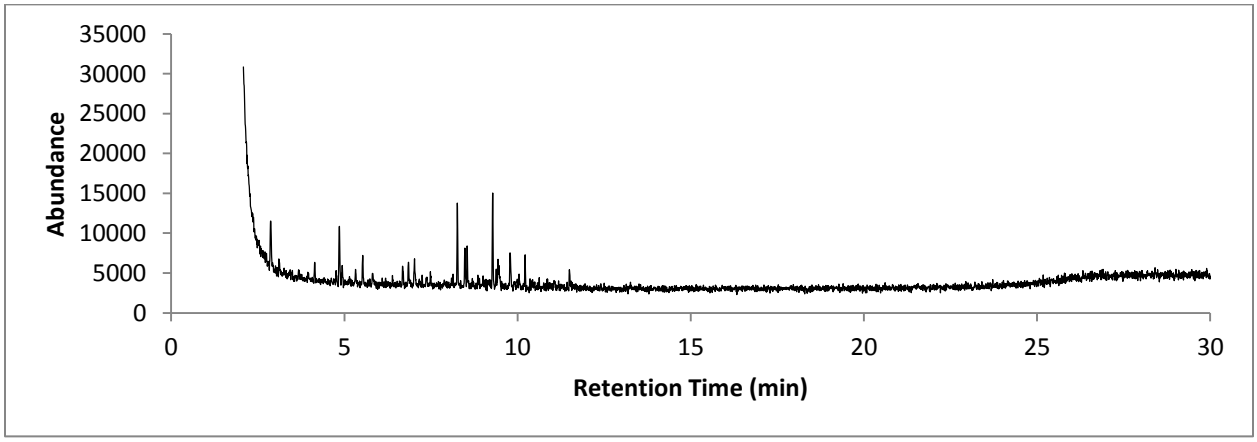

Figure 219: TIC C8-21

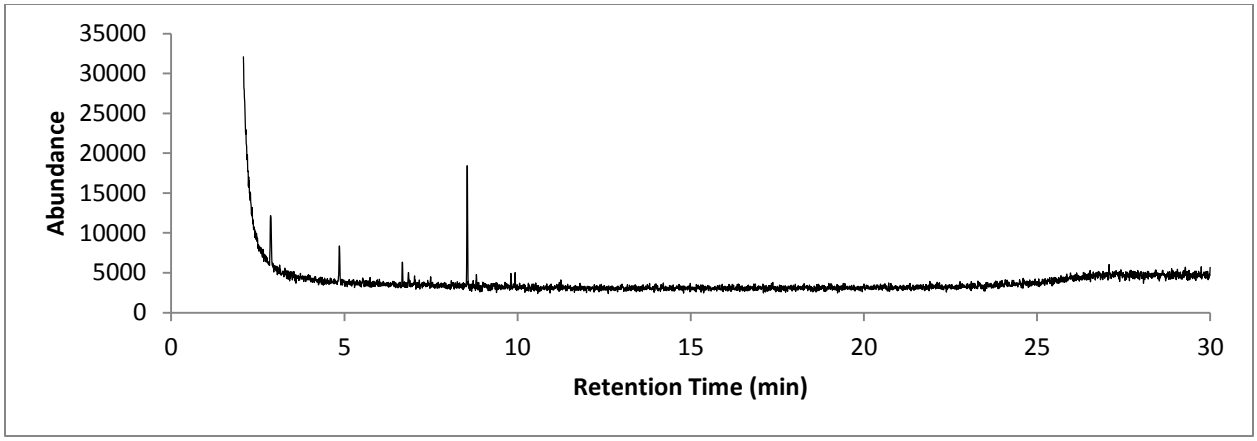

Figure 220: TIC C8-22

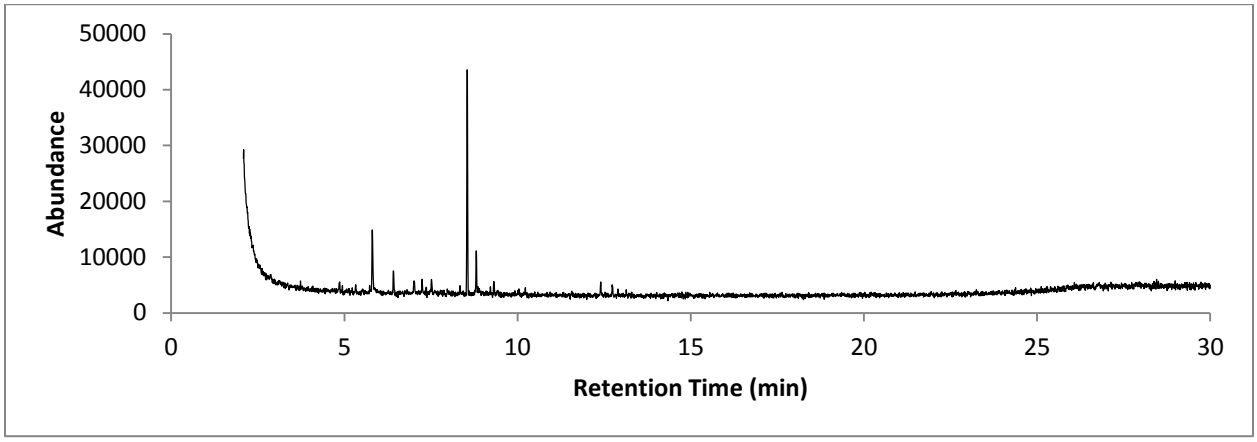

Figure 221: TIC C8-23

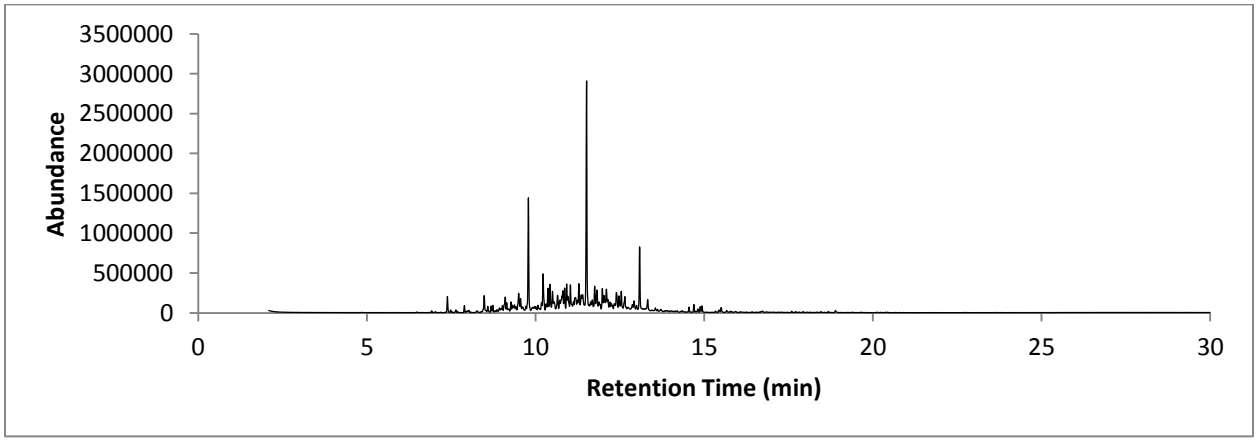

Figure 222: TIC C8-24

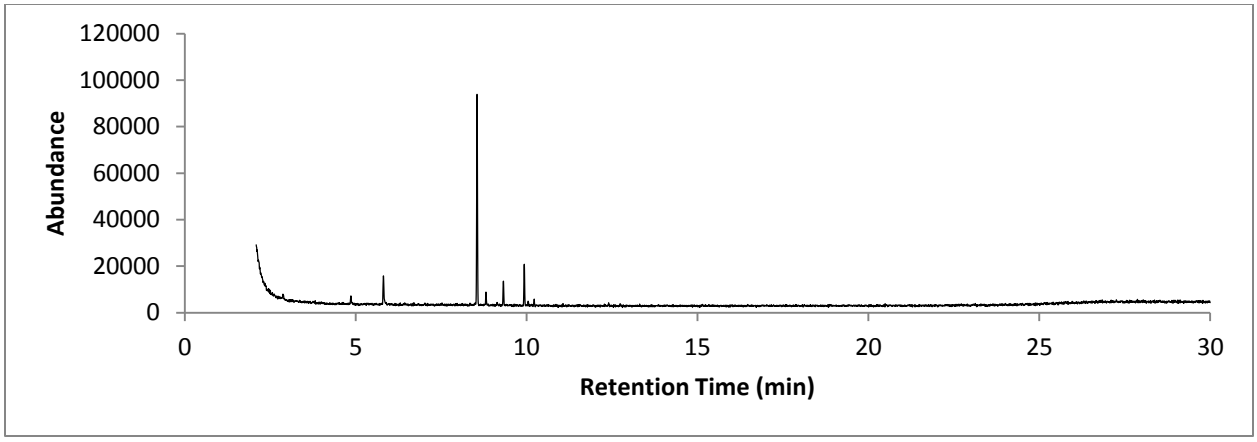

Figure 223: TIC C8-25

Sample TIS

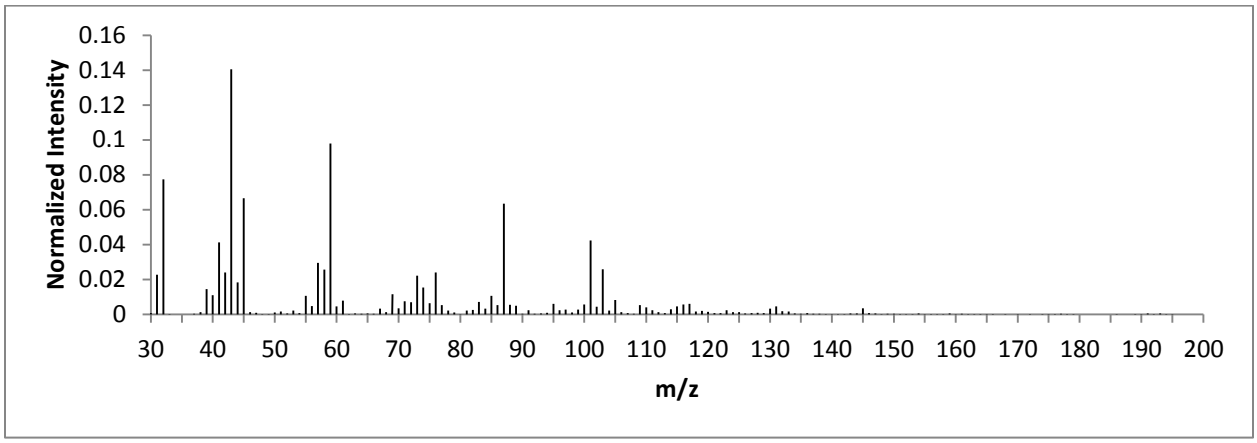

Figure 224: TIS C8-13

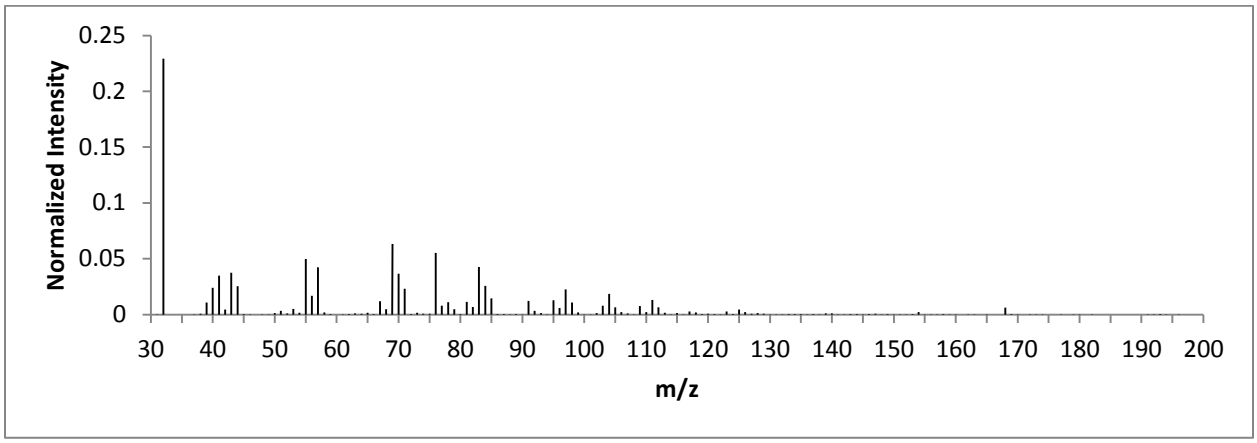

Figure 225: TIS C8-14

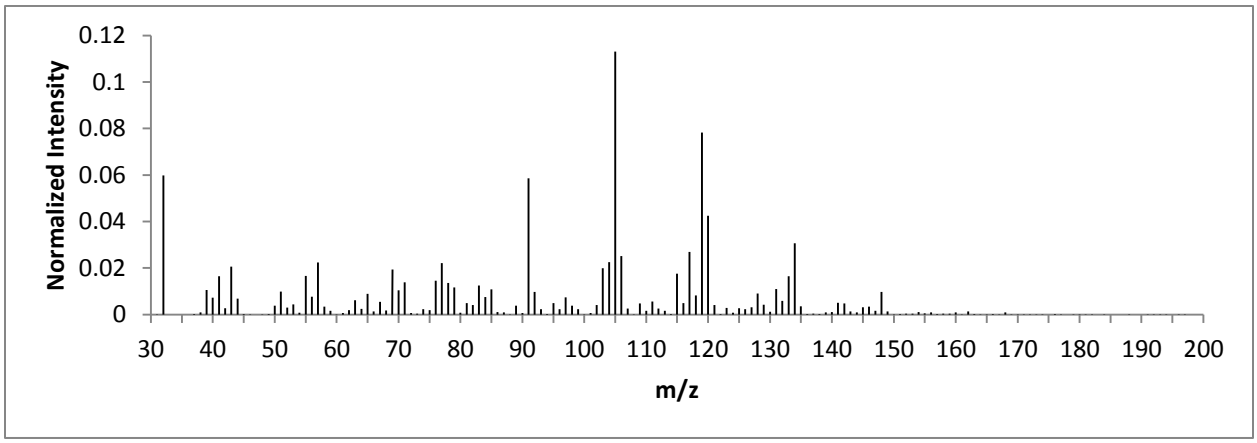

Figure 226: TIS C8-15

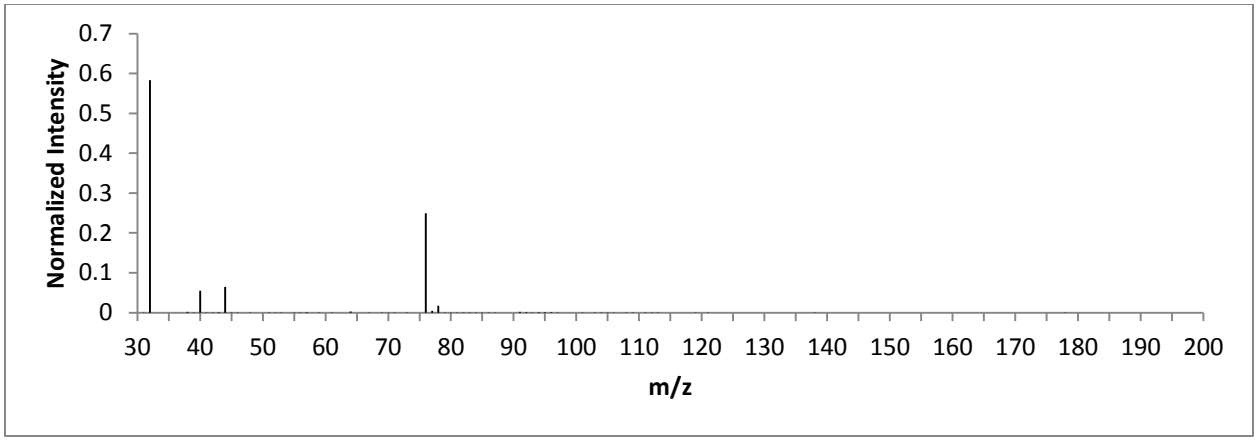

Figure 227: TIS C8-16

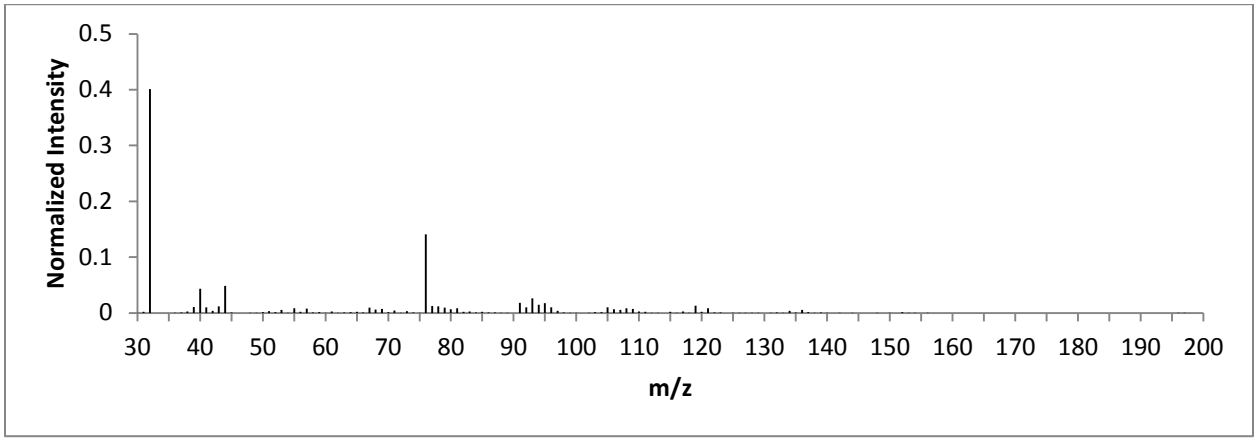

Figure 228: TIS C8-17

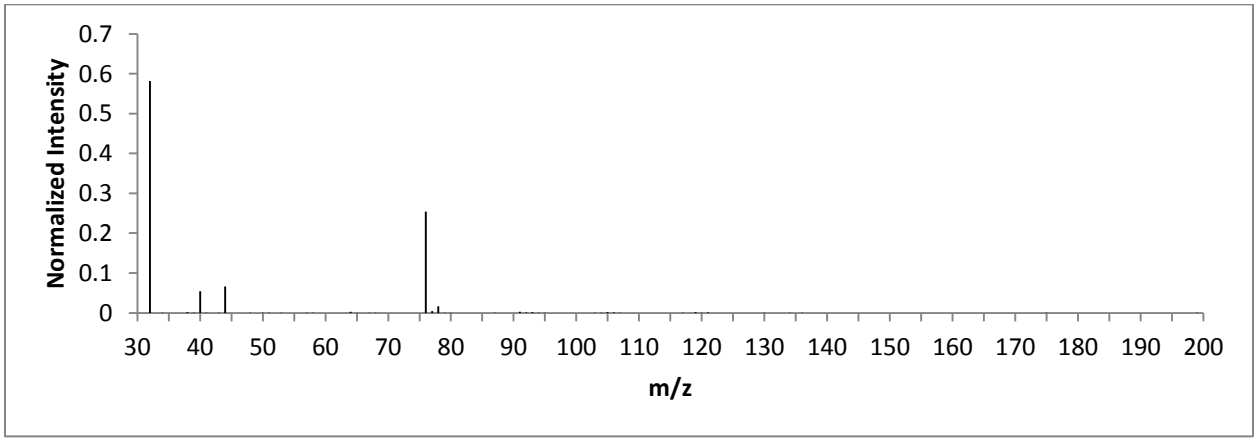

Figure 229: TIS C8-18

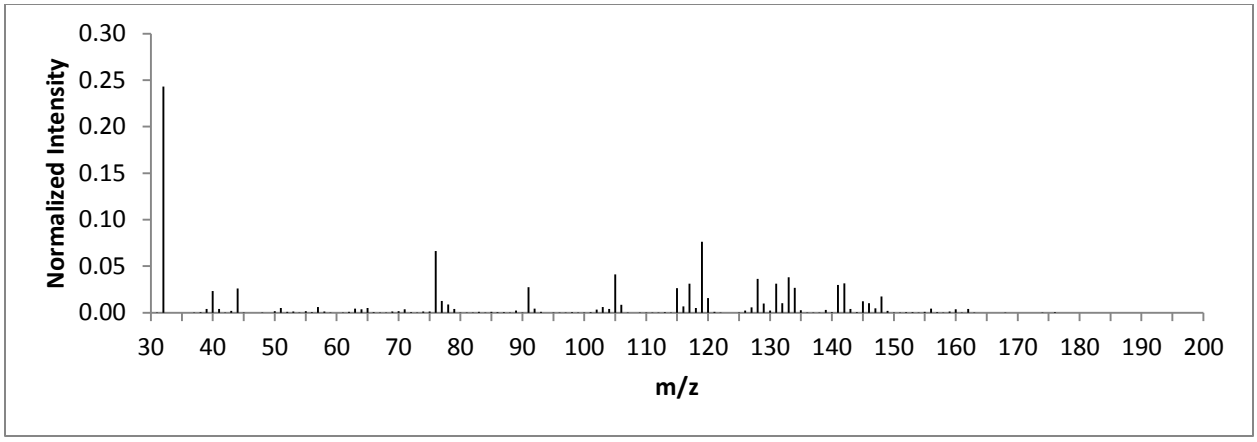

Figure 230: TIS C8-19

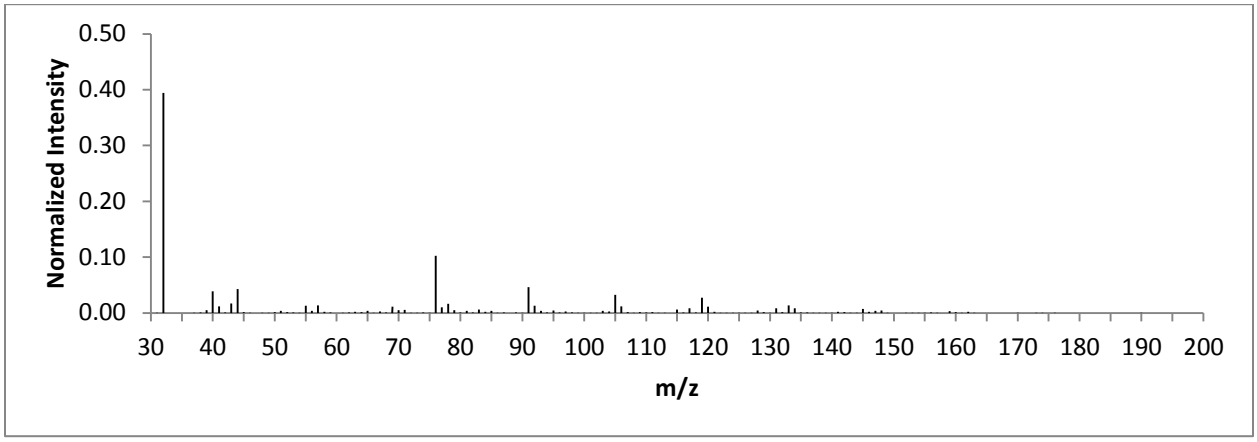

Figure 231: TIS C8-20

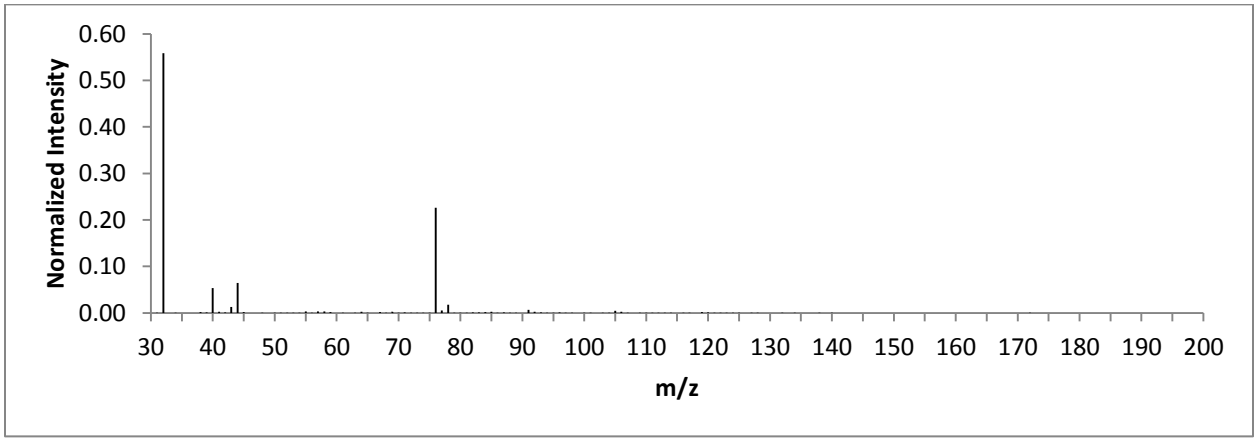

Figure 232: TIS C8-21

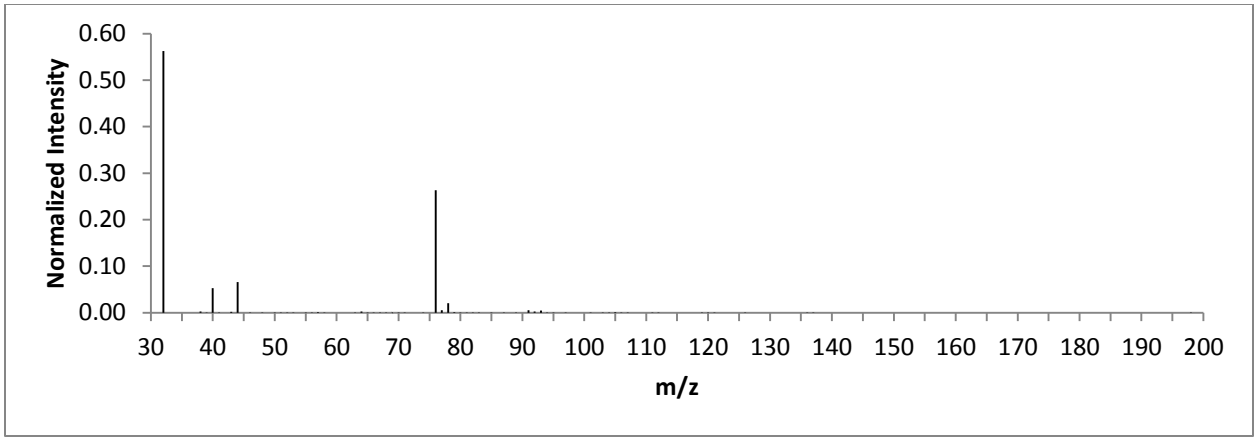

Figure 233: TIS C8-22

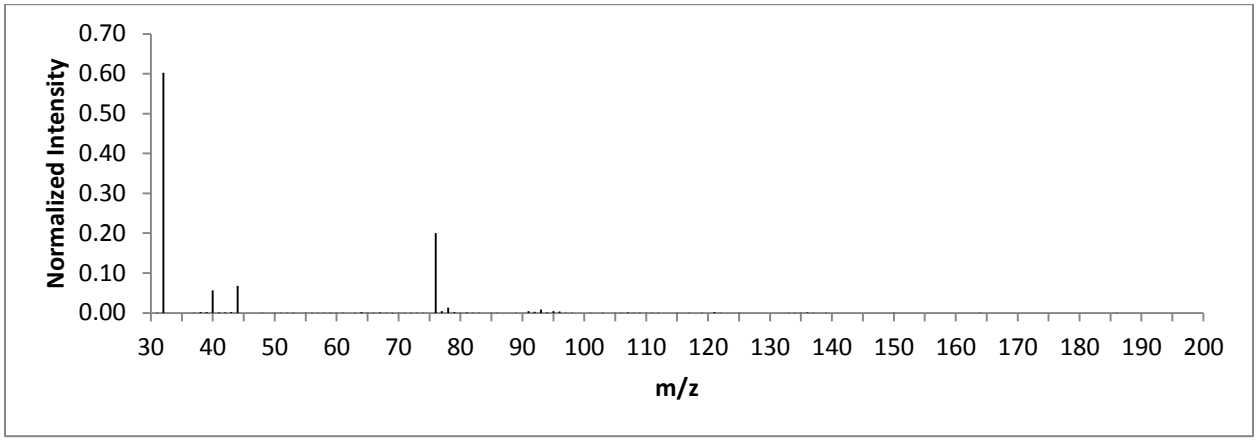

Figure 234: TIS C8-23

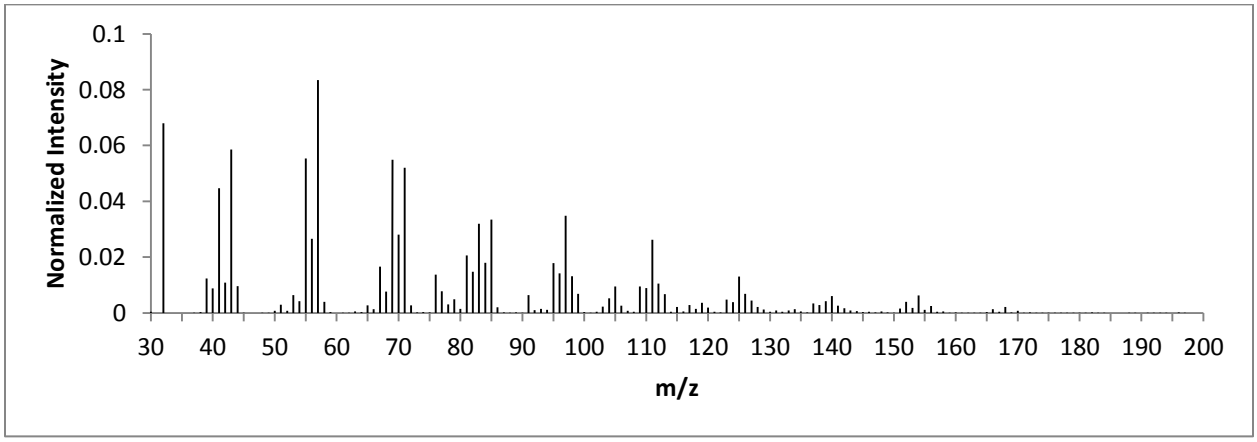

Figure 235: TIS C8-24

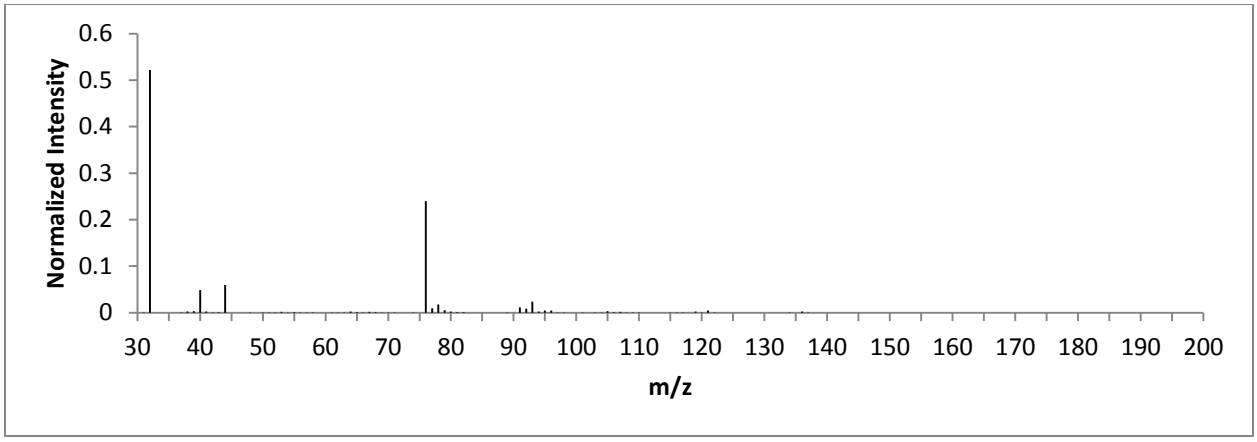

Figure 236: TIS C8-25

APPENDIX E
CONTAINER 9

Ignitable Liquid TIC

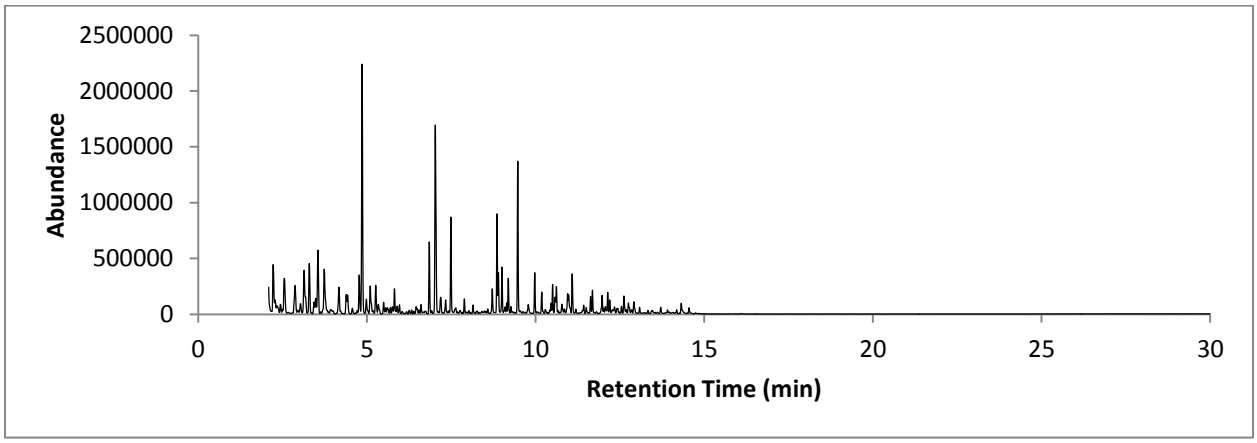

Figure 237: TIC C9 Gasoline

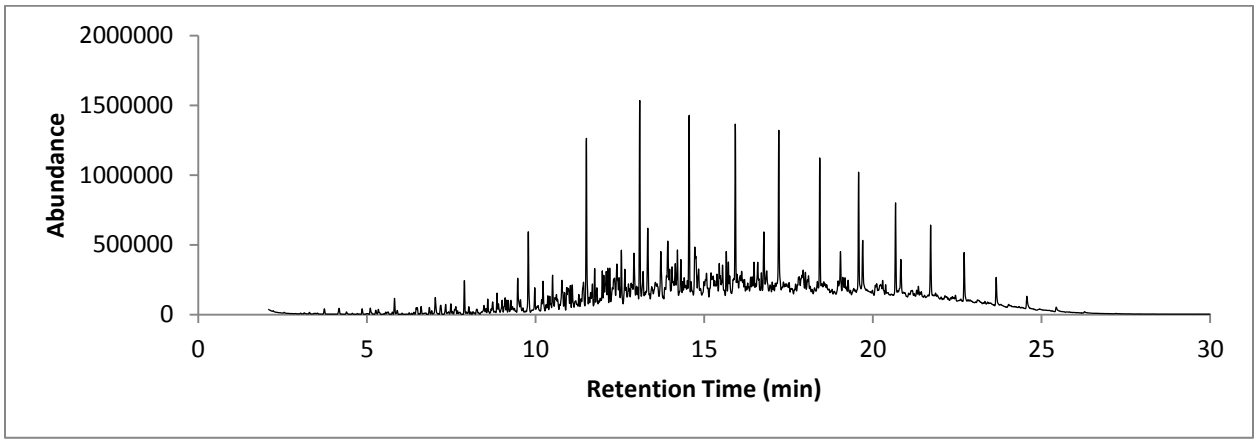

Figure 238: TIC C9 HPD

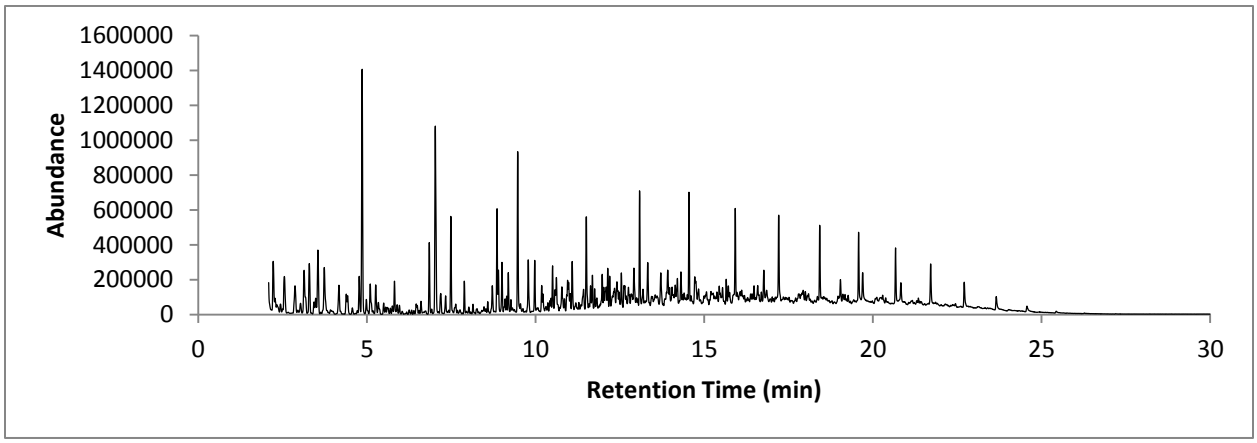

Figure 239: TIC C9 50:50 Gasoline:HPD Mixture

Ignitable Liquid TIS

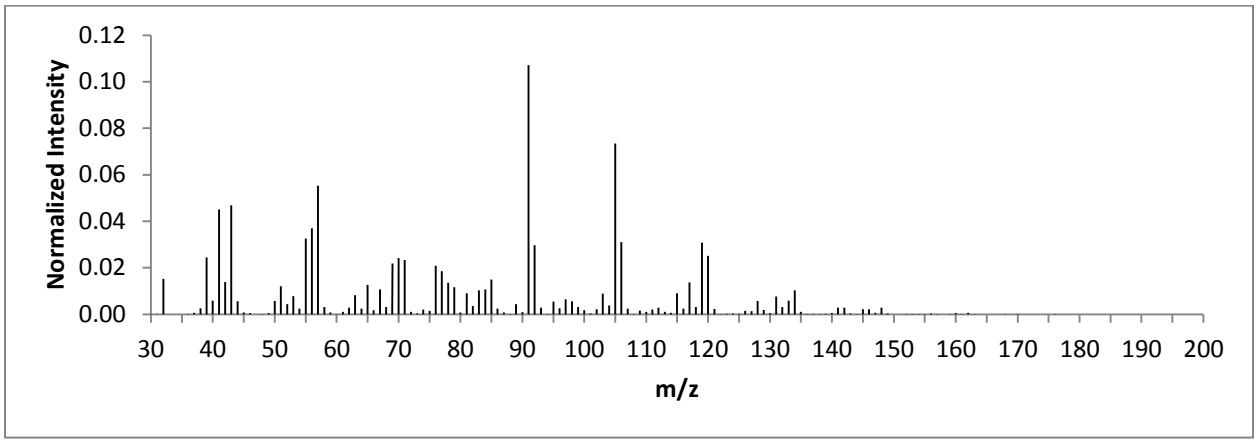

Figure 240: TIS C9 Gasoline

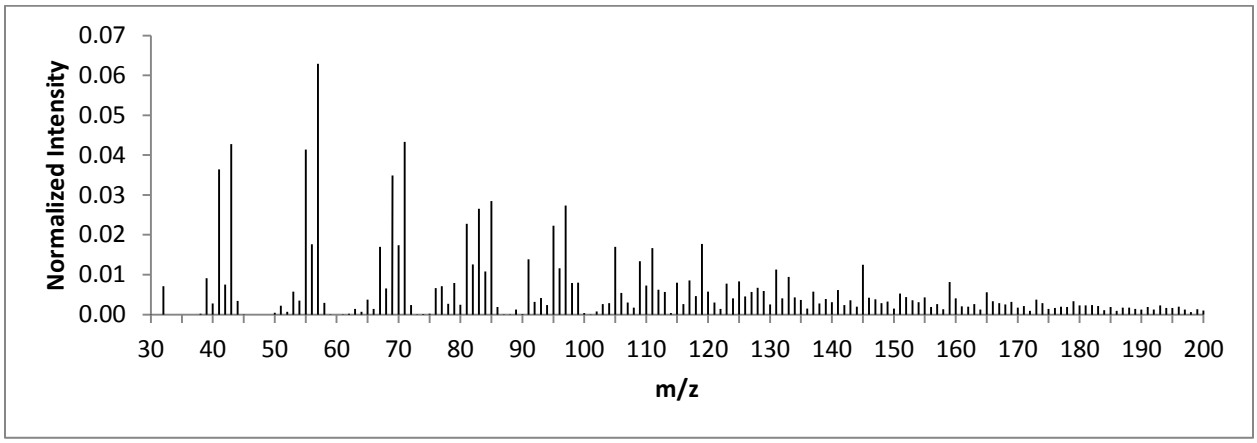

Figure 241: TIS C9 HPD

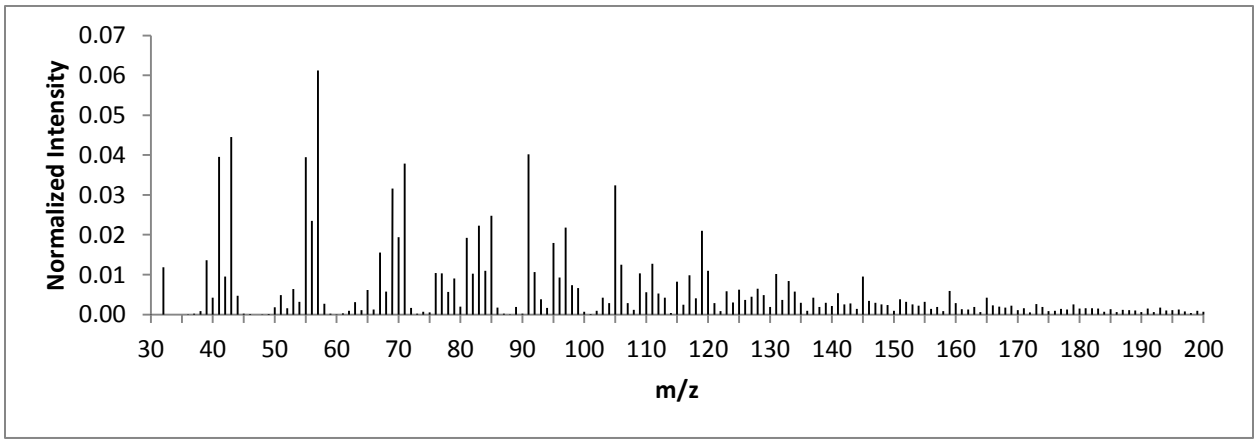

Figure 242: TIS C9 50:50 Gasoline:HPD Mixture

Sample TIC

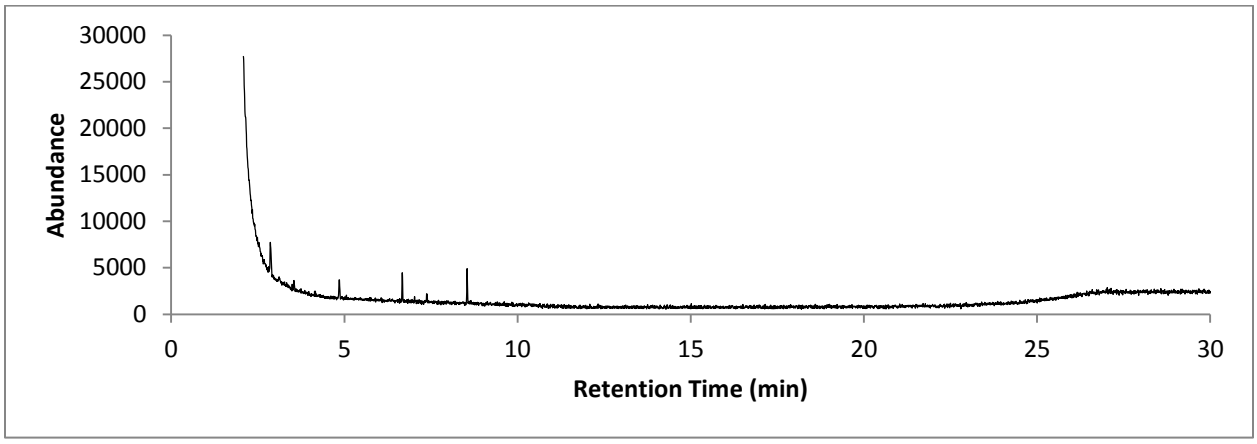

Figure 243: TIC C9-1

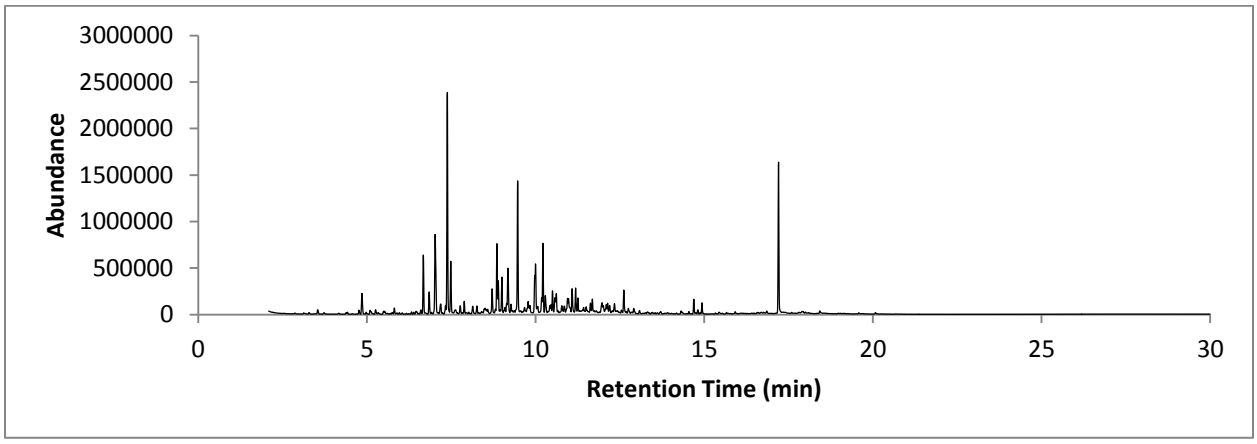

Figure 244: TIC C9-2

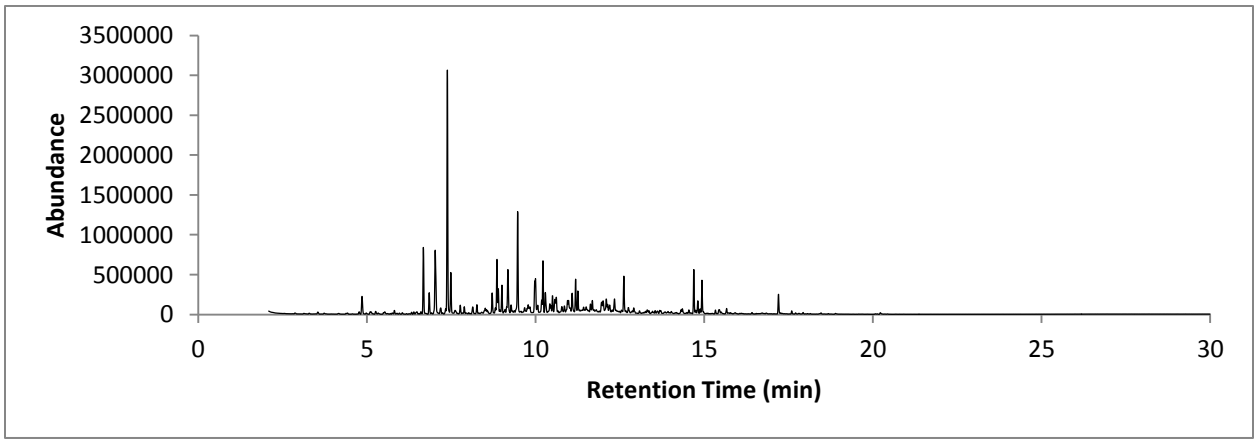

Figure 245: TIC C9-2B

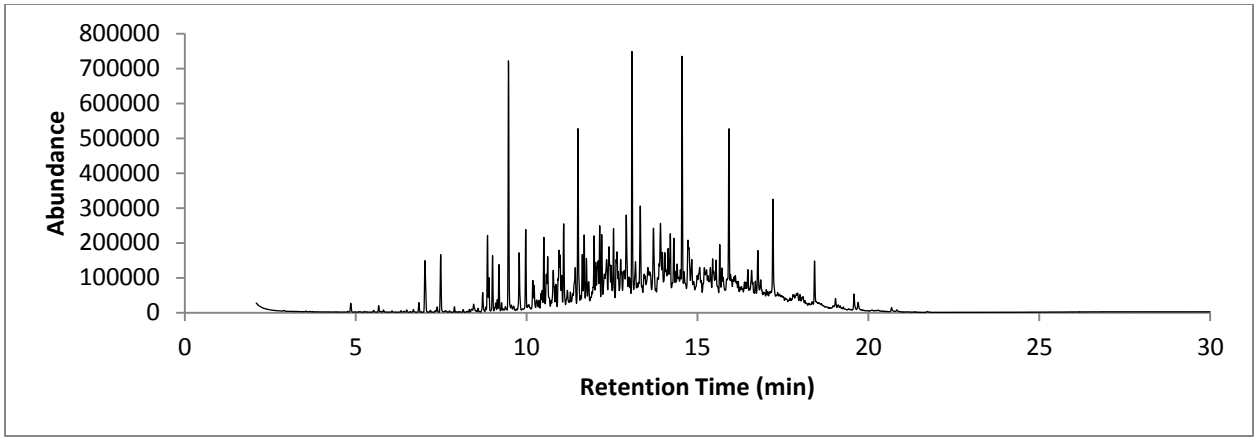

Figure 246: TIC C9-3

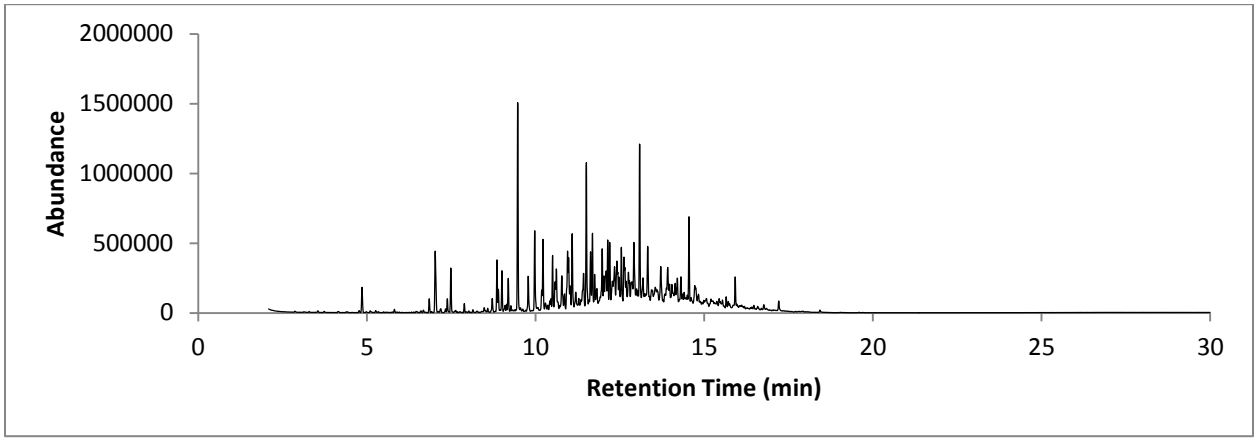

Figure 247: TIC C9-4

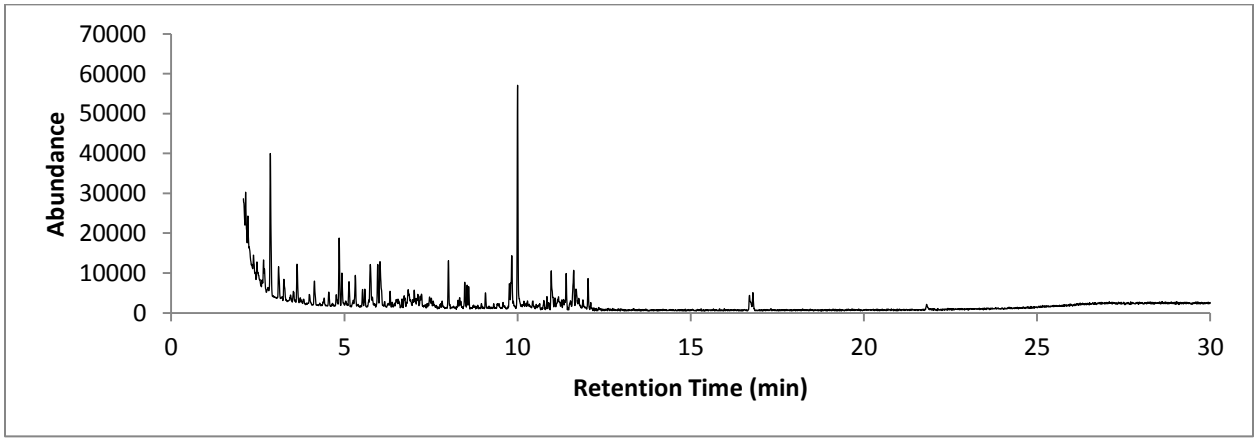

Figure 248: TIC C9-5

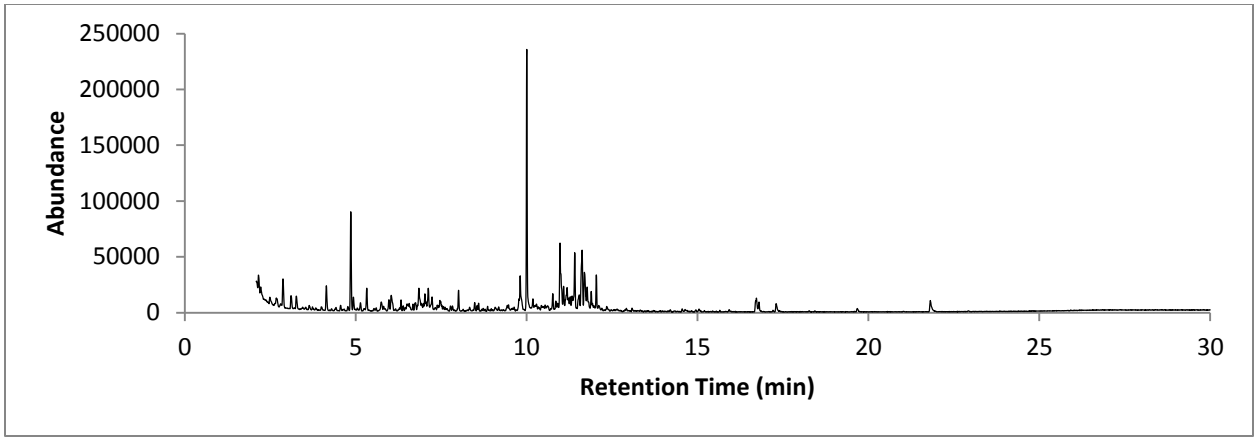

Figure 249: TIC C9-6

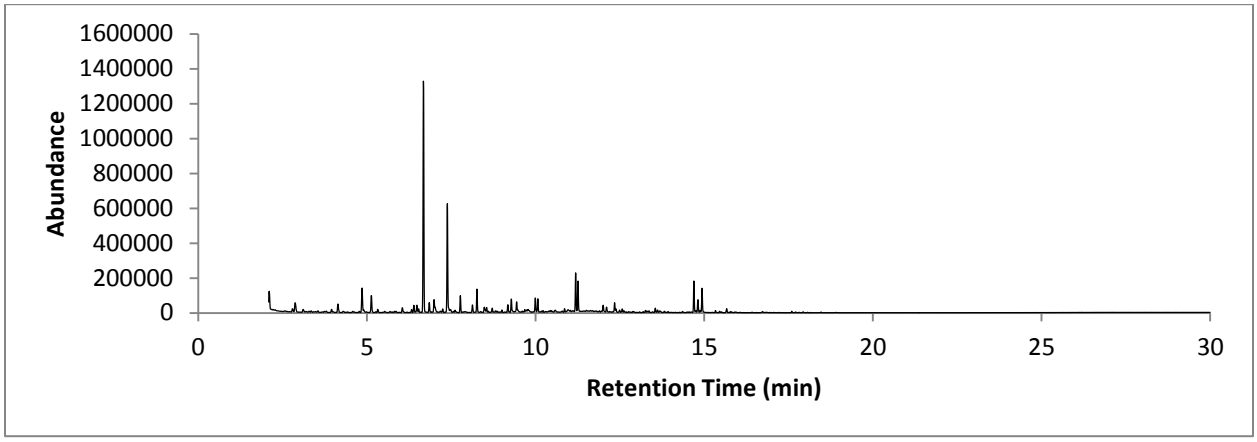

Figure 250: TIC C9-7

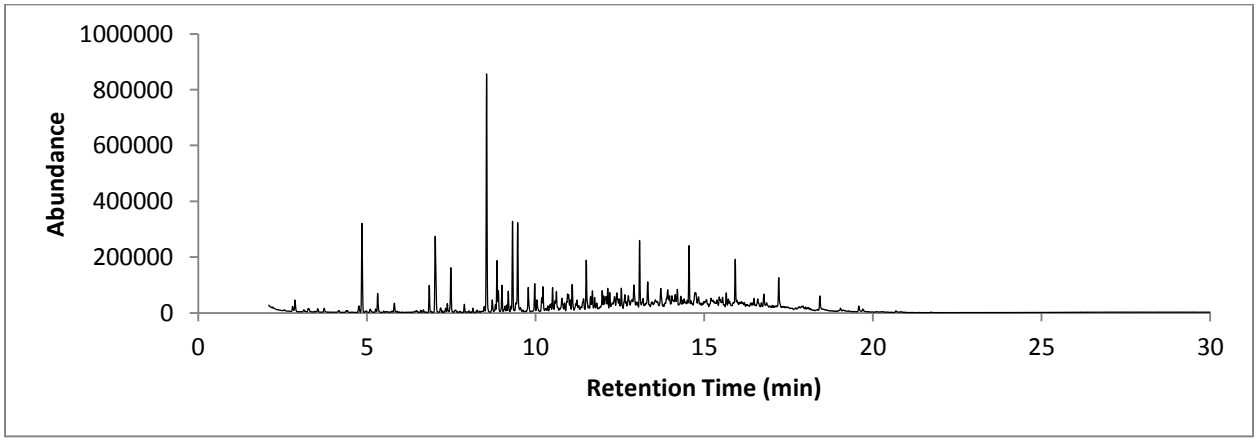

Figure 251: TIC C9-8

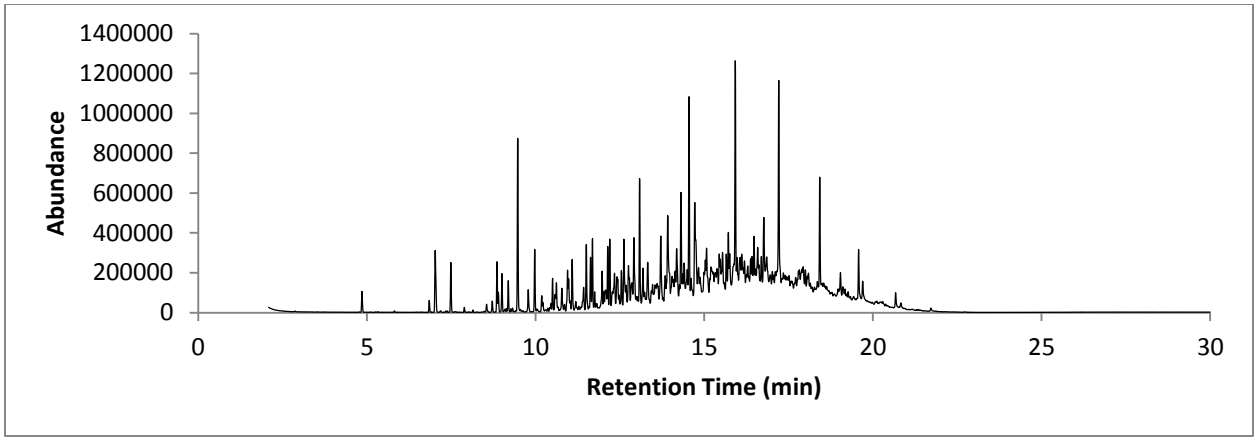

Figure 252: TIC C9-9

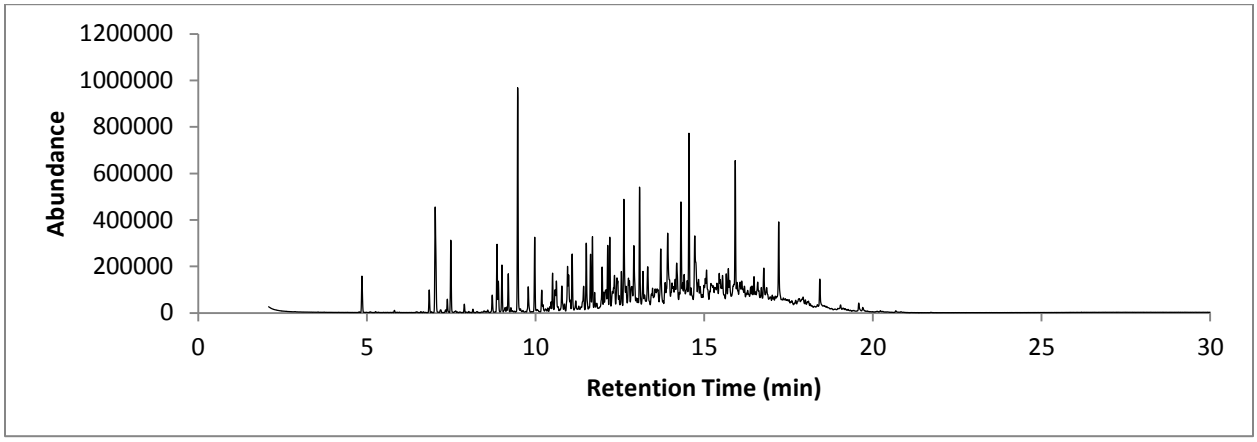

Figure 253: TIC C9-10

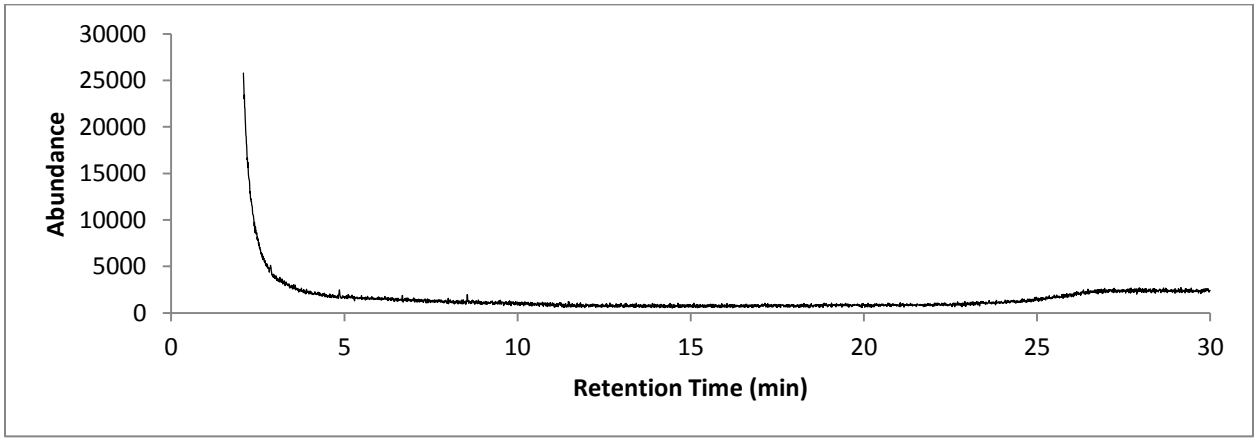

Figure 254: TIC C9-11

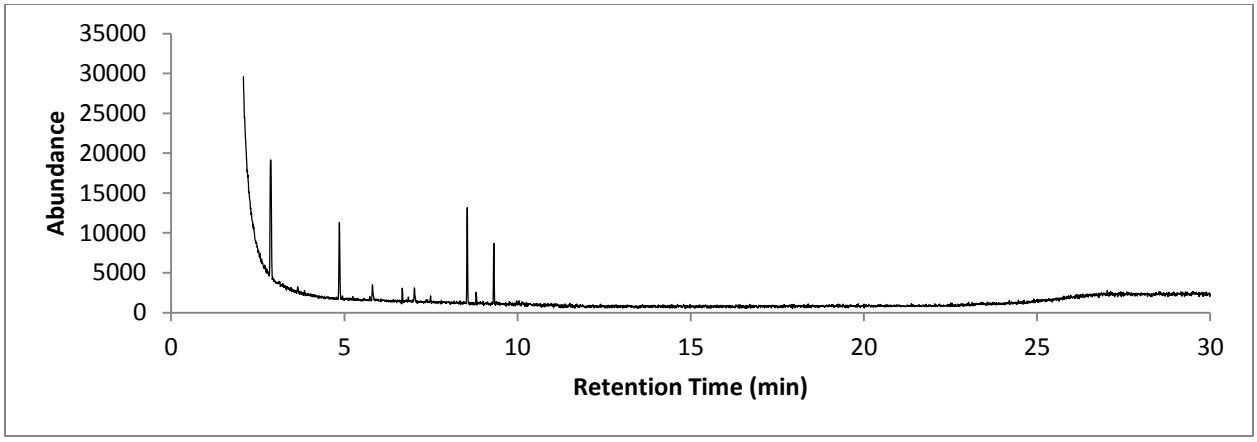

Figure 255: TIC C9-12

Sample TIS

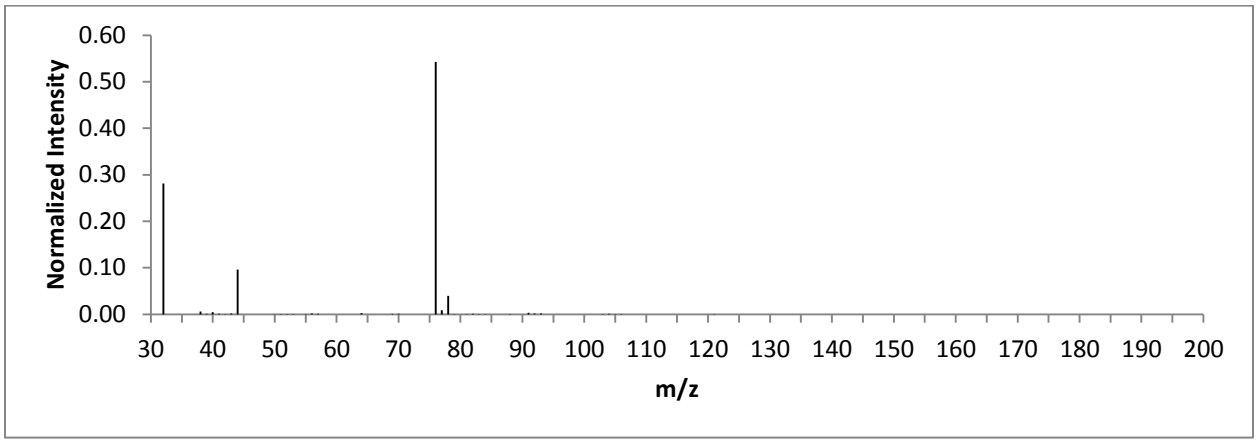

Figure 256: TIS C9-1

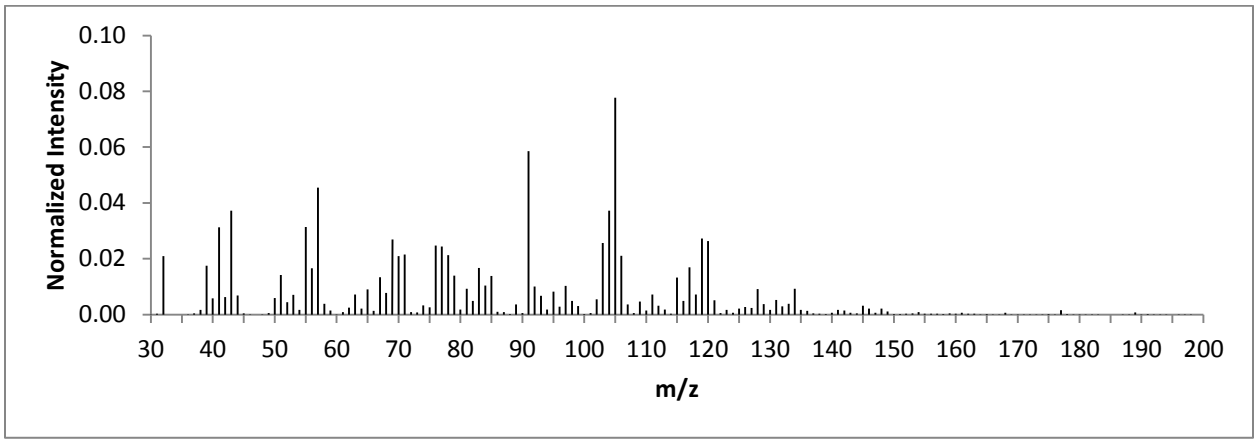

Figure 257: TIS C9-2

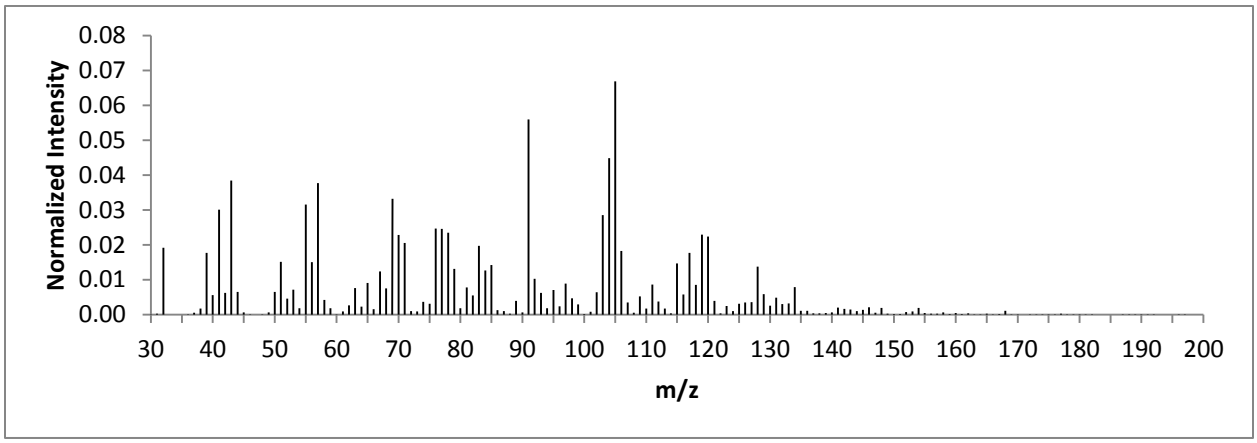

Figure 258: TIS C9-2B

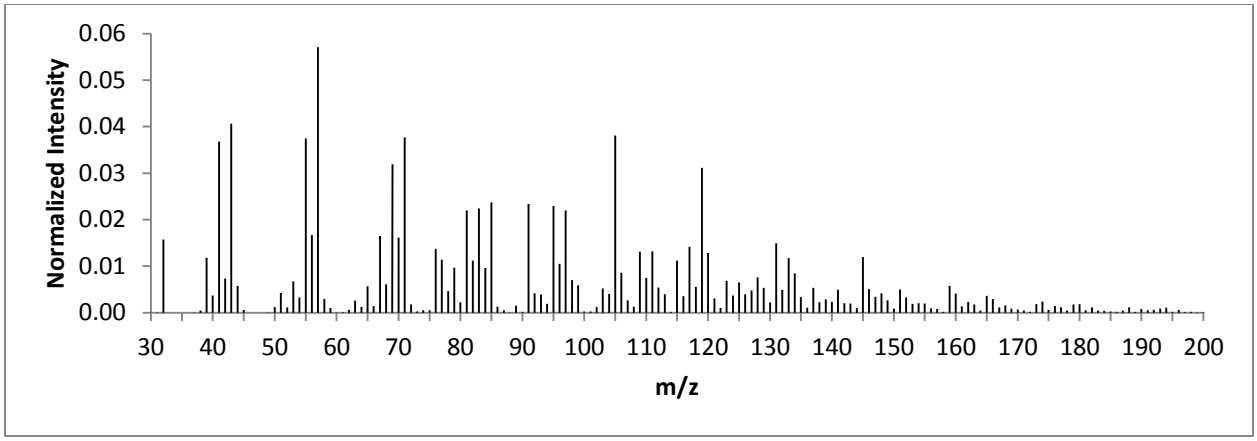

Figure 259: TIS C9-3

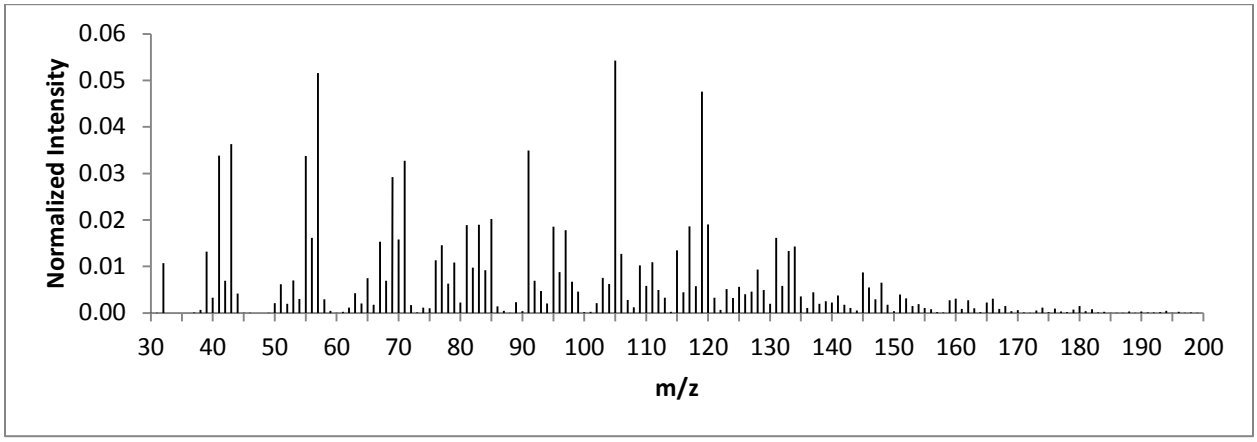

Figure 260: TIS C9-4

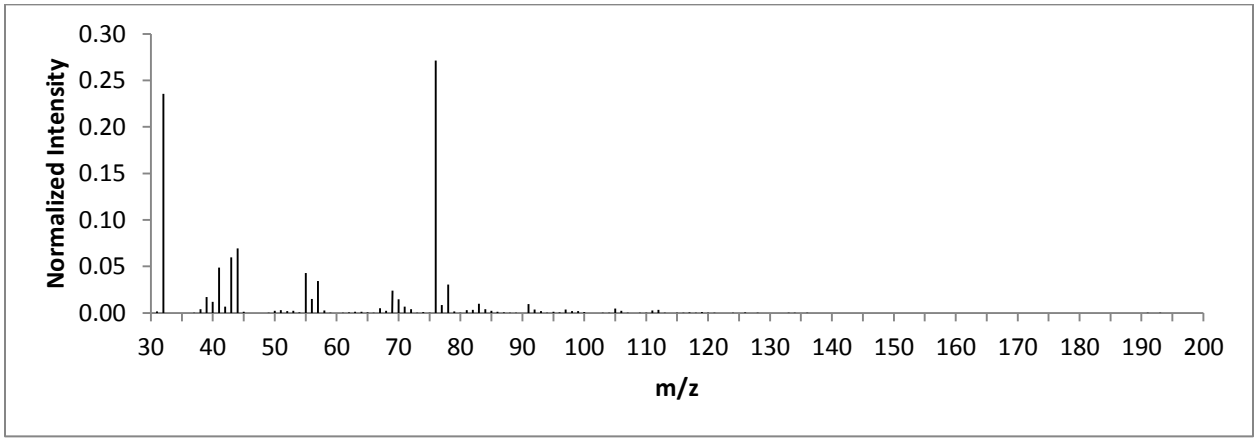

Figure 261: TIS C9-5

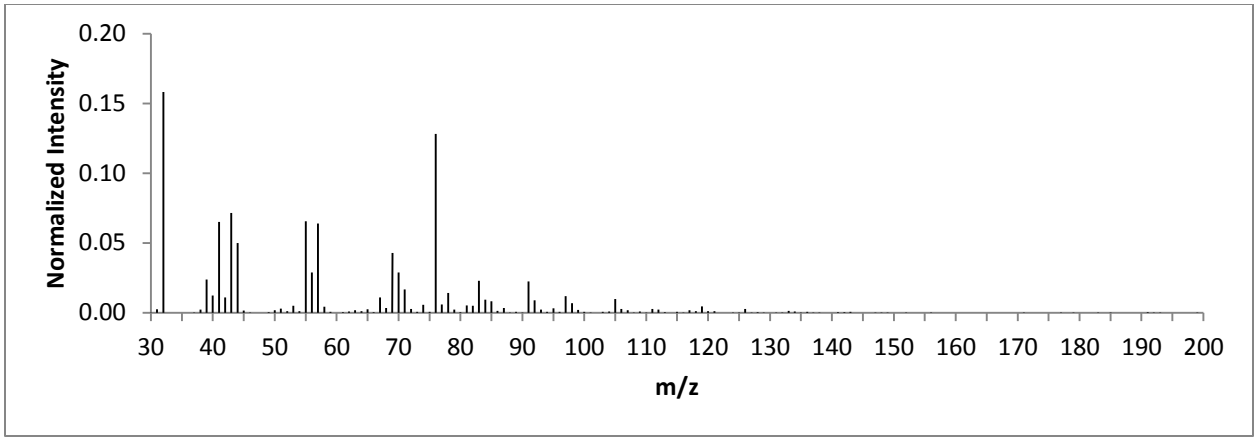

Figure 262: TIS C9-6

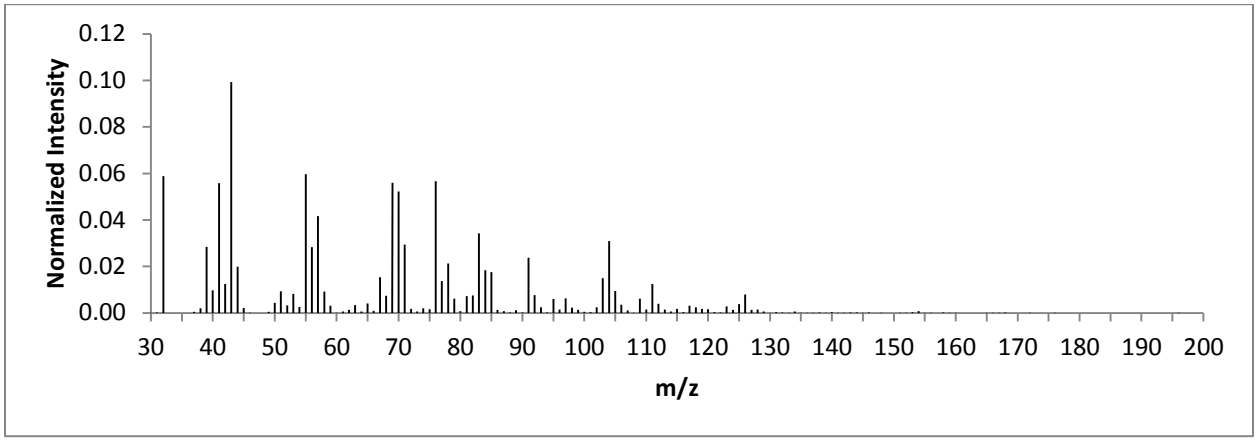

Figure 263: TIS C9-7

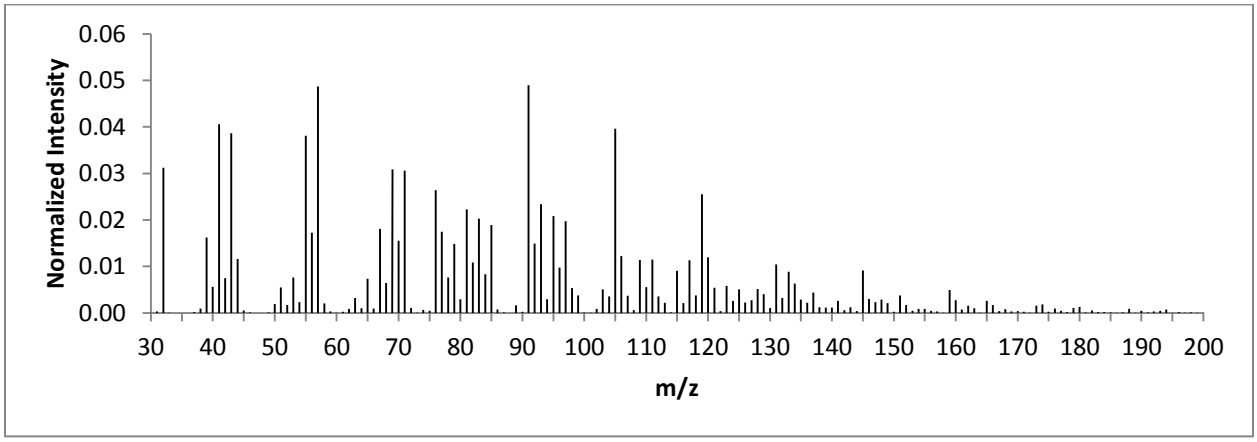

Figure 264: TIS C9-8

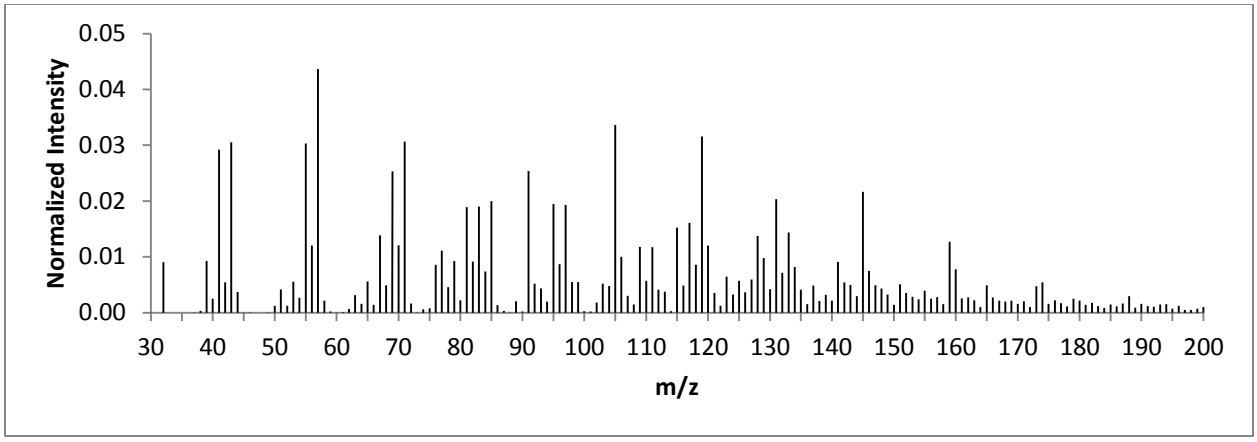

Figure 265: TIS C9-9

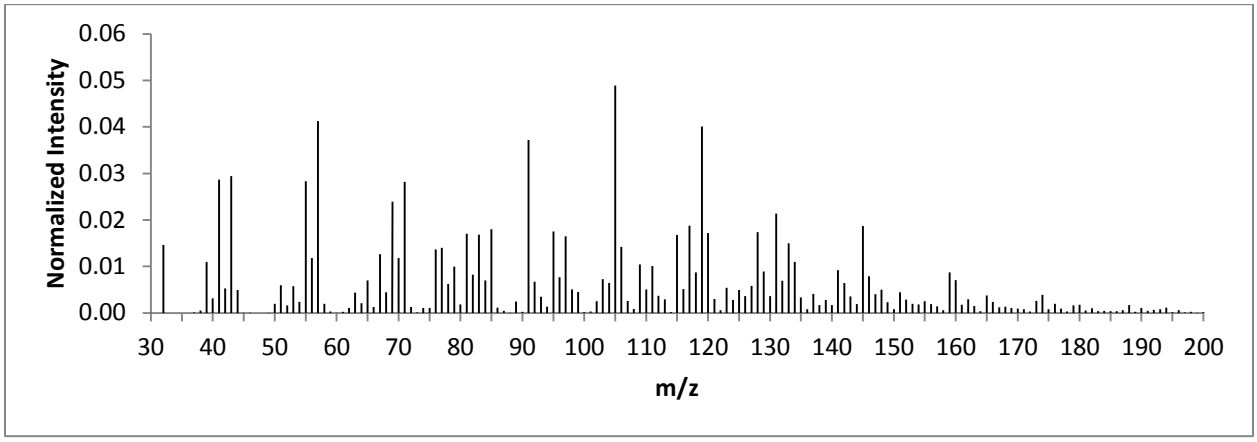

Figure 266: TIS C9-10

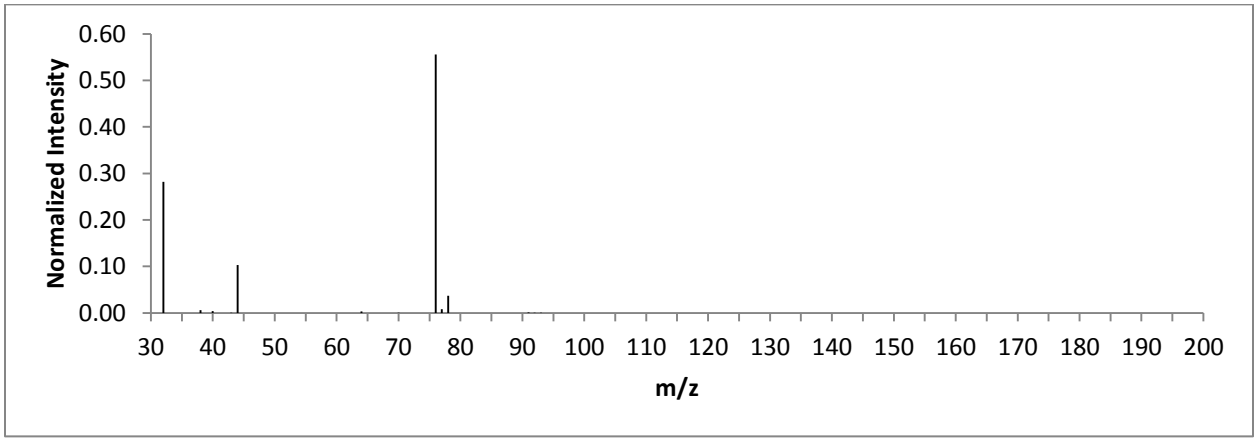

Figure 267: TIS C9-11

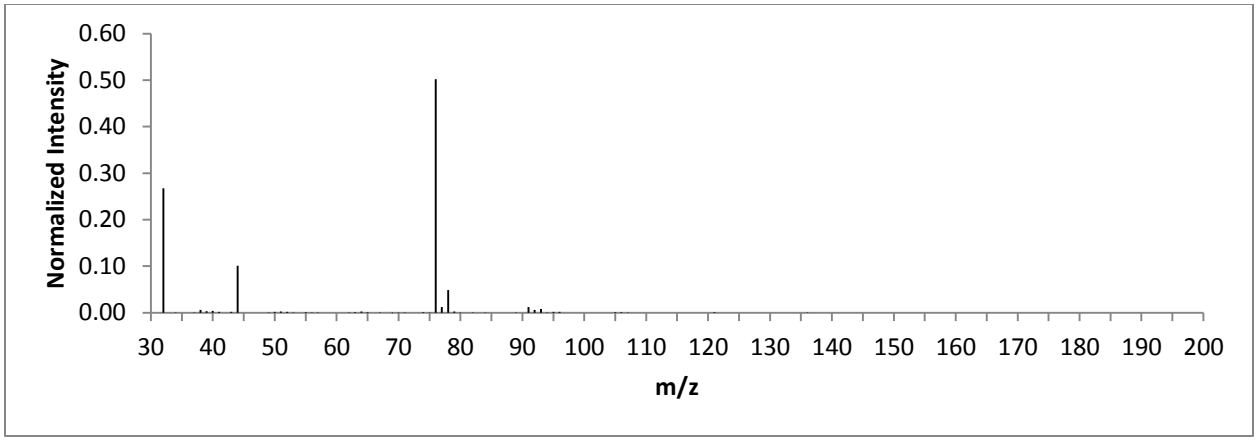

Figure 268: TIS C9-12

APPENDIX F
CONTAINER 10

Ignitable Liquid TIC

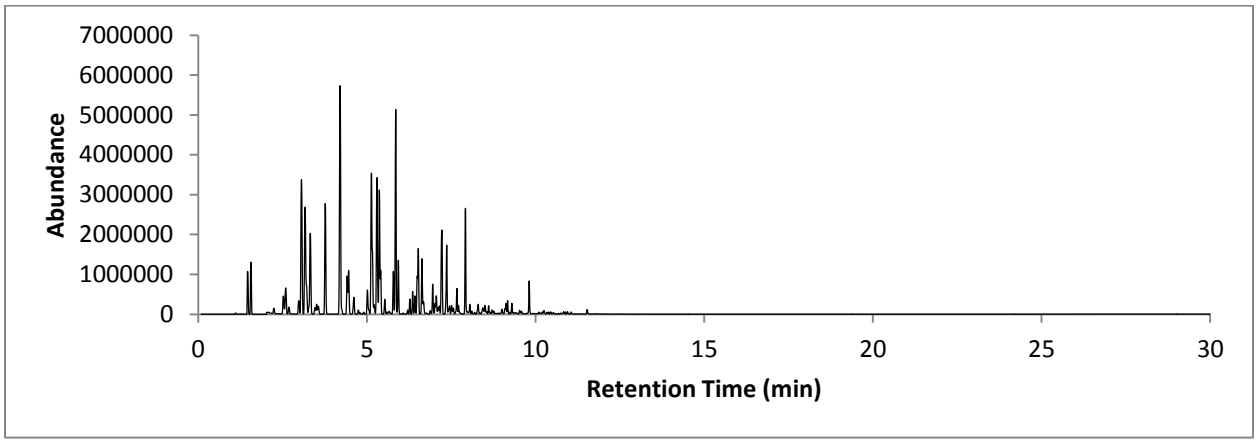

Figure 269: TIC C10 LPD

Ignitable Liquid TIS

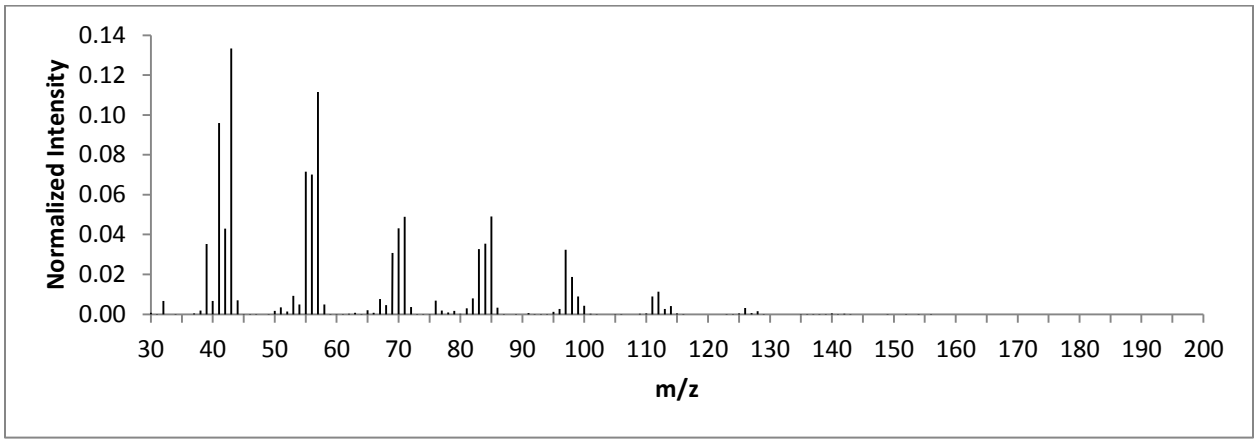

Figure 270: TIS C10 LPD

Sample TIC

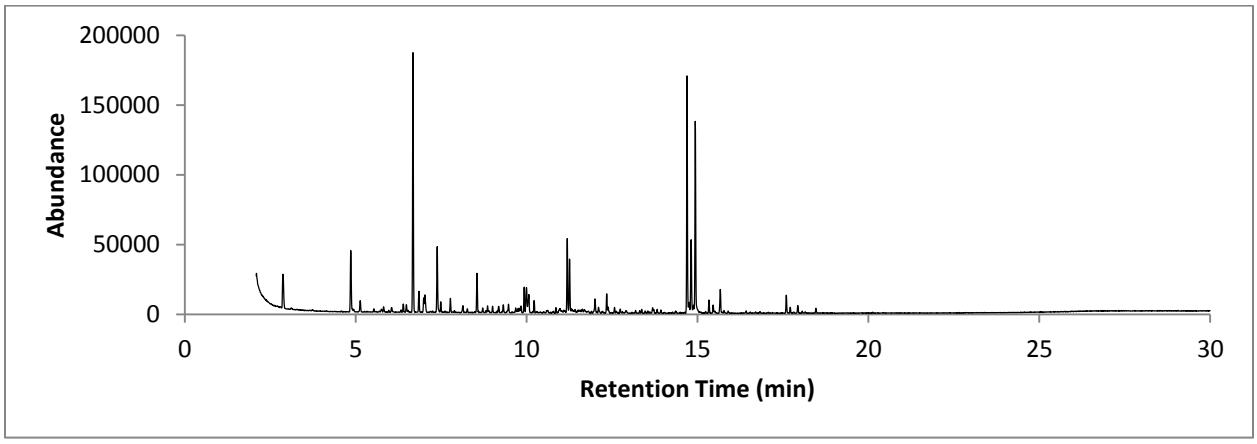

Figure 271: TIC C10-13

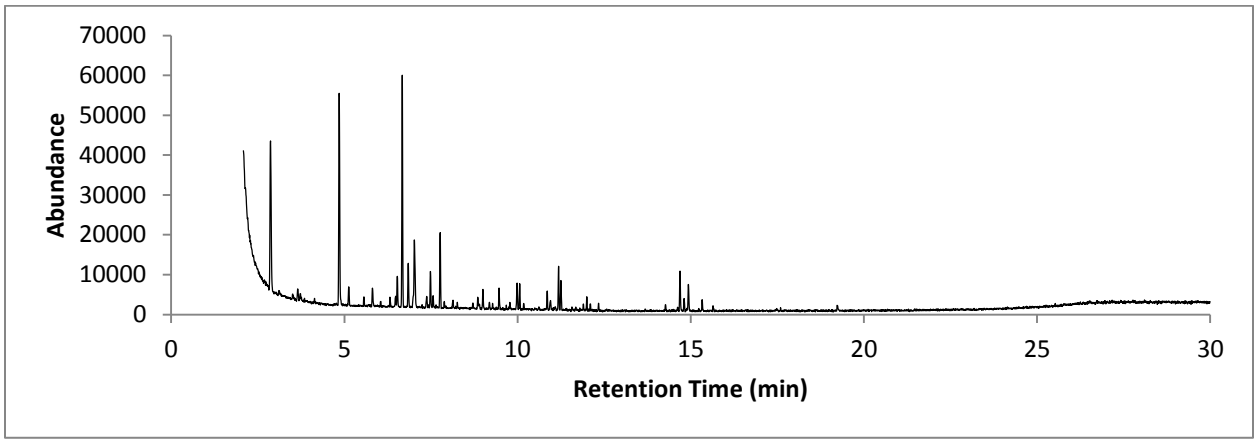

Figure 272: TIC C10-14

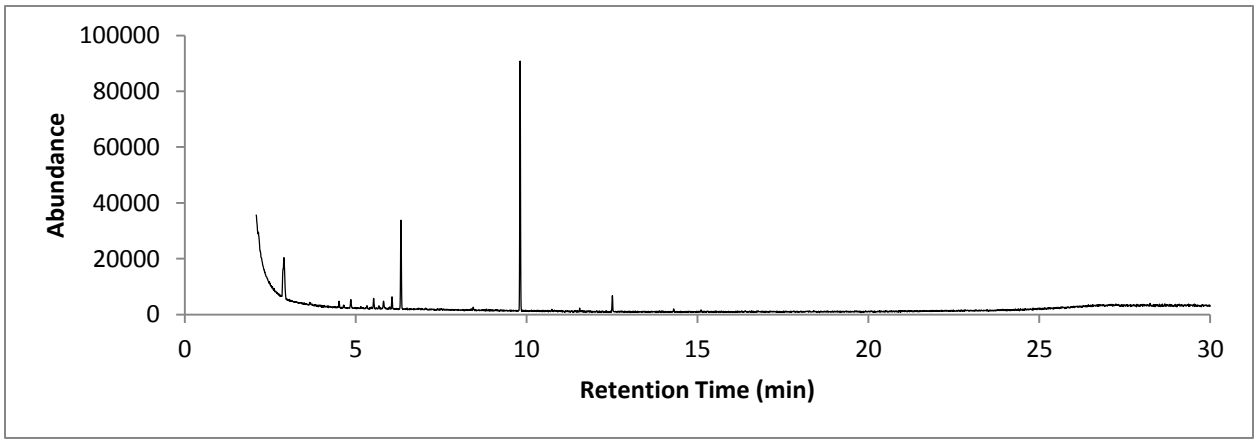

Figure 273: TIC C10-15

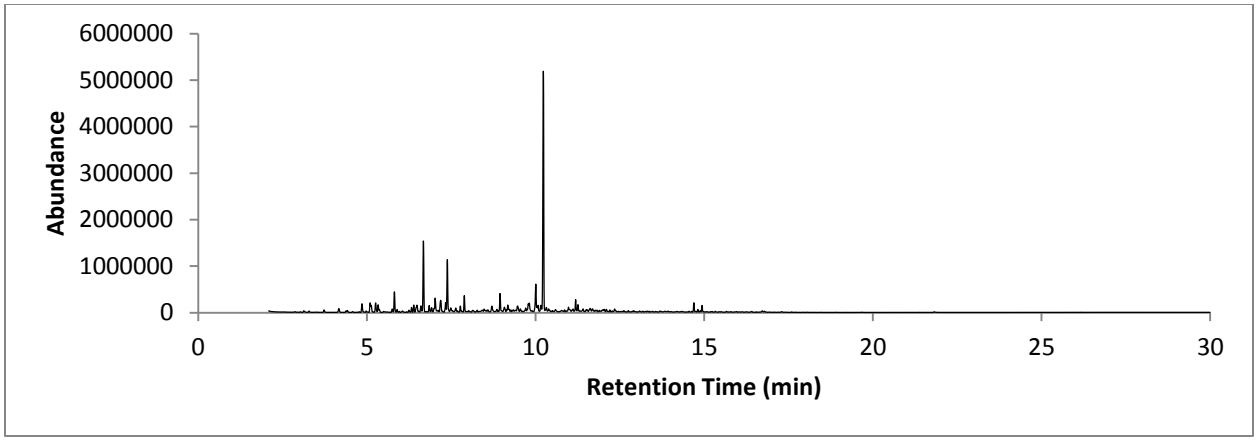

Figure 274: TIC C10-16

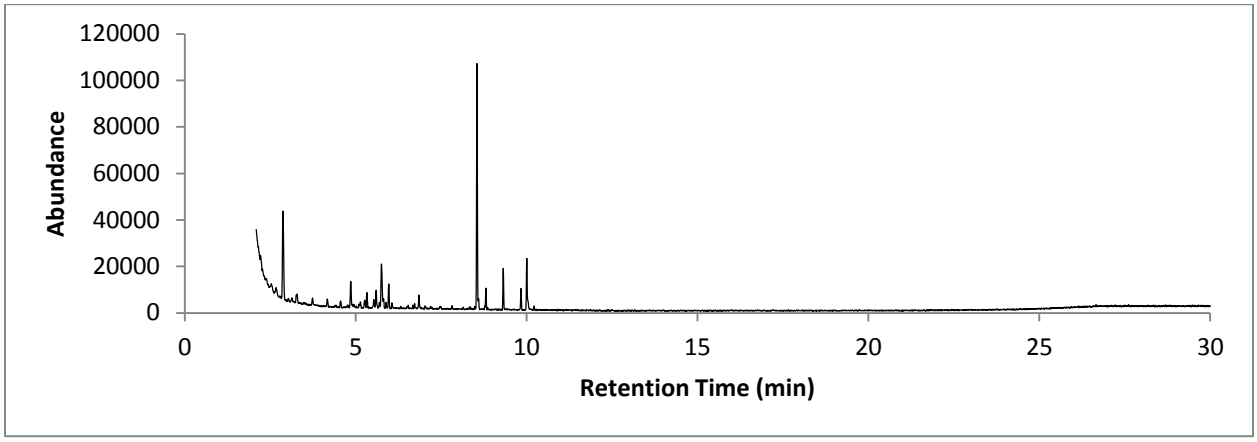

Figure 275: TIC C10-17

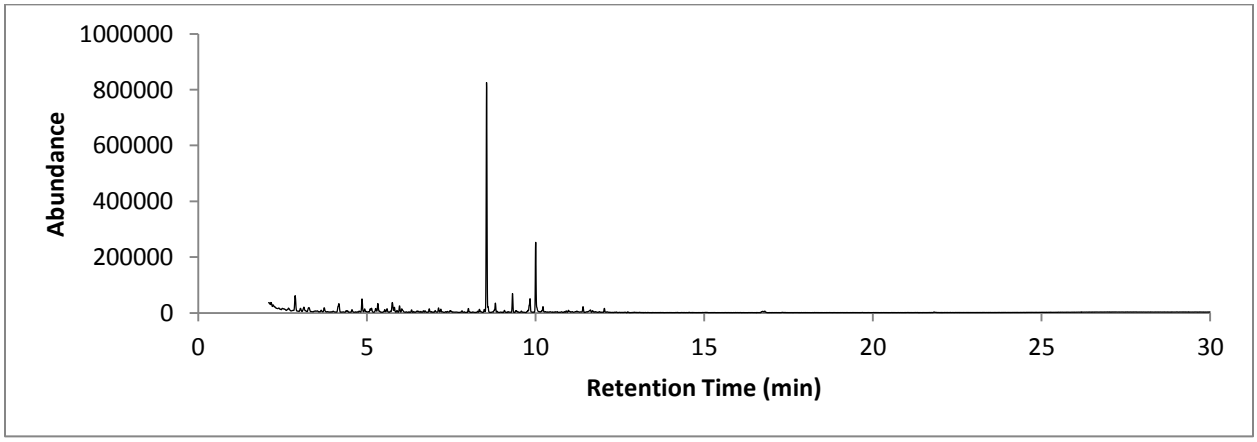

Figure 276: TIC C10-18

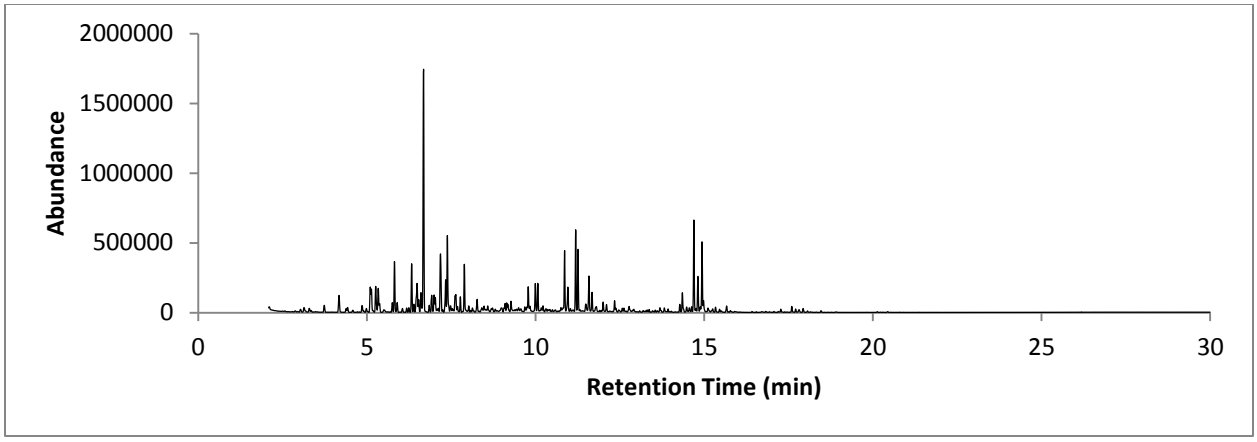

Figure 277: TIC C10-19

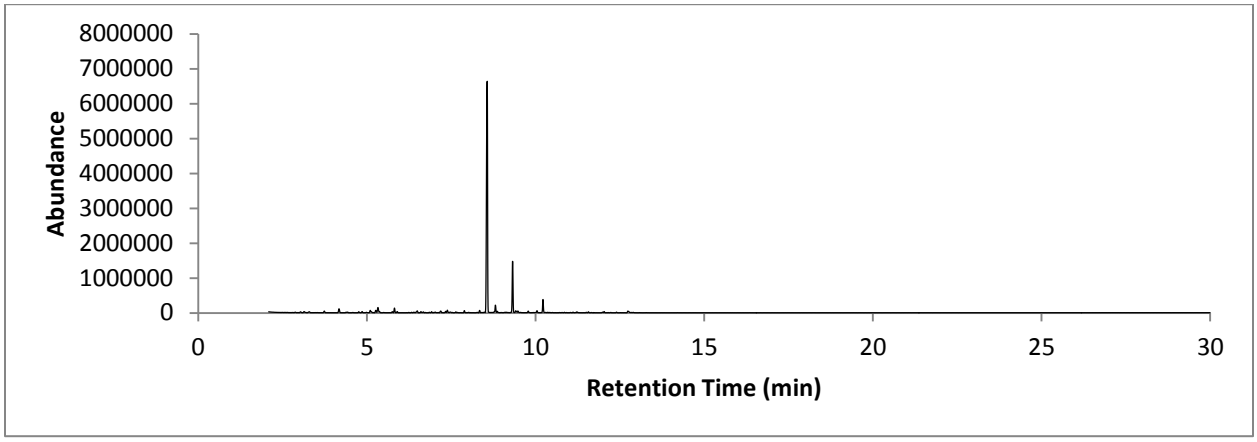

Figure 278: TIC C10-20

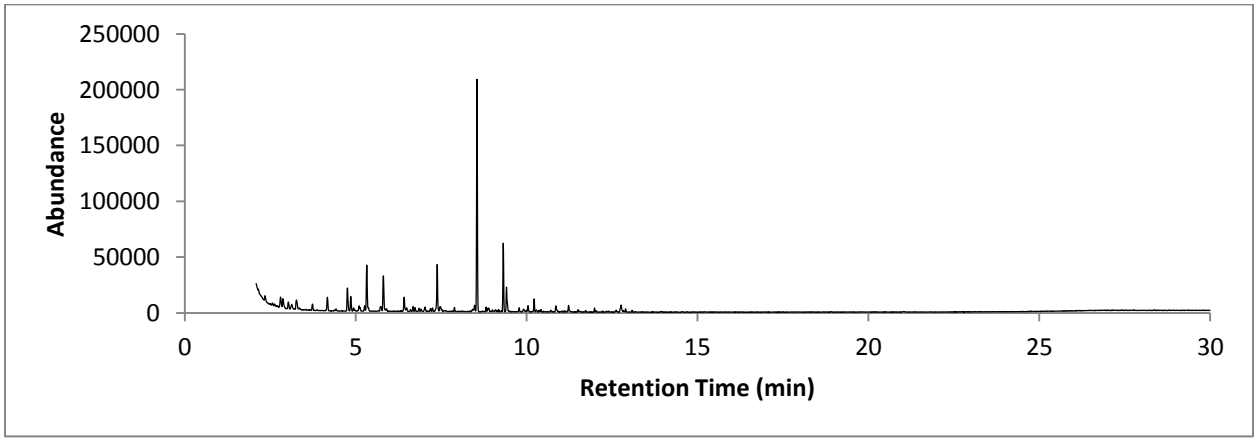

Figure 279: TIC C10-21

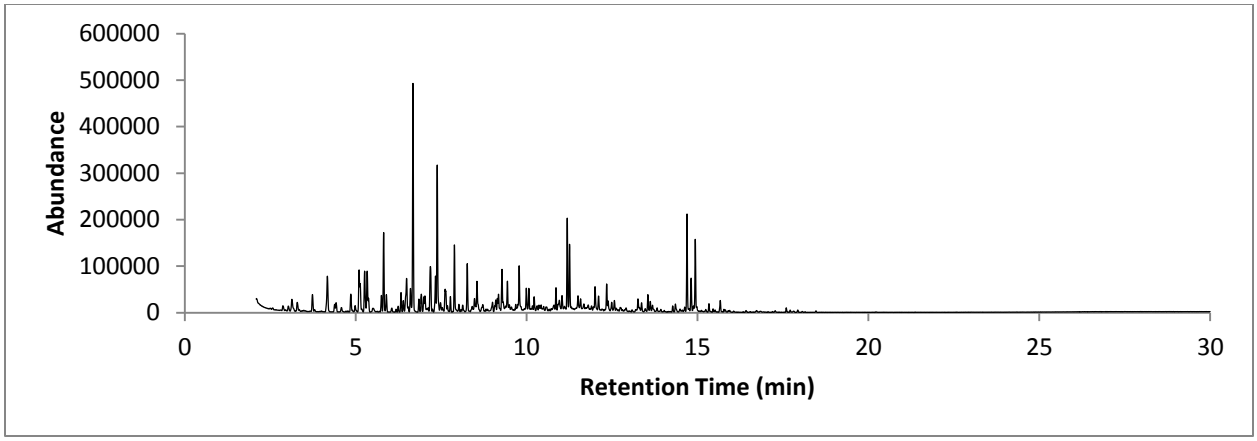

Figure 280: TIC C10-22

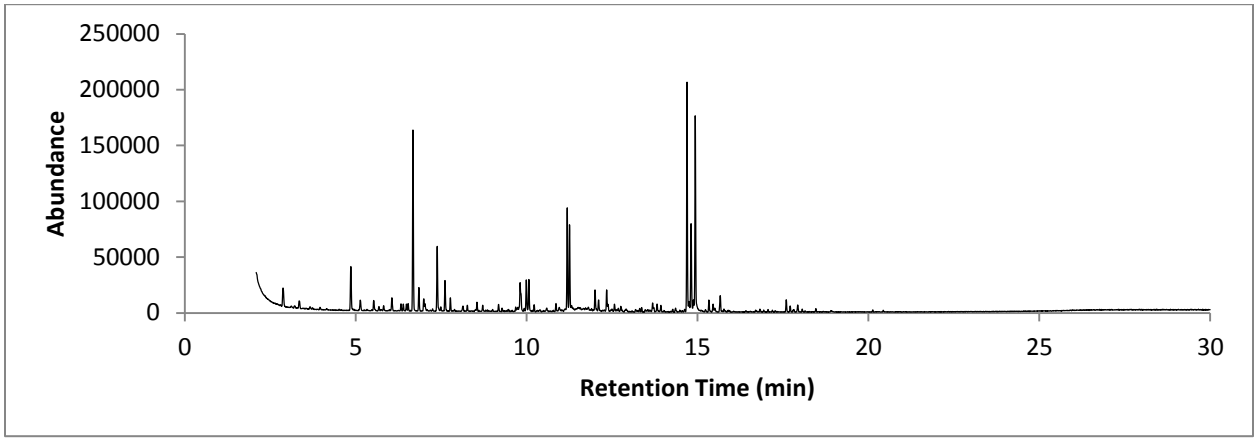

Figure 281: TIC C10-23

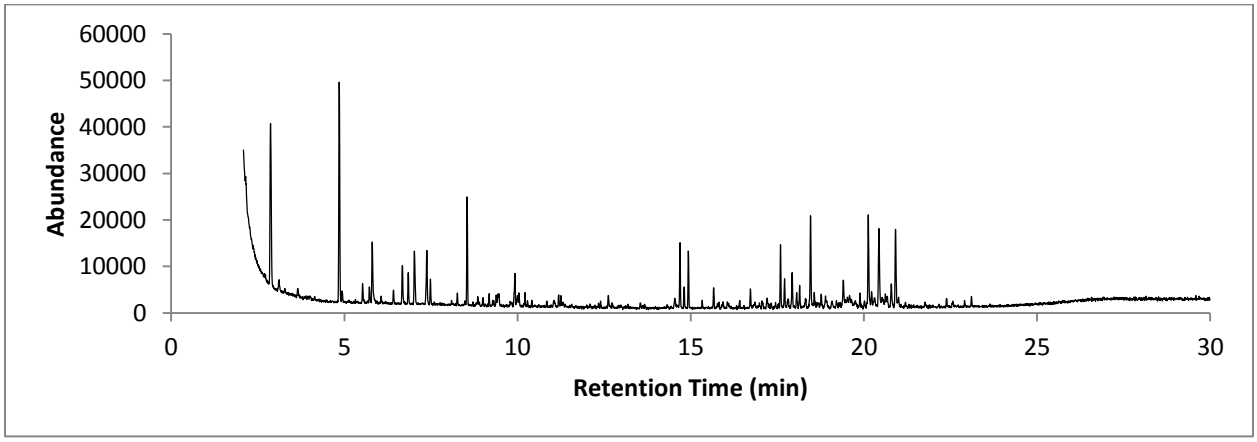

Figure 282: TIC C10-24

Sample TIS

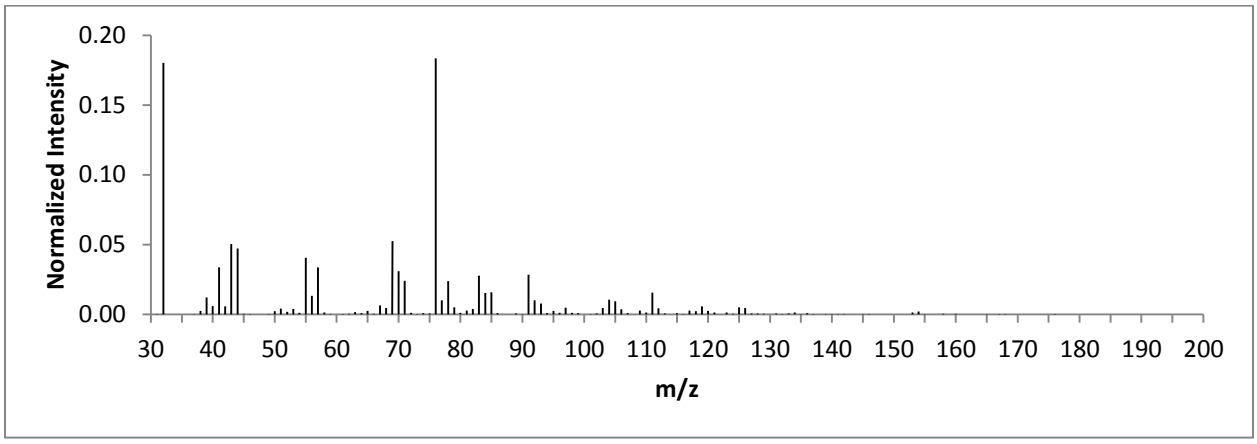

Figure 283: TIS C10-13

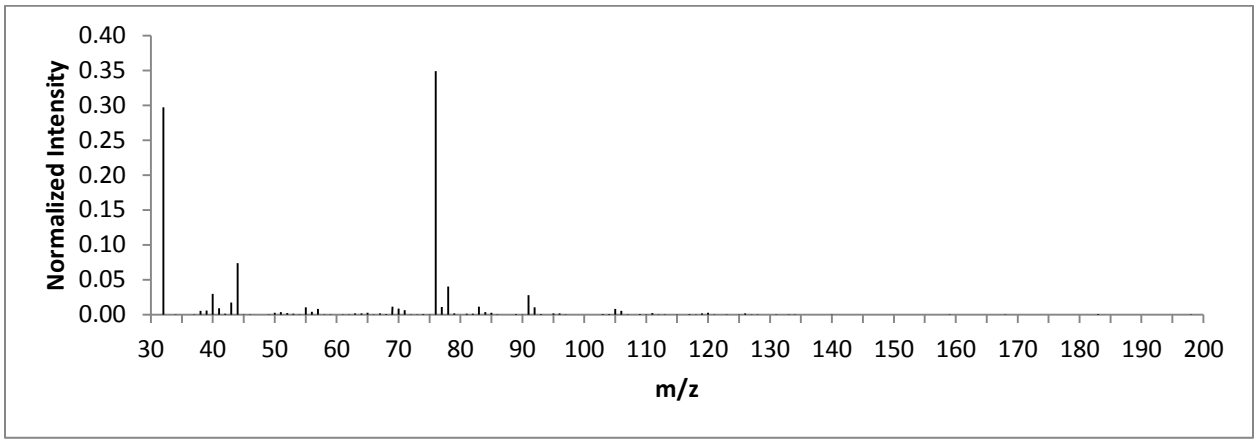

Figure 284: TIS C10-14

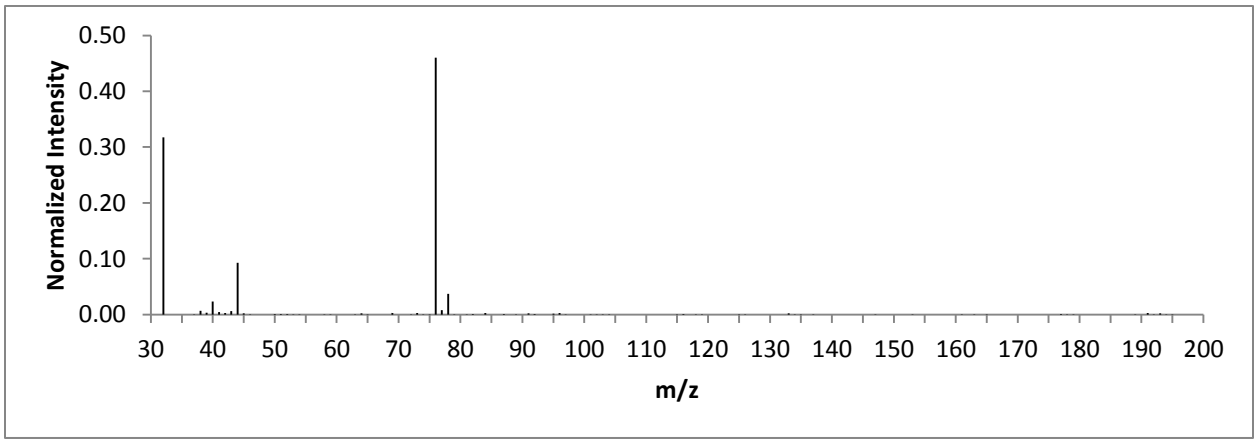

Figure 285: TIS C10-15

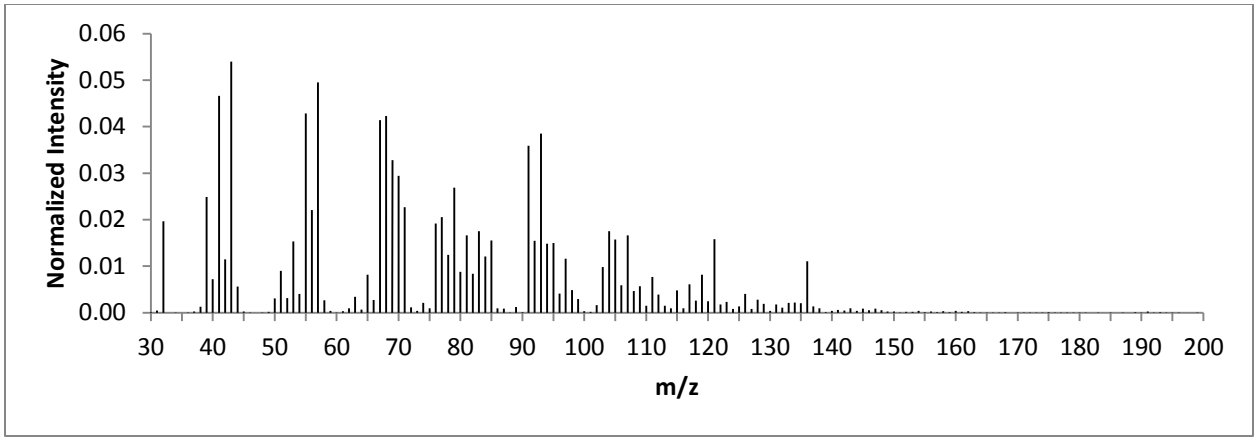

Figure 286: TIS C10-16

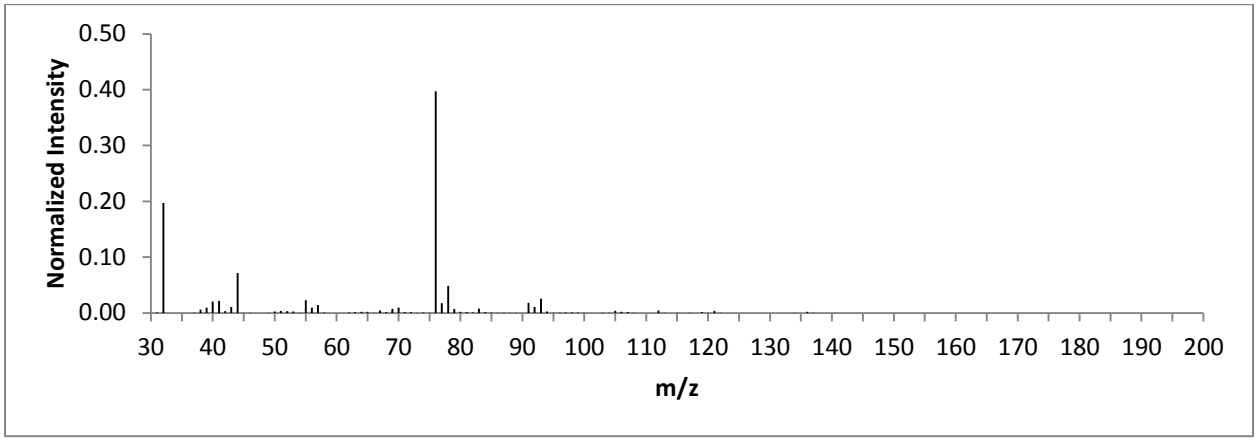

Figure 287: TIS C10-17

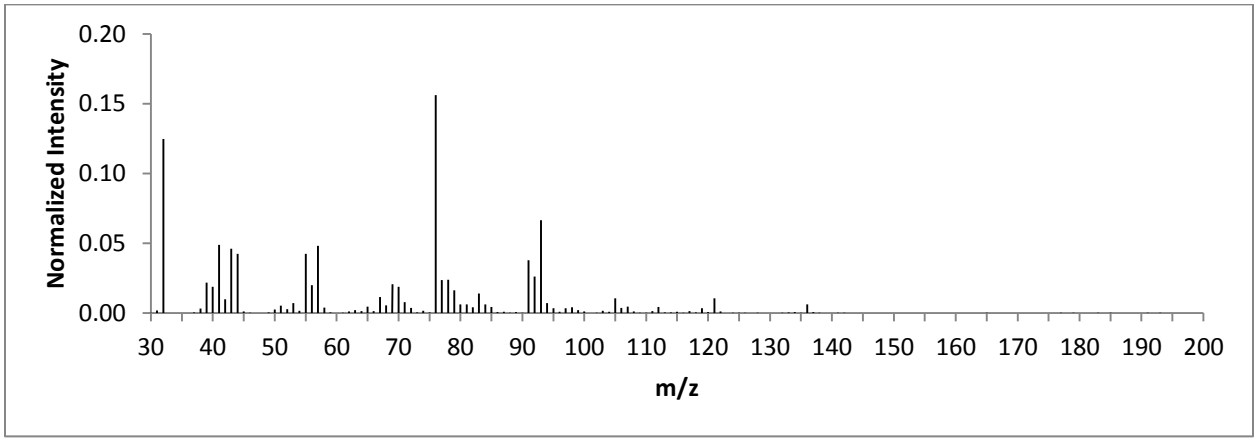

Figure 288: TIS C10-18

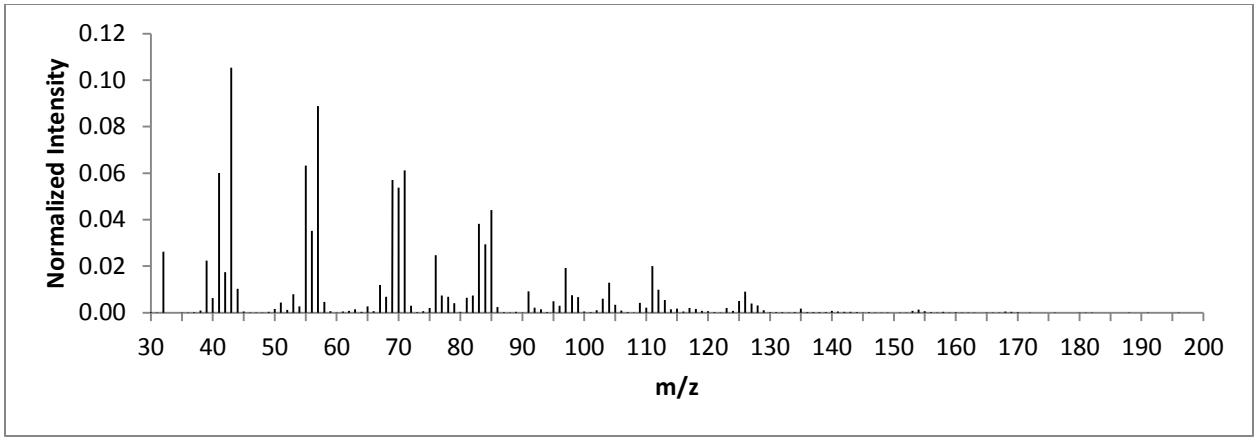

Figure 289: TIS C10-19

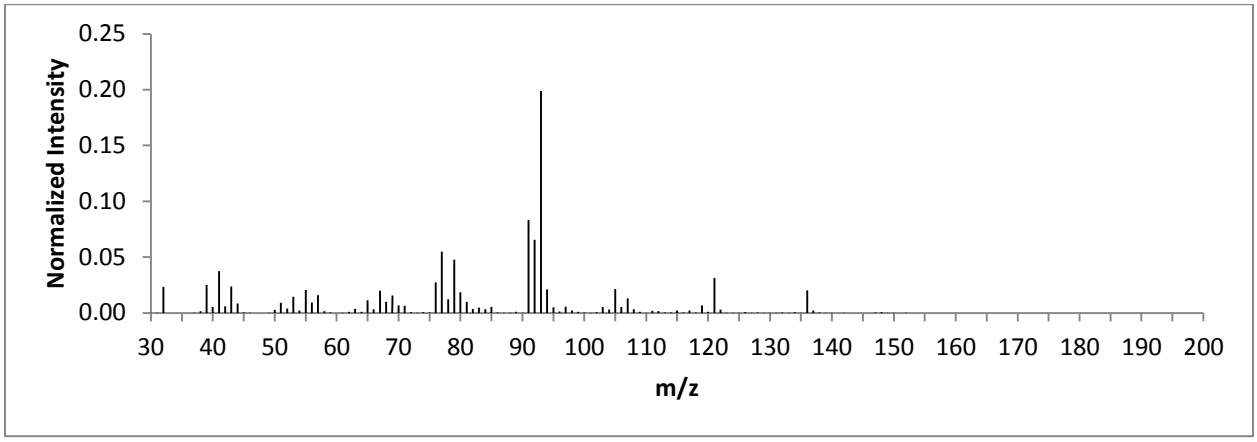

Figure 290: TIS C10-20

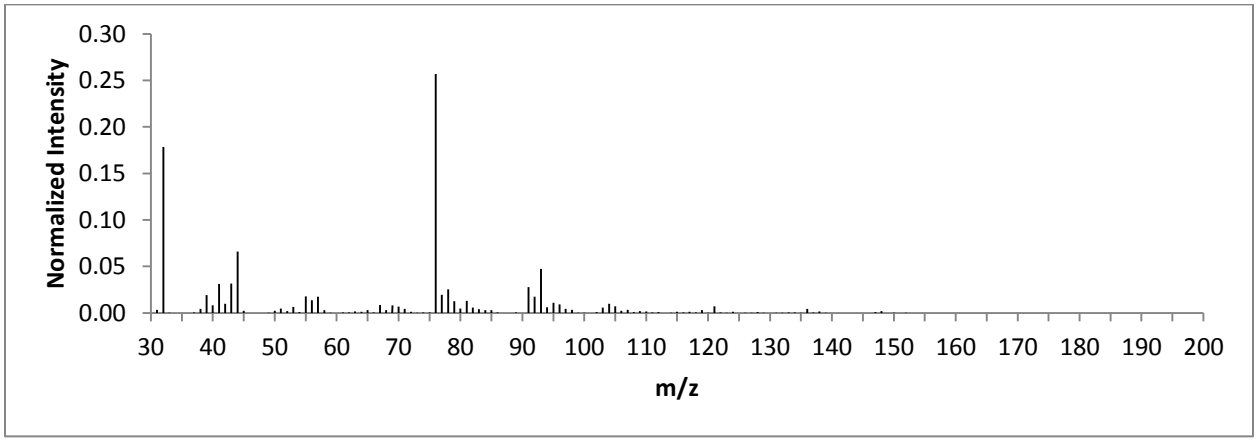

Figure 291: TIS C10-21

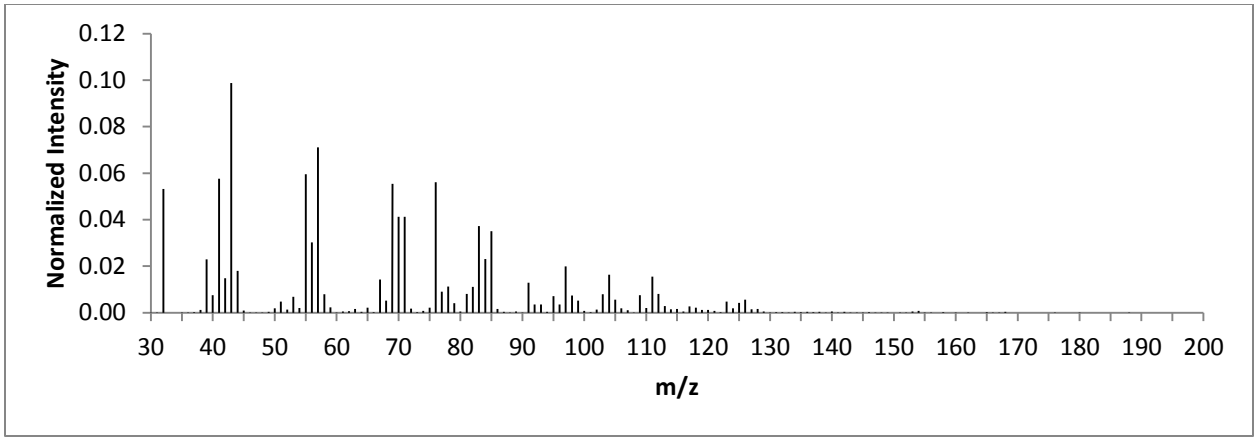

Figure 292: TIS C10-22

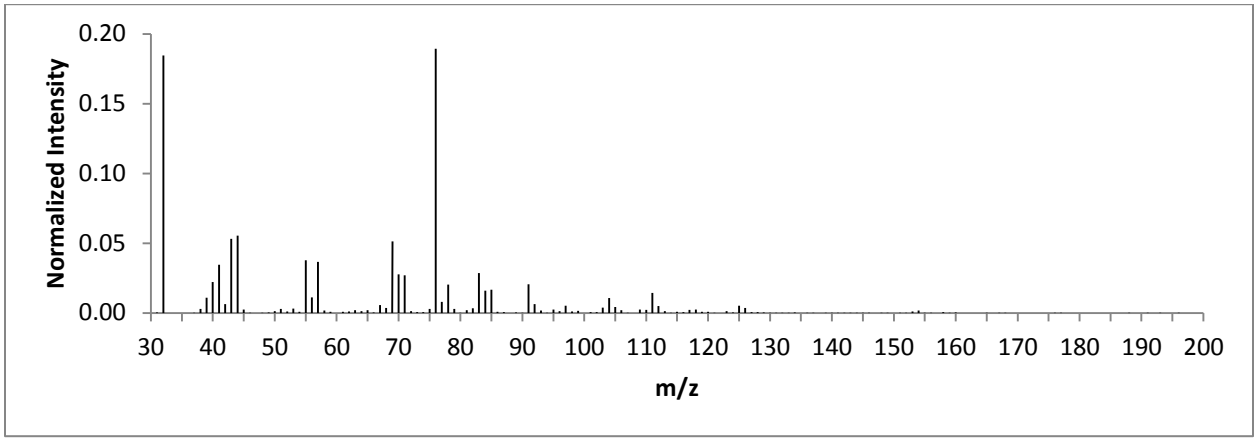

Figure 293: TIS C10-23

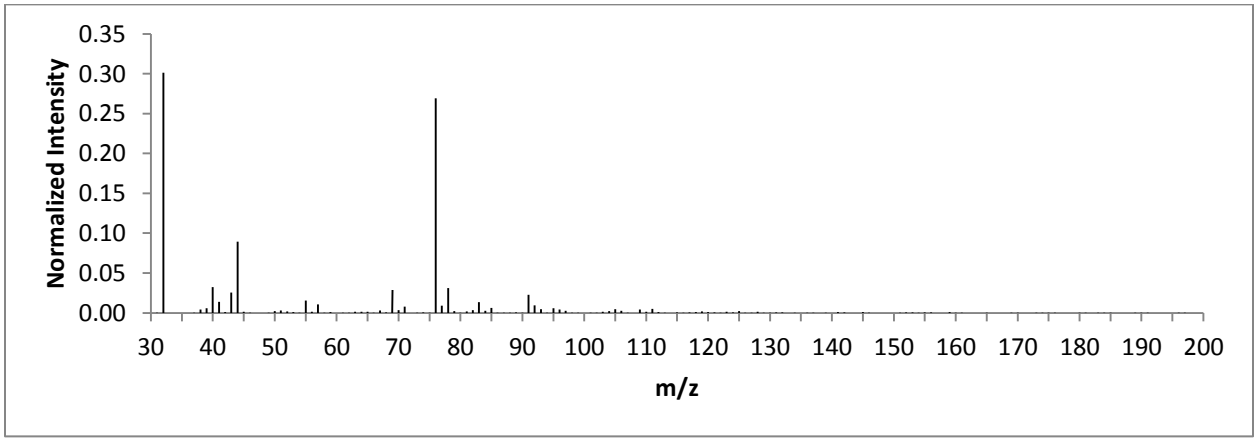

Figure 294: TIS C10-24

APPENDIX G
CONTAINER 11

Ignitable Liquid TIC

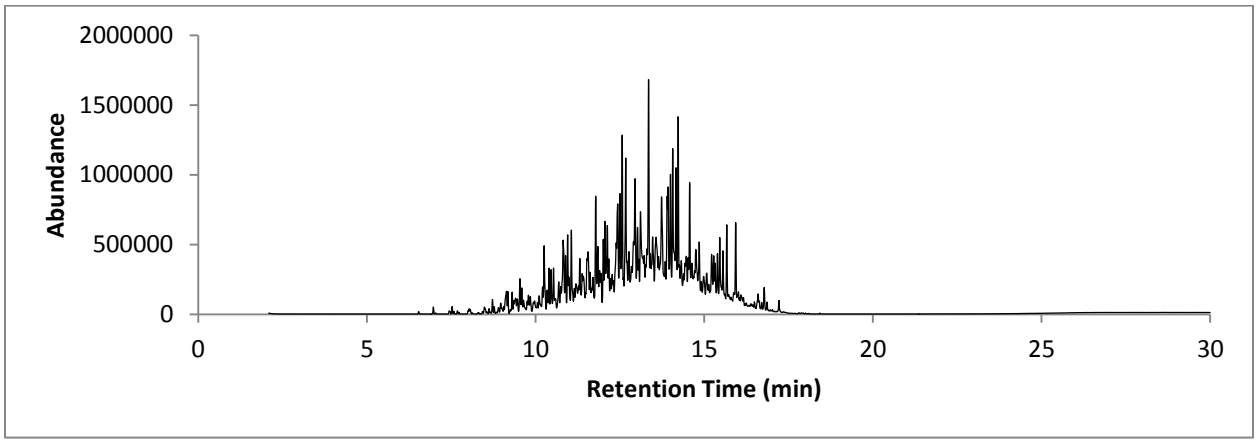

Figure 295: TIC C11 NP

Ignitable Liquid TIS

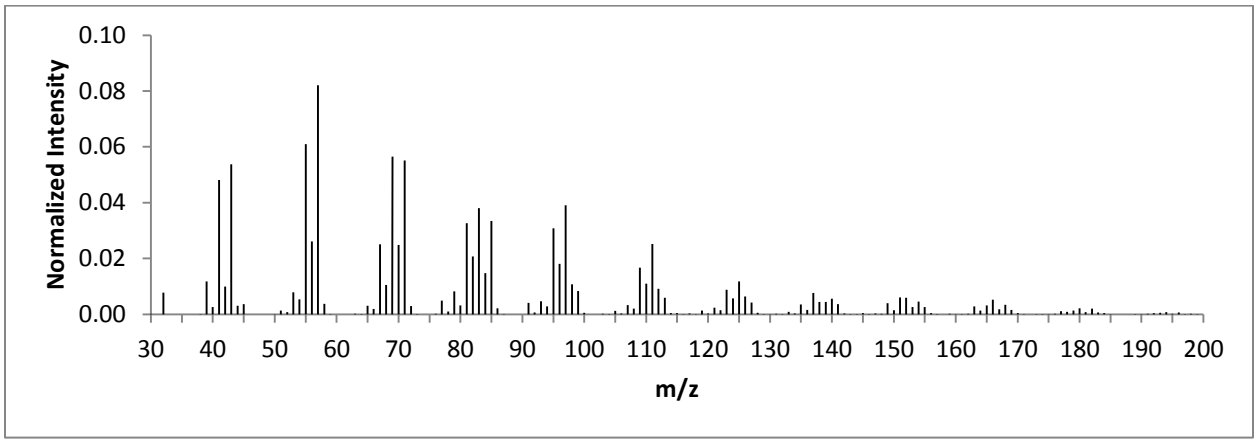

Figure 296: TIS C11 NP

Sample TIC

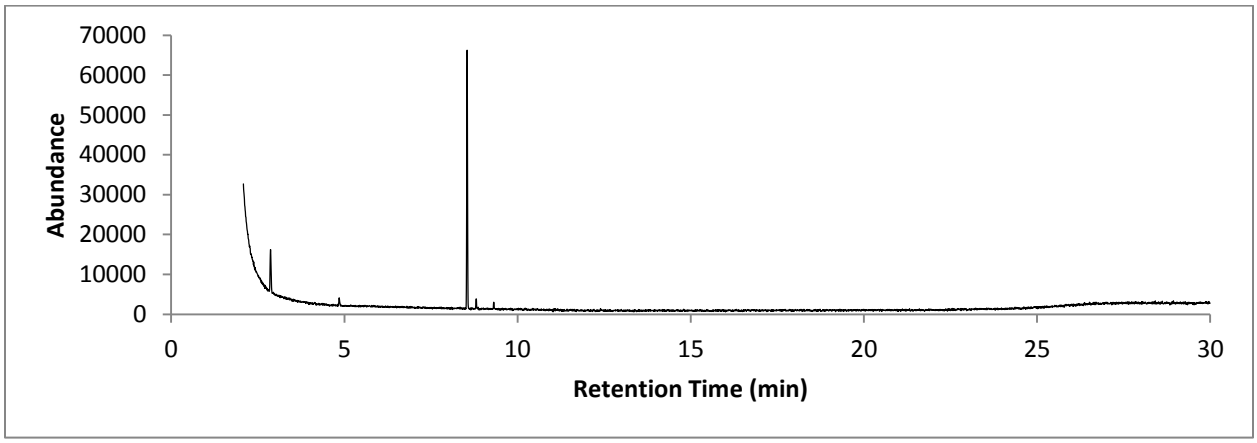

Figure 297: TIC C11-1

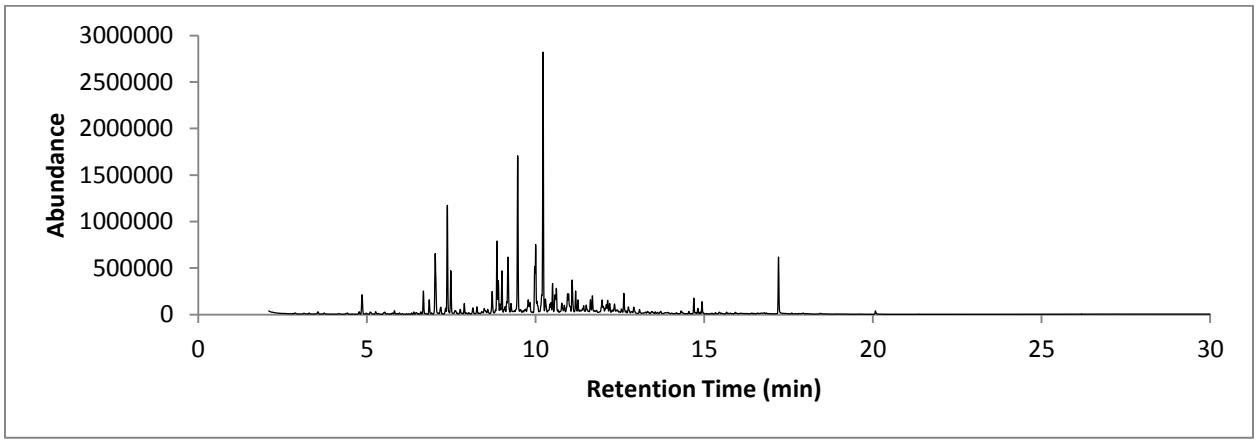

Figure 298: TIC C11-2

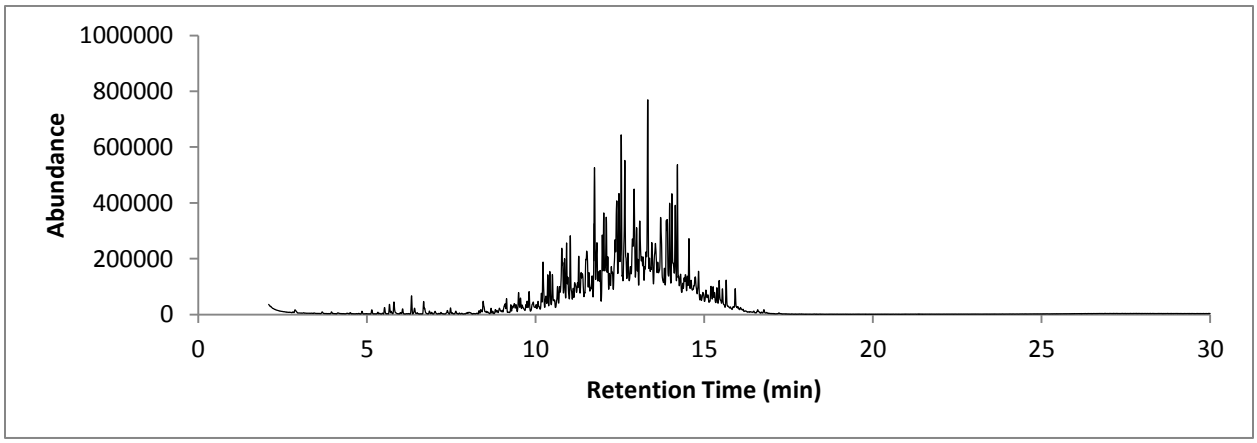

Figure 299: TIC C11-3

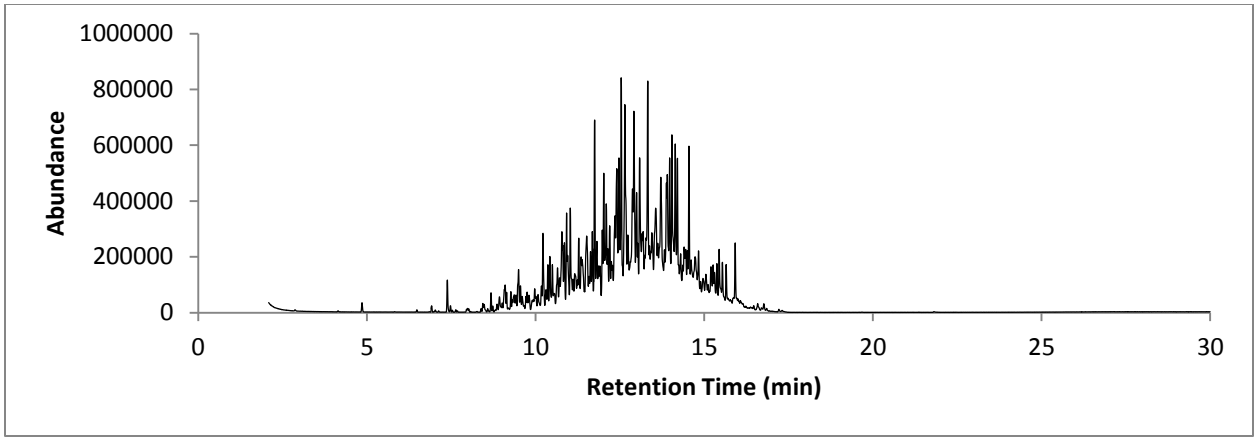

Figure 300: TIC C11-4

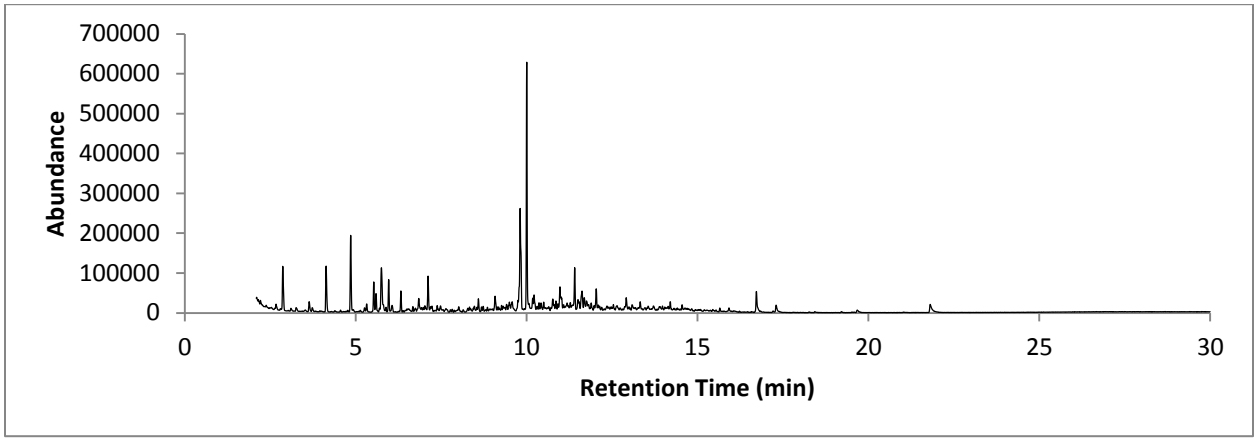

Figure 301: TIC C11-5

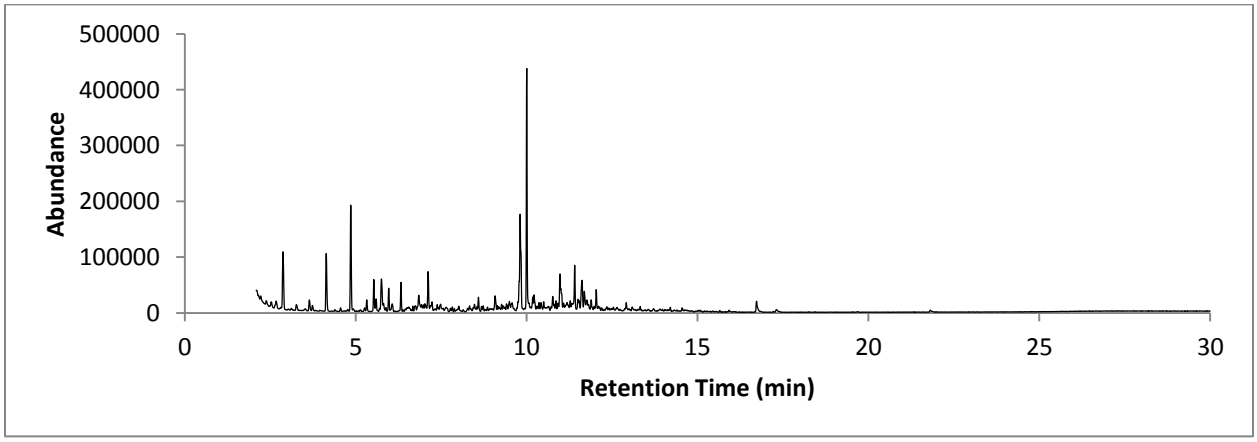

Figure 302: TIC C11-6

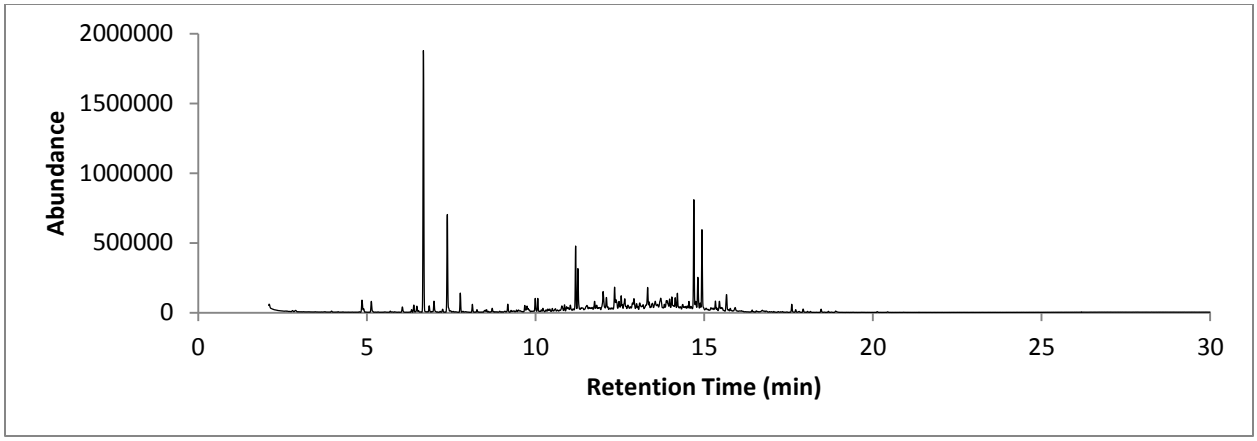

Figure 303: TIC C11-7

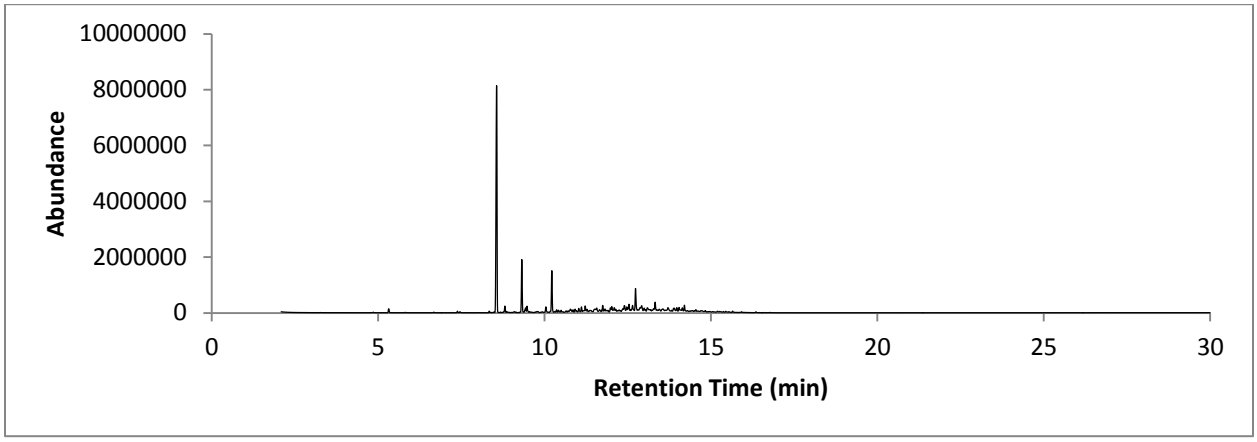

Figure 304: TIC C11-8

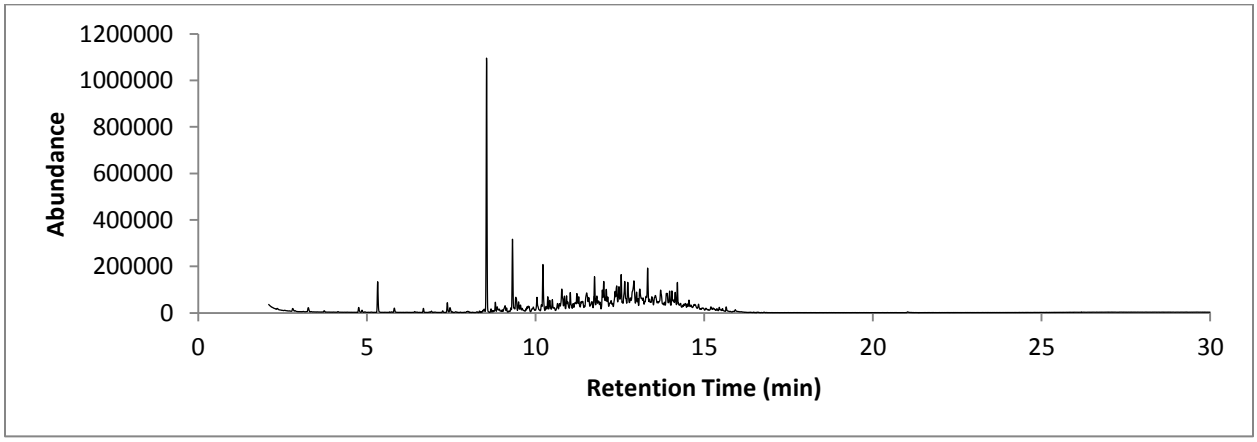

Figure 305: TIC C11-9

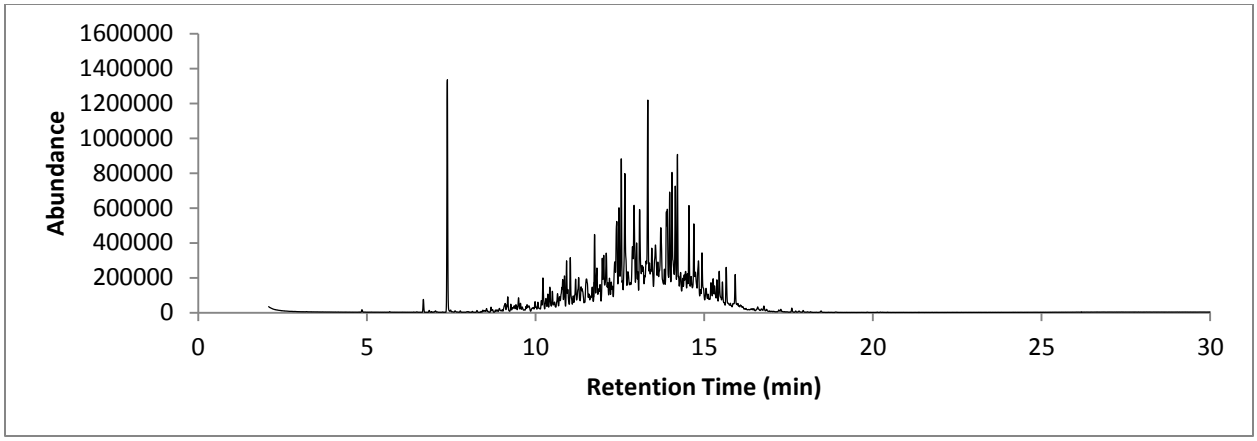

Figure 306: TIC C11-10

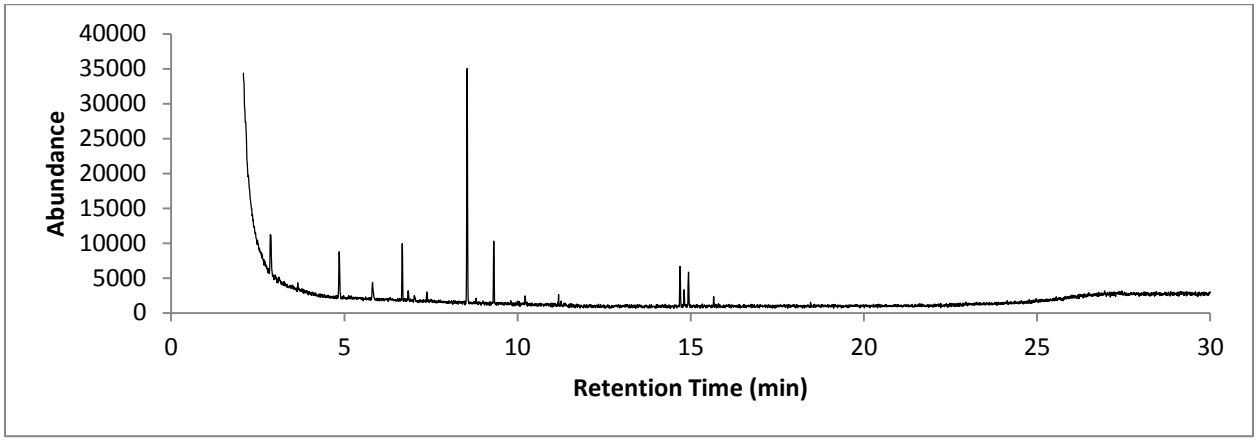

Figure 307: TIC C11-11

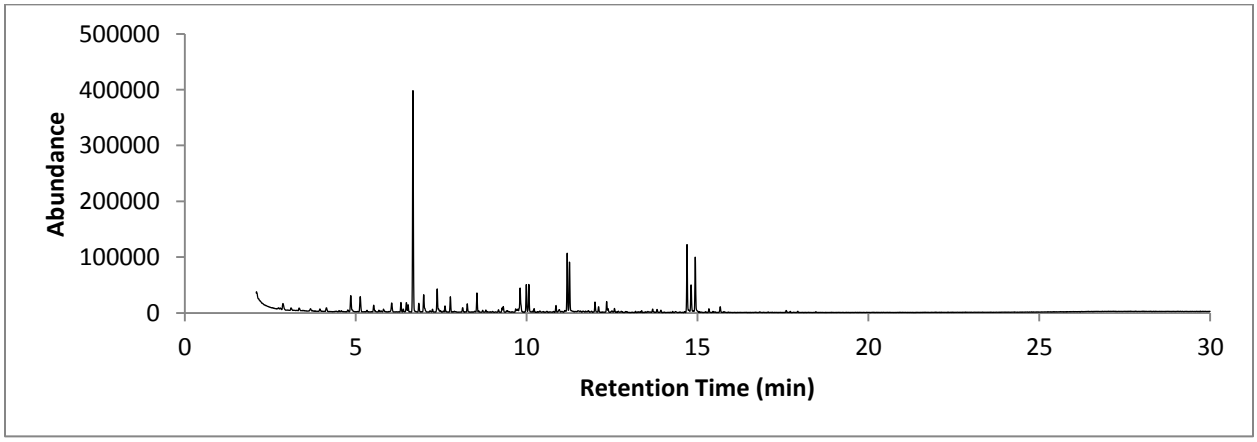

Figure 308: TIC C11-12

Sample TIS

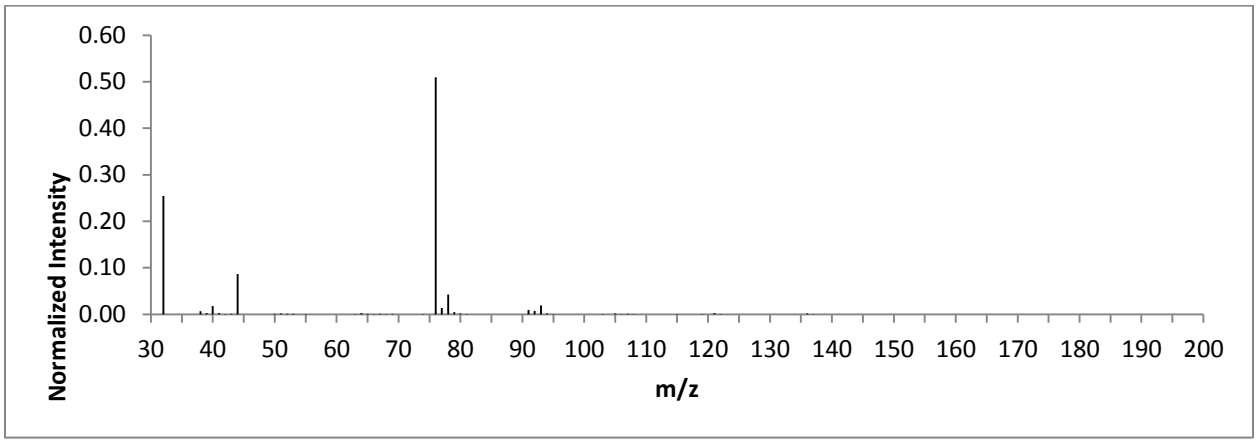

Figure 309: TIS C11-1

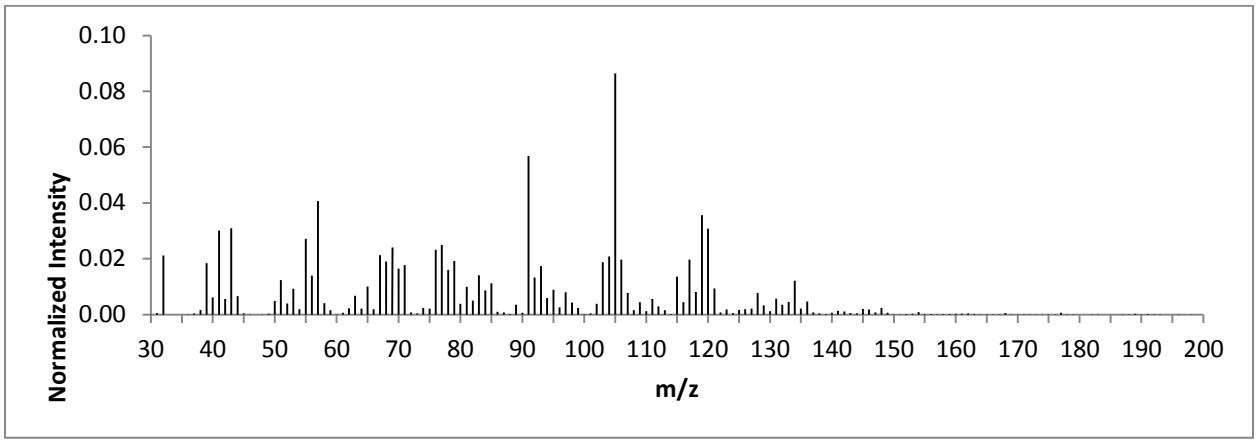

Figure 310: TIS C11-2

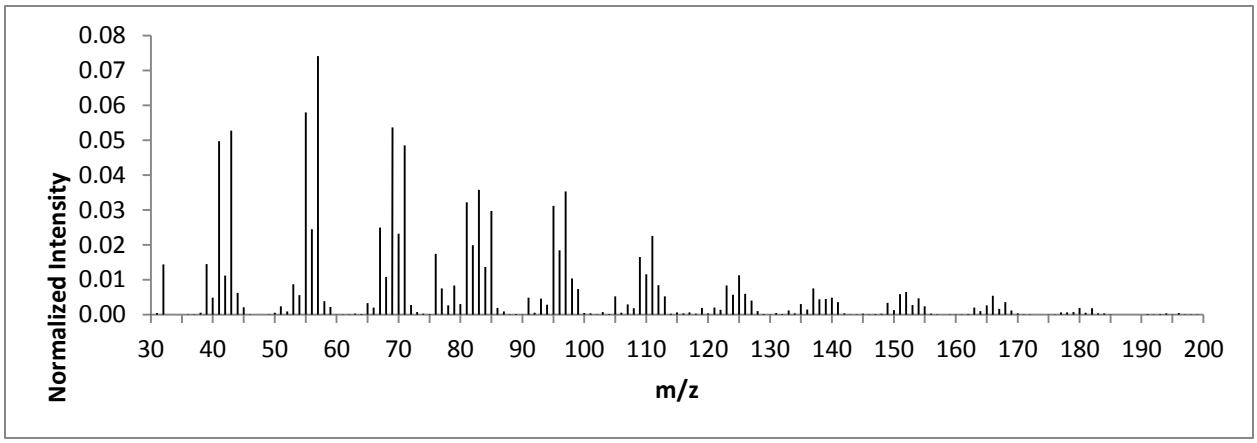

Figure 311: TIS C11-3

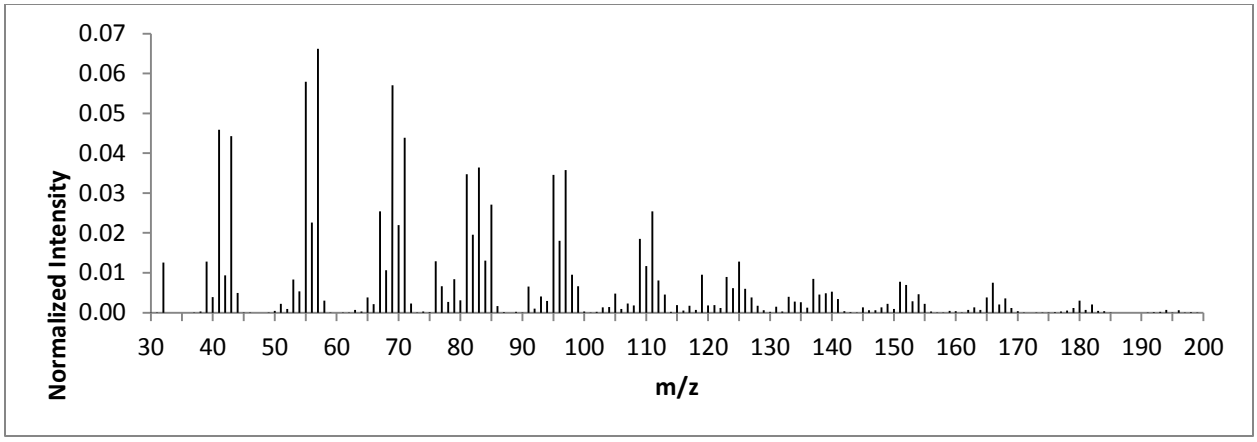

Figure 312: TIS C11-4

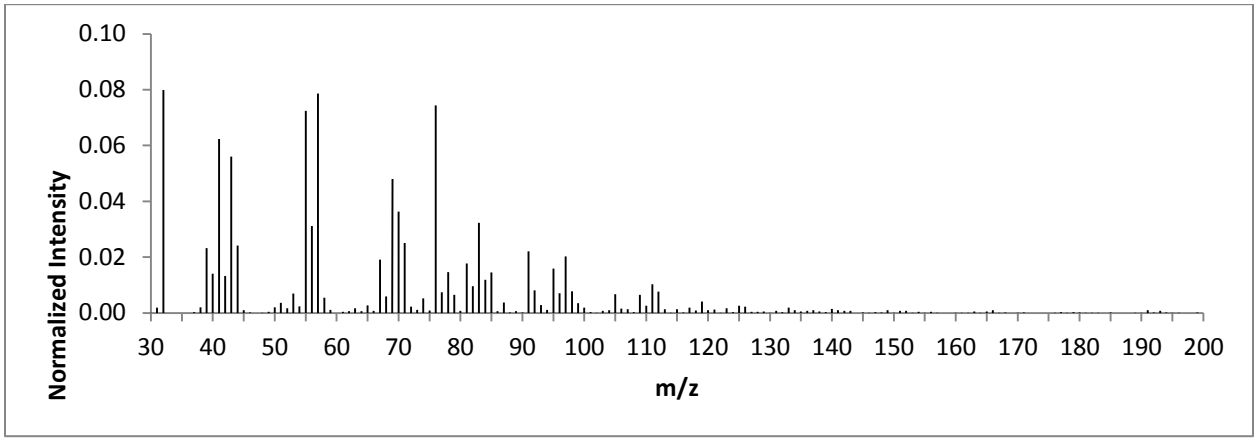

Figure 313: TIS C11-5

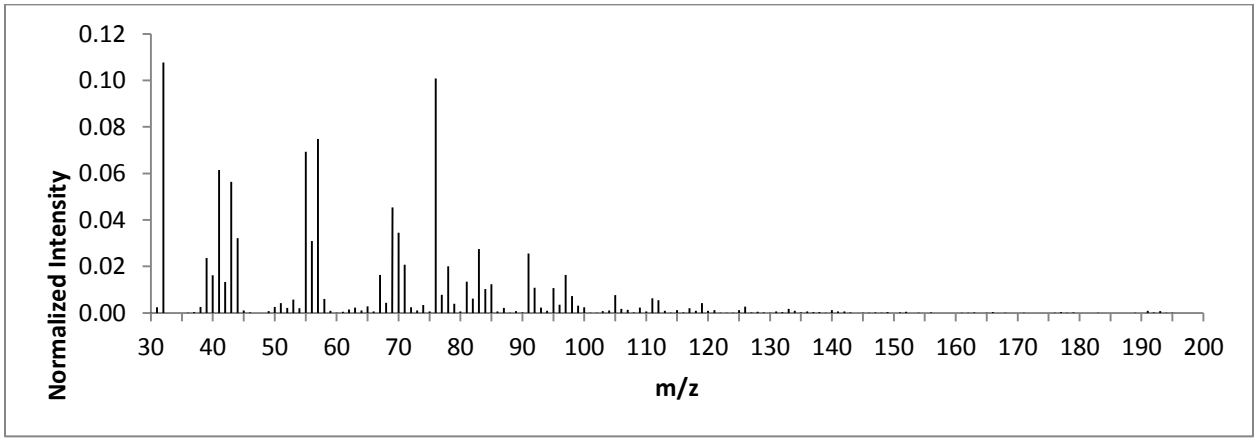

Figure 314: TIS C11-6

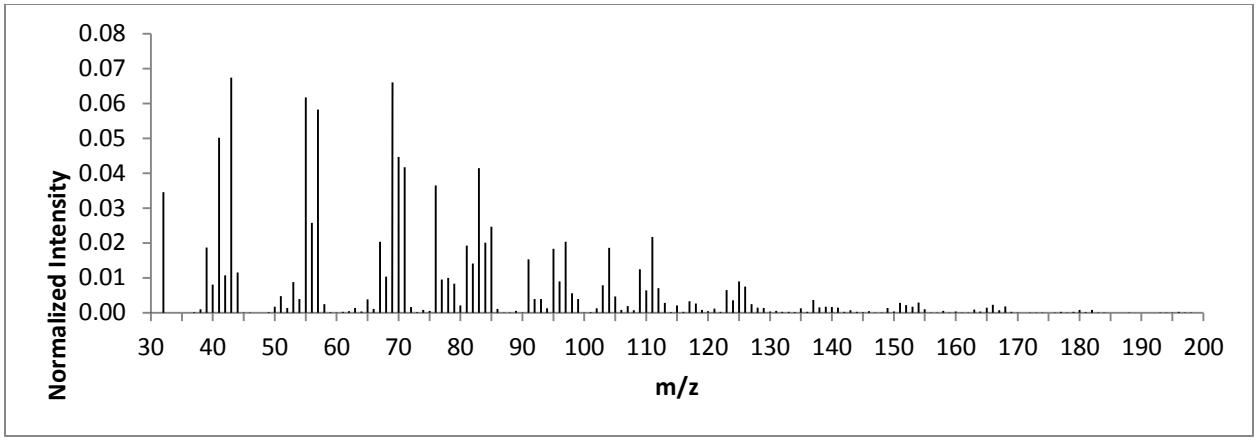

Figure 315: TIS C11-7

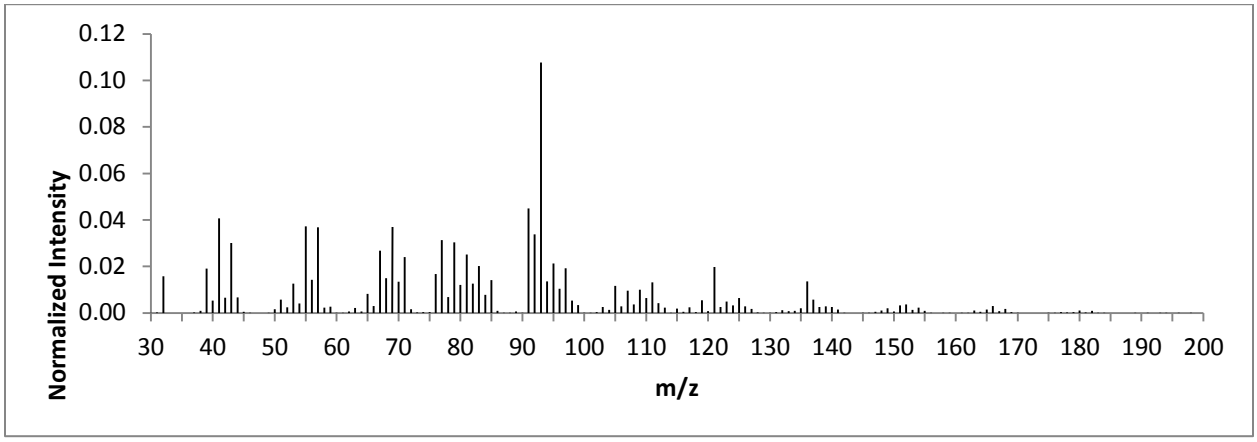

Figure 316: TIS C11-8

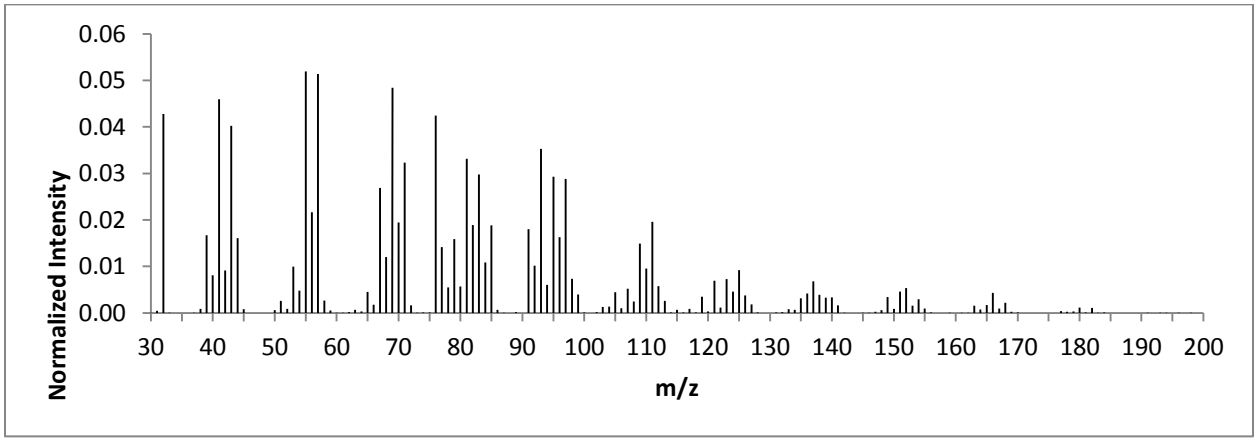

Figure 317: TIS C11-9

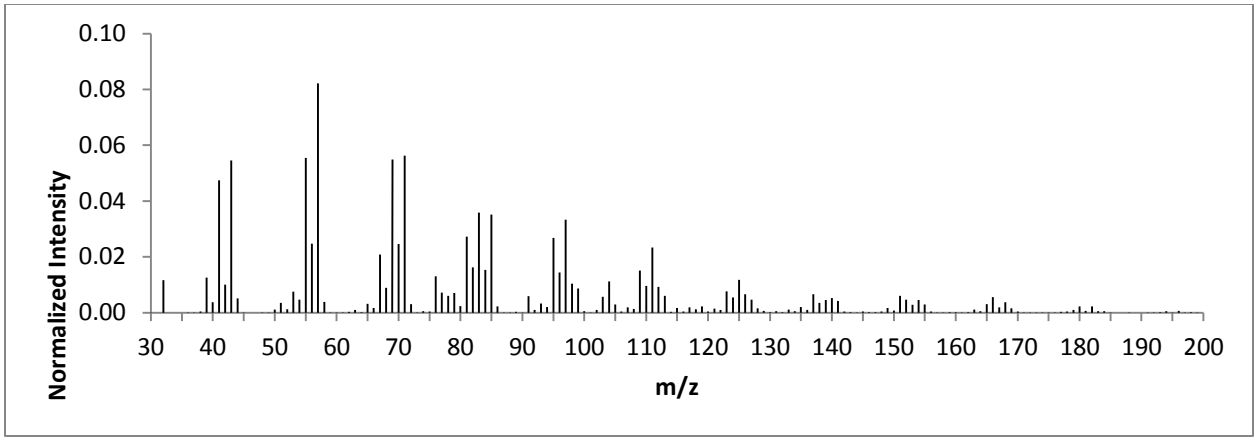

Figure 318: TIS C11-10

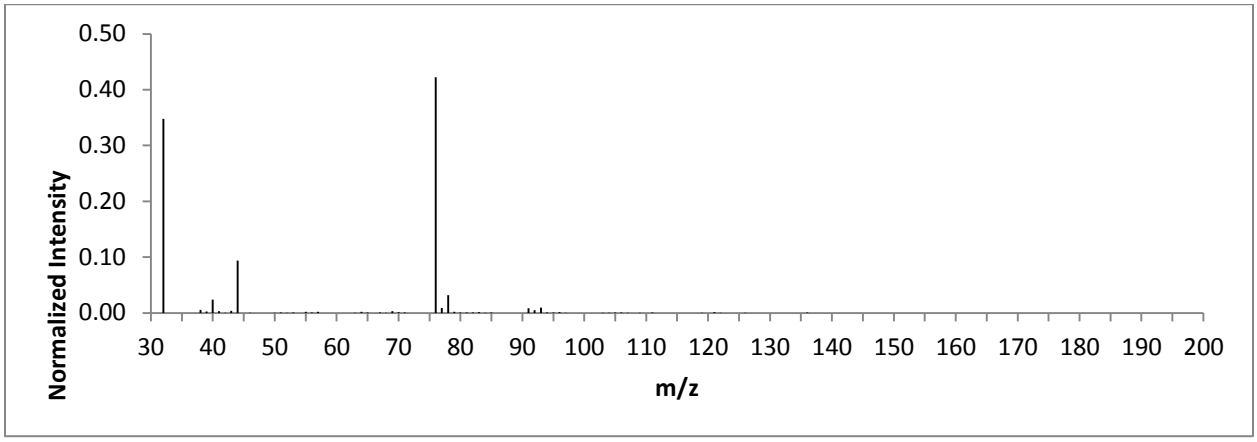

Figure 319: TIS C11-11

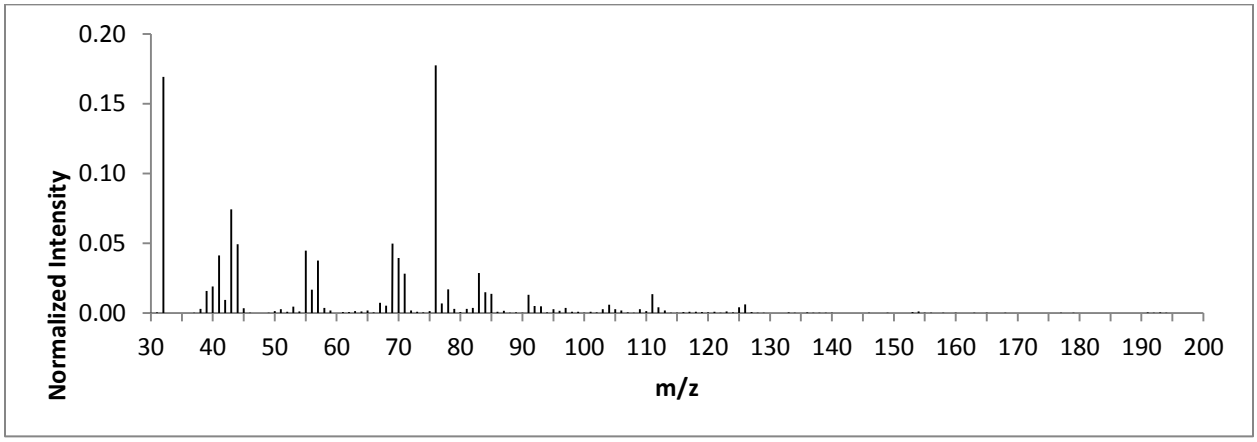

Figure 320: TIS C11-12

APPENDIX H
CONTAINER 12

Ignitable Liquid TIC

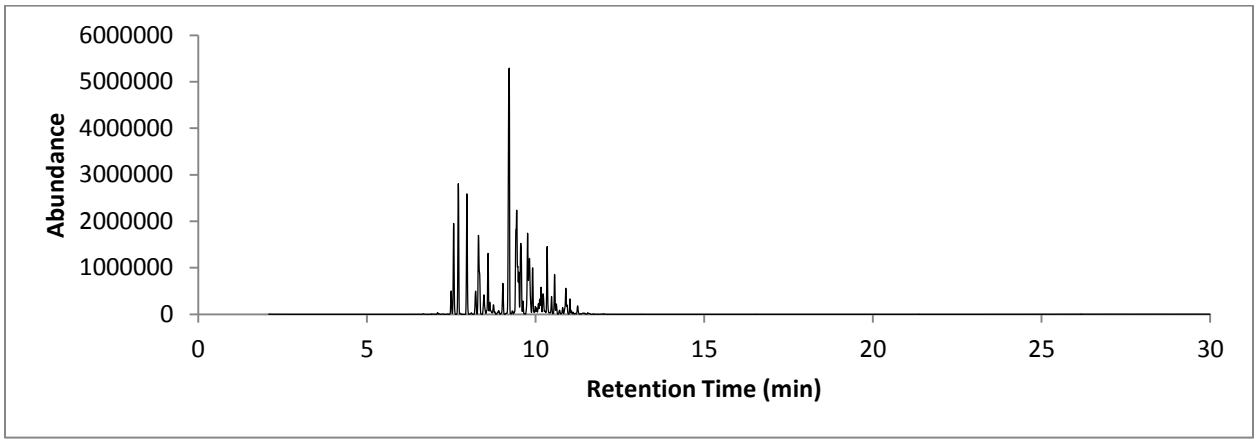

Figure 321: TIC C12 ISO

Ignitable Liquid TIS

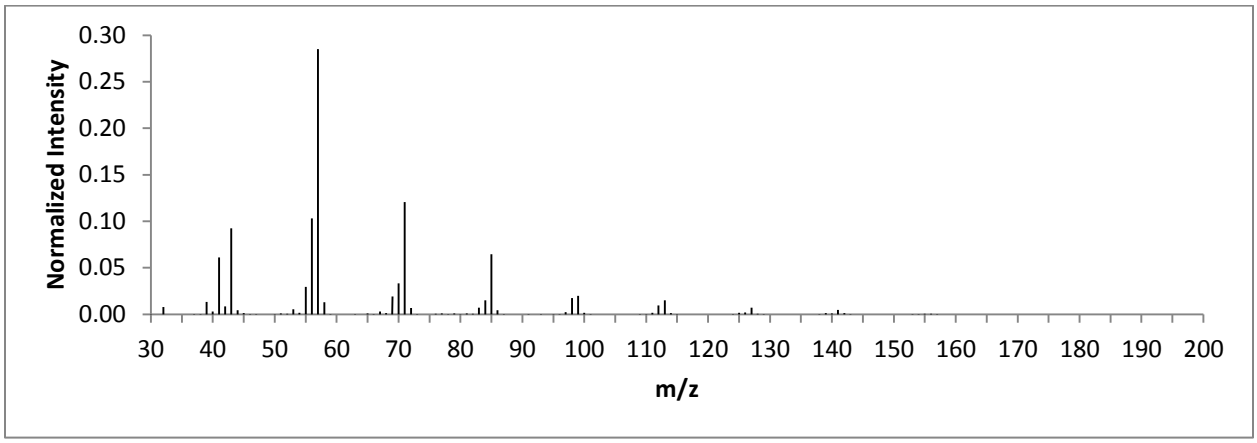

Figure 322: TIS C12 ISO

Sample TIC

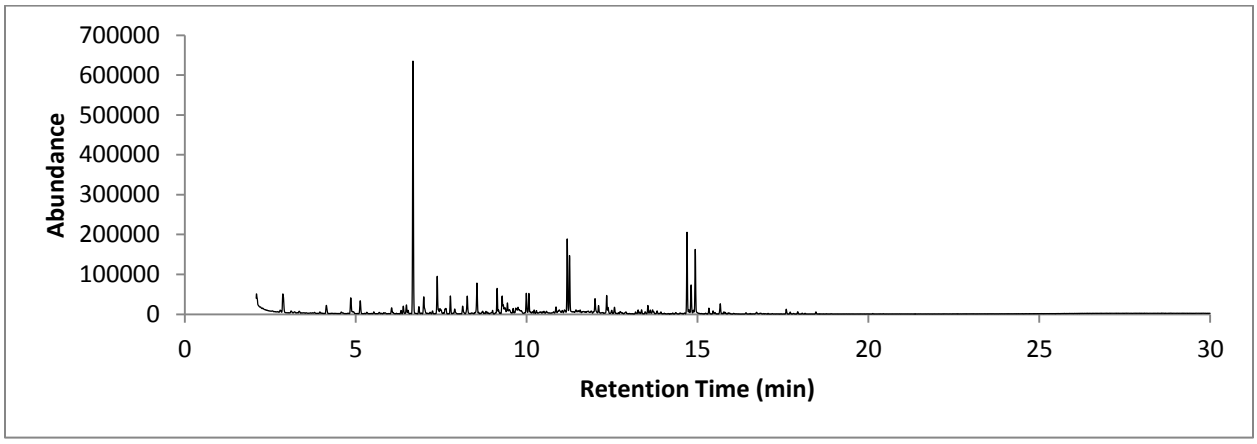

Figure 323: TIC C12-13

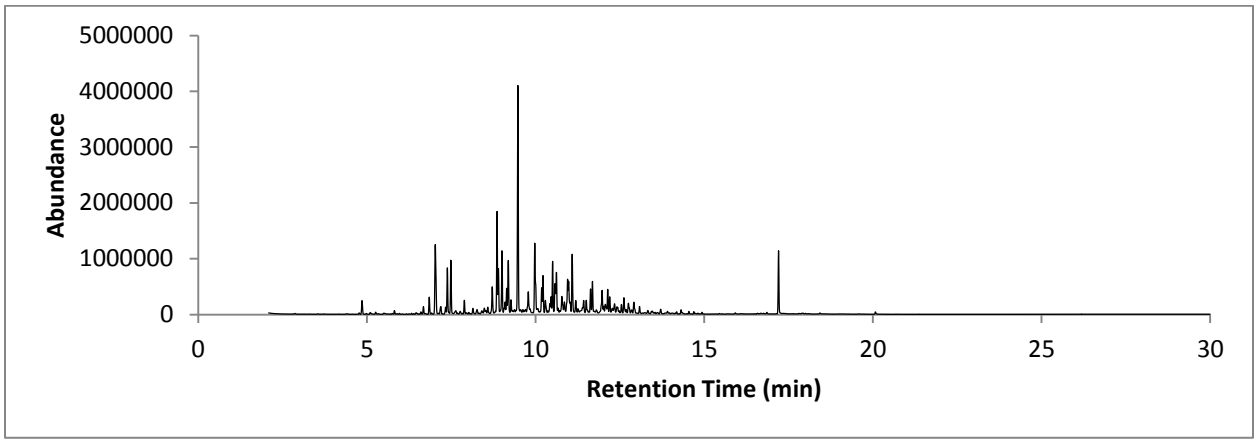

Figure 324: TIC C12-14

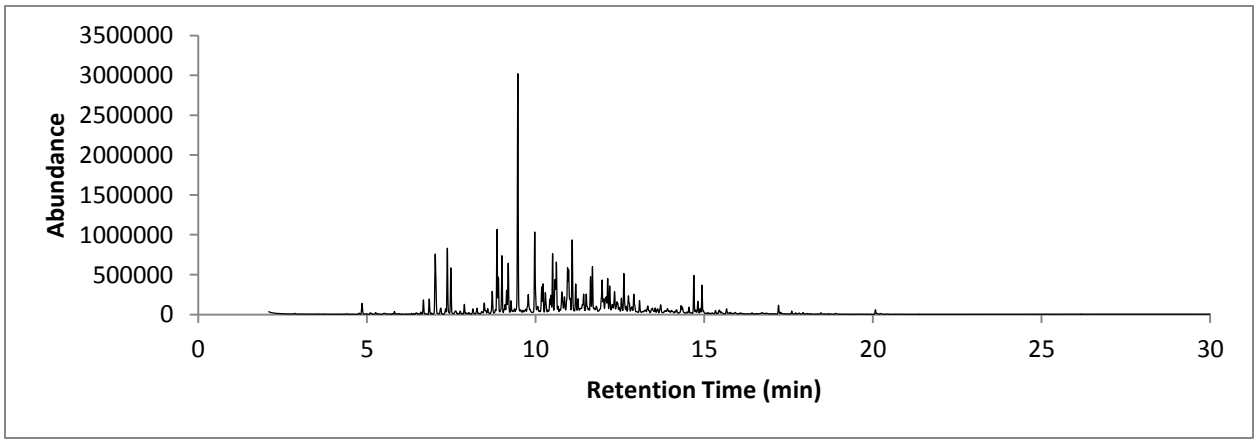

Figure 325: TIC C12-14B

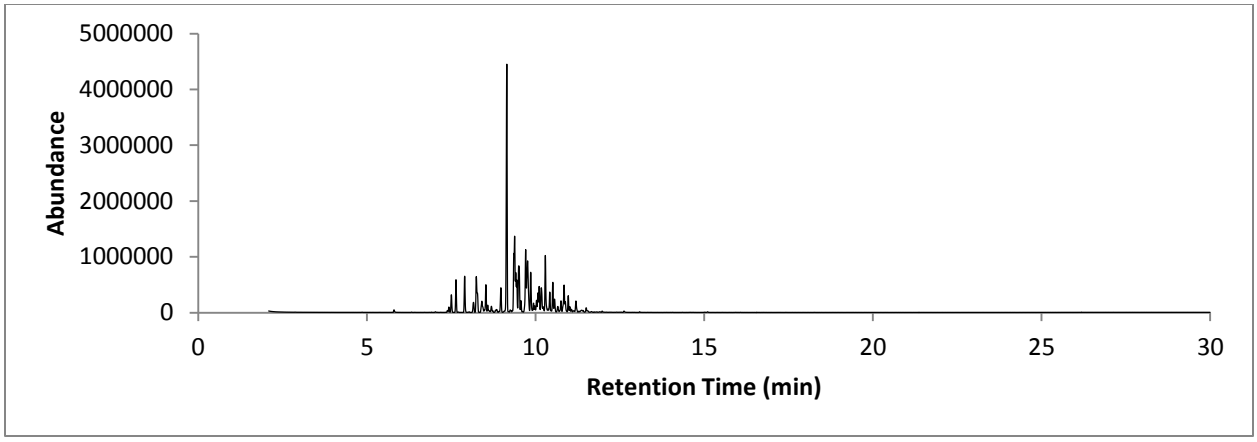

Figure 326: TIC C12-15

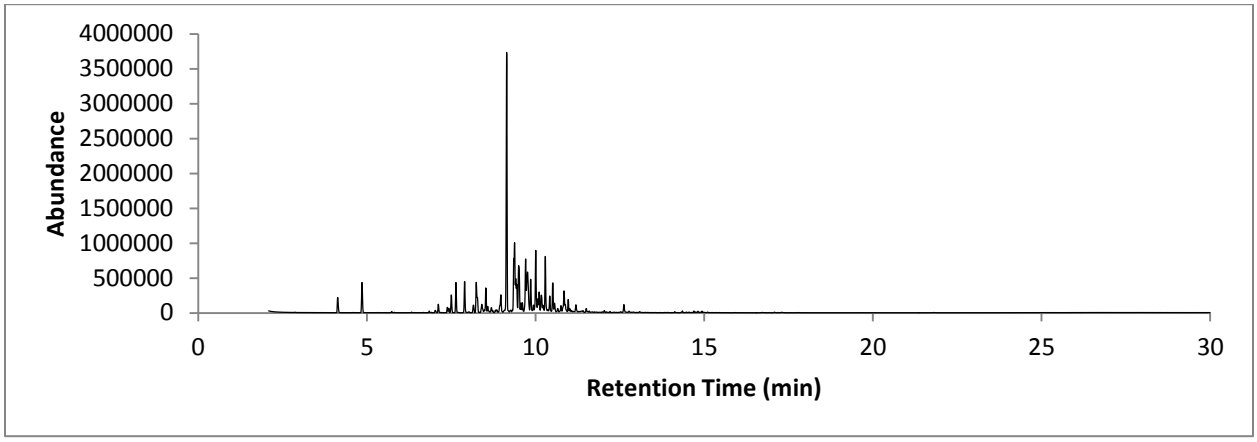

Figure 327: TIC C12-16

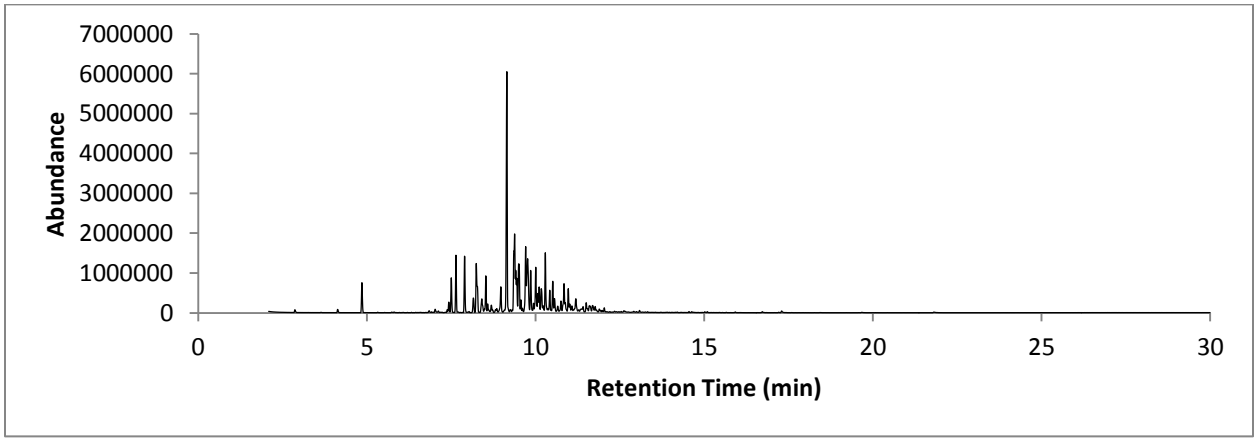

Figure 328: TIC C12-17

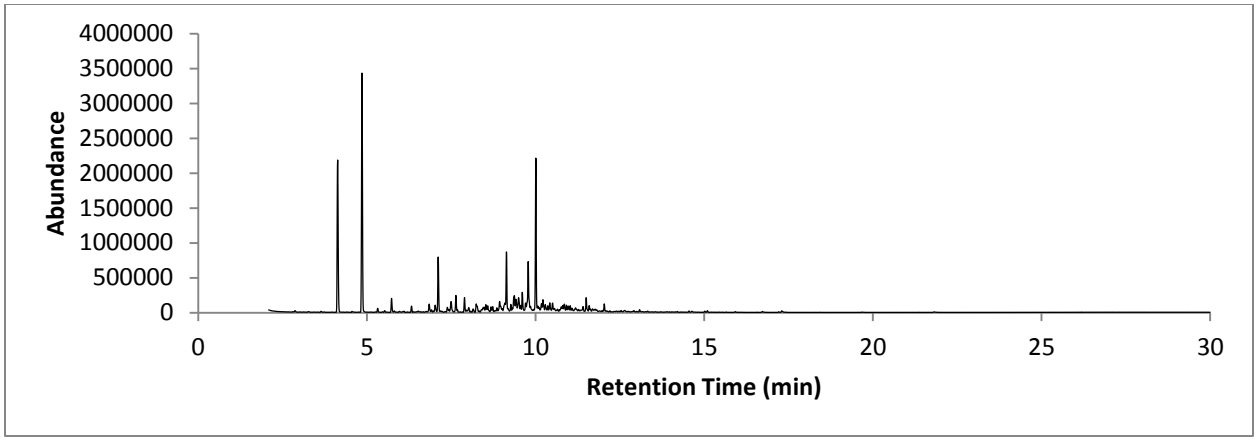

Figure 329: TIC C12-18

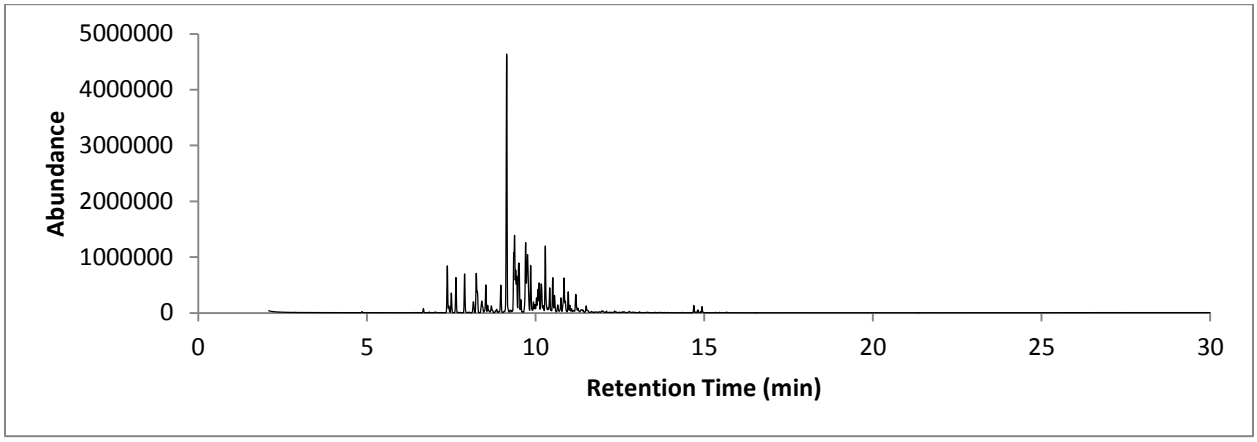

Figure 330: TIC C12-19

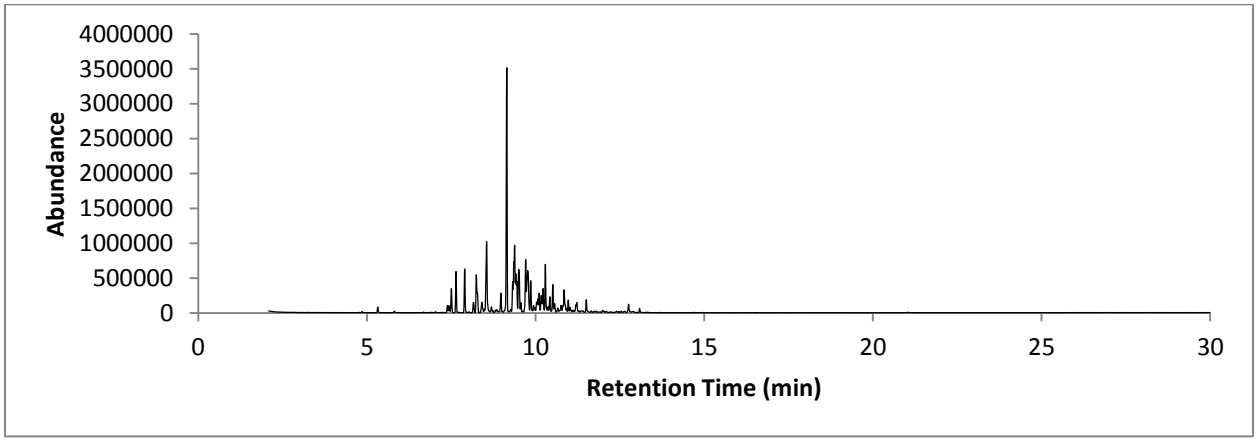

Figure 331: TIC C12-20

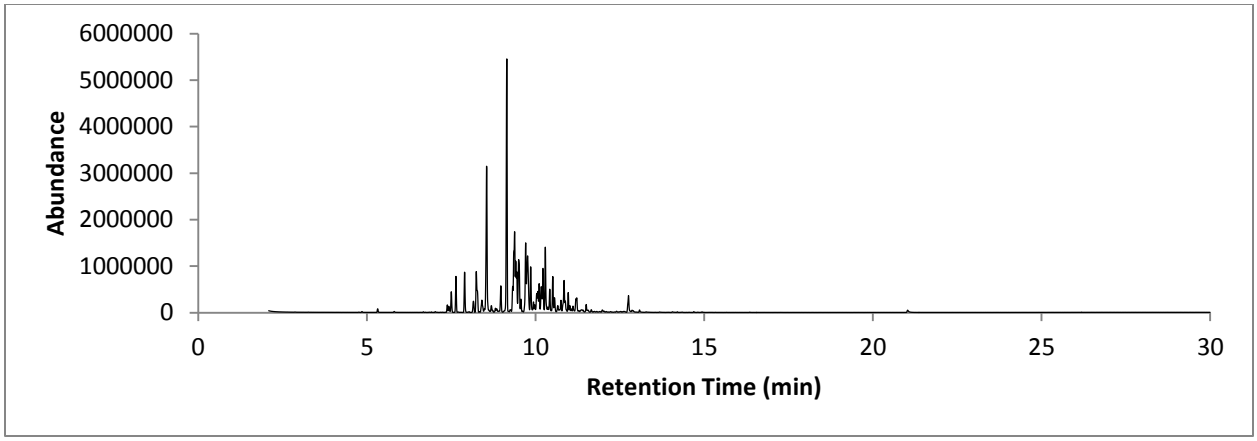

Figure 332: TIC C12-21

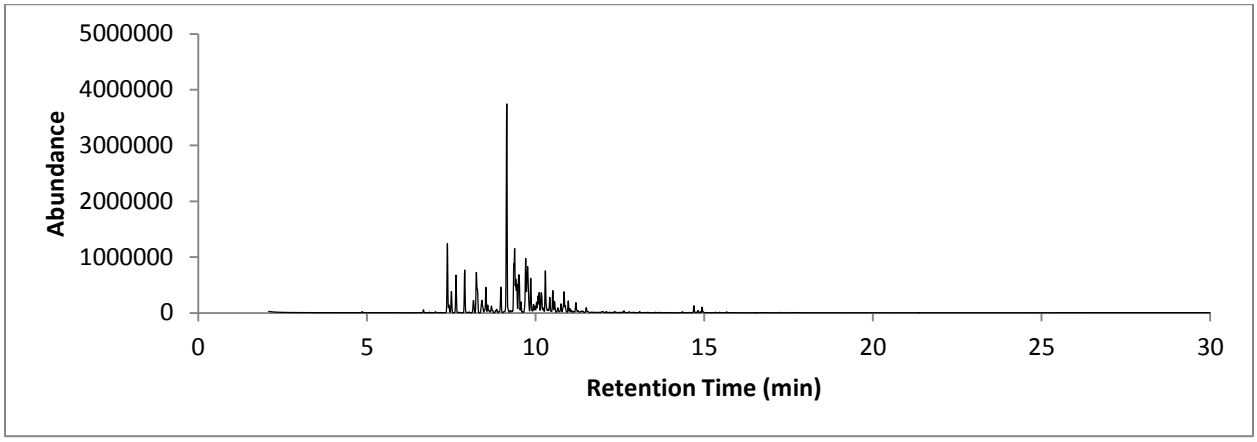

Figure 333: TIC C12-22

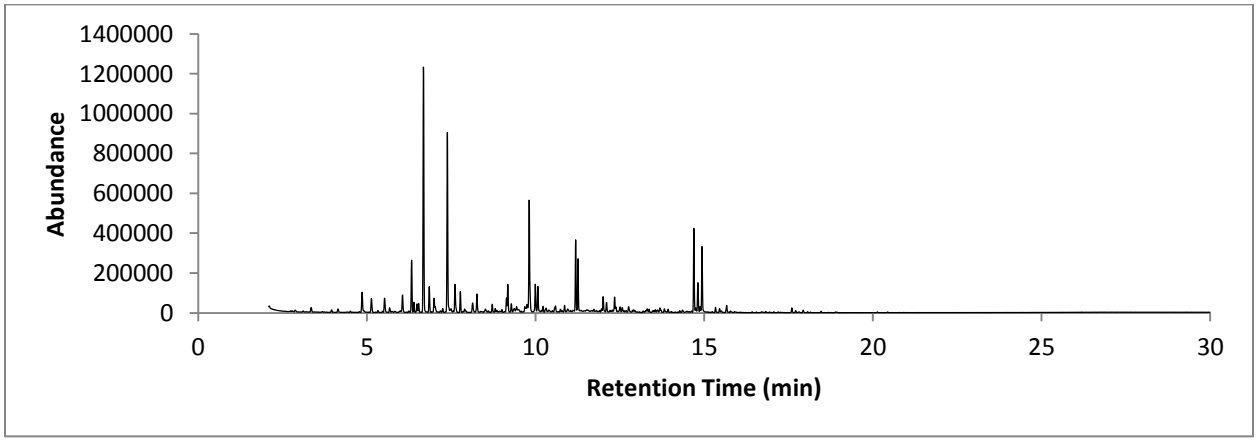

Figure 334: TIC C12-23

Sample TIS

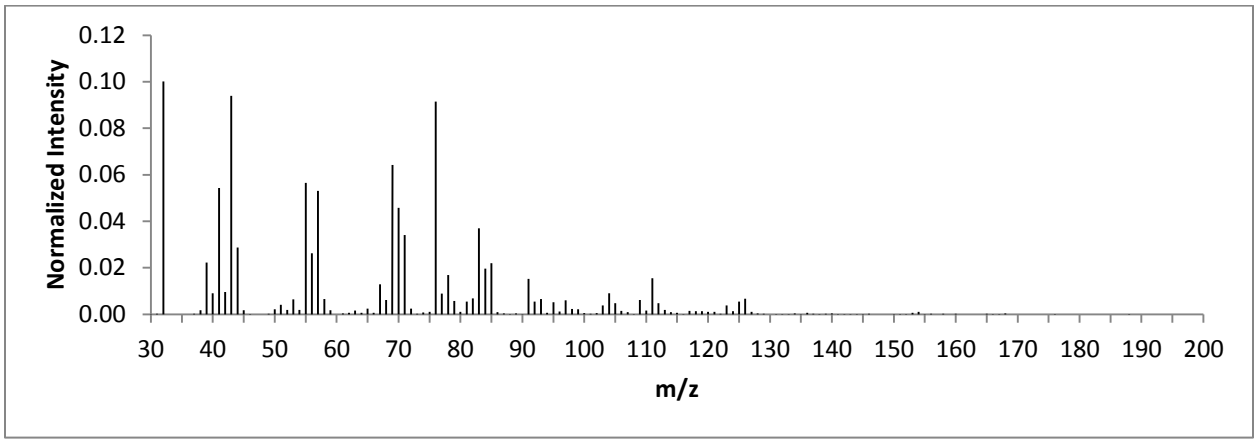

Figure 335: TIS C12-13

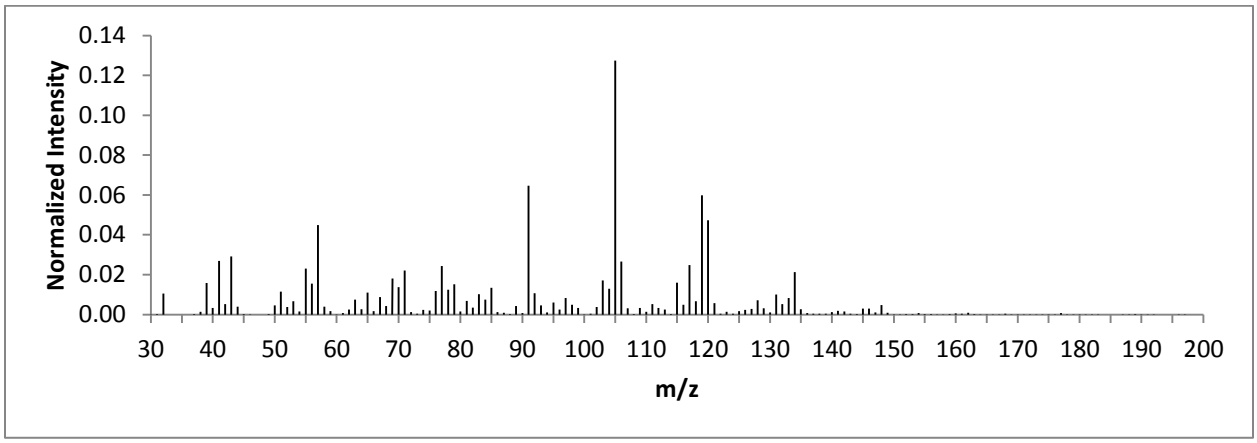

Figure 336: TIS C12-14

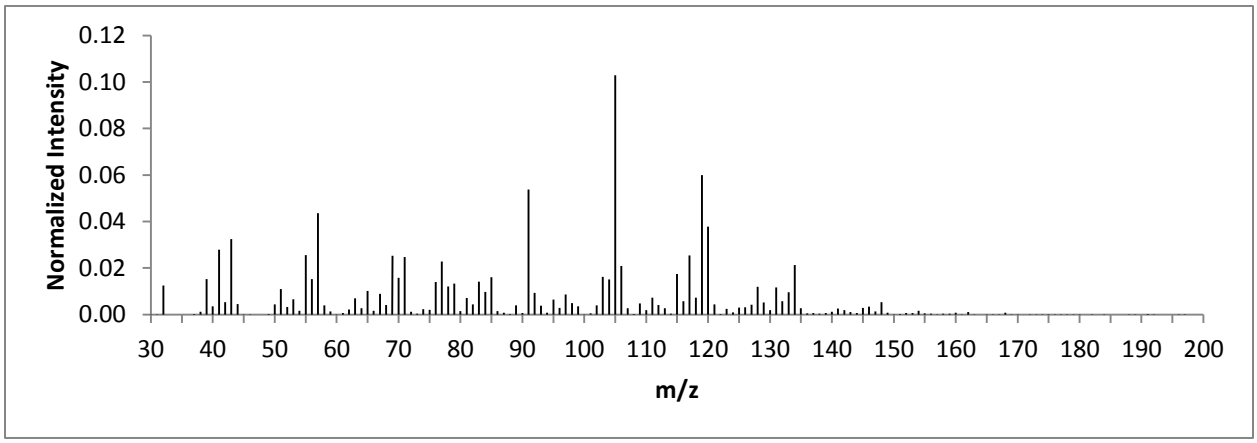

Figure 337: TIS C12-14B

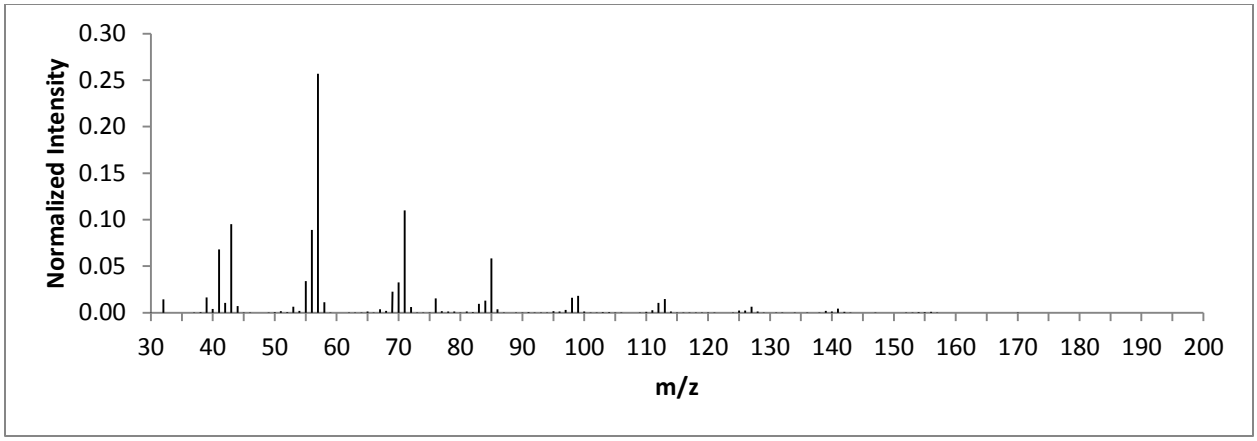

Figure 338: TIS C12-15

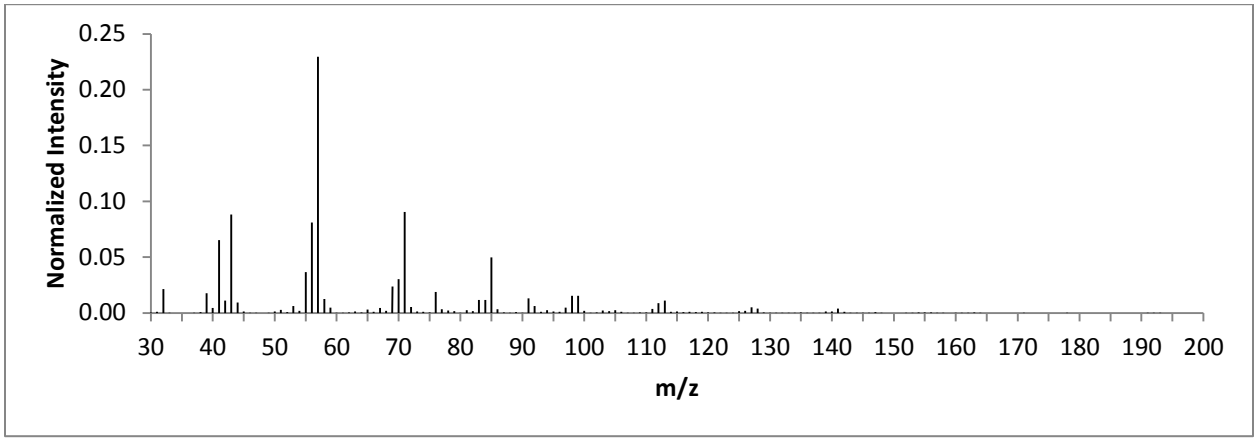

Figure 339: TIS C12-16

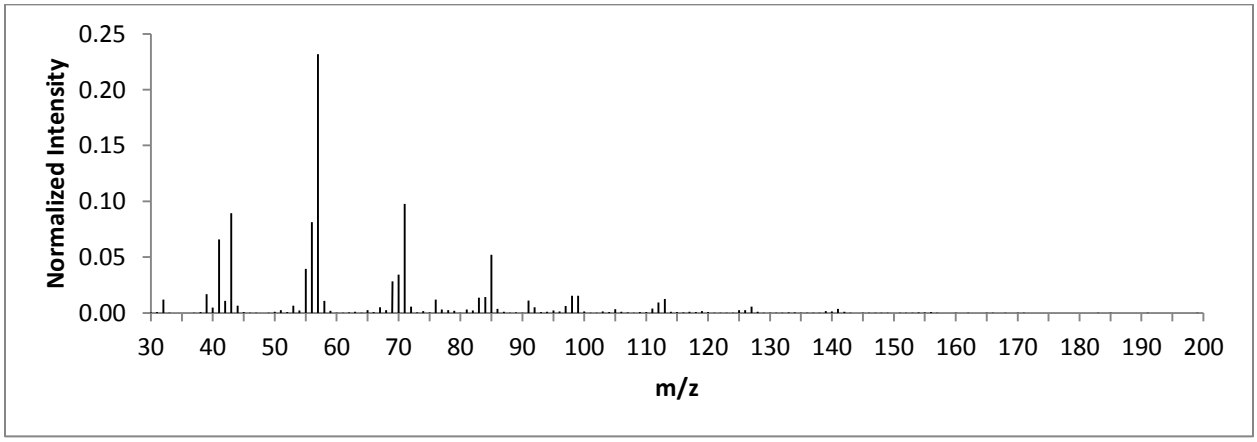

Figure 340: TIS C12-17

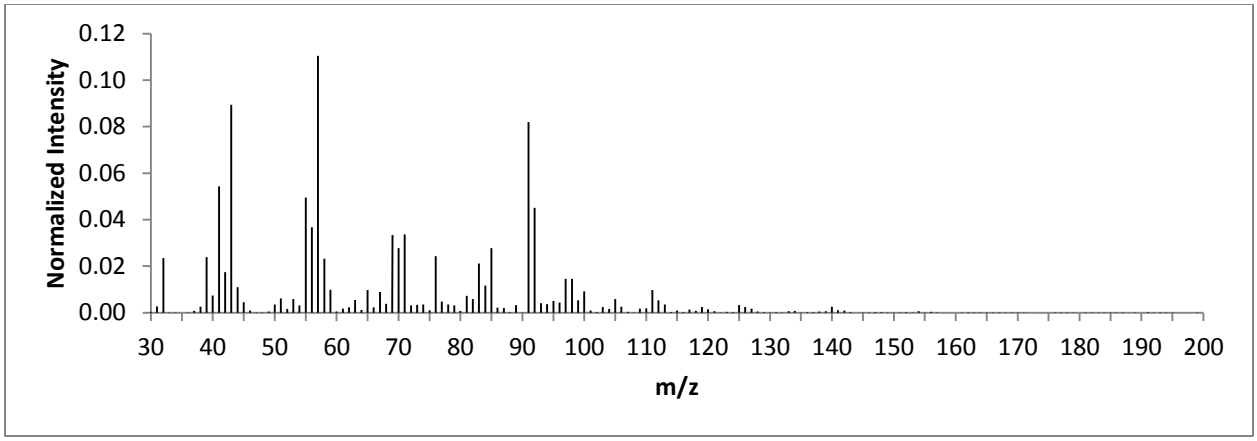

Figure 341: TIS C12-18

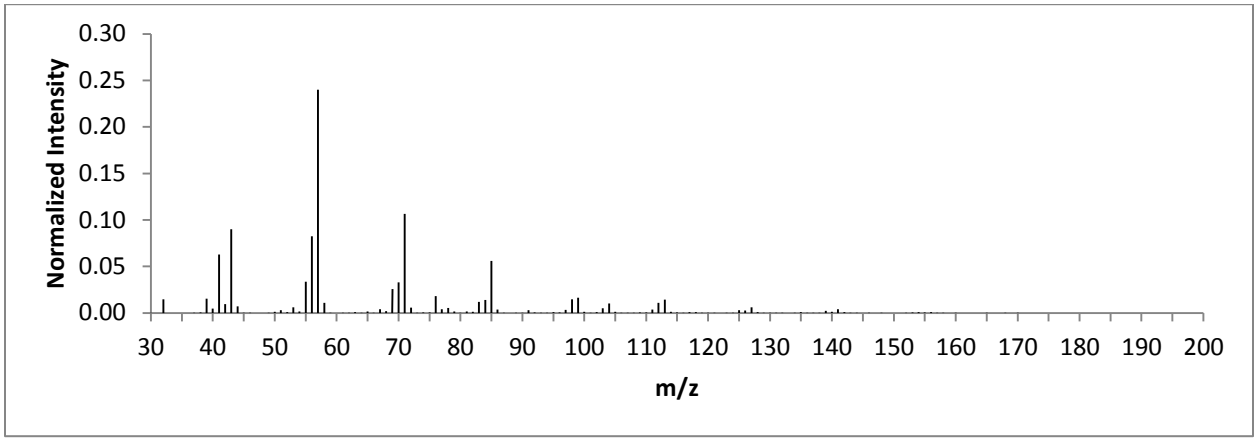

Figure 342: TIS C12-19

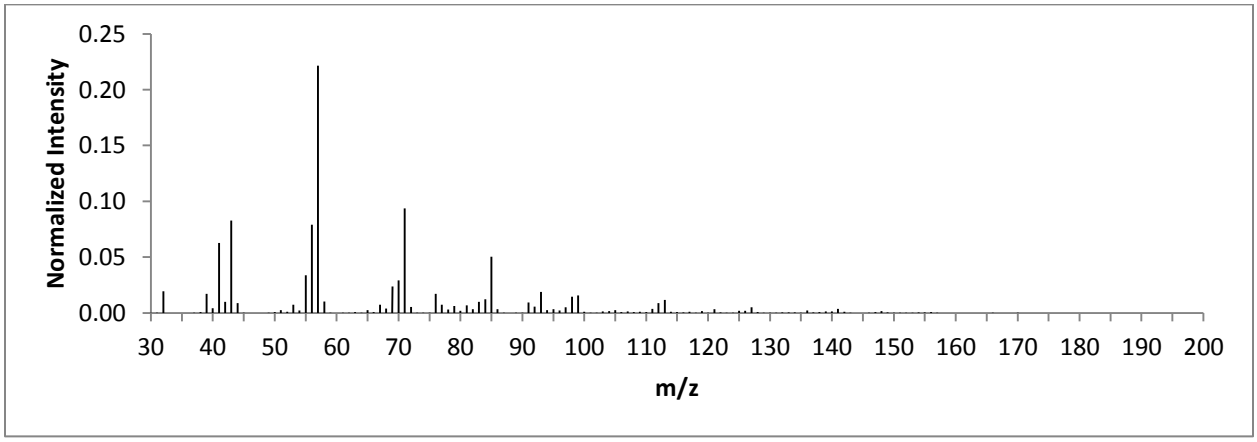

Figure 343: TIS C12-20

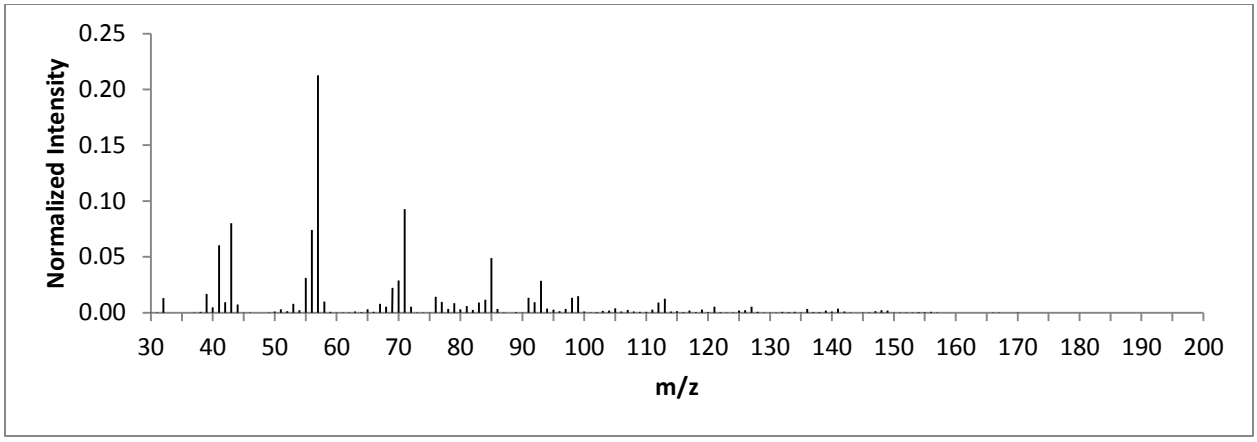

Figure 344: TIS C12-21

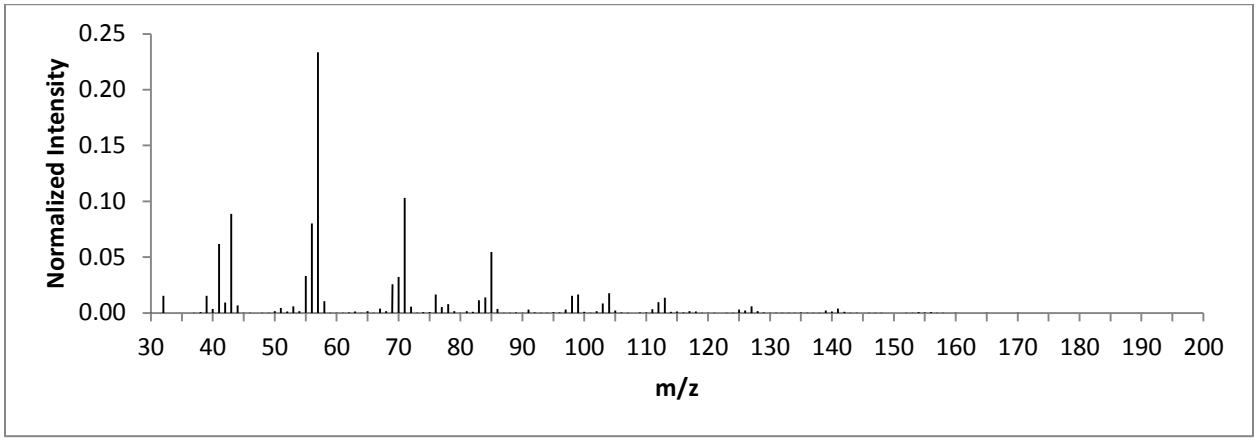

Figure 345: TIS C12-22

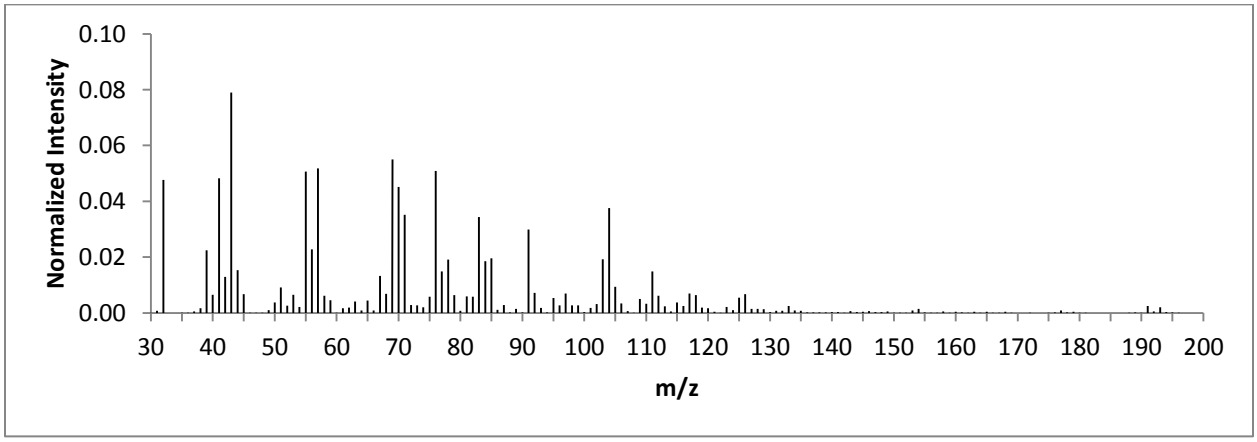

Figure 346: TIS C12-23

REFERENCES

1. *Analysis And Interpretation Of Fire Scene Evidence*. CRC Press: Boca Raton, 2004.

2. *A Profile Of Fire In The United States 2003-2007*; U.S. Fire Administration/National Fire Data Center: 2010.

3. American Standards For Testing And Materials: Standard Test Method For Ignitable Liquid Residues In Extracts From Fire Debris Sample By Gas Chromatography-Mass Spectrometry. **2006,** (E1618), 1-11.

4. Stauffer, E.; Dolan, J. A.; Newman, R., *Fire Debris Analysis*. Elsevier: Boston, 2008.

5. Almirall, J. R.; Furton, K. D., Characterization Of Background And Pyrolysis Products That May Interfere With The Forensic Analysis Of Fire Debris. *J. Anal. Appl. Pyrolysis* **2004,** *71*, 51-67.

6. Williams, M. R.; Fernandes, D.; Bridge, C.; Dorrien, D.; Elliott, S.; Sigman, M., Adsorption Saturation And Chromatographic Distortion Effects On Passive Headspace Sampling With Activated Charcoal In Fire Debris Analysis. *J. Forensic Sci.* **2005,** *50* (2), 316-325.

7. American Standards For Testing And Materials: Standard Practice For Separation And Concentration Of Ignitable Liquid Residues From Fire Debris Samples By Dynamic Headspace Concentration. **2000,** (E 1413), 1-3.

8. American Standards For Testing And Materials: Standard Practice For Separation Of Ignitable Liquid Residues From Fire Debris Samples By Passive Headspace Concentration With Activated Charcoal. **2000,** (E 1412), 1-3.

9. Varmuza, K.; Filzmoser, P., *Introduction To Multivariate Statistical Analysis In Chemometrics*. CRC Press: New York, 2009.

10. American Standards For Testing And Materials: Standard Practice For Separation And Concentration Of Ignitable Liquid Residues From Fire Debris Samples By Passive Headspace Concentration With Solid Phase Microextraction (SPME). **2001,** (E 2154), 1-3.

11. Skoog, D. A.; Holler, F. J.; Crouch, S. R., *Principles Of Instrumental Analysis*. 6th ed.; Thomson Brooks/Cole: Belmont, 2007.

12. Vestal, M. L., Methods Of Ion Generation. *Chem. Rev.* **2001,** *101*, 361-375.

13. Doble, P.; Sandercock, M.; Pasquier, E. D.; Petocz, P.; Roux, C.; Dawson, M., Classification Of Premium And Regular Gasoline By Gas Chromatography/Mass Spectrometry, Principal Component Analysis And Artificial Neural Networks. *Forensic Sci. Int.* **2003,** *132*, 26-39.

14. Sigman, M. E.; Williams, M. R.; Castelbuono, J. A.; Colca, J. G.; Clark, C. D., Ignitable Liquid Classification And Identification Using The Summed-Ion Mass Spectrum. *Instrum. Sci. Technol.* **2008,** *36* (4), 375-393.

15. Monfreda, M.; Gregori, A., Differentiation Of Unevaporated Gasoline Samples According To Their Brands, By SPME-GC-MS And Multivariate Statistical Analysis. *J. Forensic Sci* **2011,** *56* (2), 372-380.

16. Morgan, S. L.; Bartick, E. G., *Forensic Analysis On The Cutting Edge: New Methods For Trace Evidence Analysis*. John Wiley & Sons, Inc.: 2007.

17. Malinowski, E. R.; Howery, D. G., *Factor Analysis In Chemistry*. John Wiley & Sons, Inc.: New York, 1980.

18. Higgins, J. J., *An Introduction To Modern Nonparametric Statistics*. Thomson Brooks/Cole: Pacific Grove, 2004.

19. Malinowski, E. R., Determination Of Rank By Median Absolute Deviation (DRMAD): A Simple Method For Determining The Number Of Principal Factors Responsible For A Data Matrix. *J. Chemometrics* **2009,** *23*, 1-6.

20. Fadhil, G. F., Factor Analysis, Target Factor Testing And Model Designing Of Aromatic Solvent Effect Of The Formyl Proton Nuclear Magnetic Resonance Chemical Shift In Para Substituted Benzaldehydes. *Am. J. Appl. Sci.* **2010,** *7* (1), 24-32.

21. Fawcett, T., An Introduction To ROC Analysis. *Pattern Recognition Letters* **2006,** *27*, 861-874.

22. Brown, C. D.; Davis, H. T., Receiver Operating Characteristics Curves And Related Decision Measures: A Tutorial. *Chemom. Intell. Lab. Syst.* **2006,** *80*, 24-38.

23. Massart, D. L.; Vandeginste, B. G. M.; Buydens, L. M. C.; Jong, S. D.; Lewi, P. J.; Smeyers-Verbeke, J., *Handbook Of Chemometrics And Qualimetrics: Part A*. Elsevier: New York, 1997.

24. Sheskin, D. J., *Handbook Of Parametric And Nonparametric Statistical Procedures*. Chapman & Hall/CRC: New York, 2000.

25. Hanley, J. A.; McNeil, B. J., The Meaning And Use Of The Area Under A Receiver Operating Characteristic (ROC) Curve. *Radiology* **1982,** *143* (1), 29-36.

26. Sharaf, M. A.; Illman, D. L.; Kowalski, B. R., *Chemometrics*. John Wiley & Sons: New York, 1986; Vol. 82.

27. Srihera, R.; Stute, W., Kernel Adjusted Density Estimation. *Stat. Probabil. Lett.* **2011,** *81*, 571-579.

28. Castelbuono, J. A. The Identification Of Ignitable Liquids In The Presence Of Intereference Products: Generations Of A Pyrolysis Database. University of Central Florida, Orlando, 2008.

29. McHugh, K. Determining The Presence Of An Ignitable Liquid Residue In Fire Debris Samples Utilizing Target Factor Analysis. University of Central Florida, Orlando, 2010.

30. Lu, Y.; Harrington, P. B., Forensic Application of Gas Chromatography-Differential Mobility Spectrometry with Two-Way Classification of Ignitable Liquids from Fire Debris. *Anal. Chem.* **2007,** *79*, 6752-6759.

31. Benson, S.; Lennard, C.; Maynard, P.; Roux, C., Forensic Applications of Isotope Ratio Mass Spectrometry - A Review. *Forensic Sci. Int.* **2006,** *157*, 1-22.

32. Almirall, J. R.; Wang, J.; Lothridge, K.; Furton, K. G., The Detection And Analysis Of Ignitable Liquid Residues Extracted From Human Skin Ugin SPME/GC. *J. Forensic Sci* **2000,** *45* (2), 453-461.